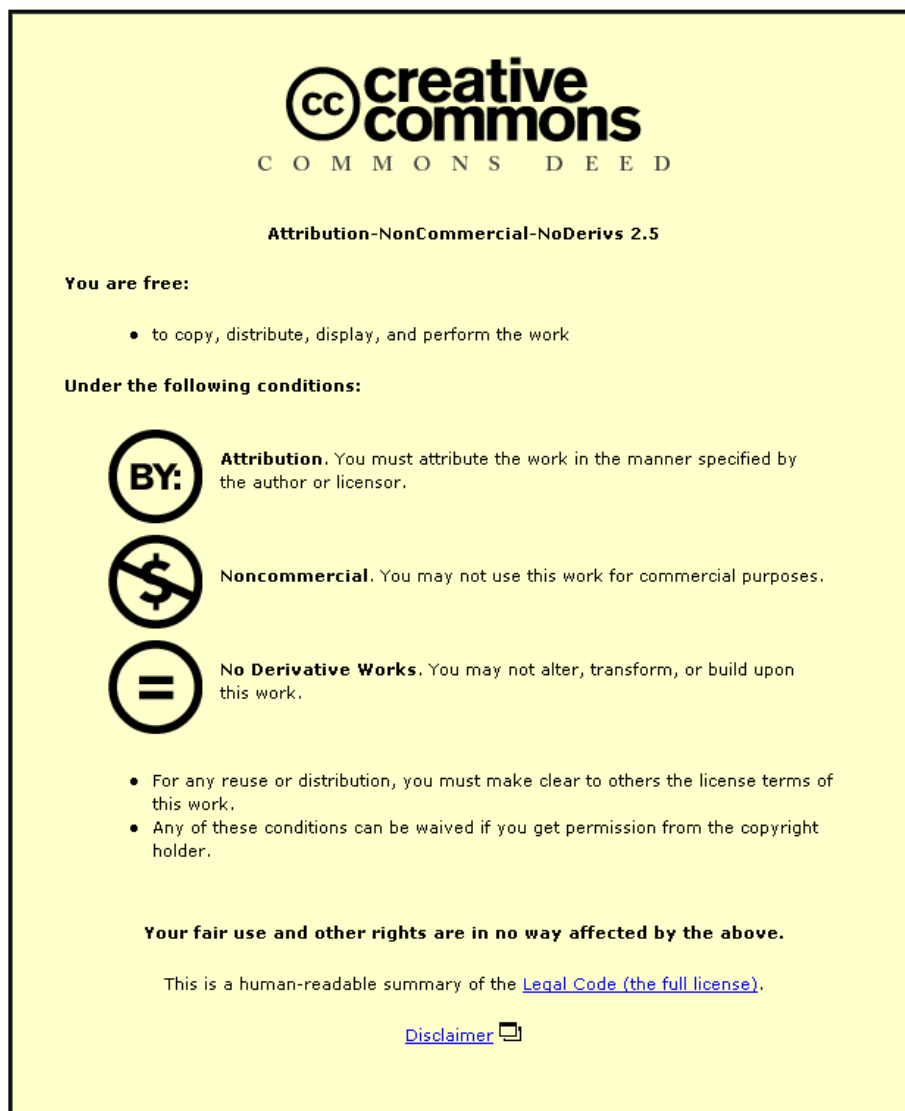


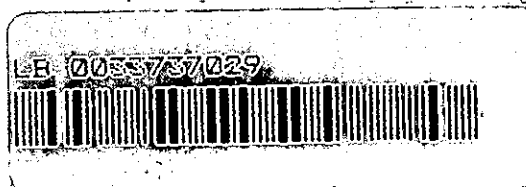
This item was submitted to Loughborough University as an MPhil thesis by the author and is made available in the Institutional Repository (<https://dspace.lboro.ac.uk/>) under the following Creative Commons Licence conditions.



For the full text of this licence, please go to:  
<http://creativecommons.org/licenses/by-nc-nd/2.5/>

LOUGHBOROUGH  
UNIVERSITY OF TECHNOLOGY  
LIBRARY

AUTHOR/FILING TITLE	
MAHDI, L T	
ACCESSION/COPY NO.	
03373702	
VOL. NO.	CLASS MARK
- 9 JAN 1998	
12 JAN 2001	



**LOUGHBOROUGH  
UNIVERSITY OF TECHNOLOGY  
LIBRARY**

AUTHOR/FILING TITLE		
MAHDI, L T		
ACCESSION/COPY NO.		
08373702		
VOL. NO.	CLASS MARK	
<div style="display: flex; justify-content: space-between;"> <div style="width: 30%;"> <p>4 JUL 1991</p> <p>- 3 JUL 1992</p> <p><del>3 JUL 1992</del></p> <p>- 2 JUL 1993</p> <p>- 2 JUL 1993</p> <p>- 2 JUL 1993</p> </div> <div style="width: 30%;"> <p>12th copy</p> <p>- 2 JUL 1993</p> <p><del>2 JUL 1993</del></p> <p>26 NOV 1992</p> <p>- 1 JUL 1994</p> </div> <div style="width: 30%;"> <p>11 NOV 1992</p> <p>no renewal</p> <p>- 2 JUL 1993</p> <p>13 JAN 1993</p> <p>2 JUL 1993</p> <p>22/6 JAN 1998</p> </div> </div>		

LB 0053737029





**THE INFLUENCE OF THE MATRIX  
ON THE BEHAVIOUR IN COMPRESSION  
OF FIBRE COMPOSITES**

by

**LAMYA T. MAHDI**

A Master's Thesis submitted in partial fulfilment  
of the requirements for the award  
of the degree of  
Master of Philosophy of the  
Loughborough University of Technology

January 1990

Supervisor: Mr J F Harper

Institute of Polymer Technology and  
Materials Engineering  
Loughborough University of Technology

© by Lamya T. Mahdi

Loughborough University of Technology Library	
Date	Oct. 90
Class	
Acc No.	03373702

49317916

—  
To my husband and  
the two A's I adore  
Ahmed and Asmaa

THE INFLUENCE OF THE MATRIX ON THE BEHAVIOUR IN COMPRESSION  
OF FIBRE COMPOSITES

**SYNOPSIS**

The behaviour of long fibre composites subjected to tensile loads has been widely studied and theories concerning the failure mechanisms are accepted and included in standard texts. In many applications compressive strength is important and in flexure failure is often initiated on the compressive side of the composite. However, compressive failure has not been studied thoroughly, partly because of the large number of failure mechanisms which can occur and the difficulties in conducting meaningful compression tests. The aim of this work was to determine the influence of the matrix on the behaviour of long fibre composites subjected to compressive loads so that failure mechanisms could be predicted more accurately.

Previous work on the compressive failure of fibre composites was reviewed. A series of unidirectional composite laminates were made using either carbon or glass fibres in an epoxy resin. The properties of the epoxy matrix were varied in an ordered way by the addition of various percentages of urethane modifier. The compressive behaviour of the resulting composites was studied using a modified Celanese jig and fracture surfaces examined using a variety of microscopic techniques. A full range of tensile and interlaminar shear tests were performed to aid in the interpretation of the results.

The behaviour of the composite under compressive loading was found to be highly dependent on the properties of the resin matrix. In tension the modulus varied only slightly, as predicted by the rule of mixtures, whereas in compression this rule was not obeyed. As the percentage of modifier in the matrix increased so the compressive strength and interlaminar shear strength decreased despite an observed increase in interfacial adhesion. In unmodified matrices both tensile and compressive failure was influenced by the interface but as the modifier addition increased there was shift from interface to matrix controlled failure. In glass reinforced composites fibre kinking was the only failure mechanism observed although the degree of damage varied considerably. In unmodified carbon reinforced specimens failure was by shear. As the percentage of modifier increased, at some critical value, the failure mode changed to one governed by fibre microbuckling, and at higher modifier content microbuckling led to kink band formation.

### ACKNOWLEDGEMENTS

I wish to express my deep sense of gratitude to my supervisor, Mr J F Harper, for his guidance, inspiration and encouragement during the preparation of this work.

Thanks are also due to the following:

- \* My husband, for his endurance and support throughout the project and to all my family
- \* Mr N A Miller (Fred) for his instruction and assistance in using the mechanical test equipment
- \* Dr T O Heumann for the stimulating discussions and practical assistance
- \* Fellow research workers in the Composites Laboratory
- \* Janet Smith for her care and attention in typing this thesis.

TABLE OF CONTENTS

	<u>Page No</u>
Synopsis . . . . .	1
Acknowledgements . . . . .	ii
Table of Contents . . . . .	iii
List of Tables . . . . .	vi
List of Figures . . . . .	vii
List of Plates . . . . .	xi
Symbols and Abbreviations . . . . .	xiv
 CHAPTER 1: INTRODUCTION . . . . .	 1
 CHAPTER 2: LITERATURE REVIEW . . . . .	 4
2.1 Introduction . . . . .	4
2.2 The Behaviour of Unidirectional Fibre Composites Under Compressive Loading . . .	5
2.3 The Influence of Test Techniques on the Compressive Strength of Unidirectional Composites . . . . .	25
2.4 Summary . . . . .	28
 CHAPTER 3: EXPERIMENTAL WORK . . . . .	 30
3.1 Introduction . . . . .	30
3.2 Materials . . . . .	31
3.2.1 Glass Fibre . . . . .	31
3.2.2 Carbon Fibre . . . . .	32
3.2.3 Epoxy Resin . . . . .	32
3.2.4 Curing Agent . . . . .	33
3.2.5 Modifier . . . . .	33
3.2.6 Solvent . . . . .	34
3.3 Equipment . . . . .	34
3.3.1 Laminate Manufacturing Equipment . .	34
3.3.2 Mechanical Testing Equipment . . . .	35

	<u>Page No</u>
3.4 Techniques . . . . .	36
3.4.1 Manufacturing of Composite Laminates	36
3.4.2 Volume Fraction Analysis Technique .	38
3.4.3 Resin Density Analysis Technique . .	39
3.4.4 Test Specimen Preparation . . . . .	40
3.5 Mechanical Testing . . . . .	44
3.5.1 Compressive Testing . . . . .	44
3.5.2 Tensile Testing . . . . .	45
3.5.3 Inter-Laminar Shear Testing . . . . .	45
3.5.4 Microscopic Testing . . . . .	46
3.5.5 Resin Tensile Testing . . . . .	46
CHAPTER 4: DATA AND RESULTS . . . . .	48
4.1 Introduction . . . . .	48
4.2 Fibre Volume Fraction . . . . .	49
4.2.1 'GRP' Specimens . . . . .	49
4.2.2 'CFRP' Specimens . . . . .	50
4.3 Voids Volume Fraction . . . . .	50
4.4 Matrix-Resin Density . . . . .	51
4.5 Matrix-Resin Properties . . . . .	52
4.6 Compressive Properties . . . . .	53
4.6.1 Compressive Strength . . . . .	53
4.6.2 Fracture Appearance . . . . .	54
4.6.3 Compressive Failure Strain . . . . .	55
4.6.4 Compressive Secant Modulus . . . . .	55
4.7 Tensile Properties . . . . .	56
4.7.1 Ultimate Tensile Strength . . . . .	56
4.7.2 Fracture Appearance . . . . .	57
4.7.3 Tensile Failure Strain . . . . .	57
4.7.4 Tensile Secant Modulus . . . . .	58
4.8 Inter-Laminar Shear Strength (ILSS) . . . . .	58
4.8.1 Appearance of Failure . . . . .	59

	<u>Page No</u>
4.9 Microscopic Results . . . . .	60
4.9.1 Fibre Distribution . . . . .	60
4.9.2 Inter-Laminar Shear Failure . . . . .	60
4.9.3 Compressive and Tensile Failures . . . . .	61
CHAPTER 5: DISCUSSION . . . . .	62
5.1 Fibre Volume Fraction and Distribution . . . . .	62
5.2 Inter-Laminar Shear Strength . . . . .	64
5.3 Tensile Properties . . . . .	67
5.3.1 Tensile Modulus . . . . .	67
5.3.2 Tensile Strength . . . . .	70
5.3.3 Tensile Failure Strain . . . . .	72
5.3.4 Failure Mechanism . . . . .	74
5.4 Compressive Properties . . . . .	77
5.4.1 Compressive Secant Modulus . . . . .	77
5.4.2 Compressive Strength . . . . .	79
5.4.3 Compressive Failure Strain . . . . .	83
5.4.4 Compressive Failure Behaviour . . . . .	84
CHAPTER 6: CONCLUSIONS . . . . .	91
REFERENCES . . . . .	95
TABLES . . . . .	100
FIGURES . . . . .	110
PLATES . . . . .	166
APPENDICES . . . . .	193

TABLESPage No

Table 4.1:	Mean values of fibres and voids volume fraction . . . . .	100
Table 4.2:	Mean values of matrix-resin density . . . .	101
Table 4.3:	Mean results of matrix-resin properties . .	101
Table 4.4:	Normalised compressive strength, GRP . . . .	102
Table 4.5:	Normalised compressive strength, CFRP . . . .	102
Table 4.6:	Normalised compressive failure strain, GRP .	103
Table 4.7:	Normalised compressive failure strain, CFRP .	103
Table 4.8:	Normalised compressive secant modulus, GRP .	104
Table 4.9:	Normalised compressive secant modulus, CFRP .	104
Table 4.10:	Normalised tensile strength, GRP . . . . .	105
Table 4.11:	Normalised tensile strength, CFRP . . . . .	105
Table 4.12:	Normalised tensile failure strain, GRP . .	106
Table 4.13:	Normalised tensile failure strain, CFRP . .	106
Table 4.14:	Normalised tensile secant modulus, GRP . .	107
Table 4.15:	Normalised tensile secant modulus, CFRP . .	107
Table 4.16:	Normalised interlaminar shear strength, GRP	108
Table 4.17:	Normalised interlaminar shear strength, CFRP	108
Table 4.18:	Macro-study of failure mechanism for compression specimens . . . . .	109

LIST OF FIGURES

CHAPTER 2	<u>Page No</u>
Figure 2.1: Rosen's analytical model for the compressive strength of unidirectional reinforced fibre composites (from Ref 1) . . . . .	110
Figure 2.2: The compressive strength of glass reinforced epoxy composites as predicted by the Rosen buckling model (from Ref 1) . . . . .	111
Figure 2.3: The critical compressive strain for glass reinforced epoxy composites as predicted by Rosen (from Ref 1) . . . . .	112
Figure 2.4: Stress-strain curves for fibres and matrix as predicted by Hayashi (from Ref 7) . . .	113
Figure 2.5: The compressive strength vs fibre volume fraction for glass-epoxy composites by Rosen and Hayashi (from Ref 7) . . . . .	114
Figure 2.6: The compressive strength of Boron-Epoxy composites calculated by Rosen and Hayashi (from Ref 7) . . . . .	115
Figure 2.7: The compressive failure showing the geometrical kink-band according to Chaplin (from Ref 15) . . . . .	116
Figure 2.8: Tensile stress-strain curves for SMC-R25A, showing the effect of rubber-toughening of the matrix on the stress and strain behaviour of the composites (from Ref 21) .	117
Figure 2.9: Piggott's consideration of interface and matrix failure as a result of sinusoidally buckled fibres (from Ref 22) . . . . .	118
Figure 2.10: Compressive failure strain vs kind of matrix by Hahn, showing the effects of fibres and matrices on the compressive failure strain (from Ref 23) . . . . .	119

	<u>Page No</u>
Figure 2.11: The dependence of compressive failure strain on modulus ratio by Hahn (from Ref 23) . .	120
Figure 2.12: Effect of resin tensile modulus on modulus of T300 and T700 composites under compression, observed by Hahn and Williams (from Ref 24) . . . . .	121
 <b>CHAPTER 3</b>	
Figure 3.13: The strain gauge bridge circuit . . . . .	122
Figure 3.14: A fibre wound steel frame ready for resin impregnation by the wet lay-up technique . .	123
Figure 3.15: The acid digestion process of the volume fraction measurement . . . . .	124
Figure 3.16: The compressive test specimen . . . . .	125
Figure 3.17: The tensile test specimen . . . . .	126
Figure 3.18: The interlaminar shear test specimen . . .	127
Figure 3.19: The resin tensile test specimen . . . . .	128
 <b>CHAPTER 4</b>	
Figure 4.20: Percentage of voids in matrix vs percentage of modifier . . . . .	129
Figure 4.21: Matrix-resin density vs percentage of modifier . . . . .	130
Figure 4.22: Load vs extension of resin-matrix systems .	131
Figure 4.23: Matrix tensile modulus vs percentage of modifier . . . . .	132
Figure 4.24: Matrix tensile strength vs percentage of modifier . . . . .	133
Figure 4.25: Compressive strength of GRP vs percentage of modifier . . . . .	134
Figure 4.26: Compressive strength of CFRP vs percentage of modifier . . . . .	135

	<u>Page No</u>
Figure 4.27: Mean compressive strength vs percentage of modifier . . . . .	136
Figure 4.28: Compressive strength retention vs percentage of modifier . . . . .	137
Figure 4.29: Compressive failure strain of GRP vs percentage of modifier . . . . .	138
Figure 4.30: Compressive failure strain of CFRP vs percentage of modifier . . . . .	139
Figure 4.31: Mean compressive failure strain vs percentage of modifier . . . . .	140
Figure 4.32: Compressive failure strain retention vs percentage of modifier . . . . .	141
Figure 4.33: Mean compressive secant modulus vs percentage of modifier . . . . .	142
Figure 4.34: Compressive secant modulus retention vs percentage of modifier . . . . .	143
Figure 4.35: Tensile strength of GRP vs percentage of modifier . . . . .	144
Figure 4.36: Tensile strength of CFRP vs percentage of modifier . . . . .	145
Figure 4.37: Mean tensile strength vs percentage of modifier . . . . .	146
Figure 4.38: Tensile strength retention vs percentage of modifier . . . . .	147
Figure 4.39: Tensile failure strain of GRP vs percentage of modifier . . . . .	148
Figure 4.40: Tensile failure strain of CFRP vs percentage of modifier . . . . .	149
Figure 4.41: Mean tensile failure strain vs percentage of modifier . . . . .	150
Figure 4.42: Tensile failure strain retention vs percentage of modifier . . . . .	151
Figure 4.43: Mean tensile secant modulus vs percentage of modifier . . . . .	152

	<u>Page No</u>
Figure 4.44: Tensile secant modulus retention vs percentage of modifier . . . . .	153
Figure 4.45: General form of curves for interlaminar shear strength test (GRP) . . . . .	154
Figure 4.46: General form of curves for interlaminar shear strength test (CFRP) . . . . .	155
Figure 4.47: Interlaminar shear strength of GRP vs percentage of modifier . . . . .	156
Figure 4.48: Interlaminar shear strength of CFRP vs percentage of modifier . . . . .	157
Figure 4.49: Mean interlaminar shear strength vs percentage of modifier . . . . .	158
Figure 4.50: Interlaminar shear strength retention vs percentage of modifier . . . . .	159
 CHAPTER 5	
Figure 5.51: The rule of mixtures relationship for the strength of unidirectional composites in which $\hat{\epsilon}_f > \hat{\epsilon}_m$ . . . . .	160
Figure 5.52: The rule of mixtures relationship for the strength of unidirectional composites in which $\hat{\epsilon}_m > \hat{\epsilon}_f$ . . . . .	161
Figure 5.53: A correlation between compression and tensile failure strain . . . . .	162
Figure 5.54: Effect of resin tensile moduli on compressive and tensile moduli of GRP . . .	163
Figure 5.55: Effect of resin tensile moduli on compressive and tensile moduli of CFRP . . .	164
Figure 5.56: Compressive failure strain vs square root of the matrix-to-fibre modulus ratio . . .	165

LIST OF PLATES

<u>Plate No</u>		<u>Page No</u>
1	The winding machine . . . . .	166
2	The leaky mould used in the wet lay-up of epoxy resin composites, showing the four G-clamps . . . . .	166
3	The Mand servo-screw test machine with which compressive tests were performed . . . . .	167
4	The Celanese compression test fixture . . . . .	168
5	The Dartec servohydraulic test machine with which tensile tests were performed . . . . .	169
6	The Instron test machine with which interlaminar shear tests were performed . . . . .	170
7	The JJ test machine with which resin tensile tests were performed . . . . .	171
8	a) Multiple kink-bands in some unmodified GRP specimens showing $70^{\circ}$ inclination of the bands to the fibre axis . . . . .	172
	b) A single kink-band observed in some unmodified GRP specimens with a $70^{\circ}$ inclination . . . . .	172
9	A narrow single kink-band in a 20% modified GRP specimen, showing a $90^{\circ}$ inclination of the band to the fibre axis . . . . .	173
10	A wider single kink-band in a 60% modified GRP specimen, showing a $90^{\circ}$ inclination of the band to the fibre axis . . . . .	174
11	A through thickness kink-band in 5% modified GRP specimens . . . . .	175
12	The shear failure mode observed in unmodified CFRP specimens . . . . .	176
13	A microbuckling mode as observed in < 5% modified CFRP specimens . . . . .	177

<u>Plate No</u>		<u>Page No</u>
14	A kink-band observed in a 30% modified CFRP specimen. The specimen did not fracture . .	178
15	A tensile failure in an unmodified GRP specimen . . . . .	179
16	A tensile failure in a 60% modified GRP specimen . . . . .	180
17	A tensile failure in an unmodified CFRP specimen . . . . .	181
18	A tensile failure in a 60% modified CFRP specimen . . . . .	182
19	The fibre distribution in an unmodified GRP specimen (x200) . . . . .	183
20	The fibre distribution in an unmodified CFRP specimen (x200) . . . . .	183
21	The fibre distribution in a 30% modified GRP specimen (x200) . . . . .	184
22	The fibre distribution in a 30% modified CFRP specimen (x200) . . . . .	184
23	An interlaminar shear crack in an unmodified GRP specimen (x500) . . . . .	185
24	An interlaminar shear crack in an unmodified CFRP specimen (x500) . . . . .	185
25	An interlaminar shear crack in a 30% modified GRP specimen (x500) . . . . .	186
26	An interlaminar shear crack in a 30% modified CFRP specimen (x500) . . . . .	186
27	An SEM micrograph of the ILSS failure surface for unmodified GRP (x660) . . . . .	187
28	An SEM micrograph of the ILSS failure surface for 60% modified GRP (x660) . . . . .	187
29	An SEM micrograph of the ILSS failure surface for unmodified CFRP (x9500) . . . . .	188

<u>Plate No</u>		<u>Page No</u>
30	An SEM micrograph of the ILSS failure surface for 60% modified CFRP (x950) . . . . .	188
31	An SEM micrograph of a part of the tensile failure surface of an unmodified GRP specimen (x450) . . . . .	189
32	An SEM micrograph of a part of the tensile failure surface of an unmodified CFRP specimen (x450) . . . . .	189
33	An SEM micrograph of the surface of shear failure observed in an unmodified CFRP compressive failure specimen (x950) . . . . .	190
34	A high magnification SEM micrograph of the end of a carbon fibre from an unmodified CFRP compressive failure. The fibre shear failure mode is clearly visible (x6500) . . . . .	190
35	An SEM micrograph of the compressive failure surface of 5% and 10% modified CFRP specimens. The characteristic steps which are the result of fibre microbuckling (x250) . . . . .	191
36	A high magnification SEM micrograph of the end of a carbon fibre from 5% and 10% modified CFRP compressive failure. The fibre microbuckling failure has resulted in well defined tensile and compressive regions of fracture being visible (x6500) . . . . .	191
37	Local buckling in the kink-band for 60% modified GRP compressive failure specimens (side view) (x50) . . . . .	192
38	Local buckling in the kink-band for 60% modified CFRP compressive failure specimens (side view) (x50) . . . . .	192

## SYMBOLS AND ABBREVIATIONS

### SYMBOLS

$\rho$	- density
$\sigma$	- stress
$\sigma_u$	- ultimate strength
$\sigma_c$	- critical strength
$\bar{\sigma}$	- mean value
$\epsilon$	- strain
$\epsilon_f$	- failure strain
$\sigma_{my}$	- matrix yield strength
$\alpha$	- kinking angle
$\tau$	- shear stress
$\phi$	- misalignment angle

### ABBREVIATIONS

c	= carbon fibre
C	= compressive
Cr	= crucible
CSA	= cross-sectional area
CFRP	= carbon fibre reinforced plastic
d	= diameter
dig	= digestion
E	= elastic modulus
$E_m$	= matrix modulus
f	= fibre
FEA	= finite-element analysis
g	= glass fibre
G	= shear modulus
g.	= gram
GRP	= glass reinforced plastic
ILSS	= inter-laminar shear strength
l	= length
L	= load
m	= matrix
% mod	= percentage of modifier
r	= resin
ROM	= role of mixture
s	= specimen
S	= inter-laminar shear strength
sec.	= secant
spec.	= specimen
T	= tensile
t	= thickness
UCS	= ultimate compressive strength
UTS	= ultimate tensile strength
UDFRCM	= unidirectional fibre reinforced composite material

V = volume fraction  
V<sub>v</sub> = voids volume fraction  
V<sub>f</sub> = fibre volume fraction  
W = weight fraction  
w = width  
W<sub>s</sub> = weight of specimen  
W<sub>wo</sub> = weight of density bottle containing water only  
wt. = weight

# CHAPTER 1

## CHAPTER 1

### INTRODUCTION

Composite materials have been classified in many ways depending on the ideas and concepts that need to be identified. This is particularly relevant to engineering components which may consist of two or more materials combined to give a performance in service which is superior to the properties of the individual materials. Thus, concrete beams which have excellent compressive strength, are given some strength in tension by reinforcing the concrete with steel bars.

There has been a rapid growth in the use of fibre reinforced material in engineering applications in the last few years and there is every indication that this will continue. Continuous Fibre Reinforced Composites are seeing significantly expanded levels of use in hardware where reduced weight is critical. This is primarily a result of their tailorability as well as their high strength and modulus-to-density ratio. In recent years these materials have seen applications ranging from mass-produced tennis rackets to relatively complex structures, such as the wings of aircraft. A range of valuable mechanical and radiological properties have allowed medical equipment and artificial limb designers to use composites to improve traditional equipment designs beyond recognition.

As the use of these materials expands, so also does the likelihood of eventual failures. As with their metal counterparts, the occurrence of failure is likely to represent a relatively rare event that is not encountered with most hardware usage. However, when such failures occur, the ability to determine their origin and cause constitutes a

critical step that is necessary in providing valuable engineering feedback and ensuring the continued integrity of the components during service.

The advantages of fibre-reinforced plastic composites to the engineering designer are well documented and indeed a great deal of information is available on tensile and impact properties and the parameters which control them. These materials are, however, often used in flexure because of the manufacturing methods employed in their production, and therefore their compressive strength and modulus are important design parameters. Compression data, however, are not so plentiful and failure processes are not so well understood.

Theoretical and experimental attempts made so far to understand the behaviour of these materials under compressive loads is limited. The progress in understanding this type of failure from the earlier theories to the current ones is outlined in Chapter 2. The measure of agreement between experimental results and various theoretical predictions are, however, limited.

There are also practical difficulties involved in compression testing. These include proper interpretation of data which generally has considerable scatter as a result of several different mechanisms inducing compressive failure. These practical difficulties are partially to blame for the lack of understanding of compressive failure mechanisms.

As yet, none of the theories proposed fully explain the behaviour of all composite systems. Despite this, much knowledge has been acquired through identifying the factors within a composite system that affects

its compressive behaviour. Amongst these the matrix properties are recognised as having a very significant effect.

The purpose of this work was to investigate the effect of matrix properties on the compressive behaviour of a unidirectional glass/carbon fibre-epoxy composite subject to compression in the direction of reinforcement. The properties of the matrix were varied by additions of an elasticising modifier to epoxy resin as appropriate. Tensile and ILSS properties were also measured in an attempt to fully understand the role of the matrix. Composite specimens were made and tested as described in Chapter 3, with the aim of establishing, comparing and contrasting the compressive behaviour that occurred over the range of matrices considered.

The benefits of such a programme will be apparent in the more effective utilisation of these systems in load bearing structures and in the ultimate development of fibre-reinforced materials with higher compressive load bearing capabilities.

# CHAPTER 2

## CHAPTER 2

### LITERATURE REVIEW

#### 2.1 INTRODUCTION

Studies of the compressive behaviour of unidirectional fibre composites frequently encounter several difficulties and many of these difficulties are associated with the proper interpretation of experimental data, which generally have considerable scatter. The scatter is associated primarily with the various failure modes that can occur in compressive failure.

The various compressive failure modes include symmetric and non-symmetric fibre microbuckling, fibre compressive failure, and delamination. These difficulties are compounded because testing is sensitive to factors such as:

- Euler buckling
- Specimen misalignment in the testing fixture
- Fibre misalignment in the laminate
- Type of fibre reinforced
- Waisted or unwaisted specimen
- Surface treatment and loading
- Fibre coupling agents
- Type of testing fixture
- Moisture present
- Fibre volume fraction
- Voids content of the matrix
- Resin ductility and toughness
- Non-isotropic properties of the fibre
- Gauge length.

Many standard test methods have become established, each of which has its own particular advantages and disadvantages, and these can yield different results for the same material. Several theories and proposals have been suggested for calculating the compressive strength of a composite material.

## 2.2 THE BEHAVIOUR OF UNIDIRECTIONAL FIBRE COMPOSITES UNDER COMPRESSIVE LOADING

In 1965 Rosen [1], believed that failure occurred due to fibre microbuckling elastically supported by the matrix. Evidence of microbuckling has been supplied by Rosen for glass fibre embedded in epoxy resins. He suggested that the deformation was due to differences in thermal expansion between the glass and resin setting up stresses on cooling, and not the direct compression load.

He noted two cases; out-of-phase buckling, the extension mode, and in-phase buckling, the shear mode, Fig. 2.1. He derived a formula for the compressive strength ( $\sigma_c$ ) of unidirectional fibre reinforced composite material, for each mode, assuming a model reinforced by equidistant plate like reinforcement. He proposed results for the extension mode be given by:

$$\sigma_c = 2 V_f \left[ \frac{V_f E_f E_m}{3(1 - V_f)} \right] \quad 2.1$$

and the results for the shear mode be given by:

$$\hat{\sigma}_c = \frac{G_m}{(1 - V_f)} \quad 2.2$$

In Fig. 2.2 the compressive strength of the composites is plotted as a function of the fibre volume fraction. It is seen that for the low fibre volume fractions the extension mode requires the lower stress, while for the high volume fractions of fibres the shear mode predominates.

However, experiments do not show good agreement with the above formulas. The equations (2.1 and 2.2) have unreasonable features such that  $(\hat{\sigma}_c)$  becomes infinite for  $V_f = 1$ , and compressive strains of greater than 5% are predicted, which would be beyond the elastic limit of the resin matrix. Rosen considered the effect of modifying the analysis to take into account these inelastic matrix deformations. He replaced the matrix modulus in equations 2.1 and 2.2 by a function which varies linearly from its elastic value at 1% strain down to a zero value at 5%. This is represented by the dotted line in Fig. 2.2. Predicted strengths however were still higher than those values obtained in experiments. Rosen then expressed his results further by showing compressive failure strain plotted as a function of fibre volume fraction for two different ratios of fibre Youngs modulus to matrix shear modulus (Fig. 2.3). These curves again showed that the shear mode of failure predominates. Also indicated was the fact that the results are very dependent on ratio of fibre to binder moduli, the critical strain being reduced as the matrix stiffness is reduced.

Schuerch [2] has studied the compressive strength in the fibre direction  $\sigma_c$  and derived the following equation, for shear mode buckling:

$$\sigma_c = \frac{G_m(\epsilon)}{(1-V_f)} \quad 2.3$$

This was the same as Rosen's equation 2.2 but the meaning of  $G_m$  is extended to the plastic range.

In 1966 Foye [3], suggested that compressive failure in a composite material could be linked with shear instability, and hence overall failure occurred if the compressive strength equalled the shear modulus of the composite. He derived the following equation in the elastic range:

$$\sigma_c = G_m \quad 2.4$$

based on textile analysis but he did not extend the property  $G$  to the plastic range.

Hayashi [4,5,6] had found shear instability phenomenon in three dimensional bulk materials and structures under compression, and proposed that the instability of the unidirectional fibre reinforced composite material will occur when:

$$\sigma_c = G_m (\sigma_c) \quad 2.5$$

where  $\sigma_c$  is the mean compressive stress in the Unidirectional Fibre Reinforced Composite Material (UDFCRM). For the shear mode equation 2.5 was found to be more reasonable than equation 2.2 by Rosen.

In 1970 Hayashi [7] extended his work by pointing out, that as far as the critical condition of the composite material is concerned, when  $(\sigma_m)$  reaches the shear instability limit

$$\sigma_m^* = G_m (\sigma_m^*) \quad 2.6$$

and some shear deformation would take place in the matrix and the matrix might lose the supporting action for the fibre.

In this state the matrix carries the load ( $\sigma_m^* (1-V_f)$ ), and the fibres carry the load ( $\sigma_f^* V_f$ ), where  $\sigma_f^*$  is the fibre stress corresponding to the same strain ( $\epsilon^*$ ) of the matrix at stress  $\sigma_m^*$  Fig. 2.4.

Therefore the compressive strength of the composite is given by:

$$\hat{\sigma}_c = \sigma_f^* V_f + \sigma_{my} (1-V_f) \quad 2.7$$

$\sigma_m^*$  will usually be greater than the matrix yield stress ( $\sigma_{my}$ ). Hence, for the safe side calculation, ( $\sigma_{my}$ ) had been used instead of ( $\sigma_m^*$ ) in equation 2.7. Hayashi plotted his rule of mixture (ROM) of expected compressive stress vs volume fraction of fibres in the composites. Comparison made with equations 2.1 and 2.2 obtained by Rosen show that equation 2.7 gave lower values over the whole region of  $V_f$  as shown in Fig. 2.5.

Previously Lager and June [8] in 1968, suggested that the shear mode buckling obtained by Rosen should be modified, because Rosen's model did not simulate well the real UDFRM. They published test results for UDFRM made of boron and epoxy resin. They used two kinds of epoxy resin A (hard) and B (soft). They found a good agreement with experiments and calculations from equations 2.1 and 2.2, when they multiplied by a reduction factor  $K = 0.63$ .

Hayashi [7] wanted to support and justify the ROM, so he plotted the results obtained from equation 2.7 using Lager and June epoxy resins properties. From Fig. 2.6 he proved that equation 2.7 gave more

reasonable values of  $\sigma_c$ , compared to Lager and June's test results than equations 2.1 and 2.2 by Rosen.

In 1971 Orringer [9] modified Rosen's theory by using tangent moduli, and by using it together with the overall composite modulus (from the rule of mixtures) to obtain the minimum strain at which buckling occurred. Finally he suggested that transverse stress concentration in the matrix influenced failure.

In 1972 Argon [10] suggested that Rosen's model acted as an upper bound prediction applicable only to composites with parallel reinforcing elements perfectly aligned with the loading axis. In practice, imperfection in the fibre alignment always exists and such regions, he suggested, form a failure nucleus by undergoing a kinking process. Although this resembles the in-phase buckling of the Rosen's model, it operates at a stress level well below the ideal buckling strength. He considered a region of initial misalignment angle ( $\gamma$ ) where the applied compressive stress produces an interlaminar shear stress ( $\tau$ ). He suggested that when this shear stress becomes equal in magnitude to the interlaminar shear strength of the material, then the lamellae in the region will slide and rotate. Argon suggested this movement increases the resolved shear stress, thus producing an instability and a shear collapse band which propagates outwards by means of the stress concentrations at the tips of the band, and thus the compressive strength should be given by:

$$\sigma_c = \frac{\tau}{\gamma} \quad 2.8$$

This decreases with increasing fibre volume loading and so presumably should ( $\gamma$ ), but it is not possible to say exactly how  $\sigma_c$  will vary with fibre content, making verification of equation 2.8 difficult.

Harris [11], showed that when a unidirectional composite is loaded in compression parallel with the fibre, the mode of failure is dependent on the strength of the fibre/matrix bond. If the bond is weak the fibres debond from the matrix at low load and the compressive strength never reaches the composite tensile strength. In addition, with brittle matrices axial cracking can occur near the loading point (which can split the composite parallel with the fibres) unless lateral spread is restrained. It is therefore important to ensure that the fibres are well aligned to avoid premature buckling fracture.

In 1973 Ewins and Ham [12] worked to find the nature of compressive failure in unidirectional composites material. They carried out longitudinal and transverse compressive tests on carbon/epoxy composites for various volume fractions. In each case a linear relationship of strength vs volume fraction was obtained. Close values of compressive strength were obtained through all results. The mode of failure for both tests (longitudinal and transverse) was shear failure of the fibre and matrix.

Ewins and Ham then performed two further series of tests in which the longitudinal and transverse compressive strength were measured at constant volume fraction but at different temperatures. These showed that below 100°C both types of test gave similar strength and the strength fell gradually with temperature.

The failure mode for both tests was shear failure through fibres and matrix. Above 100°C and for the longitudinal compressive strength, there was a sudden change in the strength and the failure mode changed to one associated with fibre microbuckling.

As temperature increased the modulus of the matrix decreased which could lead to this transition, but no quantitative agreement with existing theories based on this mode could be demonstrated.

In 1974 Greszuzuck [13] suggested that buckling was not the only failure mechanism but that a certain amount of brittle failure in the fibres also occurred.

In 1975 Hancox [14] showed that for a simple compression test on type I and type II carbon fibre/epoxy resin composites using a plane bar specimen with aluminium end tabs loaded in a compression jig, for treated fibres the failure mode was shear over a plane at 45° to the fibre axis. With untreated fibres failure was due to transverse delamination. Hancox also observed that the compression strength was reduced significantly by the presence of voids and when increasing the gauge length. He found that the variation of compressive strength, of treated material, vs fibre volume fraction was linear. The results are similar to that reported by Ewins and Ham [12] and Lager and June [8]. In magnitude the results obtained were unlike those predicted by analysis of Rosen [1] and Foye [2]. The shear modulus of the epoxy resin used was 1.4 GN m<sup>-2</sup>. When this was substituted in equation 2.2 it gave compressive strengths about three times larger than the maximum observed.

Hancox contrasted his results with Hayashi [7]. Hancox's resin yielded at 4.3% strain, which is well above the tensile and compressive failure strains for both types of carbon fibres. By Hayashi's theory one would have expected type I CFRP compressive strength to be greater than that of type II in contradiction of Hancox's results. His work supports the theory that compressive strength of unidirectional carbon fibre composite at room temperature is not governed by fibre buckling but is related to the ultimate strength of the fibre.

In 1977, Chaplin [15] attempted to understand the compressive behaviour of glass reinforced systems. He tested two kinds of glass/epoxy samples, (notched and unnotched) to demonstrate the mode of failure. The specimens were reinforced with 60% by volume of E-glass with epoxy resin (Epikote 828) cured for 2 hours at 100°C, followed by 10 hours at 125°C. He found that in unnotched specimens a band of sheared material in which extensive debonding had taken place existed, although damage was entirely restricted to this band.

The notched specimens revealed that the failed band, though at an angle to the applied load, propagated in a direction normal to the axis of loading, Fig. 2.7. Chaplin discussed the theory that the shear deformation in a band increases but without change in the orientation of the band itself. As this deformation increases there is considerable bending in the fibres at the boundaries of the bend, which results in fracture along the boundary, and further increases deformation with the adhesion between fibres and matrix breaking down. Therefore he showed that in practice it is impossible to manufacture a material totally free of defects, and under an axial compression load

the shear mode of failure starts from that region and propagates across the material with no buckling as predicted by Rosen.

In 1980, Piggott and Harris [16] investigated a number of factors which they considered could affect the calculated compressive strength of the composite. These were:

1. The character of the test specimen.
2. The compression test method used.
3. The volume fraction of fibre.
4. The effect of matrix properties.
5. The composite strength and modulus.

They carried out compressive tests on a series of polyester resins of various compositions and in different states of cure. Their mechanical characteristics having been established, the same range of resins was then used as a matrix material for a series of composites reinforced with carbon, glass and Kevlar fibres. The composites were unidirectionally reinforced. They found that the "Rule of Mixtures" behaviour occurred in glass-polyester composites up to limiting volume fractions of 31% for strength and 46% for elastic modulus. The compression modulus was found to be equal to the tensile modulus, and the apparent fibre strength in the range 1.3 to 1.6 GPa at this limiting  $V_f$ . At a  $V_f$  of 31% the strengths of reinforced polyesters were proportional to the matrix yield strength ( $\sigma_{my}$ ) and their moduli were an inverse exponential function of  $\sigma_{my}$ . For the same matrix yield strength, a similar glass fibre composite with an epoxy resin matrix was stronger than polyester based composites. At a  $V_f = 30\%$  Kevlar fibre composites behaved as though their compression modulus and strength were much smaller than their tensile modulus and

strength, while carbon fibre composites were only slightly less stiff and weaker in compression than in tension.

Failure characteristics were however different. CFRP specimens separated into two halves after removal from the grips of the test-fixture, while the GRP specimens did not. CFRP composites failed in a brittle manner with a single transverse crack which was perpendicular to the fibre axis with no splitting occurring, while GRP specimens exhibited multiple kink-bands.

Piggott and Harris found that their work did not support any of the existing theories. Certainly the linear relationship between strength and volume fraction could not be compatible with Rosen's model, and since many other results showed this same linear relationship, they suggested that it may be timely to abandon the Rosen model. The Hayashi theory although it predicts this linear relationship, also seemed inapplicable since failure should occur at the matrix yield stress. According to Piggott and Harris the failure of composites occurred while the matrix was still elastic.

In 1981 Martinez et al [17] continued experiments of previous efforts pursued by Piggott and Harris [16] in regard to the compressive strength for GRP, CFRP, and Kevlar composites. They highlighted the effects of fibre volume fraction, misalignment of fibres, and adhesion between fibres and matrix with respect to the compressive strength.

Below a  $V_f$  of 30%, the compressive strength of aligned fibre composites vs volume fraction was linear. The strength falls off when the  $V_f$  was equal to 40% with Kevlar and high strength carbon fibres. At  $V_f$  less than 40% with Kevlar fibres, the effective fibre strength

is much less than its ultimate strength but it is close to the tensile strength with E-glass fibres and high modulus carbon fibres.

The elastic moduli of these composites vary in a similar fashion with  $V_f$  up to 50% (which presumably reflects a change in mode of deformation), with the expected reasonable agreement with the rule of mixture. Only Kevlar composites do not extrapolate to a reasonable value at  $V_f = 1$ .

Misalignment of the fibres also reduces the compressive strength when the average angle of misalignment exceeds about  $10^\circ$  for GRP and CFRP. However, with Kevlar no such reduction is observed because the compressive strength of Kevlar reinforced resin is only a very little better than that of the unreinforced resin. Kinking of fibres reduced composite strength considerably if the minimum radius of curvature of the fibre axis was below 5 mm. Kinking defects in composites could therefore be quite critical while misalignments may not be if they are kept to within  $10^\circ$  of the fibre axes.

The last effect was the adhesion between fibres and matrix. They showed that with poor adhesion, the compressive strength was reduced. Martinez et al commented on the similarity between these strength results and those of Hancox [14], with poor bonding apparently causing strength to fall increasingly further from the ROM expression applied to compressive strength:

$$\hat{\sigma}_c = V_f f + V_m \sigma_{m1} \quad 2.9$$

where  $\sigma_{m1}$  is the matrix stress at the failure strain of the composite assuming the matrix is still elastic at the instant of composite failure.

Hull [18] points out Rosen's theories of microbuckling are likely to be correct for some composite systems, although they require modification to take into account the material effects that reduce the theoretical strength. These include resin rich regions (caused by fibre bunching), voids, fibre misalignment, and poor fibre matrix bonding, all of which reduce the fibre support and allow buckling of the fibres to occur more easily.

In 1982 Parry and Wronski [19] published several papers concerning the compressive behaviour of composites. Experiments were carried out on type III carbon fibre with epoxy resin. They managed to analyse the failure mechanism by encapsulating specimens in resin, thus causing failure to be arrested during its propagation through the test piece. They concluded that the fibres involved in microbuckling at the edge of a kink-band failed by a tensile failure mechanism and that this occurs before permanent deformation within the kink band, which supports the previous work of Chaplin [15]. They suggested that the strengths of CFRP materials are not related to the moduli of the resin but rather to their strength, ductility and even toughness.

Wronski and Parry [20] also studied the failure of high volume fraction GRP using atmospheric and superposed hydrostatic pressure. All experiments were performed on 6 mm diameter pultruded rod containing 60% of S-glass fibres in an epoxy resin matrix. The specimens were fabricated to the same design as reported previously for CFRP [19].

In atmospheric pressure the compressive strength of GRP/epoxy was found somewhat lower than the tensile strength. Compressive strength was found to increase linearly with pressure. Failures were

catastrophic and separation occurred at an angle of approximately  $30^\circ$  to the fibre axis. The mode of failure could be identified as kinking, involving buckling of fibre bundles as the mechanism of failure propagation, but the critical stage was suggested as being yielding of the matrix, which initially restrains surface bundles from buckling. Other systems, particularly CFRP, in which there appears to be a transition in the critical stage of failure from bundle buckling to matrix yielding with increasing superposed pressure, were also considered.

Lee et al [21] studied the effect of matrix toughening on the tensile strength and strain properties of SMC. They reviewed briefly matrix cracking problems of fibre-reinforced resin composites in general, and examined how rubber-toughening of unsaturated polyester resin matrix affects critical stress and strain properties of SMC-R25. The addition of rubber to the matrix was found to decrease slightly the initial tangent modulus of elasticity, but increase the (knee) stress and strain, the secant modulus above the knee, and the ultimate tensile strength and strain of SMC-R25, Fig. 2.8.

In 1984 Piggott [22] and in his latest piece of work, presented experimental data to investigate three theories of failure:

1. Fibre failure.
2. Matrix yielding.
3. Interface failure and matrix tensile failure.

In the fibre failure mode (1), composite strength obeys the ROM relationship:

$$\hat{\sigma}_c = V_f \hat{\sigma}_f + V_m E_m / E_f \hat{\sigma}_f \quad 2.10$$

where  $\hat{\sigma}_f$  is the compressive stress in the fibres when they fail in the composite and may not necessarily be the ultimate compressive strength of the fibres. This type of failure has been observed in Kevlar composites since these fibres have a very low yield stress in compression. For GRP this type of failure would give the composite strength up to 2.4 GPa, so it is almost certainly not the governing failure mode. This theory was supported by experimental observation of Chaplin [15], and Piggott and Harris [16].

The matrix yielding mode of failure (2) occurs due to the fact that fibres cannot be perfectly straight. Piggott assumed that the fibre axis is in a sinusoidally buckled shape and that to start with there is perfect adhesion with the matrix. On the outer edge of the fibre displacement, a pressure is created between the fibre and matrix. When this pressure reaches the matrix yield stress, an unstable state is reached since further deflection would result in further increasing pressure. Piggott used these assumptions to derive the following equations which predict composite strength and modulus governed by this failure mode:

$$\hat{\sigma}_C = (2 \lambda^2 \sigma_{my} / a \pi^3) (V_f + V_m E_m / E_f) \quad 2.11$$

$$E_1 = V_f / (1/E_f + 1/E_{f1}) + V_m E_m \quad 2.12$$

where  $\lambda d$  = wavelength of sinusoidal buckling

$a d$  = amplitude of sinusoidal buckling

if  $d$  = diameter of fibre

$E_f$  = fibre modulus due to elastic shortening

$E_{f1}$  = fibre modulus resulting from increase in  $(a)$  and decrease in  $(\lambda)$  due to the matrix pressure.

He found that experimental data in [14,15] fitted the equations well for GRP up to  $\sigma_{my}$ , approximately 60 MPa. However, this failure relationship breaks down at a low value with Kevlar fibres composites because fibre yielding mode takes over.

The interface failure and matrix tensile failure mode (3) occurs when the interface is weak, causing separation of the fibre from the matrix followed by matrix splitting. As in (2) above, there is a sinusoidal shape except that this time the pressure under consideration is the negative one on the inside of the fibre curve as Figure 2.9. Taking into account the relative areas over which these stresses act, he obtained an equation for the equilibrium of forces, from which he derived the composite strength equation for this type of failure.

$$\hat{\sigma}_c = \left(\frac{4R}{\pi d}\right) (\pi \hat{\sigma}_a + \{\sqrt{(P_f/V_f)} - 2\} \hat{\sigma}_{mt})(V_f + V_m E_m/E_f) \quad 2.13$$

where  $R$  = radius of curvature of fibre

$\hat{\sigma}_a$  = adhesion strength

$P_f$  = factor representing fibre packing arrangement

=  $2\pi\sqrt{3}$  for hexagonal packing

$\hat{\sigma}_{mt}$  = matrix tensile strength.

Piggott in his later work [22] presented experimental data which fitted the equations well. At low  $V_f$  equation 2.11 gives the lower stress and would therefore define the failure process while at higher  $V_f$  equation 2.13 would take over.

In 1985 Hahn [23] published a paper to delineate compressive failure mechanisms in unidirectional composites, and to identify material parameters that control compressive strength. He used specimens consisting of a fibre bundle embedded in epoxy, to monitor the sequence of failure within the bundle, because the bundle is well contained and can be monitored during testing.

Four different fibres (E-glass fibre, T700, T300, and P75 graphite fibres) were combined with two different epoxy resins. Epon 815/V140 was chosen to represent a soft resin, and Epon 828/Z, a stiff resin. The (IITRI) compressive fixture was used with a specimen of 13 mm gauge length and of 6.5 mm width, while the thickness varied from 4 to 6.5 mm.

After bundle failure, the specimens were examined and the modes of failure were noted. High modulus P75 fibres failed in shear. Buckling induced failure was most evident for the E-glass fibre, while kinking type of failure was also common for the T300 and T700 graphite fibres. It was found that no distinction could be detected between stiff and soft resin.

The measured compressive strains at failure are shown in Figure 2.10. The E-glass fibre was seen to have the highest failure strain, while the P75 had the lowest. As expected from the buckling theory, the stiffer epoxy yields higher failure strains. However, the difference in failure strain due to the matrix for T300 and T700 graphite fibres was much less than for the E-glass, and disappeared for the P75. Since the failure of P75 fibres was in shear without buckling, resin stiffness had no effect.

Fibres having a higher tensile failure strain were seen to buckle at higher strain.

Buckling of a single fibre embedded in epoxy resin has been analysed by Rosen [1]. The analysis indicates that the buckling strain for the extension mode, out of phase buckling is:

$$\epsilon_b \propto \left(\frac{E_m}{E_f}\right)^{1/2} \quad 2.14$$

where  $\epsilon_b$  = buckling strain

$E_m$  = matrix modulus

$E_f$  = fibre modulus

Hahn's results for compressive failure strain were seen to be fairly proportional to the square root of the matrix to fibre modulus ratio, Fig. 2.11, although a bundle of fibres rather than a single fibre was used.

Finally Hahn concluded that the yield stress and the tensile fracture stress of the matrix and the interface play a role in determining compressive failure under appropriate conditions.

In 1986 Hahn and Williams [24] examined the effect of resin tensile modulus on the compression failure mechanisms in unidirectional composites. They used two different graphite fibres (T300 and T700) combined with four different epoxy resins. Compression tests were performed on an Instron machine at a speed of 1 mm/min. All the compression specimens failed without warning. The predominant failure

mode was identified as shear crippling. When the matrix was stiff, shear crippling was the result of fibre kinking. However, for soft resins microbuckling failure was a result of high bending strains in the fibre in the post-buckled state.

The effect of resin tensile modulus on the composite strength and axial modulus were noted. According to the rule of mixtures the composite modulus was given by:

$$E_c = V_f E_f + V_m E_m \quad 2.15$$

For a laminate with a 60% fibre volume fraction, a change of resin modulus from 3 to 5.5 GPa will result in an increase in composite modulus of 1 GPa. This increase is insignificant in comparison to the original composite modulus magnitude, which is of the order of 100 GPa.

Hahn and Williams' results indicate an increase in composite modulus with resin tensile modulus much higher than predicted by equation 2.15, see Fig. 2.12. The compressive strength also increased with resin tensile modulus.

Using other researchers' results they observed that the compressive modulus of a composite was more dependent on the resin modulus than was the tensile modulus. The other feature was that the composite tensile modulus was greater than the composite compressive modulus, for resin modulus values less than approximately 5 GPa. The compressive strength is seen to increase with increasing resin modulus. Again when compared with previous published results, they confirmed a strong correlation between compressive strength and resins

modulus, but a weak correlation between tensile strength and resin modulus.

This theory can be represented by the formula for a non-linear model:

$$\sigma_c = V_f G_{LT} \frac{\gamma_{LT}}{\gamma_{LT} + \pi f_o / l} \quad 2.16$$

where  $G_{LT}$  = composite shear modulus

$\gamma_{LT}$  = average shear strain

$f_o / l$  = calculated parameter =  $0.295 \gamma_{LT}$  (thus if  $\gamma_{LT} = 1\%$ ,  
 $f_o / l = 0.295\%$ )

Furthermore, if no initial defect was assumed, that is  $f_o / l = 0$ , equation 2.16 yields:

$$\sigma_c = V_f G_{LT} \quad 2.17$$

The calculated compression strength predicted by equation 2.16 was compared with experimental results. Equation 2.16 was seen to overestimate the composite compressive strength when the matrix resin tensile modulus was less than 3 GPa, but in general was in reasonable agreement with observed experimental data, even when non-linear material properties and initial curvature of fibres were not included.

In 1987 Heumann [25] carried out a study of elastic properties and failure mechanisms in unidirectional glass/carbon hybrid composites. Included in this work was a discussion of test results from GRP and CFRP monofibre composites with vinyl ester and epoxy matrices in both tension and compression.

In tension, the type of failures which occurred in the GRP composites indicated that the fibre-resin bond was weaker than in the CFRP composites. In addition the vinyl ester composites demonstrated weaker bonding than the epoxies in both the CFRP and GRP laminates. The results however, showed that this weaker bonding in the vinyl esters did not adversely affect the tensile strength. The weaker bonding in the GRP specimens resulted in bond failure at relatively low loads, which affected the mechanism by which failure propagated through the specimen.

'K factors' were calculated as a simple ratio of the composite strength over expected rule-of-mixtures predictions using fibre strength data. It was suggested that these represented some indication of the fibres surface damage, from which it was concluded that the glass fibres in the composite suffered more from damage than the carbon.

In the compressive tests, different failure mechanisms occurred depending upon the type of fibres and matrix in the composite. The four main mechanisms of compressive failure were:

- a) longitudinal splitting
- b) kink-bands
- c) fibre and matrix shear failure
- d) microbuckling.

Longitudinal splitting and kink-band failures were observed in the GRP specimens of both vinyl ester and epoxies. It was concluded that these failures were the result of transverse tensile failure of the matrix due to the Poisson stress distribution as the composite was subjected

to uniaxial compressive load. There appeared to be no significant difference in the strengths which resulted from kink-bands, those which exhibited splitting, but rather that the difference was the result of restrictions on the propagation of the failure (between end tabs), dependent upon the location of its initiation.

Fibre and matrix shear failure was observed in all the epoxy CFRP specimens while microbuckling occurred in the CFRP with the vinyl ester matrix. It was concluded that the difference in the method of manufacture of the specimens was a significant factor contributing to this change in failure mechanism. The flaws introduced during the wet lay-up laminating process apparently encouraged the early initiation of microbuckling which did not occur in the prepreg epoxies.

### 2.3 THE INFLUENCE OF TEST TECHNIQUE ON THE COMPRESSIVE STRENGTH OF UNIDIRECTIONAL COMPOSITES

Compression strength is one of the most difficult intrinsic composite material properties to measure. The results are often dependent on loading geometry and test conditions. Several papers have discussed test techniques for evaluating the compressive strength of unidirectional composites.

Woolstencroft et al [26] showed that each test fixture has its own particular advantages. However these test methods can yield different compressive strength results even on the same material. A series of tests has been undertaken using different test methods on composites of prepreg material. To ascertain the optimum test technique, tests were performed using the following specimens:

1. Celanese specimen.
2. RAE specimen.
3. Modified ASTM DG95 specimen.
4. Modified Celanese specimen.
5. BAe modulus specimen.

The optimum test method was the RAE method. The results showed that at failure there were negligible additional secondary stress systems in the specimen due to its configuration.

Chamis and Sinclair [27] conducted experiments and analysed the effects of end attachments on longitudinal compressive failure of (IITRI) type specimens.

Unidirectional fibre composites were assessed using finite-element-analysis (FEA), in conjunction with composite mechanics. Analyses were performed to evaluate end attachment effects (such as degree of misalignment, type of misalignment, progressive end-tab debonding, and specimen thickness).

Two types of eccentricities were assumed (lateral and cantilever type displacements) and two different gauge lengths were selected to illustrate and evaluate the effects of specimen misalignment on the stress distribution, on the buckling load, and on the buckling shape.

The results obtained from the (FEA) and comparisons with fractured specimens showed that eccentricities induce bending type stresses which peak near the end-tabs and cause flexural type failure. It was also concluded that back-to-back strain gauges should be placed to measure the presence/absence of possible end attachment and eccentricity effects.

Lee [28] has investigated the selection of suitable test methods for measuring compressive strength and has looked in detail at a wide range of unidirectional carbon fibre reinforced thermoplastics fabricated by film stacking or by melt impregnation.

In order to achieve an accurate strength measurement, he used special loading fixtures and specimens to overcome three basic problems:

- a) Specimen buckling; by ensuring that column length is less than the critical Euler buckling length.
- b) 'Brooming' of ends of solid column specimens; by using compression rated wedge action grips and load diffusion tabs, bonded over a large area of the specimen.
- c) Axial misalignment; which required well controlled bondline thickness for the end tabs, to ensure that the platens are parallel.

Two test fixtures were used:

- 1. Celanese jig.
- 2. End loaded compression fixture.

Lee made a comparison between his work and with aerospace epoxide systems. The results indicated that the polyetheretherketone based laminates, despite having a lower shear modulus, have similar compression strength to the epoxide systems. On the other hand the end loaded compression fixture gave lower values of compressive strength than the 6 mm. celanese jig.

Finally the experimental results suggested that failure was not by macrobuckling.

Barker and Balasundaram [29] developed a compression test jig which they used in the measurement of the compressive strength of both unidirectional and multidirectional CFRP. The jig has the merit that small specimens may be tested without the necessity of end tabbing which is especially useful for specimens exposed to an environment of high humidity. Therefore, the test specimen must be relatively small in order to ensure that water absorption can be predicted with reasonable accuracy. The results of tests on the compressive strength of waisted unidirectional specimens support the usefulness of the test technique in comparison with alternative methods.

## 2.4 SUMMARY

In short, the Discussion can be summed up in the following way.

Rosen's buckling model [1] was the first attempt to explain the compressive failure behaviour of unidirectionally reinforced fibre composites. There have been many attempts to modify Rosen's model [2,8,9] but they have not solved the basic problem, because Rosen's model predicts strengths far in excess of those achieved in practice. Other workers showed in practice imperfection in the fibre alignment always existed initiating failure at earlier stages. They showed that when the fibre was carefully made, the composite was much stronger than when no such care was taken. Thus the fibre straightness is an important factor in avoiding microbuckling. There are several amounts of experimental evidence to support this [10,15,19,20]. However, Rosen's theory does not predict the correct variation of compressive strength with volume fraction, as has been observed [6,7,14].

Other theories showed that the matrix yield stress is an important factor controlling compression properties, both strength and modulus are much reduced, when the matrix is soft [16,22,23,24]. The other important factor is the adhesion between fibres and matrix, when this is poor the composite is weaker in compression [14,25].

This type of buckling failure is not the only type of failure mechanism, other workers have observed a shear type of failure along a plane inclined at  $45^\circ$  to the fibre axis [12,13,14,25]. Therefore, depending upon the characteristics of the constituent materials and the condition of testing, a transition can occur from one type of failure to another [26,27,28,29]. This idea of several different failure mechanisms has been reinforced by other researchers and experimental results have backed up the theory [22].

# **CHAPTER 3**

## CHAPTER 3

### EXPERIMENTAL WORK

#### 3.1 INTRODUCTION

The aim of the experimental work was to provide data which would clarify the influence of the modified matrix-resin on the compressive properties of reinforced unidirectional composites.

The programme was to produce a series of GRP and CFRP laminates by wet-lay-up techniques using modified epoxy resin.

Eight main matrix systems for each of GRP and CFRP were studied and a series of tests (tensile, compression, interlaminar shear and microscopic) were carried out for each of the systems, so that the effect of the resin-matrix could be properly investigated. Every effort was made to keep the variable characteristics of these systems constant. Therefore it was necessary to make two slabs of each laminate configuration, so that the effect of any variability was reduced.

Also eight slabs of the matrix-resin systems were produced. A tensile test was carried out and the densities of the matrices were calculated.

The series of matrix-system properties which were used are shown in Table 3.1.

Resin (% Modifier)	Desmocap 11 (gm)	Epikote 828 (gm)	Ancamine MCA (gm)	Heloxyl WC-68 (gm)
0	-	100	55	10
5	7.75	100	55	10
10	15.50	100	55	10
20	31.00	100	55	10
30	46.50	100	55	10
40	62.00	100	55	10
50	77.50	100	55	10
60	93.00	100	55	10

TABLE 3.1: THE PROPORTION OF CONSTITUENTS FOR EACH MATRIX SYSTEM

## 3.2 MATERIALS

### 3.2.1 Glass Fibre

The glass fibre used in this work was fibre glass Equerove 23/14. It was purchased on 10 kg cheeses and wound onto the laminate frames as required. Equerove is an untwisted, reinforced roving which had been designed to give fast wet-out and good release properties. The properties of glass fibre are shown below:

Material	E-glass fibre
Roving	Equerove 23/14
Tensile strength	2.4 GPa
Tensile modulus	71 GPa
Elongation	3.37%
Density	2.55 g/cm <sup>3</sup>
Coefficient of thermal expansion	$5 \times 10^{-6} \text{ K}^{-1}$
Mass/unit length	600 mg/m
Linking agent	Silane
Filament diameter	13 $\mu\text{m}$

### 3.2.2 Carbon Fibre

The carbon fibre used was Grafil E/XA-S 10K, a high performance twist free tow. The fibres are surface treated for good fibre/matrix bond properties and have an epoxy resin size to assist handling. The properties are shown below:

---

Material	PAN based carbon fibre
Roving	Grafil E/XAS 10K
Tensile strength	3.43 GPa
Tensile modulus	237 GPa
Elongation	1.44%
Density	1.81 g/cm <sup>3</sup>
Coefficient of thermal expansion	-1.0 x 10 <sup>-6</sup> K <sup>-1</sup>
Mass/unit length	730 mg/m
Size contents	0.7 % mass
Filament diameter	7.2 µm

---

### 3.2.3 Epoxy Resin

Epikote 828 epoxy resin was used in this work. Epikote 828 is an unmodified liquid bisphenol A - epichlorohydrin epoxide resin of medium viscosity, combining reasonable ease of handling with high chemical resistance and mechanical performance after cure. Cured either at room temperature or elevated temperature. Typical properties are shown below:

---

Epoxy group content	5150-5490 mmol/kg
Viscosity at 25°C	9-14 Pa.s
Density at 25°C	1.16 kg/l
Flash point	>150 °C
Specific heat	1.9 kJ/kg°C

---

### 3.2.4 Curing Agent

Ancamine MCA is a modified aliphatic amine of high reactivity used as a curing agent for epoxy resins, and contains Phenol, Isophorone-diamine and Benzyl Alcohol. It will aid curing under a variety of conditions including high humidity, low temperature and underwater. Special features of this curing agent include good gloss and smooth finishing in cured films, excellent chemical resistance and low viscosity, low water miscibility and a reduced tendency to form carbamates with carbon dioxide in the atmosphere during cure. Recommended usage was 55 parts of MCA per 100 parts of liquid epoxy resins. Ancamine MCA had a gel time of 23 minutes and curing time of 2-7 days at ambient temperature. Its typical properties are shown below:

---

Viscosity at 25°C	0.2 Pa.s
Specific gravity at 25°C	1.03
Flash point	110°C
Gel time	23 min
Curing (at ambient temperature)	2-7 days

---

### 3.2.5 Modifier

Desmocap 11 is used for elasticising epoxy resins, containing crosslinking, blocked isocyanate groups. The reaction of Desmocap 11 with amines makes it possible to combine some of the good properties of the polyurethane resins with those of the amine-cured epoxy resin. This is especially true for the flexibility. The additions of Desmocap 11 to epoxy resin results in a continuous increase in flexibility which is retained in the products even at low temperature. Its data characteristics are shown below:

---

Density at 20°C	1.05 g/cm <sup>3</sup>
Viscosity at 25°C	80 ± 15 cPa.s
Flash point	>200°C

---

### 3.2.6 Solvent

Heloxy WC-68 was used in this work as an efficient diluent for viscosity reduction of epoxy resins with minimum loss of properties. Heloxy WC-68 is a technical grade of the Diglycidyl Ether of Neopentyl Glycol. It will completely react with the curing agent. This means that the physical properties of a system containing Heloxy WC-68 are similar to a non-modified system. Blends of Heloxy WC-68 with liquid bisphenol A-epichlorohydrin type resin (Epikote 828) can be cured with amines (Ancamine MCA) and other curing agents used in epoxy systems. The low volatility of Heloxy WC-68 makes elevated temperature curing feasible. Its physical properties are:

---

Viscosity at 25°C	(14-18) cPa.s
Specific gravity at 25°C	1.05-1.08
Flash point (open cup) °C	127

---

## 3.3 EQUIPMENT

### 3.3.1 Laminate Manufacturing Equipment

A filament winder was used to wind fibres onto steel frames for making the laminates. In order to get good alignment a low transverse speed was used; see Plate 1.

A leaky mould was used for making epoxy resin composite laminates. These moulds gave laminate dimensions of approximately (200 mm x 155 mm), and with a thickness of 2-2.5 mm since 2 or 2.25 mm spacers were used on the edges of moulds. The clamping force was provided by means of four G clamps (see Plate 2).

A diamond studded cut-off wheel was used to cut the laminates into the required specimens. Finally a finisher machine was used for smoothing the specimen edges.

### 3.3.2 Mechanical Testing Equipment

Compression testing was carried out on a "Mand servo-screw" test machine shown in Plate 3, using a Celanese compression test jig (Plate 4). It was designed to support a specimen as it is loaded in uniaxial compression and to prevent it from buckling. Compressive loads were applied by means of flat platens which pressed directly onto the tapered sleeves of the compression test jig. The maximum load capacity of this machine was 100 kN. For strain measurement, strain gauges were used for measuring extension through the test, due to the small size of the specimen's gauge length.

The bridge circuit used for processing the strain gauge signals was situated in a strain gauge connector box (SGCB), (see Fig. 3.13) and results were recorded in the form of load-strain curves on a chart plotter.

Tensile testing was carried out on a "Dartec Servohydraulic" testing machine, shown in Plate 5, at a constant rate of extension. An extensometer was used for strain measurement instead of strain gauges due to the large size of the specimen's gauge length. This was fitted

onto the specimen by means of knife edge jaws. The results were recorded directly on a chart plotter in the form of load-strain curves. The maximum load capacity of the machine was 100 kN.

Interlaminar shear testing was carried out on an "Instron" testing machine. The maximum load capacity of the machine was 500 kg. The maximum force was read directly from the test machine's built in load/time plotter as shown in Plate 6. A crosshead speed of 5 mm/min was used.

Resin tensile testing was carried out on a "J.J. Lloyd" testing machine, as shown in Plate 7. The maximum load capacity of the machine was 5000 Newtons. A crosshead speed of 5 mm/min was used. The J.J. pulsed infra-red non-contacting extensometer was used to read accurate measurements of extension. This was fed to the X input of the X-Y plotter, giving a graph of load against extension.

### 3.4 TECHNIQUES

#### 3.4.1 Manufacturing of Composite Laminates

A filament winding, wet-lay-up technique was used in which the fibres were wound from the "cheese" onto a steel frame. A total of eight passes (or sixteen layers) were used in each laminate. In this work 50 turns per pass were used for glass fibre and 25 turns per pass were used for carbon fibre. It was found that this was suitable for a laminate with a fibre volume fraction of between 45% and 50%. 100 gms of the resin were weighed and mixed with 55 gms of hardener, then different percentages of modifier were added each time and mixed as shown in Table 3.1.

The whole mixture was then placed under vacuum for a few minutes to allow the gas produced by the reaction to escape. The fibres were then wetted by the epoxy resin in the leaky mould, see Figure 3.14. The best way to impregnate the fibres was found to be to pour half the quantity of the resin on the upper side of the frame, and then speed up the wetting by using a laminating roller. The frame was then turned upside down and the remaining half of the resin poured onto the fibres. The laminating roller was again used to help wetting which had to be completed within the gel time of 23 minutes. The excess resin was then squeezed out by the use of a straight metal edge strip. Every effort was made to keep the amount of fibre damage at the surface layer down to a minimum. The leaky mould's lid was placed on the mould and suitable spacers inserted in the gaps on both sides of the mould to obtain the required thickness of laminate. Four G-clamps were applied to the corners of the mould to provide compression force so that the remaining excess resin and air were squeezed out of the ends, thus producing a low voids content. A curing period of 2-7 days was then allowed at room temperature. The laminate slab was then cut out of the steel frame using a diamond studded wheel. The slabs were kept in a desiccated cabinet until required for cutting and testing.

During the process of impregnating the glass fibres with epoxy resin, it was found that due to the high viscosity of resin, the inside layers were difficult to wet properly and evenly. To prevent this phenomena from happening with carbon fibre, 10 gms of solvent (Heloxyl WC-68) were added to the resin in order to reduce viscosity. Carbon fibres were then wetted as described above, however before the lid was closed, the leaky mould was put in a vacuum chamber for 15 minutes in order for the solvent and the voids to be released. Four G-clamps and spacers were applied as described earlier.

It was ensured that all the metallic objects, including the leaky mould, spacers and frames with which the resin came into contact, were previously coated with a release agent. The type of release agent used in this work was "FREKOTE 1711" Mould Release, which was sprayed on the metallic objects. Recoating was required for each moulding.

### 3.4.2 Volume Fraction Analysis Technique

#### a) Glass Fibre Composite Specimens

Two small samples were cut from the centre of each slab in order to analyse the fibre content. The density of these specimens was measured by using a density bottle and distilled water. Furthermore an accurate balance was used to weigh these samples from each laminate before placing them in a known weight crucible and burning them. The crucible was then placed in the furnace at 600°C for three hours. The resin was burned off leaving the fibres. After cooling for 24 hours in a dessicator, the remaining glass fibre was weighed. These results were used subsequently for the calculation of fibres and voids volume fraction as described in Chapter 4.

#### b) Carbon Fibre Composite Specimens

The acid digestion method was used to determine the volume fraction of carbon fibres by Haynes and Talbert's method [30]. One inch long samples were cut from the centre of each slab. The density of these samples was measured by using a density bottle and distilled water.

#### STAGE 1: Acid Digestion

Each sample was placed in a beaker after being weighed accurately. Twenty mls of concentrated sulphuric acid were added. The mixture was then placed on a hot plate heated to 70°C until the acid began to fume, and the composite began to visibly disintegrate. The beaker was

then removed from the hot plate. Hydrogen peroxide of 50% solution was carefully added dropwise down the side of the beaker (the addition was carried out slowly at first to avoid splattering of the mixture), until the acid solution became clear and colourless. The beaker was again placed on the hot plate, and 2 mls of hydrogen peroxide was added to the mixture. The mixture was heated to fumes for another 10 minutes in order to complete decomposition.

#### STAGE 2: Filtering and Washing

The beaker, after being removed from the hot plate, was subsequently placed in cold water to allow to cool. The fibres were then filtered in a known weight sintered glass crucible and washed with distilled water by vacuum filtration until the filtrate had a neutral pH value. An alcohol rinse then aided the removal of surface moisture.

#### STAGE 3: Drying

Finally the fibres were dried in an air oven at 120°C for three hours and cooled in a desiccator for at least twelve hours, then weighed.

The above stages of the acid digestion process are shown in Figure 3.15. These parameters were then used for the calculation of fibre volume fraction and voids volume fraction as shown in Chapter 4.

#### **3.4.3 Resin Density Analysis Technique**

In order to analyse the densities of the matrices used in this work, resin slabs were manufactured using the same resin mixtures used in the composites. After the required amount of resin was mixed in a beaker, the beaker was placed in an air oven at 90°-100°C for a few minutes in order to reduce the mixture's viscosity, and to speed up the reaction. The beaker was then removed from the oven and placed in

a vacuum dessicator to release the voids to the surface of the mixture.

The mixture was then poured into a leaky mould after the open ends had been sealed with plasticine, to provide a slab size (200 x 155 x 3 mm). The resin was left uncovered to cure for a period of 2-3 days. After curing, the upper surface of the slab was machined off to ensure the complete removal of the remaining voids on the surface during the last process.

Resin density was determined by measuring the water displaced by the specimen using a density bottle and distilled water. The technique was used to weigh small specimens cut from the resin slab. Care was taken to avoid specimens with air voids. The weight of the density bottle filled with distilled water was taken. The bottle was always dried on the outside. The specimen was then placed in the density bottle and the whole weight was taken. These results were then used for the calculation of resin density (Chapter 4, Section 4.3). Four specimens for each slab were analysed and the resin density was taken as the average of these.

#### 3.4.4 Test Specimen Preparation

##### a) Compression Test Specimens

Four compressive specimens were obtained from each laminate, each 10 mm wide and 142.5 mm long as shown in Fig. 3.16, according to ASTM standard: D3410-87 [31].

For each laminate the edge 1 cm was discarded in order to minimise edge effects in the laminate resulting from laying up. The cutting was carried out on a diamond studded wheel and care was taken to

ensure accurate alignment of the specimen. The edges were smoothed on a linisher first then polished down to 1200 grade silicon carbide paper. Aluminium alloy HS30 end tabs were cut of dimension (10 mm x 65 mm) from sheet and the edges were smoothed on a linisher and the surface roughened by hand with coarse grit paper. A 12.5 mm gauge length was marked on both sides of the specimen and the remaining areas of the specimen were roughened with coarse grit paper. The tabs were bonded using Araldite MY-750 epoxy resin with HY-951 hardener 100:10 in ratio. A load was applied to the tabs to provide compression force to get a good bonding. A curing period of 2-3 days was allowed at room temperature.

For measuring the extension through the test, strain gauges were used instead of an extensometer, due to the small size of the gauge length. One strain gauge for each side of the specimen was used to eliminate errors due to bonding. It was essential to have a good and uniform bond between the gauge and the specimen. A description of the strain gauge used is as follows:

---

TECHNI-MEASURE	
Type	Metal foil/FLA-3-11
Gauge length	3 mm
Gauge resistance	120 $\Omega$
Gauge factor	2.12

---

According to the recommendations of M-Line Measurements Group [34], the following procedure was used:

1. Degreased with Freon on a clean cloth.
2. Dry lapped with 240 grit silicon carbide paper.
3. M-Prep Conditioner-A applied and wet lapped, keeping surface wet. Wiped with cloth.
4. Items 2 and 3 repeated with 600 grit paper.
5. Re-wet with Conditioner-A. Scrubbed with cotton buds until one remained clean. Wiped dry with cloth.
6. M-Prep Neutralizer-5 applied. Scrubbed with cotton buds keeping surface wet. Directly wiped dry with clean cloth.
7. Strain gauge removed from acetate with tweezers and placed on a clean glass slide, bonding side down.
8. Two terminal strips cut and aligned alongside strain gauge.
9. Cellophane tape stuck over gauge in one wiping action, and removed by lifting at  $45^{\circ}$  to the surface.
10. Tape with gauge and terminal strips positioned on specimen and lifted off so that the gauge and terminal were free but the remainder of the tape stuck.
11. M-Bond 200 catalyst applied in a thin and uniform coat to the bond surface of the gauge and terminal. The catalyst was then allowed to dry for at least one minute in normal ambient conditions.
12. M-Bond 200 adhesive applied at the fold, formed by the junction of the tape and specimen surface, according to M-Line instructions for strain gauge installations [35].
13. The tape was rotated at  $30^{\circ}$  angle so that the gauge was bridged over the installation area. The tape surface was then wiped by a clean cloth.
14. Pressure applied by thumb to the gauge and terminal for at least one minute.

15. Finally, the tape was removed after a period of two minutes. This was done by pulling it back directly over itself. The gauge and terminal strip were then solidly bonded in place.

Wires from the strain gauges were soldered to the terminal strip. These wires were then soldered to the wires from the strain gauge connector box (SGCB) which contained the bridge circuit. This was done after the specimen had been mounted in the compression test fixture.

b) Tensile Test Specimens

Two tensile test specimens were obtained from each laminate, each 25 mm wide and 200 mm long as shown in Fig. 3.17. This is in accordance with BS-2782 specification, method 320E [32].

Cutting was carried out on a diamond studded wheel and care was taken to ensure accurate alignment of the specimens in the fibre direction. The edges of these specimens were then smoothed by a linisher and by fine silicon carbide paper. A 110 mm gauge length was marked on the specimen, and the surfaces at the ends of the specimen were roughened by hand with coarse grit paper. Aluminium alloy HS30 end tabs were cut (25 mm x 45 mm) from a sheet, their edges were smoothed by a linisher and the surface roughened by hand with coarse grit paper. The end tabs were bonded to the specimen using Araldite MY-750 epoxy resin with HY-951 hardener, 10:1 in ratio. A load was then applied to the tabs provide compression force in order to obtain a good bond. A curing period of 2-3 days was allowed at room temperature.

For measuring the extension throughout the test an extensometer was used rather than strain gauges, due to the larger size of gauge length. Heumann [25] tested two tensile specimens fitted with strain

gauges and the results were compared with the readings taken by the extensometer. The readings obtained by each of these methods agreed to within 0.5% of the readings up to a value of 2% strain. He therefore confirmed that both methods of strain measurement were accurate.

#### c) Inter-Laminar Shear Test Specimens

Three specimens were cut from each of three longitudinal strips of each slab with dimensions of 10 mm width and 18 mm length as shown in Fig. 3.18 and according to BS 2782: Part 3: Method 341A [33], making a total of six specimens.

The cut edges were smoothed down to 1200 grade silicon carbide paper. Care was taken to keep the corners of the specimen square.

#### d) Resin Tensile Test Specimens

Four tensile test specimens were obtained from each slab. The specimens were 200 mm long and 2-3 mm thick. They were fabricated using a steel mould and cast as rectangular pieces (see Section 3.4.3). The specimens were then configured into a dogbone shape using a high speed router (see Fig. 3.19).

### 3.5 MECHANICAL TESTING

#### 3.5.1 Compressive Testing

The specimens were tested in compression using the Celanese compression test fixture. A compression speed of 1.2 mm/min was used. Strain gauges were used to measure the strain via an amplifier in a bridge circuit and load was monitored directly via the load cell of the test machine. Load and strain were fed into a chart plotter to produce load vs strain curves. The curves thus obtained were generally

linear and only deviated as the maximum load was approached. When mounting specimens, an initial preload of 5 kN was given to each specimen. This reduced the initial irregular part of the load-strain curve down to a minimum.

### 3.5.2 Tensile Testing

A servohydraulic test machine was used to test the specimens to failure. The tests were carried out at a constant rate of grip separation of 5 mm/min. The load was measured directly through the load cell of the test machine. Strain was measured with an extensometer which was fed via an amplifier into a chart plotter. The specimen was covered with a strip of double sided tape in order to eliminate the effects of slippage of the extensometer knife edges and to prevent any damage being caused to the surface layers of the composites. Results obtained were a graphical plot of load vs strain to failure.

### 3.5.3 Inter-Laminar Shear Testing

An Instron machine was used for obtaining the inter-laminar shear strength of the material. The machine was fitted with a 200 kg load cell and geared to give a crosshead speed of 0.1 cm/min and chart speed of 5 cm/min.

The dimensions of the specimens to be tested were measured and the load obtained was read directly from the test machine's built in load/time plotter. Finally the specimens were checked for the existence of shear mode failure.

### 3.5.4 Microscopic Testing

The microscopic examination was carried out on two levels using:

1. An optical microscope.
2. A scanning electron microscope (SEM).

An optical microscope was used (Olympus) to observe the fibre distribution in the composites and to investigate the form of interlaminar shear failure in the different matrices.

Small specimens ( 5 mm long) were mounted in a resin. The surface was polished and subjected to the microscope. The polishing of the surface consisted of wet grinding on consecutively finer silicon carbide paper. The fine scratches from grit papers were removed by using a 5 micron alumina wheel for GRP specimens with alumina powder and water as lubricant. For CFRP specimens 6 and 1 micron diamond wheels were used.

Scanning Electron Microscopy was used (Cambridge Instruments Microscope) to investigate the fibre-matrix interfacial bond and also the condition of failure under compressive, tensile, and interlaminar shear. The fracture surface was cleaned ultrasonically and gold coated, before examination, to prevent them charging up in the SEM. The SEM was used at both high and low magnifications.

### 3.5.5 Resin Tensile Testing

To avoid fracture at the grips when testing brittle and ductile materials, dogbone shape specimens were used for tensile tests. The J.J. machine was used to test the specimens to failure. The load was measured directly through the test machine and fed onto a chart plotter. Strain was measured with an infrared extensometer instead of

a clip-on extensometer because the latter was not capable of measuring high strains. Two marks were applied to the sample to obtain a 50 mm gauge length. A powerful light source in the follower head illuminated the mark and detected the contrast of the reflected light from a dark mark applied to a light coloured sample.

As the sample was extended during the test, the two followers followed their respective gauge marks. A transducer in the extensometer generated a DC voltage proportional to the separation between the followers and hence proportional to the separation between the gauge marks. A transducer output was initially zeroed at the start of the test and this output applied to the X-axis of the X-Y recorder to plot a graph of load against extension.

# **CHAPTER 4**

## CHAPTER 4

### DATA AND RESULTS

#### 4.1 INTRODUCTION

This Chapter presents the results of the experimental work. For each composite laminate the following parameters were measured.

- Fibre Volume Fraction
- Matrix-Resin Density
- Matrix-Resin Tensile Properties
- Composite Compressive Properties
- Composite Tensile Properties
- Inter-Laminar Shear Strength.

The individual test results are listed in Appendices A,B, C, D and E. The mean values are presented in Tables 4.1-4.18. (The results are shown graphically in Figs. 4.20-4.50).

The fibre volume fraction was calculated for each laminate (this will be shown later in Section 4.2). However, since there was a variation about the mean, it was thought appropriate to assume a Law-of Mixtures relationship for the mechanical properties (tensile and compression) over the range and normalise these results to a standard fibre volume fraction of 45% using the following equations:

$$\sigma_{(T,C)} = \sigma^*_{(T,C)} \times \frac{0.45}{V_f} \quad (4.1)$$

$$\epsilon_{(T,C)} = \epsilon^*_{(T,C)} \times \frac{0.45}{V_f} \quad (4.2)$$

$$E_{(T,C)} = E^*_{(T,C)} \times \frac{0.45}{V_f} \quad (4.3)$$

where  $\sigma_{(T,C)}$  = normalised tensile or compressive strength  
 $\sigma^*_{(T,C)}$  = measured tensile or compressive strength  
 $\epsilon_{(T,C)}$  = normalised tensile or compressive failure strain  
 $\epsilon^*_{(T,C)}$  = measured tensile or compressive failure strain  
 $E_{(T,C)}$  = normalised tensile or compressive modulus  
 $E^*_{(T,C)}$  = measured tensile or compressive modulus

Throughout the following section, the word 'composite' will be used to mean "GRP and CFRP composites".

## 4.2 FIBRE VOLUME FRACTION

### 4.2.1 'GRP' Specimens

For laminates containing Glass Fibre Reinforcement, the resin burn-off procedure was carried out (see Section 3.4.2). For each laminate two samples were tested. A set of results is listed in Appendix A, Table A-1. The fibre volume fraction was calculated by the following equation:

$$V_{fg} = \frac{1}{1 + \frac{\rho_g}{\rho_m} \left( \frac{c-f}{f} \right)} \quad (4.4)$$

where  $\rho_g$  = density of glass fibre (= 2.55 gm/cm<sup>3</sup>)

$\rho_m$  = density of resin

c = weight of composite sample before burn-off

f = weight of remaining fibre after burn-off.

The mean value per laminate is presented in Table 4.1 and was used in subsequent calculations.

#### 4.2.2 'CFRP' Specimens

For laminates containing Carbon Fibre Reinforcement, the acid digestion technique was carried out to determine fibre volume fraction (see Section 3.4.2).

For each laminate two samples were tested. A set of results is listed in Appendix A, Table A-2. The fibre volume fraction was calculated by the following equation:

$$V_{fc} = \frac{1}{1 + \frac{\rho_c}{\rho_m} \left( \frac{c-f}{f} \right)} \quad (4.5)$$

where  $\rho_c$  = density of carbon fibre (= 1.81 g/cm<sup>3</sup>)

The mean value per laminate is shown in Table 4.1 and used in subsequent calculations.

#### 4.3 VOIDS VOLUME FRACTION

For both composites, the method of determining the volume fraction of voids is based on density measurements. From the weight of the fibres and the weight of the resin in a known weight of the composite material, the voids volume fraction was calculated by the following equation:

$$V_v = 100 - \rho_c (W_f/\rho_f + W_R/\rho_R) \times 100 \quad (4.6)$$

where  $V_v$  = voids volume fraction  
 $W_f$  = fibres weight fraction  
 $W_R$  = resin weight fraction  
 $\rho_C$  = composite density.

The mean values per laminate for both composites are presented in Table 4.1, which will be used in a subsequent discussion in Chapter 5. The mean value of voids is shown graphically as a function of the percentage modifier in Fig. 4.20.

#### 4.4 MATRIX-RESIN DENSITY

Matrix density was measured by means of a water displacement method. Density was then calculated using the following equation:

$$\rho_s = \frac{W_s \rho_w}{W_{wo} + W_s - W_{w+s}} \quad (4.7)$$

where  $\rho_s$  = specimen density  
 $\rho_w$  = distilled water density ( $= 1\text{g/cm}^3$ )  
 $W_s$  = weight of specimen  
 $W_{wo}$  = weight of density bottle containing water only  
 $W_{w+s}$  = weight of density bottle containing water + specimen.

A set of results is shown in Appendix B, Table B-1. The mean value of four specimens from each sheet were then plotted as a function of the percentage of modifier content, as shown in Fig. 4.21.

The accurate resin density value for each laminate was deduced from the plotted graph and is presented in Table 4.2. Resin density was required in volume fraction calculations (see Section 4.2).

#### 4.5 MATRIX-RESIN PROPERTIES

The resin tensile strengths were calculated from the highest point reached by the load-extension curves obtained from the test. The general form of these curves is shown in Fig. 4.22.

The tensile failure strain was then calculated:

$$\epsilon_m = \frac{\Delta L}{L} \quad (4.8)$$

where  $\Delta L$  = extended length

$L$  = the specimen's gauge length.

The resin tensile modulus was obtained after measuring the load at 2% strain.

The average results of the above properties are shown in Table 4.3. A complete set of results is recorded in Appendix B, Table B-2. The mean value of resin tensile moduli, strengths results are shown graphically as a function of the percentage of modifier content in the matrix, Figs. 4.23-4.24.

The unmodified matrix had a tensile strength of 58 MPa and a modulus of 2.98 GPa. With the addition of 20% modifier the value of tensile strength dropped to 50% of its original value (see Fig. 4.24). The modulus showed the same behaviour as that of tensile strength.

## 4.6 COMPRESSIVE PROPERTIES

### 4.6.1 Compressive Strength

From the load/strain curves the maximum load applied to each specimen was obtained by reading the highest point reached by the curve. The UCS was then calculated using the following equation:

$$\sigma_c = \frac{L}{wt} \quad (4.9)$$

where  $\sigma_c$  = ultimate compressive strength (UCS) (MPa)

$L$  = load at failure (kN)

$w$  = width of specimen (mm)

$t$  = thickness of specimen (mm).

The complete sets of test results for GRP and CFRP specimens are listed in Appendix C, Tables C-1 and C-2. The mean normalised compressive strength of five specimens from each laminate for both GRP and CFRP are given in Tables 4.4 and 4.5. These results are plotted as a function of percentage of modifier content in the matrix in Figs. 4.25-4.28.

The compressive strength of CFRP specimens was observed to be higher than those of GRP. As the percentage of modifier increased, the compressive strength decreased. With the addition of a small amount of modifier (5%) to GRP there was a 15% decrease in strength. With the addition of 20% modifier the compressive strength showed a decrease of about 50%. The CFRP specimens seemed to follow the same behaviour in decrease as in the GRP, although the initial rate of decrease was greater.

#### 4.6.2 Fracture Appearance

In all compressive tests carried out the failure occurred suddenly and catastrophically as compared with tensile failure. This led to different types of failure across the range of specimens tested.

1. Unmodified specimens of GRP failed by splitting and kinking. The single or multiple kink-band structure made an angle of  $70^{\circ}$  with the fibre axis, as shown in Plate 8. With unmodified CFRP specimens the failure was by shear on a plane at about  $45^{\circ}$  with the loading direction, as seen in Plate 12. All failures were accompanied by a clear cracking sound.
2. GRP specimens, with small percentages of modifier ( $<20\%$ ), exhibited clear narrow single kink bands. These kink bands were perpendicular to the fibre direction across the specimen's width, as shown in Plate 9. Using the same amount of modifier with CFRP, the failure was fibre microbuckling on a  $70^{\circ}$  plane. The failures were accompanied by a clear cracking sound, see Plate 13.
3. GRP and CFRP specimens with higher percentages of modifier ( $>30\%$ ) failed by wider single kink bands, as shown in Plates 10 and 14. Only a faint sound accompanied these failures.

A  $70^{\circ}$  inclination of the kink band to the fibre through the thickness of the specimen was observed in all modified specimens, see Plate 11. Table 4.18 shows the four different mechanisms of failure for both composites in which they occurred.

#### 4.6.3 Compressive Failure Strain

The compressive failure strain of composites ( $\epsilon_c$ ) was obtained from the load/strain curve. Mean normalised results are presented in Tables 4.6 and 4.7. A complete set of results is given in Appendix C, Tables C-1 and C-2. These results are plotted as a function of percentage of modifier in the matrix in Figs. 4.29-4.32.

The failure strains were 1.26% and 1.15% for unmodified GRP and CFRP specimens respectively. However, as percentage modifier increased, the compressive strain decreased. With GRP, the addition of 60% modifier led to a drop of 50% in the strain value (i.e. 0.67%). In CFRP specimens, however, a 30% addition of modifier led to a drop of 50% in its strain value (i.e. 0.52%).

#### 4.6.4 Compressive Secant Modulus

In the case of any discontinuity or non-linear elastic variation in the load/strain curve, the secant modulus was measured instead of elastic modulus.

The compressive secant modulus was obtained by measuring load at 0.5% strain from the load/strain curve. Then the modulus was calculated from the following:

$$E_c = \frac{\sigma_c}{\epsilon_c} \quad (4.10)$$

where  $E_c$  = compressive secant modulus

$\sigma_c$  = compressive strength at 0.5% strain

$\epsilon_c$  = compressive strain (= 0.5%).

The calculated results from each laminate were normalised to 45%  $V_f$ . Details of mean results are presented in Tables 4.8 and 4.9. A complete set of results is recorded in Appendix C, Tables C-1 and C-2. These results are plotted as a function of percentage modifier in the matrix in Figs. 4.33-4.34.

The results show a decrease in modulus with an increase in modifier content in the matrix.

In GRP specimens, a 50% drop in modulus was noticed with the addition of 30% modifier. On the other hand CFRP specimens showed a drop of 50% in modulus with 60% addition of modifier.

Secant modulus is used for assessing differences in uniaxial stiffness between composites.

## 4.7 TENSILE PROPERTIES

### 4.7.1 Ultimate Tensile Strength

The UTS ( $\sigma_T$ ) was calculated using the point of greatest load supported by the specimen during the test (obtained from load/strain curves).  $\sigma_T$  was calculated as follows:

$$\sigma_T = \frac{L}{t \cdot w} \quad (4.11)$$

where  $L$  = maximum tensile load.

The mean normalised tensile strength results of composites are presented in Tables 4.10 and 4.11. A complete set of results is recorded in Appendix D, Tables D-1 and D-2. These results are plotted as a function of percentage modifier in the matrix, in Figs. 4.35-4.38.

The average tensile strength of unmodified GRP specimens was 978 MPa. This fell to 512 MPa with a 60% addition of modifier (i.e. a decrease of  $\sim 48\%$ ).

In CFRP specimens, however, the average tensile strength was 1392 MPa. This fell to 898 MPa with 60% addition of modifier (i.e. a decrease of 35%).

#### 4.7.2 Fracture Appearance

During the test, loud cracking noises were heard in unmodified GRP specimens; this was due to a gradual failure, starting at a low load, near the edges of the specimen. This was prior to specimen tensile failure. The appearance of the failure was brush like. This is shown in Plate 15. When increasing the percentage of modifier the tensile failure load was reached before the cracks spread across all the specimens, see Plate 16.

In unmodified CFRP specimens, failure was sudden and catastrophic. It was observed that the specimens failed by transverse cracking with few longitudinal cracks, Plate 17. With higher modifier content the failures resembled the modified GRP failures. Plate 18 shows a typical example.

#### 4.7.3 Tensile Failure Strain

The tensile failure strain of composites was obtained directly from the load/strain curve. The average normalised results are presented in Tables 4.12 and 4.13. A complete set of results is recorded in Appendix D, Tables D-1 and D-2. These results are shown graphically in Figs. 4.39-4.42.

With GRP specimens, a large scatter was observed. The highest failure strain was in unmodified specimens and the lowest was in specimens with 60% addition of modifier. The CFRP specimens exhibited considerably lower strains than the GRP specimens. Yet a clear descending curve was observed with little scatter in direct comparison with the GRP results.

#### 4.7.4 Tensile Secant Modulus

The analysis of tensile secant modulus was obtained in the same way as the compressive modulus (see Section 4.6.3). The average normalised results are represented in Tables 4.14 and 4.15. A complete set of results is recorded in Appendix D, Tables D-1 and D-2. These results are shown graphically in Figs. 4.43-4.44.

Unmodified GRP specimens had an average tensile modulus of 43.42 GPa, which is equivalent to the value measured in compression. In modified specimens a lower modulus was produced.

In CFRP, the difference between tensile and compressive values was much greater. The tensile modulus for unmodified specimens being 109.98 GPa. However, there was a very large variation between tensile and compressive results for modified composites.

#### 4.8 INTER-LAMINAR SHEAR STRENGTH (ILSS)

From the inter-laminar shear test, a curve of load against extension was obtained for all composites. Typical sets of curves are shown in Figs. 4.45-4.46.

The ILSS was calculated using the following equation:

$$S = \frac{0.75F}{bd} \quad (4.12)$$

where  $S$  = ILSS (MPa)

$F$  = force of fracture (N)

$b$  = width of specimen (mm)

$d$  = thickness of specimen (mm)

The average normalised results are given in Tables 4.16 and 4.17. A complete set of results for all tests carried out on the specimens is given in Appendix E, Tables E-1 and E-2. These results are plotted as a function of percentage of modifier content in the matrix, in Figs. 4.47-4.50.

The unmodified specimens had the highest inter-laminar shear strengths. This was true for both GRP and CFRP laminates. It was noted that the ILSS for GRP and CFRP followed the same trend; an increase in the amount of modifier created a decrease in shear strength.

#### 4.8.1 Appearance of Failures

All GRP specimens showed either single or multiple shear failures. In unmodified CFRP specimens and those with a small addition of modifier (5%) a clear crack was seen. With higher modifier content however, the mode of failure was the same as with GRP.

The results of these tests give an indication of fibre matrix interface bonding. With this information it is possible to discuss the mode of tensile failure.

## 4.9 MICROSCOPIC RESULTS

### 4.9.1 Fibre Distribution

Samples of different concentrations of modifier (0%, 30%, 60%) from each composite, were examined under an optical microscope (Olympus) to observe how the fibres were distributed within the composite, and to investigate the presence of voids.

Within each unmodified composite, fibres were found in a good distribution without too much fibre bunching, see Plates 19 and 20. Also there was no evidence of voids.

With modified composites (30%) the fibres were more bunched and there were rich resin areas. There was also a significant proportion of voidage, see Plates 21 and 22. It was noticed that with the increase in percentage of modifier, more resin rich areas were created. This, in effect, led to an increase in the number of voids within each sample.

### 4.9.2 Inter-Laminar Shear Failure

Failed inter-laminar shear specimens were examined under optical and electronic scanning microscopes.

Under an optical microscope, unmodified specimens showed clear crack propagation through the fibre-matrix interface, see Plate 23. CFRP specimens showed a much better bonding than was the case with GRP, see Plate 24.

Plates 25 and 26 show highly modified specimens (30%) with good bonding between the matrix and the fibre. The crack propagated through the matrix and appeared to have branched. There were clumps of matrix material still attached to some fibres.

SEM micrographs of the fibres from the ILSS failed specimens also showed that the matrix in modified specimens adhered better than in unmodified specimens, see Plates 27-30. It was noticed that all GRP specimens showed poor bonding relative to CFRP specimens.

#### 4.9.3 Compressive and Tensile Failures

It is important to discuss the mode of failure of each composite, and find the influence of the matrix on the mechanical properties (see Chapter 5).

For this reason, small pieces of failed specimens from compressive and tensile tests were examined under the SEM.

Plates 31-32 show high magnification SEM micrographs of the tensile failure surface of unmodified GRP and CFRP specimens.

Plates 33-34 show high magnification SEM micrographs of the compressive failure (shear) in unmodified CFRP specimens, while Plates 35-36 show the compressive failure surfaces (fibre microbuckling) in slightly modified CFRP specimens (5%).

Plates 37-38 show the sides of failed 60% modified GRP and CFRP specimens, under an optical microscope. Kinking in compressive regions of fracture is visible.

# CHAPTER 5

## CHAPTER 5

### DISCUSSION

#### 5.1 FIBRE VOLUME FRACTION AND DISTRIBUTION

Theoretically in a unidirectional composite all the fibres are well aligned parallel to each other. The fibres can be considered to be arranged on a square or hexagonal lattice, with each fibre having a circular cross-section and the same diameter. In practice, however, these ideal distributions do not occur except in localised regions.

In low  $V_f$  composites, for example,  $V_f = 0.30$ , the packing is often very irregular; some fibre bunching and large resin rich regions may occur. Misalignment of the fibres is also more pronounced in low  $V_f$  laminates. The irregular dispersion of the fibres may have a significant effect on properties such as the transverse strength and modulus [Hull, 18].

It is possible to calculate the distribution of stress and strain in a composite material in terms of the:

- geometry
- $V_f$  of the fibres and distribution
- elastic properties of the fibres and the matrix.

In the work reported here there was a difference between the fibre volume fraction of modified and unmodified laminates; also between GRP and CFRP composites. To minimise the effect of these differences,

the results were normalised to a constant fibre volume fraction of 0.45.

With regard to fibre distribution, plates 19 and 20 show the fibre distribution in unmodified composites. It can be seen that there is not too much fibre bunching and no evidence of voidage in the matrix. With modified composites, however, there are significant voids. The fibres were irregularly packed and resin rich regions occurred throughout the laminate (see Plates 21 and 22). It was noticed that the resin became considerably more viscous as the modifier additions were increased. This caused a decrease both in the wetting process and also in the escape of entrapped air from the matrix. The tendency for voidage in the matrix, therefore, increased with the increase in modifier additions.

The presence of voids may have affected the mechanical properties of the composites. Hancox [14] noticed a steady decline in compressive strength of CFRP composites with increasing voidage. Above 5% voids, the compression strength is most reduced, while the modulus is least affected. Hancox also noted the effect of voidage on inter-laminar shear strength. This property was very sensitive up to approximately 1% voidage. Inter-laminar shear strength decreased by about 7% for each 1% voids up to a total voids content of about 4%. He concluded that the lack of correlation between these different strength properties indicated that voidage has a different effect in each case.

The percentage of voids in the resin system studied ranged between 0% (in unmodified composites) to 2% in higher percentages of modifier (60%), see Fig. 4.20. It was noticed that with 10% addition of modifier, the inter-laminar shear strength for GRP and CFRP composites

decreased by 23% and 19% respectively. Hence it is concluded that the presence of voids is not totally responsible or behind the drop in mechanical properties of the composites.

## 5.2 INTER-LAMINAR SHEAR STRENGTH

The inter-laminar shear strength (ILSS) of a composite depends on the direction of the shear displacements. For a given matrix, ILSS depends upon the stress concentration effects associated with the presence of fibres, the voids, and the interfacial adhesion.

In the modified composites the fibres are strongly bonded to the matrix. The ILSS will depend on the strength of the matrix and the interface bond. If the bond does not fail there is a stress in the resin which is a maximum near the fibres. This stress concentration effect results in a reduction in ILSS. As the modifier addition increases with a corresponding reduction in the modulus and strength of the matrix, the stress concentration effect decreases and the ILSS could also be expected to decrease.

At low fibre volume fraction the stress concentration factor is relatively insensitive to  $V_f$ , but it rises rapidly when  $V_f$  is greater than 0.60. In the specimens tested the fibre volume fractions were not large enough to have a significant effect on the stress concentration factor.

Hancock [14] noted the sensitivity of ILSS to voidage. Voids act as stress-raisers and tend to reduce ILSS. In these experiments the tendency for voidage in the matrix increased with higher modifier additions. Consequently a decrease in ILSS was to be expected and this

is apparent in Figs. 4.47-4.49. However, the question has to be asked as to whether all of the decrease was due to voids.

From the micrographs of ILSS fracture surfaces it appears that the interfacial adhesion improved with higher modifier additions. Plates 27-30 show this fact for both composites.

In unmodified resin composites, ILSS was controlled by 'interfacial adhesion'. Since the unmodified matrix was brittle and had a higher yield strength, the interlaminar shear cracks travelled preferentially through the fibre-matrix interfaces. As modifier additions increased, the matrix yield strength was reduced, whilst the interfacial adhesion improved. It therefore became easier for the interlaminar shear cracks to travel through the matrix itself. ILSS became matrix controlled. The modifier allowed stress relieving processes to operate which reduced thermal and shrinkage stresses within the cured composite as well as local stress concentrations through plastic flow.

The general trend of decreasing ILSS with higher modifier additions represents the conjoint action of a shift from interface to matrix control of the interlaminar cracking as the matrix yield strength decreased, and increased local stress concentration due to the presence of voidage.

The results in Fig. 4.50 show that the higher percentage of modifier had a weakening effect on the interlaminar shear strength. The percentage of drop in shear strength for CFRP composites at less than 15% modifier additions was smaller than for the GRP composites, although the amount of modifier addition was the same. It is believed that this was due to the interfacial adhesion in CFRP being better

than in GRP. As the modifier addition increased above 15%, the results show that the shear strength of CFRP composites was worst affected. This is seen from the sharp drop in the curve for CFRP in Fig. 4.50. It can thus be suggested that 15% modifier addition was a transition point for failure mechanisms in CFRP. Above 15% modifier any stress concentrations are relaxed by local deformation processes.

Examination of polished fracture surfaces under an optical microscope showed the interlaminar shear crack for unmodified composites, Plates 23-24. It is apparent that failure occurred by shear off the resin close to or at the fibre matrix interface. Shear zones have grown ahead of the crack and some local interface debonding has occurred. SEM micrographs of a shear fracture surface of each composite are shown in Plates 27-29. The most significant difference is that the CFRP shows stronger adhesion than the GRP. This leads to increased ILSS for unmodified CFRP.

Plates 25 and 26 show GRP and CFRP polished interlaminar shear fracture surfaces at 30% modifier additions under the optical microscope. In both cases there is evidence of resin adhering to fibres, while glass fibre forms relatively poor bonds. Plates 28 and 30 show modified GRP and CFRP interlaminar shear fracture surfaces at high magnification.

The typical load/extension curves to failure for both unidirectional composites tested in interlaminar shear are shown in Figs. 4.45-4.46. The non-linearity in the composites is due to the properties of the resin. With flexible resin matrices some viscoelastic or plastic flow occurs. The extension at failure of the composites appears to be related to those of the matrices shown in Fig. 4.22 and especially for GRP.

Further discussion on tensile and compressive failure strain for composites and their dependence on the matrix properties will be included in successive sections.

### 5.3 TENSILE PROPERTIES

#### 5.3.1 Tensile Modulus

From the distribution of stress, the elastic properties of the composites material can be calculated. For unidirectional composites, the simple rule of mixtures can be used to calculate the modulus of the composites for given fibre and resin matrix moduli:

$$E_C = E_f V_f + E_m (1 - V_f) \quad 5.1$$

where  $E_C$  = composite elastic modulus

$E_f$  = fibre elastic modulus

$E_m$  = matrix elastic modulus

The rule of mixtures is important because of its simplicity which has led to its widespread usage and because it does not require determination of the less readily known properties of composites such as effective fibre pull out length at a break, or the statistical function describing the distribution of weak points.

It is assumed that all the fibres behave elastically in tension up to the fracture strength. However, epoxy resins have non-linear load-extension curves, see Fig. 4.22 and may undergo considerable viscoelastic deformation before fracture.

In this work the term modulus has been used to describe the elastic stiffness of the composites, calculated by taking a secant of the stress-strain curve as described in Section 4.7.4.

Fig. 4.43 shows the mean tensile moduli for both GRP and CFRP composites against the percentage of modifier addition. In general the tensile moduli for CFRP specimens is higher than for GRP specimens. This is due to the higher modulus of carbon fibres when compared with glass fibres. It was observed that the stiffness of the CFRP composites was about 34% higher than in GRP composites under tension.

The results show that the modulus of modified specimens obeys the rule of mixtures. However, as the matrix moduli is small in comparison with the fibre modulus, the change in moduli of the matrix has little effect on the moduli of the composite.

The stress-strain curves for all specimens were initially linear elastic but became non-linear as failure approached. As the modifier increased the composites showed more non-linearity. This was due to the change in matrix modulus and resulting reduction in local stress concentration.

In CFRP composites small modifier additions (i.e. 5% and 10%) resulted in a small improvement in tensile moduli with respect to the unmodified samples. This increase can be attributed to the brittleness of the unmodified matrix being removed. Initially the modifier allowed a stress relieving process which reduced thermal and shrinkage stress within the cured composite as well as local stress concentrations, through plastic flow. It is suggested that carbon

fibre composites were more greatly affected than glass because the difference in coefficient of thermal expansion between the carbon fibres and the matrix resulted in much higher thermal stresses than was the case with glass fibres. The increased adhesion due to the modifier addition also could initially lead to an increase in the modulus of the composites.

In general the GRP and CFRP composites showed similar rates of decrease in moduli, as can be seen from the results in Fig. 4.44. It was thus observed that the decrease in modulus of matrix had a similar effect on GRP and CFRP and that this effect was to only lower the modulus of the composites by a small amount, as predicted by the rule of mixtures.

Fig. 4.23 shows the matrix tensile modulus as a function of modifier addition. The unmodified matrix had a tensile modulus of 2.98 GPa, while with a 60% addition of modifier the modulus had dropped to 0.17 GPa. From the rule of mixtures equation 5.1 and for laminates with 0.45 fibre volume fraction, this decrease in resin moduli will result in a decrease of 1.5 GPa in composite modulus. This decrease is insignificant in comparison to the original composite modulus magnitude, which was of the order of 110 GPa for CFRP and 43 GPa for GRP.

Thus it can be concluded that the modulus of the composites under tension was controlled by fibre and not matrix stiffness.

### 5.3.2 Tensile Strength

From an analysis of the tensile strength of the various fibre-resin matrix systems used in this work, the tensile strength of composites was found to decrease as the modifier addition in the matrix increased. A little scatter was expected in tensile properties as discussed in Section 5.3.1. The results are presented in Figs. 4.35-4.37.

In the tensile tests the fibre failure mode predominated. The main parameters which affect the tensile strength are:

- Fibre tensile strength
- Interface adhesion
- Resin tensile strength
- Voids

As shown in Tables 4.10 and 4.11, and Fig. 4.37, the average tensile strength of unmodified GRP specimens was 978 MPa and this decreased by 48% at 60% modifier addition, while in unmodified CFRP specimens the average tensile strength was 1392 MPa which decreased by 35% at 60% modifier addition. The rate of decrease is shown in Fig. 4.38. With a small amount of modifier addition, 5%, GRP specimens showed a sharp decrease about 23% in tensile strength. CFRP specimens showed a 1% decrease at 5% modifier addition. This was evidence of a better interface adhesion in carbon fibres. However, as the percentage of modifier increased, >10%, a gap of approximately 10% retention between the two composites could be clearly seen. A similar observation has been noted with ILSS and tensile failure strain results (Sections 5.2 and 5.3.3) which suggests this to be a general phenomenon. In general the ultimate tensile strength of all CFRP composites was higher than

GRP. This is due to the fact that the carbon fibres have a much higher strength than the glass fibres.

SEM micrographs of the fibres from the interlaminar shear failure, Plates 27-30, showed that matrix adhesion in both modified composites is greater than in unmodified composites. In both modified composites there was evidence of resin remaining adhered to the fibres, although this was more apparent in the case of carbon fibres.

From an analysis of the tensile strength of the various fibre-resin systems used in this work, together with a comparative consideration of the interlaminar shear strength failure results, the relative adhesion of the fibre-matrix interface has been ascertained. While glass fibres show less matrix adhesion than carbon fibres, it is also clear that unmodified resins produce composites with less adhesion than do the modified resins with respect to the fibre systems used in this work. However, the lower adhesion formed by unmodified resins does not result in weaker composite strength. The reason for this is the large reduction in tensile strength of the matrix (see Fig. 4.24). In unmodified composites (brittle matrix) the matrix had a higher yield strength. When the tensile load was applied parallel to the fibres, the fibres bore the major part of the load, and the matrix takes only a small proportion. The matrix fractures before the fibre and then all the load is transferred to the neighbouring fibres, but complete unloading does not occur until final fracture. As modifier addition increased, the matrix yield strength was reduced. When the fibres fracture the load transfers to the matrix and this cannot support the load, so that the matrix fractures when the fibres fracture.

Tensile strength is particularly sensitive to the presence of voids. The increasing addition of modifier increases the amount of voids in the composites. Higher modifier addition hinders the escape of trapped air from the matrix resulting in more voids. The presence of voidage tends to increase the local stress concentration. This may be part of the explanation of the poor tensile strength results with high modifier.

It is clear that any factors that affect redistribution of load from fibre to matrix influence tensile strength.

### 5.3.3 Tensile Failure Strain

The tensile failure strains of the composites are presented in Figs. 4.39-4.41. In all cases as the modifier is increased the tensile failure strain decreases. Fig. 4.41 shows that the tensile failure strain of all GRP specimens is higher than CFRP. This is due to the fact that the carbon fibres have a much lower strain to failure (1.44%) than the glass (3.37%).

The response of the composite depends on the relative strain to failure of the matrix and the fibre. When the tensile load is applied, and the strain to failure in the fibres is greater than in the matrix,  $\epsilon_f > \epsilon_m$ , the matrix takes only a small proportion of the load assuming the fibre modulus is greater than matrix modulus,  $E_f > E_m$ . When the matrix fractures the transfer of load to the fibres is insufficient to cause fracture provided it is still possible to transfer the load to the fibres. The load on the laminate can be increased until the fracture strength of the fibres is reached. At this point  $\sigma_c^* = \sigma_f^* V_f$ , as shown in Fig. 5.51.

This theory can be applied to the unmodified GRP composites, since the failure strain of glass fibre used in this work is 3.37%, while the failure strain of the unmodified matrix was 2%. In the case of carbon fibres the failure strain was 1.44%, which is lower than the matrix failure strain.

Modifier additions have the effect of reducing the elastic moduli of the matrix. Therefore the ultimate tensile strength of the composites is reduced as discussed in Section 5.3.2.

When  $\epsilon_m > \epsilon_f$ , the fibres fracture before the matrix. The load transferred to the matrix is very large and cannot be supported, so that the matrix fractures when fibres fracture. In this case  $\sigma_c^* = \sigma_f^* V_f + \sigma_m' (1 - V_f)$ , Fig. 5.52.

This theory can be applied to all modified GRP composites and CFRP composites. (Since a small addition of modifier increased the strain to failure of the matrix, and this in turn reduced the mechanical properties of the composites).

The decrease in tensile failure strain was 33% in GRP samples with 60% modifier added to the matrix, and 44% in CFRP with the same percentage of modifier added. Fig. 4.42 shows percentage retention of failure strain in both composites. The percentage of retention decreased gradually with increase of modifier. At lower values of modifier additions, percentage retention is the same for both composites. However, as the percentage of modifier is increased (>5%), a gap of approximately 10% retention opens between the two curves. This same behaviour was observed earlier in tensile strength (Fig. 4.38). The decrease in tensile strain at failure was accompanied by a decrease in

tensile strength. The modulus of the composite however obeyed the rule of mixtures and showed little decrease.

Working with different fibres in different matrices, Hahn [23] observed that the compressive failure strain increased with the tensile failure strain. He concluded that this same defect mechanism may operate in compression as well as in tension. The defect sensitivity in compressive buckling however, would be less in tension. A correlation between compression and tension failure strain for both composites is shown in Fig. 5.53. Linear regression analysis was performed. One feature that stands out is that the tensile and compressive failure strains for both composites were reduced by reducing the stiffness of the matrix.

#### 5.3.4 Failure Mechanism

Two main types of tensile failure modes were observed in this work, as shown in Plates 15-18.

When the composite is loaded the stress in the fibres is related to the stress in the laminate by:

$$\sigma_c = \sigma_f V_f + \sigma_m (1 - V_f) \quad 5.2$$

where  $\sigma_c$  = stress on the laminate

$\sigma_f$  = stress on the fibres

$\sigma_m$  = stress on the matrix

As the force was applied longitudinal cracks caused by shear stress at the interface appeared in the bulk of the specimens and propagated rapidly along the fibre-resin interface to occupy the complete length of the specimen. This debonding was followed by pronounced audible signals of cracking as fibres pull-out, usually starting at the specimen edge and propagating across the entire width. This caused total destruction of the laminate and the force drop.

In the unmodified GRP specimens tested, debonding occurred throughout the gauge length. This was evidence of a weak interface bond. Brush-like failure is typical of unidirectional GRP tensile failure with fibre pull-out.

When a composite is loaded and the load increases, a fibre fracture will occur at one of the serious flaws or imperfections. When such a fibre breaks, the stress in the vicinity of the broken fibre is disturbed substantially so that the axial stress in the fibre vanishes at the fibre break and gradually builds up to its undisturbed stress value due to shear stresses being transferred across the fibre matrix interface. The cracking of fibre and matrix can occur before complete separation of the fracture surfaces, hence brush-type fractures. Failures of this nature have been observed recently by Heumann [25] and many other workers, see Plate 15.

Plate 16 shows failed modified GRP specimens. There is a significant difference between modified and unmodified specimen failure. There was less debonding in modified specimens and the UTS was reached before interface cracks propagated through the specimen. When modifier addition increased, the matrix yield strength was reduced, whilst the amount of interfacial adhesion increased. Therefore when a fibre

fractured the load was transferred over a greater distance to surrounding fibres and ultimately because the average stress carried per fibre was reduced, the tensile strength of the composite was reduced. The specimens showed small clumps of resins and fibres intact, while the main failure was brush type.

An observation of a typical unmodified CFRP failure pattern is shown in Plate 17. This composite failed by fibre breakage with failure surfaces roughly perpendicular and parallel to the direction of loading with little debonding. It is therefore believed that certain amounts of fibre failure do occur in unmodified CFRP composites before final catastrophic failure, amounting to many small group failures which then link up at the point of ultimate tensile failure.

SEM micrographs of the tensile failure surface for both unmodified composites are shown in Plates 31 and 32. There is evidence of weaker adhesion in the glass fibres witnessed by the finer fibre separation which occurs, while Plate 32 shows good interfacial adhesion in the fracture surface of an unmodified CFRP specimen failure.

In CFRP laminates with higher modifier content, Plate 18, debonding occurs but still fibres clump together. The process of failure in the carbon fibre reinforced specimens appears to be simpler. The lower yield strength of the matrix allows some debonding between fibre bundles by shear. The fracture of modified CFRP specimens falls into a category somewhere between unmodified GRP failure and unmodified CFRP failure.

## 5.4 COMPRESSIVE PROPERTIES

### 5.4.1 Compressive Secant Modulus

The secant modulus represents an approximation to the stress-strain relationship which, for most comparison purposes, is quite valid. It is used for assessing differences in stiffness between composites with different matrices.

The average results of compressive secant moduli for both composites are presented in Fig. 4.33. They show straight parallel lines which indicate that as the percentage of modifier increases the modulus decreases.

There was a significant difference in the secant modulus results for glass and carbon reinforced matrices. Fig. 4.34 shows the rate of decrease in compressive modulus for both composites as a function of percentage of modifier. At small modifier additions, the carbon fibre composites were affected more than glass fibre composites. At 10% modifier addition, CFRP compressive modulus decreased about 18%, while the GRP decreased about 6%.

The compressive moduli for both composites were compared with tensile moduli, see Section 5.3.1. Unmodified GRP specimens had a compressive secant modulus of 43.42 GPa and a similar tensile secant modulus value (i.e. the stiffness in compression and tension was the same). The variation between tensile and compressive values in unmodified CFRP specimens was much greater. The stiffness in compression was 47% lower than in tension. This is due to the fact that carbon fibres have a lower modulus in compression than in tension as discussed recently by Harper and Heumann [37].

The compressive moduli for both modified composites proved to disobey the RCM (rule of mixtures). This is shown in Figs. 5.54 and 5.55. The variation in modulus between tensile and compressive increases as the percentage of modifier increases. This is due to the fact that the failure mechanism under tension is completely different to that in compression. Defect sensitivity in buckling being a major factor in compression failure.

Hahn and Williams [24] in their work observed that the compressive modulus of carbon reinforced composites is more dependent on the resin modulus than is the tensile modulus. They also observed that the composite tensile modulus is greater than the compressive modulus for a resin modulus value less than 5 GPa. Above 5 GPa the difference in compressive and tensile moduli was not as great. In this work the unmodified matrix had a resin tensile modulus  $\approx 3$  GPa. As the modifier percentage increased the resin tensile modulus became less than 1 GPa. Therefore the observed differences in moduli, in the carbon fibre reinforced samples, support Hahn and Williams' findings.

The lower composite modulus in compression rather than in tension can be explained by the following facts:

- i) the fibres themselves are less stiff in compression than in tension
- ii) the fibres themselves are not perfectly aligned within the laminate; the initial misalignment and curvature of the fibres may impose disproportionately high stress on the matrix, locally pushing the matrix into the non-linear range at an early stage of loading

- iii) different thermal expansion could cause thermal compressive stresses in the fibres or in extreme cases buckling of the fibres. However calculation using known coefficient of thermal expansion for the fibre and the matrix show in this case that such stresses are low and not sufficient in themselves to cause failure.

The mode of failure observed in all GRP specimens was kinking due to fibre buckling. Unmodified CFRP specimens showed a shear mode from the rough failure surface, but as the modifier was added the mode of failure changed and showed a similar attitude of kinking, see Section 5.4.4. A SEM micrograph of a surface failure of CFRP with 5% modifier is shown in Plate 35. Characteristic steps associated with fibre microbuckling are clearly visible. Therefore it can be suggested that as the modifier increases the matrix is not a good support to the fibres and fibre buckling occurs very easily. This results in a low modulus and resulting lower compressive strength which is observed widely in this work.

#### 5.4.2 Compressive Strength

The compressive strength results of both composites are shown in Figs. 4.25 and 4.26. GRP and CFRP results showed similar scatter, however, this was not larger than found by other workers.

A comparison of the compressive strength of both composites is shown in Fig. 4.27.

The average compressive strength of GRP in an unmodified matrix was 488 MPa with a fibre volume fraction of 0.45. This is shown in Table 4.4. All results in the table are markedly lower than those of Chaplin

[15] which he obtained from extremely carefully made specimens. Chaplin's compressive strength result was 950 MPa for a fibre volume fraction of 0.60.

In the case of CFRP composites, the compressive strength showed the same trend as with GRP mentioned earlier, the results are shown in Table 4.5. The average compressive strength of unmodified specimens is 602 MPa for a fibre volume fraction of 0.45. This is much lower compared to the results obtained by Hahn and Williams [24] and by various other workers [12,16,19,25].

The lower compressive strength observed in GRP and CFRP composites in this work can be explained by reference to the manufacturing techniques and lower volume fractions. These points are discussed in more detail later in this section.

In Fig. 4.27, the compressive strength of both unmodified and slightly modified CFRP composites is higher than those of GRP specimens. However, as the percentage of modifier increases the compressive strength of both composites starts to coincide. The initial higher compressive strength of CFRP composites with respect to GRP composites is due to the high fibre strength of carbon and better bonding with epoxy resin.

Fig. 4.28 shows the percentage retention of compressive strength as a function of modifier content for CFRP and GRP. The compressive strength curves for both composites coincide.

The longitudinal compressive strength is dependent on many factors including the fibre and resin properties, the interface bond strength and void content. Any factor which leads to a reduction in the support that the matrix and the surrounding fibres give to the fibre to prevent microbuckling will lead to a reduction in compressive strength [19,24].

The scatter observed in this work was not unexpected; composite materials are notorious for it when tested in compression. Neither was its reduction with higher modifier additions. The principal cause is a reduction in matrix modulus caused by matrix plasticisation. These more ductile matrices allowed plastic flow and stress relieving processes to operate which lessened any local stress concentrations.

The interfacial adhesion improved with higher modifier additions, whilst the mechanical properties decreased. In the case of GRP the weak adhesion in unmodified matrices allowed fibre debonding and thus easier kinking of the fibres. However, the hard brittle matrices initially tended to support the fibre but once they had kinked the composite failed by splitting and cracking due to transverse expansion. As the modifier additions increased there was a shift from interface to a matrix controlled failure process. The soft, ductile matrices offered little support for the fibres and kinking occurred at low strain energies.

Early theoretical treatments of failure are based on one suggested by Rosen [1] in which failure is attributed to fibre instability (buckling), within an essentially elastic matrix. However, in the case of unidirectional CFRP, agreement was particularly poor (Ewins and Potter [36]).

Ewins and Hain [12] suggested that, while fibre instability could cause failure, a more usual mode of failure for carbon fibres in an epoxy matrix, particularly at or below room temperature, was one depending on the compressive strength of the fibres themselves. It was suggested that shear failure occurred when initiated at fibre flaws. While the fibre strength dominated mode, sets an upper bound on compressive strength, it does not preclude the occurrence of other failure modes at lower stresses under different circumstances.

Hancox [14] suggested that poor ILSS and high void content can depress the compressive strength substantially and it is possible that these factors might also reflect a change in failure mode. Increased voidage in the matrices decreased their compressive strength. Hancox found that 15% of voids in the composites decreased the compressive strength by half. The voidage increased with high percentage of modifier. Voids may have also introduced excessive fibre misalignment into the specimens.

Matrix stiffness, especially shear modulus, is a major parameter in stability analysis. With unmodified CFRP composites the failure mode was shear. As the matrix stiffness decreased the mode changed to one of fibre instability. Further modifier additions and corresponding reductions in matrix modulus are likely to result in a rapid reduction in compressive strength. Ewins and Hain [12] showed that a moderate temperature increase will cause sufficient reduction in matrix stiffness to allow instability modes to dominate and compressive strengths to be substantially reduced.

The variation in compressive strength with percentage modifier, showed a similar relationship to that found for tensile strength and interlaminar shear strength.

#### 5.4.3 Compressive Failure Strain

The average compressive failure strain results for both composites are presented in Fig. 4.31 plotted vs the percentage of modifier content in the matrix. By observation a curve is more suitable for the CFRP results, while a regression line is better for GRP results.

The same analysis used previously in obtaining rate of decrease was applied to the compressive failure strain results. It can be seen (by comparison of Figs. 4.32 and 4.42) that there is a similar behaviour in compression and in tensile failure strain for GRP composites. The compressive failure strain of the CFRP composites does not show as much fluctuation as the GRP but continuously decreases.

At a 10% modifier addition, both composites showed a similar 15% decrease. As the modifier increases the carbon fibre composites were more affected. This is due to the greater interfacial adhesion improvement in carbon fibre composites compared with glass fibre composites. (This does not appear to such a great extent in tensile failure strain since they fail by a totally different mechanism).

The basis of Rosen's compressive strength model for unidirectional fibre composite materials was that microbuckling of fibres occurs throughout the composites. If this could begin to occur before failure, then the modulus of the composites would certainly be affected. Buckled fibres would result in lower composite modulus than straight fibres. Fig. 5.56 represents results of the compressive

failure strain as a function of the square root of the matrix-to-fibre modulus ratio. It is seen to be fairly proportional. This conforms with the equation predicted by Rosen [1] and Hahn [24], (i.e. compressive failure strain is proportional to the square root of the matrix-to-fibre modulus ratio).

$$\epsilon_c \propto \left(\frac{E_m}{E_f}\right)^{1/2} \quad 5.3$$

where  $\epsilon_c$  = compressive failure strain

$E_m$  = matrix modulus

$E_f$  = fibre modulus

In Plate 37, the side of a failed modified GRP specimen clearly shows kinking induced failure over one wavelength. Plate 38 shows the failure side of a high modified CFRP specimen. More localised buckling failure than GRP is apparent. If failure does not follow immediately, buckling may spread along the fibre axis. Since the carbon fibres have lower tensile failure strain than glass, the modified CFRP fails immediately after buckling causing low strain results and compressive strength. Unmodified CFRP failed in shear without buckling, resulting in higher strain. Buckling induced failure became more evident with low modulus fibre in softer matrices.

#### 5.4.4 Compressive Failure Behaviour

In this work there was a transition from one mode of failure to another across the range of specimens tested. The kinking failure mechanism was observed in both composites. The kink-band usually occurred on a plane at an angle to the direction of loading. All the compression specimens failed suddenly without warning.

The failure mode observed in unmodified GRP specimens is shown in Plate 8. The fibre kinking/splitting shown was typical of all GRP composites. The  $70^{\circ}$  plane of the single or multiple kink-band fracture appeared to be a characteristic of this type of failure.

Plate 9 shows the failure mode in a GRP specimen with 20% addition of modifier to the matrix. The kink-band pattern consists of a narrow single band, oriented at approximately  $90^{\circ}$  to the direction of the applied load. In the specimens with higher modifier content (i.e. 60%), the kink-band was wider and near the end tabs, and approximately at  $90^{\circ}$  to the specimen axis (Plate 10). In all modified GRP specimens, kinking also occurred through the specimen thickness. A typical example is shown in Plate 11.

This type of kink-band failure was also observed in modified CFRP specimens with >10% modifier addition (see Plate 14). It is concluded therefore that the  $70^{\circ}$  kink-band is not a function of fibre parameter, but is a characteristic of this type of failure. Heumann [25] recently observed the same type of failure in vinyl ester GRP composites made by similar wet lay-up techniques.

Plate 12 shows an unmodified CFRP specimen. The mode of failure was by shear on a plane at about  $45^{\circ}$  with loading direction. SEM micrographs of the fracture surface, shown in Plates 33 and 34, confirm this type of failure.

As the modifier addition slightly increased (i.e. <10%), the compressive strength decreased, probably due to a decrease in the contribution to strength of the matrix. As the modifier increased and the matrix modulus decreased at some critical percentage of modifier

the failure mode changed to one governed by fibre instability. The fracture surface appeared to be at  $70^{\circ}$  to the axis of loading (Plate 13).

An SEM micrograph of the fracture surface of a 5% modified CFRP specimen is shown in Plate 35. It revealed steps in the fracture surface also typical of microbuckling. Clearly several planes of fracture are formed and the transmission of this type of failure through the cross-section takes place at an angle to the specimen's cross-sectional plane. A high magnification SEM micrograph of individual fibres on the fracture surface of a 5% modified CFRP, shown in Plate 36, supplies clear evidence of fibre microbuckling. This suggests that the microbuckling of fibre starts with buckling of a single fibre and progresses with additional fibres as the damage propagates. Similar behaviour was confirmed by Ewins and Hain, when they raised the temperature of the composite to reduce the matrix stiffness.

In CFRP specimens with greater than 10% modifier the fibre microbuckling did not lead to actual fracture of the specimen. Instead kink bands formed as already described in GRP.

It can be concluded that in all the GRP composites and modified CFRP composites studied in this work, failure took the form of kinking, or microbuckling. Kinking involved the formation of a regular kink band pattern oriented at  $70^{\circ}$  or less than  $90^{\circ}$  to the direction of the applied load. While microbuckling fracture involves large post-buckling deformation of the fibre in which multiple or single fracture occurred due to the high bending strains.

The failure sequence involving both the above mechanisms for unidirectional composites is proposed as follows. As the compression load is increased, the weakest fibres, or the fibres that have the least lateral support because of a free boundary, poor fibre to matrix bond, or voids fail first. The failure initiation may also be due to the stress concentration introduced by test hardware.

The behaviour observed by Chaplin [15] was very similar to that observed in this work. His proposal that kink bands initiate at defects and propagate from them to cause total compressive failure, appears to offer an acceptable account of the observed behaviour. Chaplin proposed that the formation of kink bands arose from a shear instability in a volume of material. He considered a shear instability of the type shown in Fig. 2.7a, which gives the same theoretical results as Rosen's [1] shear instability model (in-phase mode, shown in Fig. 2.1b), in a band of material inclined at an angle to the compression axis. Neglecting the effects of any changes in axial stress and considering only the effects of shear rotation within the band, Chaplin suggested that the volumetric strain within the sheared band is given by:

$$\epsilon_{vol} = \frac{\cos(\alpha - \tau)}{\alpha} - 1 \quad 5.4$$

where  $\epsilon_{vol}$  = volumetric strain

$\tau$  = shear strain

$\alpha$  = kink band angle.

Therefore, for  $\alpha > 0$  the volumetric strain will initially be positive, returning to zero when  $\tau = 2\alpha$ . This volumetric strain argument is dependent on assuming that as the shear deformation increases the orientation of the kink band and the length of fibres within it do not change.

In a unidirectional fibre composite under axial compression, once there has been any significant amount of interfacial failure, then there will be little resistance to a large positive volumetric strain. However, if transverse expansion is restricted in any way, then the expected effect of this constraint would be an increase in compressive strength. There is therefore a limit set on the axial compressive displacement associated with a shear failure in terms of the inclination of the kink band, and the associated maximum shear strain equal to  $2\alpha (= \tau)$ .

Using notched specimens, Chaplin demonstrated that compressive failure can propagate from a pre-existing defect through the formation of a kink band. The sequence of events in such a failure was as follows:

- i) Shear deformation in a band of material which increased, but without a change in the orientation of the band itself.
- ii) As deformation increased considerable kinking of the fibres at the boundary of the band. This often resulted in fibres fracturing at the boundaries.
- iii) As deformation increased further, the adhesion between fibre and matrix broke down. As this interlaminar failure occurred after fibre kinking it was arrested at the boundaries.

Once initiated the kink bands often propagated very rapidly through the specimens. The varying amounts of damage associated with the kink band mechanism may be explained in terms of strain energy consideration.

An unmodified matrix (brittle), stores more strain energy prior to failure than a (ductile) highly modified matrix, by virtue of its higher yield strength and stiffness. Upon failure this energy is released. If the level of strain energy is high, the kink band mechanism may not consume it all. The excess energy manifests itself as clearly audible longitudinal resin cracking, surface layer delamination, etc. As the matrix properties decreased with higher modifier additions, so the strain energy decreased. As modifier additions increased specimens tended to show single kink bands through their thickness rather than the multiple kink bands across their widths. This was noticed in GRP composites. In the case of CFRP composites with modifier additions, specimens again tended to show single kink bands without fibres fracturing. This trend simply reflects the progressively lower strain energies associated with the formation of kink bands at higher modifier additions.

It may be true that it is not easy to manufacture a specimen which is totally free of defect. In practice, imperfection in the fibre alignment always exists and such regions form a failure nucleus by undergoing a kinking process [10].

In this work the method of preparing GRP and CFRP laminates, was the manual winding process and impregnation with resin which resulted in a certain amount of fibre breakage and misalignment. The reason why the Rosen [1] prediction of strength appears to be so high is because it

considers the composite to be made up of perfectly straight, aligned fibres. Lager and June [8] found good agreement to Rosen's theory when they multiplied the results by a constant reduction factor, when using two kinds of epoxy resin (i.e. hard and soft).

Piggott and Harris [16] observed very similar behaviour in specimens when the same resins were used as a matrix for composites reinforced with carbon and glass fibres. CFRP composites failed in a brittle manner in two halves with a single transverse crack, when a fully cured resin matrix was used, while GRP specimens exhibited multiple kink bands. With a just gelled matrix the behaviour showed localised narrow kink bands through the thickness, which had also been noted by Chaplin previously and was apparent in this work.

The fibre microbuckling in CFRP composites under compression has been noted by Yasushi [38]. He confirmed the fact that the time and temperature dependence of compressive strength in unidirectional CFRP is the same as the viscoelastic behaviour of the matrix epoxy resin. He also concluded that the longitudinal compressive strength of CFRP was dominated by the deformation properties of the matrix resin, as illustrated in the work reported here.

# CHAPTER 6

## CHAPTER 6

### CONCLUSIONS

The use of glass fibres and carbon fibres with a variety of epoxy resin systems can provide much information on the compressive failure mechanisms in fibre composite materials. The work presented in this study indicates that there are two kinds of failure which can be clearly distinguished. Kinking-induced failures and shear-induced failures. Further specific conclusions are described below.

1. The tensile secant moduli for both modified and unmodified composites obey the rule of mixtures. The compressive moduli disobeys the ROM.
2. The composite compressive modulus is more dependent on the resin modulus than is the tensile modulus. This is due to the fibre being less stiff in compression than in tension due to buckling. An additional reason is that under compression the initial misalignment of the fibres may impose high local stress on the matrix, thus pushing the matrix into a non-linear range at an early stage of loading.
3. The stiffness of unmodified GRP composites in compression and tension was the same, while the stiffness of unmodified CFRP composites in compression was 47% lower than in tension.
4. Modified and unmodified CFRP composites had a higher tensile moduli than similar glass reinforced composites. This variation is due to the fibre modulus itself.

5. Generally tensile, compressive and inter-laminar shear strength decreased with increasing percentage modifier in the matrix.
6. The matrix properties had a significant effect on the compression behaviour of the composites during increasing matrix plasticisation. They controlled both the compressive strength and failure behaviour observed.
7. Interfacial adhesion improved with higher modifier additions, whilst the matrix properties decreased. Adhesion was better with carbon, compared with glass, for all the matrices. However, these differences did not have a significant effect on strength when compared to other matrix properties.
8. The tensile and compressive strengths of the composites with unmodified brittle matrices was interface controlled. As the modifier addition increased there was a shift from interface to matrix controlled failure.
9. The tensile failure appearance for unmodified GRP was brush-type. The modified GRP showed less debonding and the UTS was reached before interface cracks propagated through the specimen, therefore only parts of the failures were brush-types. Unmodified CFRP failed by crack propagation, both transverse and parallel to the direction of loading. The modified CFRP specimens failed by multiple cracking parallel to the loading axis but was not as brush-like as the unmodified GRP.

10. The tensile strength of CFRP showed a 1% decrease with 5% modifier addition, while GRP showed a 23% decrease. This was believed to be due to the better interface adhesion in carbon fibres.
11. Fibre misalignment defects had the most significant effect in highly modified composites, reducing compressive strength considerably. Such defects are a considerably more important factor in compressive as compared with tensile failure.
12. In GRP composites the only general compressive failure mechanism was kinking. The degree of this varied across the range of specimens tested. The amount of damage associated with failure decreased progressively with modifier addition. Initially multiple or single kinking, splitting behaviour at  $70^{\circ}$  to the fibre axis was noted and this gradually changed to a single kink band  $90^{\circ}$  to the fibre axis.
13. In the CFRP systems studied, three different mechanisms of compressive failure occurred. Unmodified CFRP failed by fibre and matrix shear. With modifier increases the matrix modulus decreased and at some critical percentage of modifier (<10%), the failure mode changed to one governed by fibre instability (fibre microbuckling). At higher modifier >10% the fibre microbuckling did not lead to actual fracture of the specimen, instead kink bands formed.
14. The best compressive strengths were exhibited by unmodified CFRP composites in which shear failure occurred. In this mode strength was limited only by fibre properties.

15. Voidage increased with percentage of modifier in the matrix. The voids acted as stress-raisers and contributed to the reduction in composite properties but were not solely responsible.

# REFERENCES

REFERENCES

1. Rosen, B.W. "Mechanics of Composite Strengthening", Fibre Composite Materials, Chapter 2, American Society for Metals, 1965, pp 58-65.
2. Schuerch, H. "Compressive Strength of Boron/Metal Composites", April 1965, NASA CR-202.
3. Foye, R.L. "Compression Strength of Unidirectional Composites", AIAA Third Aerospace Sciences Meeting, New York, USA, 1966, pp 66-143.
4. Hayashi, T. "Mechanics of Fibre Reinforced Materials", Jour. Japan Soc. Mech. Eng. Vol. 71, No. 593, 1968.
5. Hayashi, T. "Strength Theory of Fibre Reinforced Composite Materials". Jour. Japan Soc. Aero. Space Sci., Vol. 71, No 183, 1969.
6. Hayashi, T. "On the Shear Instability of Structures Caused by Compressive Loads", Proc. 16th Japan Nat. Congress for Applied Mechanics, 1966, pp 149-157.
7. Hayashi, T. "Compressive Strength of Unidirectionally Fibre Reinforced Composite Materials", 7th International Reinforced Plastics Conf., Brighton, UK, 1970, Paper 11.
8. Lager, J.R. and June, R.R. "Design Analysis Fabrication and Test of a Boron Composite Beam", J. Comp. Mat., April 1968, pp 178.
9. Orringer, O. AFOSR, TR 71 3098, 1971.

10. Argon, A.S. "Fracture of Composites", Treatise on Mats. Sci. and Tech., Edited by H. Herman, Academic Press, 1972, pp 79-114.
11. Harris, B. "The Strength of Fibre Composites", Composites 3 (July 1972), pp 152-167.
12. Ewins, P.D. and Ham, A.C. "The Nature of Compressive Failure in Unidirectional Carbon Fibre Reinforced Plastics", Royal Aircraft Establishment, TR 73057, 1973.
13. Greszczuk, L.B. "Consideration of Failure Modes in the Design of Composite Material", AGARD Conference Proceedings, 163, Paper 12, 1974.
14. Hancox, N.L. "The Compressive Strength of Unidirectional Carbon Fibre Reinforced Plastics", J. of Mats. Sci. 10, 1975, pp 234-242.
15. Chaplin C.R. "Compressive Fracture in Unidirectional Glass-Reinforced Plastics", J. of Mats. Sci. 12, 1977, pp 347-352.
16. Piggott, M.R. and Harris, B. "Compression Strength of Carbon, Glass and Kevlar-49 Fibre Reinforced Polyester Resins", J. of Mats. Sci. 15, 1980, pp 2523-2538.
17. Martinez, G.M., Piggott, M.R., Bainbridge, D.M.R. and Harris, B. "The Compression Strength of Composites with Kinked, Misaligned and Poorly Adhering Fibres", J. of Mats. Sci., 1981, pp 2831-2836.
18. Hull, D. "An Introduction to Composite Materials", Cambridge University Press, (1981), Chapter 7.

19. Parry, T.V. and Wronski, A.S. "Kinking and Compressive Failure in Uniaxially Aligned Carbon Fibre Composites Tested Under Superposed Hydrostatic Pressure", J. of Mats. Sci., 17, 1982, pp 893-900.
20. Wronski, A.S. and Parry, T.V. "Compressive Failure and Kinking in Uniaxially Aligned Glass-Resin Composites Under Superposed Hydrostatic Pressure", J. of Mats. Sci., 17, 1982, pp 3656-3662.
21. Lee, B.L. and Howard, F.H. "Effect of Matrix Toughening on the Strength and Strain Properties of SMC", Proc. of 36th Ann. Tech. Conf. of SPI Reinf. Plastics/Comp. Inst., Sect. 23E (1981).
22. Piggott, M.R. "Compressive Properties of Resins and Composites", Chapter 4, 1984, Development in Reinforced Plastics, pp 131-163.
23. Hahn, H.T. "Effects of Constituent Properties on Compression Failure Mechanisms", Tough Composite Materials, NASA, Langley Research Centre, 1985, pp 72-88.
24. Hahn, H.T. and Williams, J.G. "Compression Failure Mechanisms in Unidirectional Composites", Composite Materials Testing and Design, 7th Conf. (1986), pp 115-139.
25. Heumann, T.O. "Elastic Properties and Failure Mechanisms in Hybrid Composites with Differing Resin Matrices", A Doctoral Thesis, Loughborough University of Technology, 1987.
26. Woolstencroft, D.H., Curtis, A.R. and Haresceugh, R.I. "A Comparison of Test Techniques Used for the Evaluation of the Unidirectional Compressive Strength of Carbon-Fibre Reinforced Plastic", Composites, Vol. 12, Oct. (1981), pp 275-280.

27. Chamis, C.C. and Sinclair, J.H. "Longitudinal Compressive Failure Modes in Fibre Composites: End Attachment Effects on IITRI Type Test Specimens", J. of Comp. Tech. and Res., Vol. 7, No. 4 (1985), pp 129-135.
28. Lee, R.J. "Compression Strength of Aligned Carbon-Fibre Reinforced Thermoplastic Laminates", Composites, Vol. 18, No. 1 (1987), pp 35-39.
29. Barker, A.J. and Balasundaram, V. "Compression Testing of Carbon-Fibre-Reinforced Plastics Exposed to Humid Environments", Composites, Vol. 18, No. 3 (1987), pp 217-226.
30. Haynes, W.M. and Tolbert, T.L. "Determination of the Graphite Fibre Content of Plastic Composites", J. Composite Materials, Vol. 3, October 1969, pp 709-712.
31. ASTM Standard Test Methods: D3410-87 for Compressive Properties of Unidirectional or Crossply Fibre-Resin Composites 1987.
32. British Standard Methods of Testing Plastics: 2782: Part 3 - Mechanical Properties Methods 320A to 320F. Tensile Strength, Elongation, and Elastic Modulus, 1976.
33. British Standard Methods of Testing Plastics 2782: Part 3: Method 341A: 1977, Determination of Apparent Interlaminar Shear Strength of Reinforced Plastics.
34. M-Line Accessories: "Surface Preparation for Strain Gauge Bonding", Instruction Bulletin B-129, May 1976.
35. M-Line Accessories: "Strain Gauge Installations with M-Bond 200 Adhesive", Instruction Bulletin B-127-9, 1979.

36. Ewins, P.D. and Potter, R.T. "Some Observations on the Nature of Fibre Reinforced Plastics and the Implications for Structural Design", Phil. Trans. R. Soc. Lond. A294, 1980, pp 507-517.
37. Harper, J.F. and Heumann, T.O. "The Strain Dependence of Elastic Modulus in Unidirectional Composites", Composite Evaluation, Ed. J. Herriott, Proceedings Testing Evaluation and Quality Control of Composites, 22-24 Sept. 1987, Pub. Butterworths.
38. Yasushi, M. and Manabu, K. "Role of Matrix Resin on Fracture Strength of Unidirectional CFRP", J. of Composite Mat., Vol. 20, Nov. 1986, pp 520-538.

# TABLES

TABLE 4.1: MEAN VALUES OF FIBRE VOLUME FRACTION.

% Mod Spec No	$V_{fg}$ (%)	$V_{fc}$ (%)	$V_{voids}$ (%)
0% - 1	44.4	42.7	0.71
0% - 2	43.4	45.8	
5% - 1	46.9	45.8	0.95
5% - 2	46.0	44.4	
10% - 1	40.8	40.7	0.93
10% - 2	40.3	48.2	
20% - 1	47.2	44.9	1.06
20% - 2	41.0	54.3	
30% - 1	45.4	51.6	1.55
30% - 2	42.0	55.1	
40% - 1	46.3	49.3	1.26
40% - 2	44.2	51.6	
50% - 1	48.1	49.3	1.95
50% - 2	41.2	50.7	
60% - 1	45.2	50.3	1.78
60% - 2	43.0	50.4	

TABLE 4.2: MEAN VALUE OF MATRIX RESIN DENSITY

Laminate % Modifier	Mean Value $m \text{ (gcm}^{-3}\text{)}$	Deduced Value $m \text{ (gcm}^{-3}\text{)}$
0%	1.123	1.127
5%	*	1.121
10%	1.118	1.116
20%	1.080	1.104
30%	1.094	1.093
40%	1.087	1.081
50%	1.063	1.070
60%	1.060	1.058

TABLE 4.3: MEAN RESULTS OF MATRIX-RESIN PROPERTIES

Laminate % Modifier	$\sigma_T \text{ (MPa)}$	$\sigma_T \text{ (\%)}$	$E_T \text{ (GPa)}$
0%	58	1.95	2.98
5%	*	*	*
10%	40	8.20	2.00
20%	30	14.35	1.39
30%	21	16.30	0.88
40%	15	34.41	0.58
50%	11	33.90	0.30
60%	9	36.40	0.17

TABLE 4.4: NORMALISED COMPRESSIVE STRENGTH, GRP

Laminate % Modifier	$\sigma_c$ (MPa)	Retention (%)
0%	488	100
5%	412	84
10%	355	73
20%	257	53
30%	206	42
40%	171	35
50%	168	34
60%	96	20

TABLE 4.5: NORMALISED COMPRESSIVE STRENGTH, CFRP

Laminate % Modifier	$\sigma_c$ (MPa)	Retention (%)
0%	602	100
5%	519	86
10%	404	67
20%	313	52
30%	212	35
40%	203	34
50%	162	27
60%	109	18

TABLE 4.6: NORMALISED COMPRESSIVE FAILURE STRAIN, GRP

Laminate % Modifier	$\epsilon_c$ (%)	Retention (%)
0%	1.26	100
5%	1.09	87
10%	1.04	83
20%	1.11	88
30%	0.83	66
40%	0.92	73
50%	0.81	64
60%	0.67	53

TABLE 4.7: NORMALISED COMPRESSIVE FAILURE STRAIN, CFRP

Laminate % Modifier	$\epsilon_c$ (%)	Retention (%)
0%	1.15	100
5%	1.16	100
10%	1.00	87
20%	0.67	58
30%	0.52	45
40%	0.46	40
50%	0.44	38
60%	0.34	30

TABLE 4.8: NORMALISED COMPRESSIVE SECANT MODULUS, GRP

Laminate % Modifier	$E_c$ (GPa)	Retention (%)
0%	43.04	100
5%	39.86	93
10%	40.54	94
20%	26.38	61
30%	21.41	50
40%	20.65	48
50%	19.81	46
60%	13.42	31

TABLE 4.9: NORMALISED COMPRESSIVE SECANT MODULUS, CFRP

Laminate % Modifier	$E_c$ (GPa)	Retention (%)
0%	58.54	100
5%	52.36	89
10%	47.95	82
20%	46.68	80
30%	34.97	60
40%	38.26	65
50%	33.73	58
60%	27.89	48

TABLE 4.10: NORMALISED TENSILE STRNGHT, GRP

Laminate % Modifier	$\sigma_T$ (MPa)	Retention (%)
0%	978	100
5%	754	77
10%	761	78
20%	698	71
30%	672	69
40%	609	62
50%	577	59
60%	512	52

TABLE 4.11: NORMALISED TENSILE STRENGTH, CFRP

Laminate % Modifier	$\sigma_T$ (MPa)	Retention (%)
0%	1392	100
5%	1382	99
10%	1211	87
20%	1236	89
30%	1091	78
40%	1035	74
50%	985	71
60%	898	65

TABLE 4.12: NORMALISED TENSILE FAILURE STRAIN, GRP

Laminate % Modifier	$\epsilon_T$ (%)	Retention (%)
0%	2.37	100
5%	2.04	86
10%	2.11	89
20%	2.14	90
30%	1.97	83
40%	1.74	73
50%	1.78	75
60%	1.58	67

TABLE 4.13: NORMALISED TENSILE FAILURE STRAIN, CFRP

Laminate % Modifier	$\epsilon_T$ (%)	Retention (%)
0%	1.44	100
5%	1.21	84
10%	1.14	79
20%	1.16	81
30%	1.04	72
40%	0.96	67
50%	0.90	63
60%	0.80	56

TABLE 4.14: NORMALISED TENSILE SECANT MODULUS, GRP

Laminate % Modifier	$E_T$ (GPa)	Retention (%)
0%	43.42	100
5%	36.06	83
10%	39.52	91
20%	33.37	77
30%	37.50	86
40%	38.48	89
50%	35.79	82
60%	33.62	77

TABLE 4.15: NORMALISED TENSILE SECANT MODULUS, CFRP

Laminate % Modifier	$E_T$ (GPa)	Retention (%)
0%	109.98	100
5%	117.04	106
10%	115.57	105
20%	107.14	97
30%	95.19	87
40%	105.67	96
50%	109.73	100
60%	108.84	99

TABLE 4.16: NORMALISED INTER-LAMINAR SHEAR STRENGTH, GRP

Laminate % Modifier	ILSS (GPa)	Retention (%)
0%	48.29	100
5%	38.78	80
10%	37.32	77
20%	34.49	71
30%	28.58	59
40%	23.27	48
50%	25.17	52
60%	15.49	32

TABLE 4.17: NORMALISED INTER-LAMINAR SHEAR STRENGTH, CFRP

Laminate % Modifier	ILSS (GPa)	Retention (%)
0%	56.26	100
5%	52.40	93
10%	46.17	82
20%	32.71	58
30%	24.95	44
40%	23.07	41
50%	24.03	43
60%	15.81	28

TABLE 4.18: MACRO-STUDY OF FAILURE MECHANISM FOR COMPRESSION SPECIMENS

% Modifier	Fibre Reinforced	Failure Mechanism	Angle Across
0	GRP	Splitting/kinking (multiple or single kink-band)	70
0	CFRP	Fibre and matrix shear failure	45
5	GRP	Splitting/kinking (multiple or single kink-band)	70
5	CFRP	Fibre shear failure on fibre microbuckling	70
10	GRP	Kinking (single kink-band)	70
10	CFRP	Fibre microbuckling	70
20	GRP	Kinking (narrow single kink-band)	70-90
20	CFRP	Kinking (narrow single kink-band)	70-90
30	GRP	Kinking (narrow single kink-band)	70-90
30	CFRP	Kinking (narrow single kink-band)	70-90
40	GRP	Kinking (narrow single kink-band)	90
40	CFRP	Kinking (narrow single kink-band)	90
50	GRP	Kinking (wide single kink-band)	90
50	CFRP	Kinking (wide single kink-band)	90
60	GRP	Kinking (wide single kink-band)	90
60	CFRP	Kinking (wide single kink-band)	90

# FIGURES

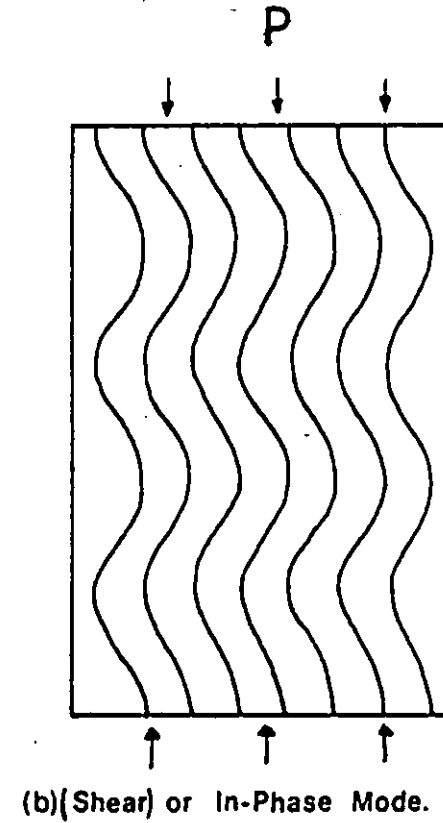
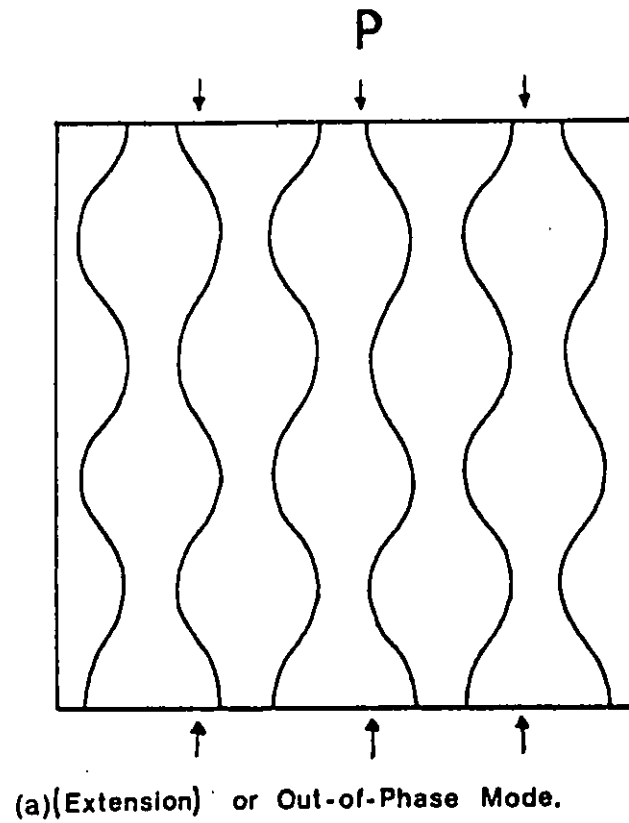


FIGURE 2.1: ROSEN'S ANALYTICAL MODEL FOR THE COMPRESSIVE STRENGTH OF UNIDIRECTIONAL REINFORCED FIBRE COMPOSITES (From Ref 1)

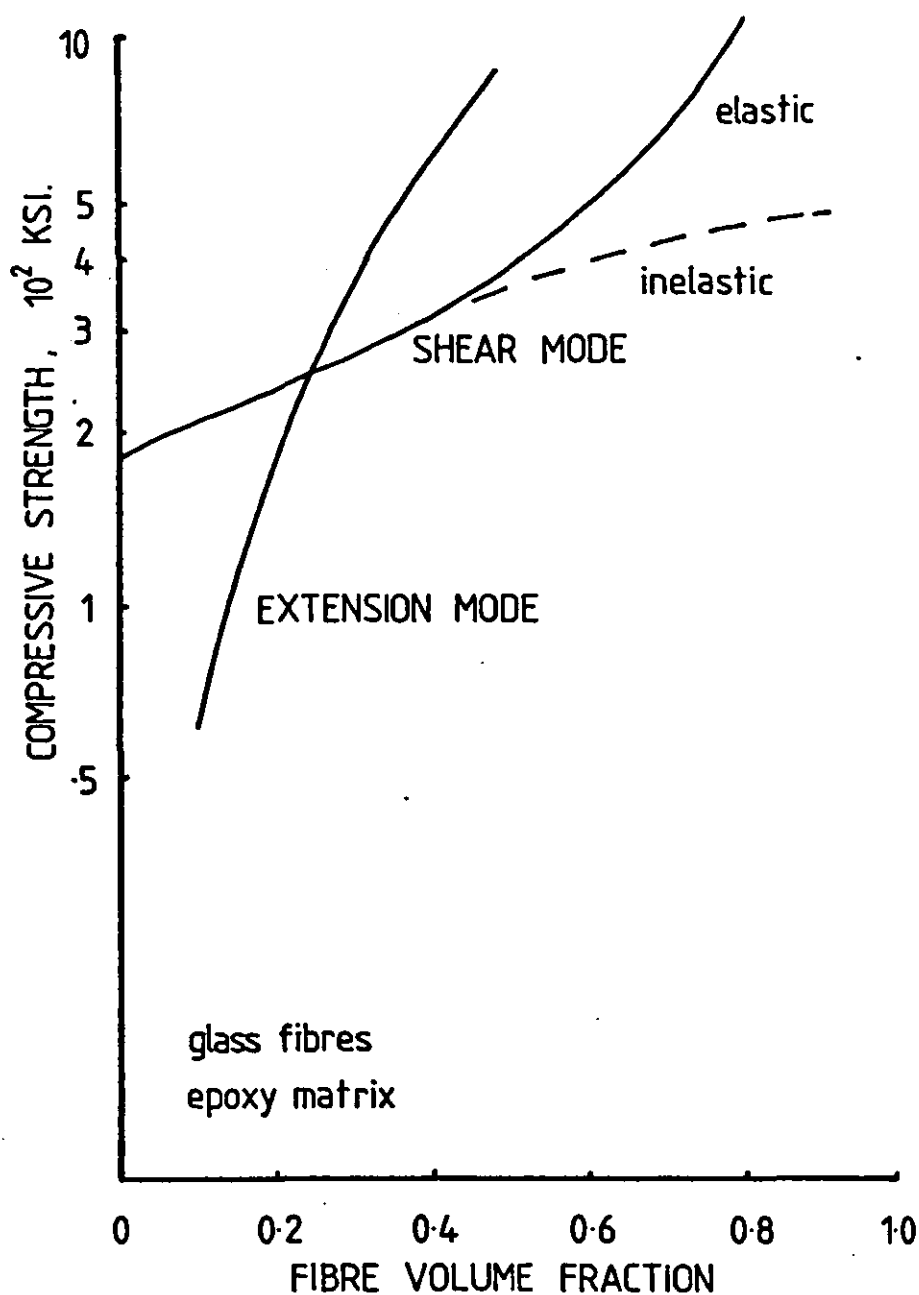


FIGURE 2.2: THE COMPRESSIVE STRENGTH OF GLASS REINFORCED EPOXY COMPOSITES AS PREDICTED BY THE ROSEN BUCKLING MODEL (From Ref 1.)

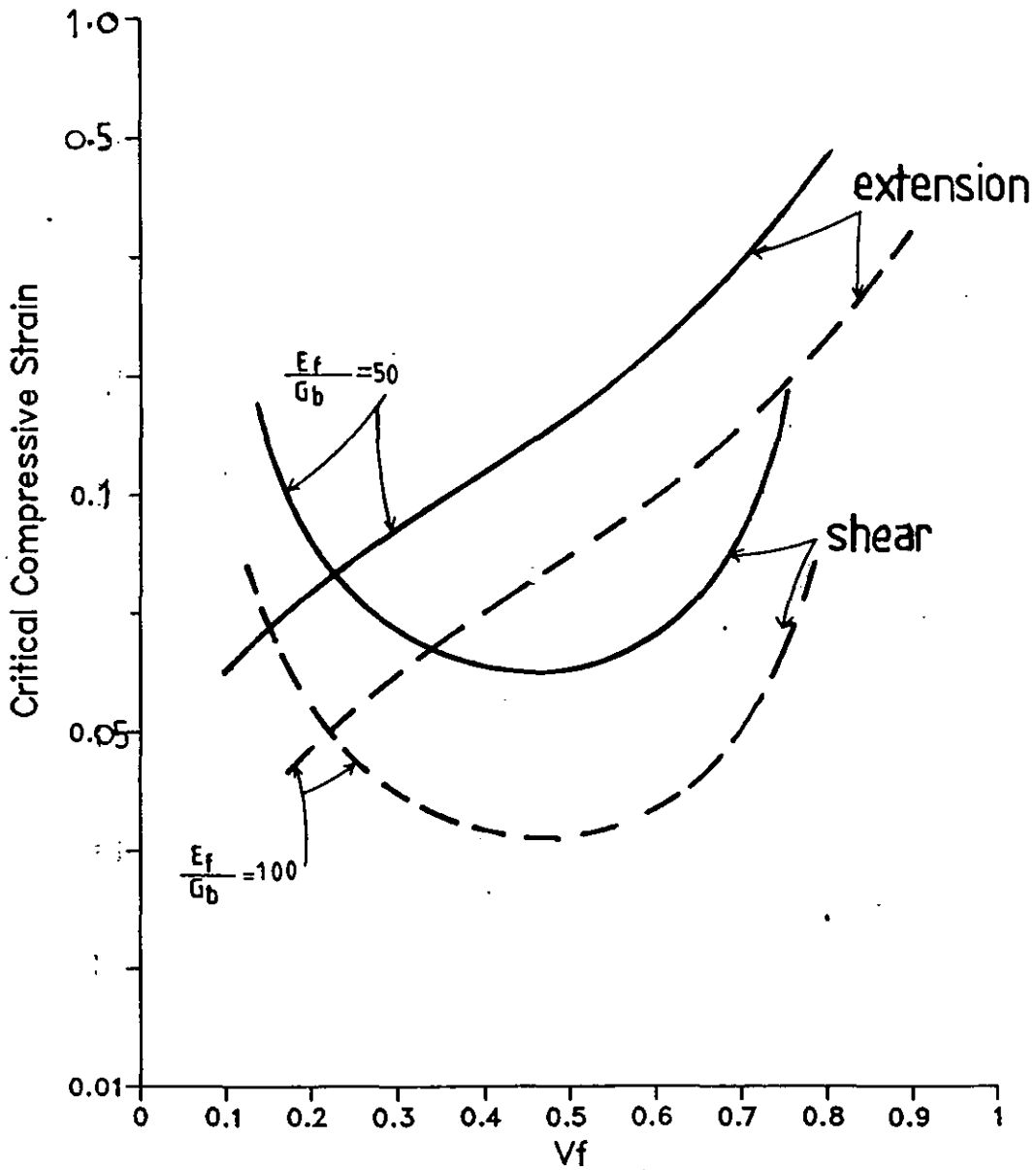


FIGURE 2.3: THE CRITICAL COMPRESSIVE STRENGTH FOR GLASS REINFORCED EPOXY COMPOSITES PREDICTED BY ROSEN (From Ref 1)

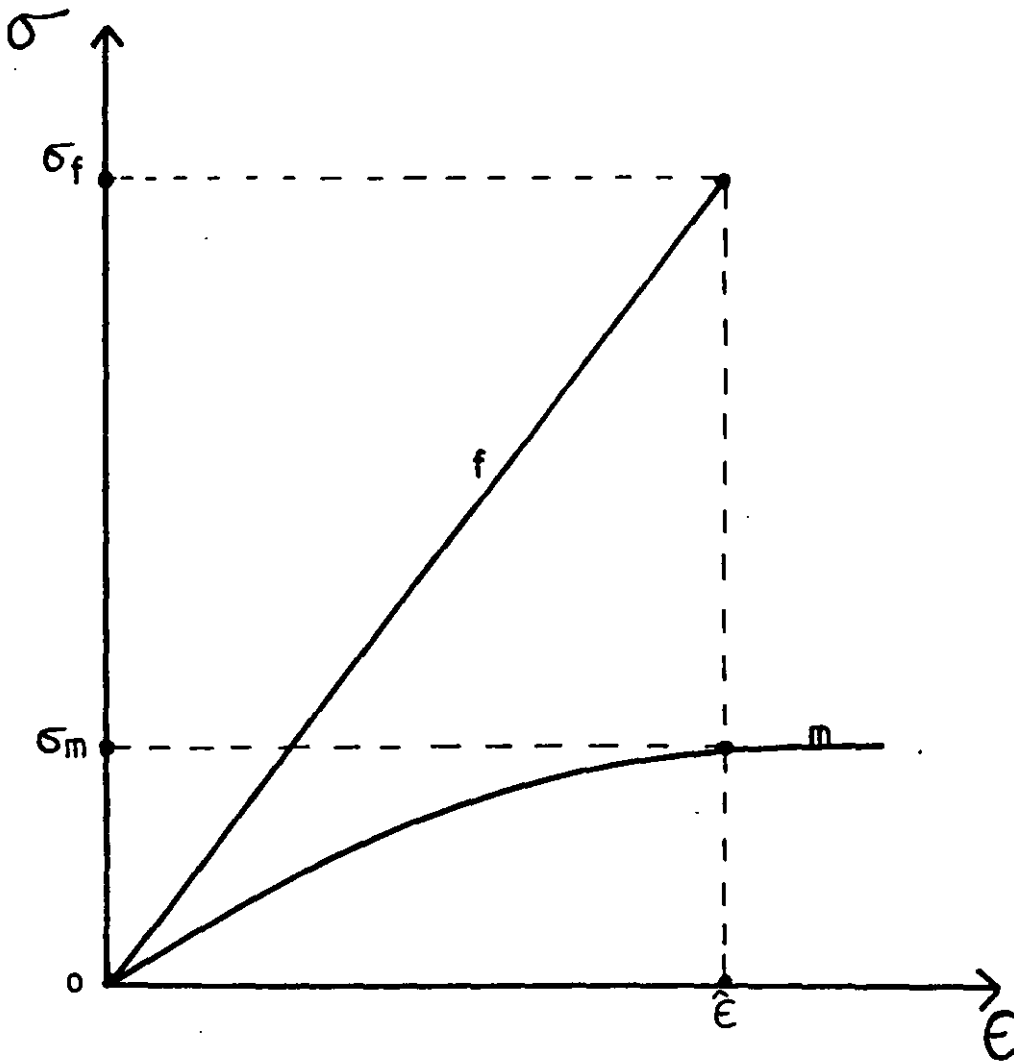


FIGURE 2.4: STRESS-STRAIN CURVES FOR FIBRES AND MATRIX AS PREDICTED BY HAYASHI (From Ref 7)

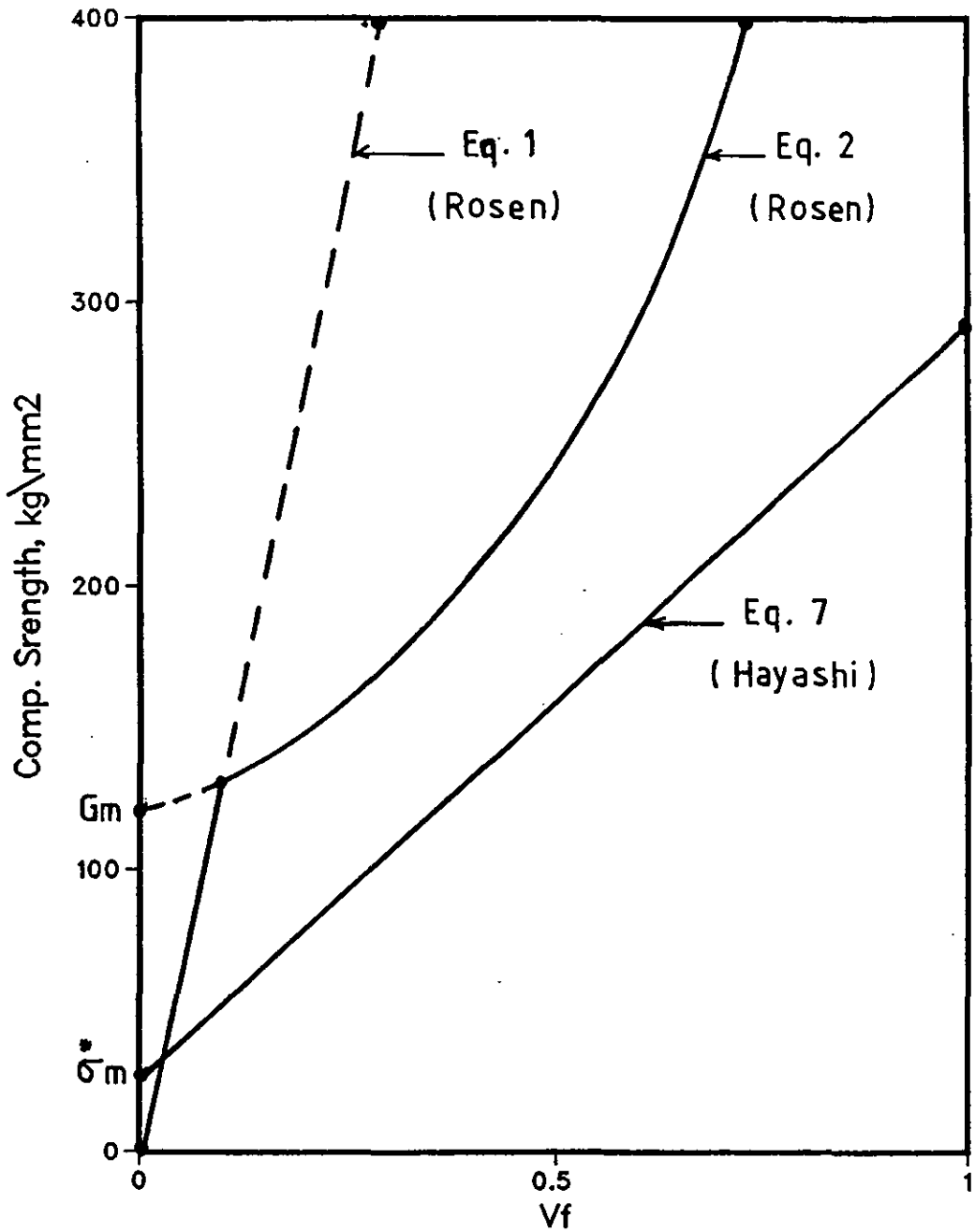


FIGURE 2.5: THE COMPRESSIVE STRENGTH vs FIBRE VOLUME FRACTION CURVES FOR GLASS/EPOXY COMPOSITE BY ROSEN AND HAYASHI (From Ref 7)

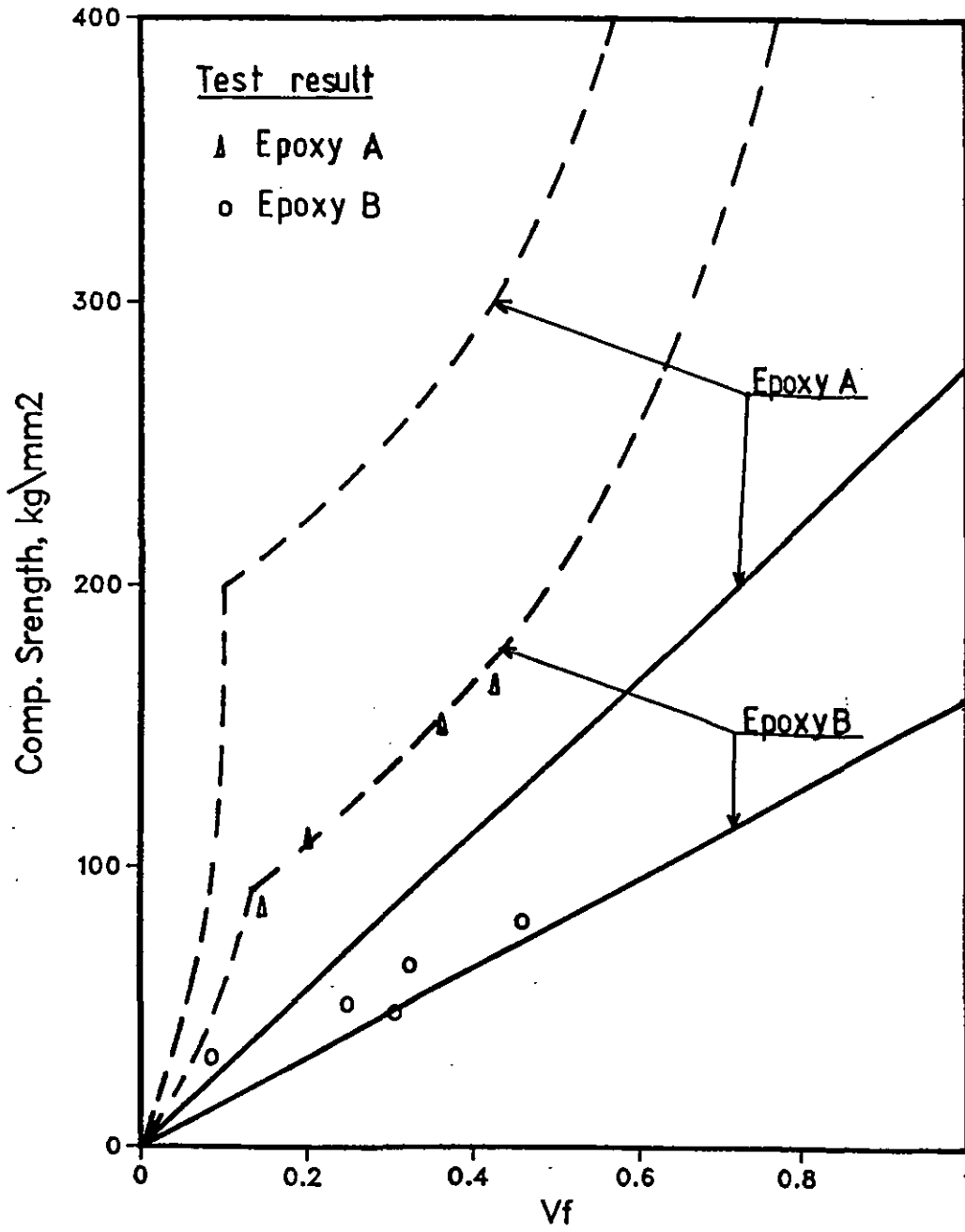


FIGURE 2.6: THE COMPRESSIVE STRENGTH OF BORON/EPOXY COMPOSITE

----- Calculated by Rosen (from Ref 7)

———— Calculated by Hayashi (from Ref 7)

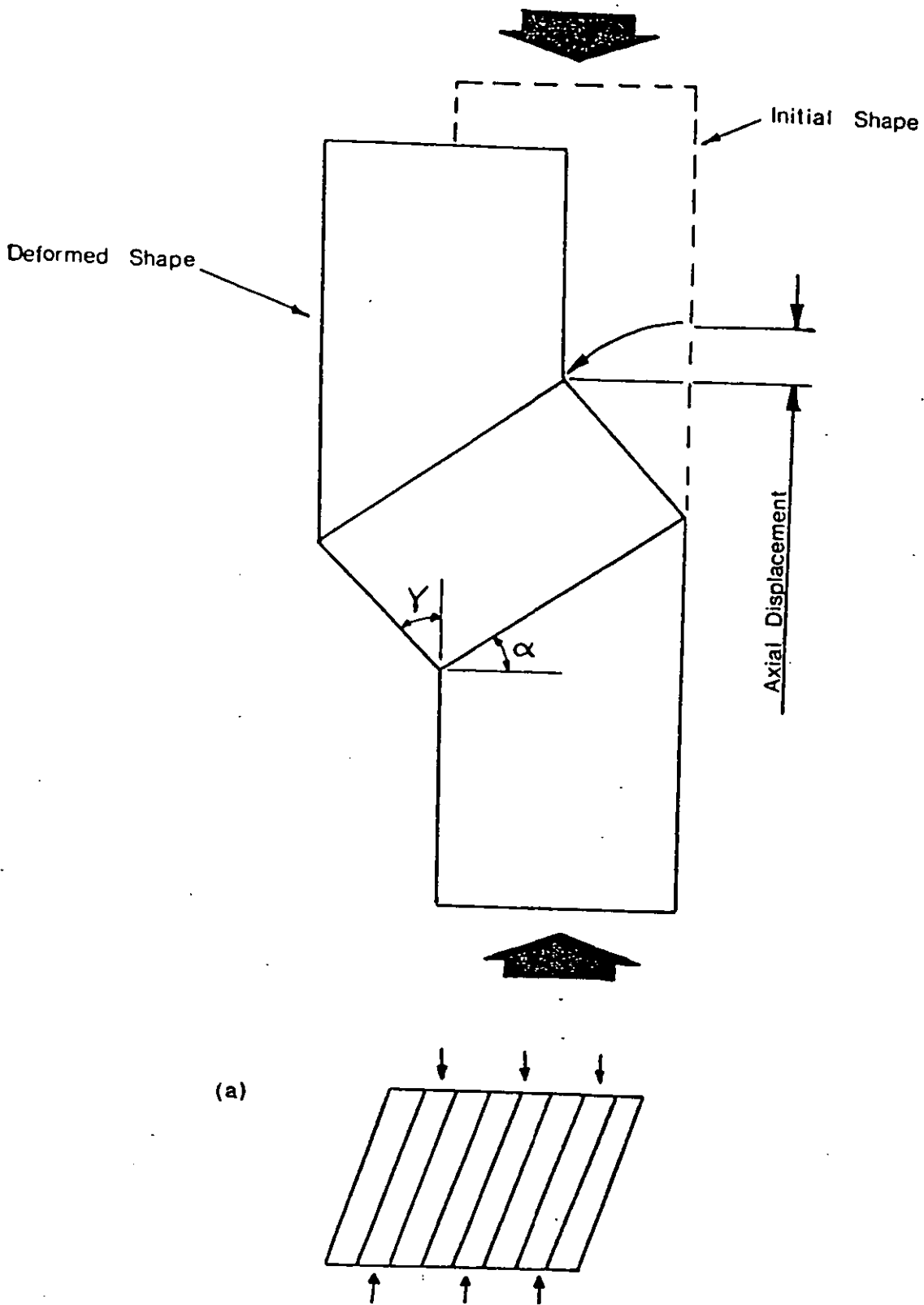


FIGURE 2.7: COMPRESSIVE FAILURE SHOWING THE GEOMETRY OF THE KINK-BAND ACCORDING TO CHAPLIN (From Ref 15)

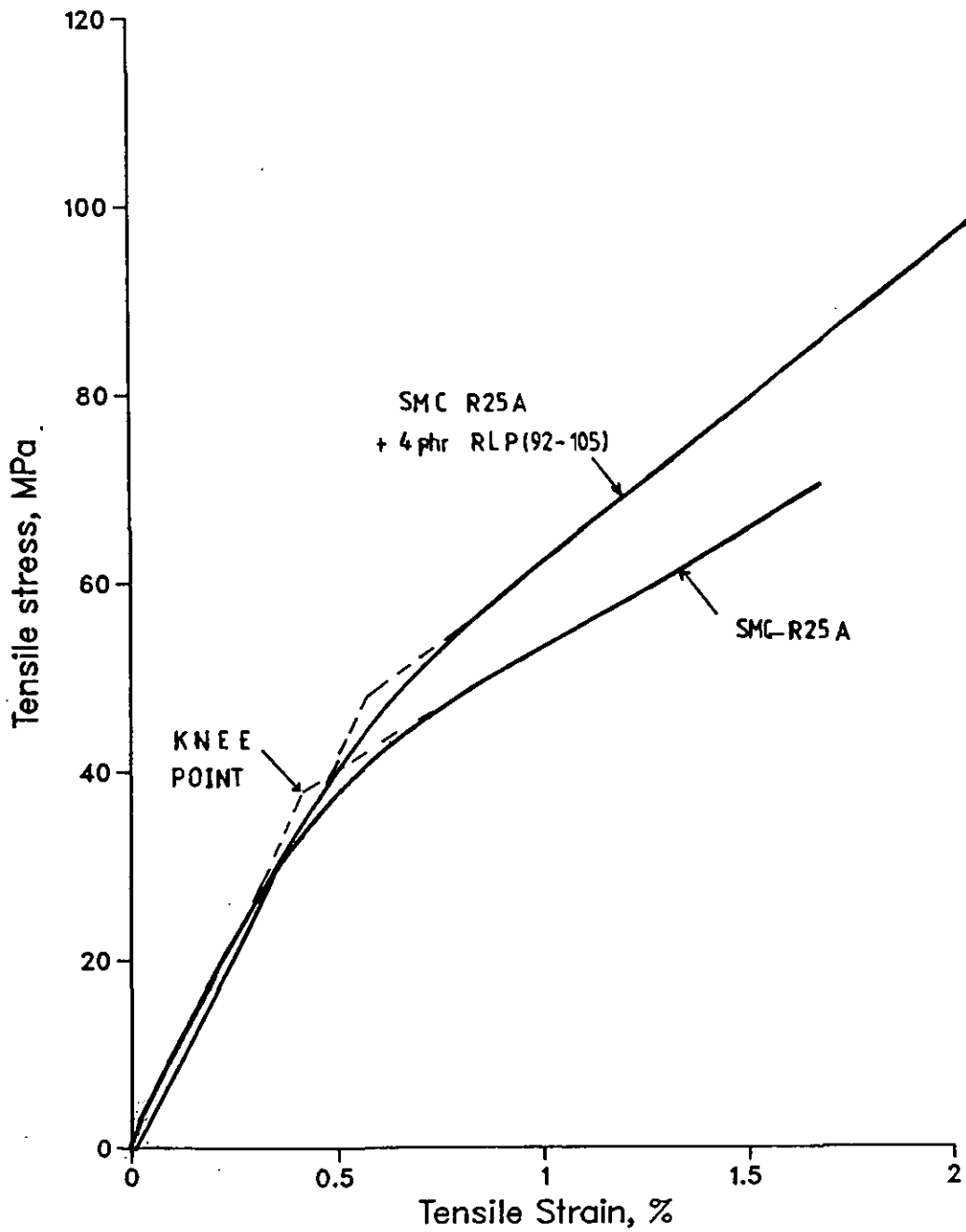


FIGURE 2.8: TENSILE STRESS-STRAIN CURVES FOR SMC-R25A, SHOWING THE EFFECT OF RUBBER TOUGHENING OF THE MATRIX ON THE STRESS AND STRAIN BEHAVIOUR OF THE COMPOSITES (From Ref 20)

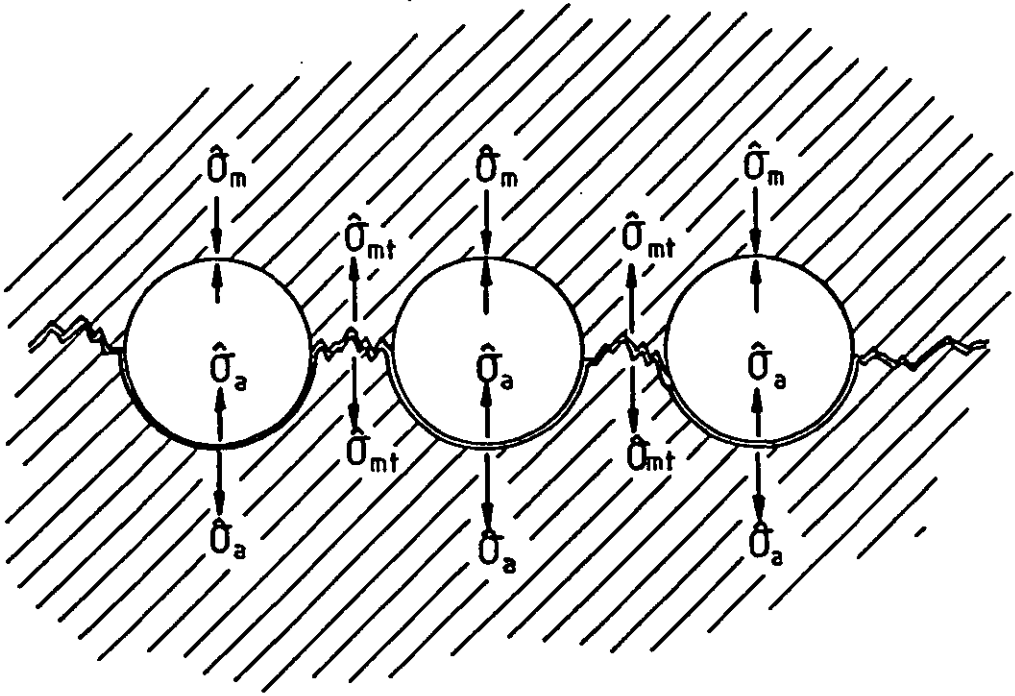


FIGURE 2.9: PIGGOTT'S CONSIDERATION OF INTERFACE AND MATRIX FAILURE AS A RESULT OF SINUSOIDALLY BUCKLED FIBRES (From Ref 22)

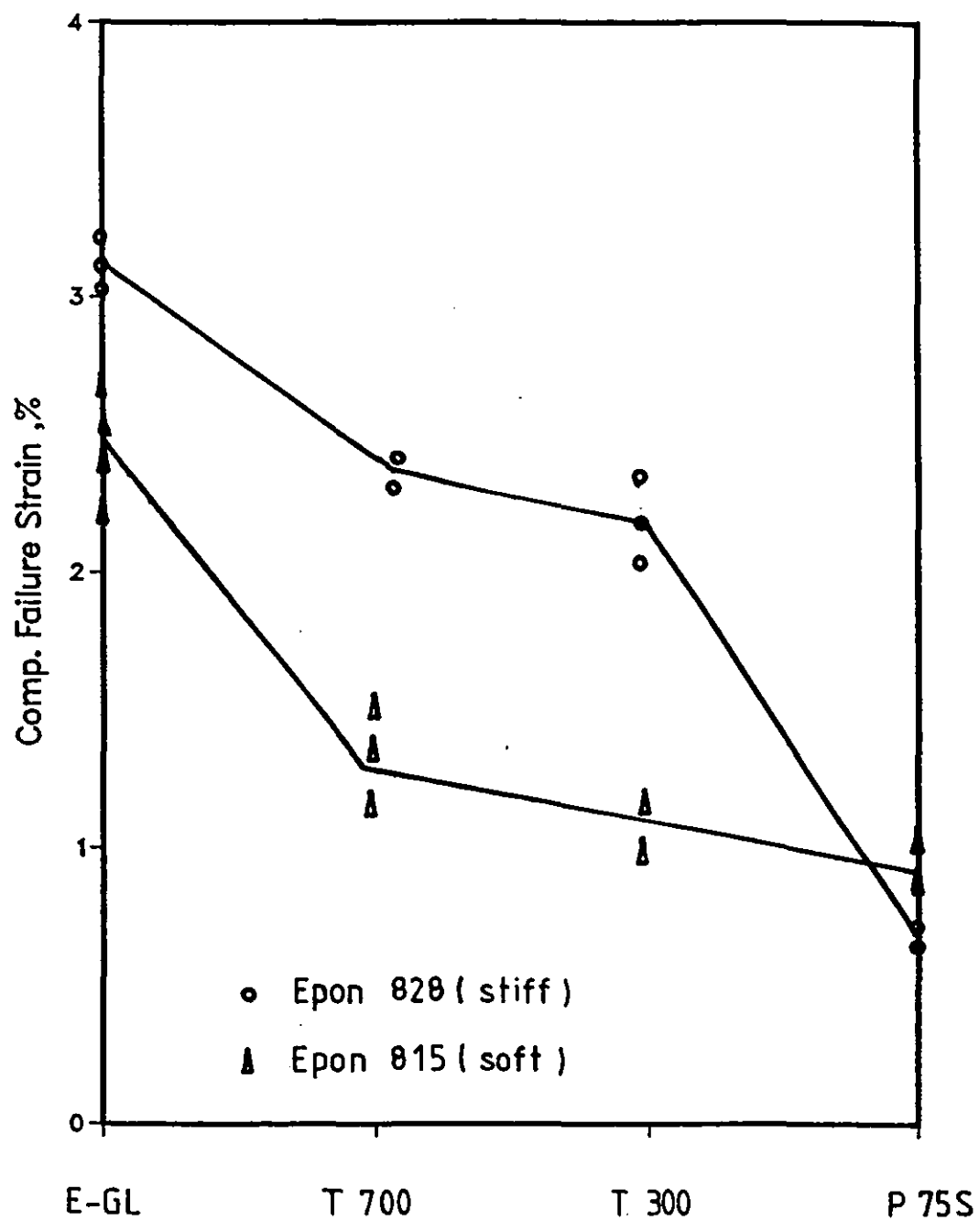


FIGURE 2.10: COMPRESSIVE FAILURE STRAIN vs KIND OF MATRIX BY HAHN, SHOWING THE EFFECTS OF FIBRES AND MATRICES ON THE COMPRESSIVE FAILURE STRAIN (From Ref 23)

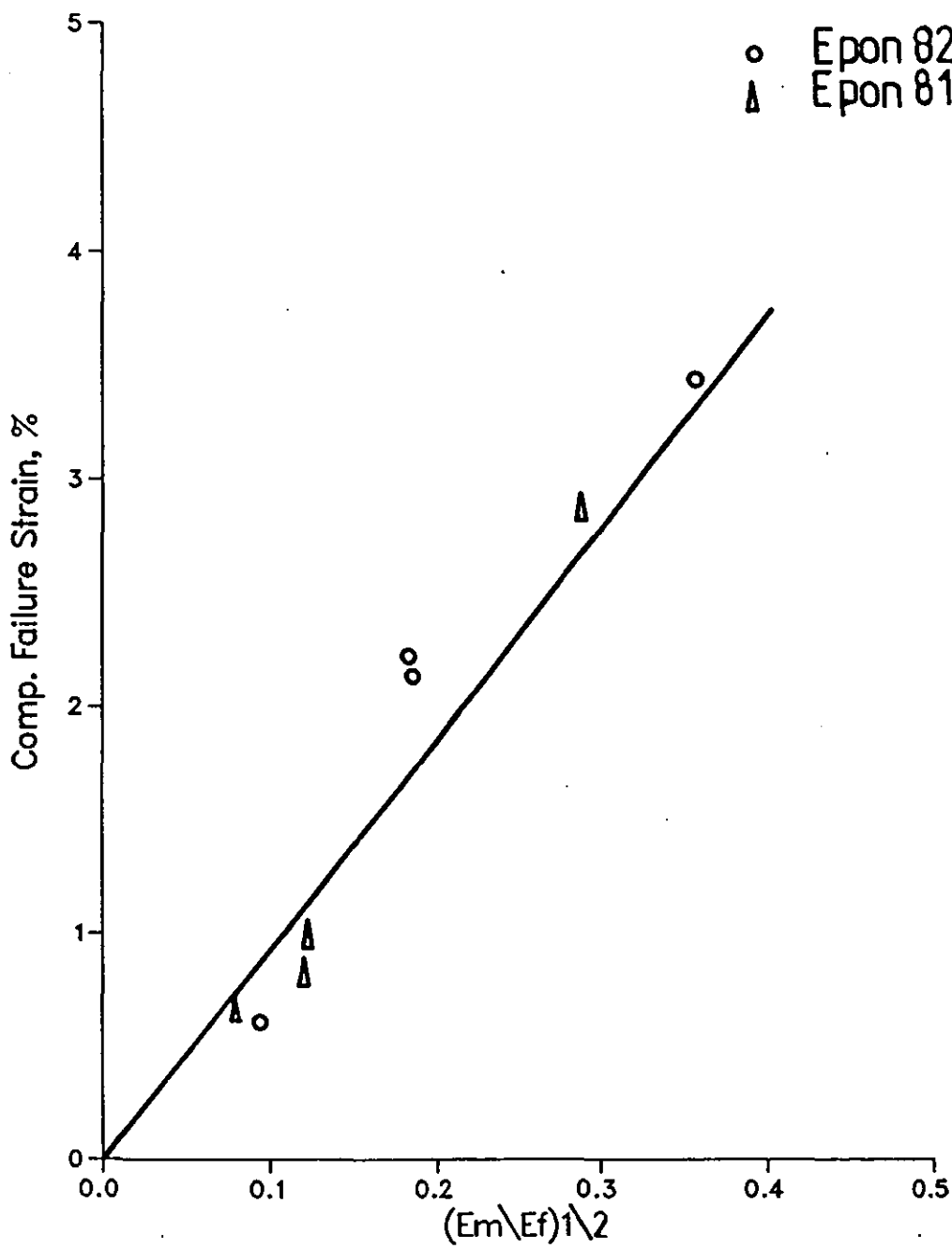


FIGURE 2.11: THE DEPENDENCE OF COMPRESSIVE FAILURE STRAIN ON MODULUS RATIO BY HAHN (From Ref, 23)

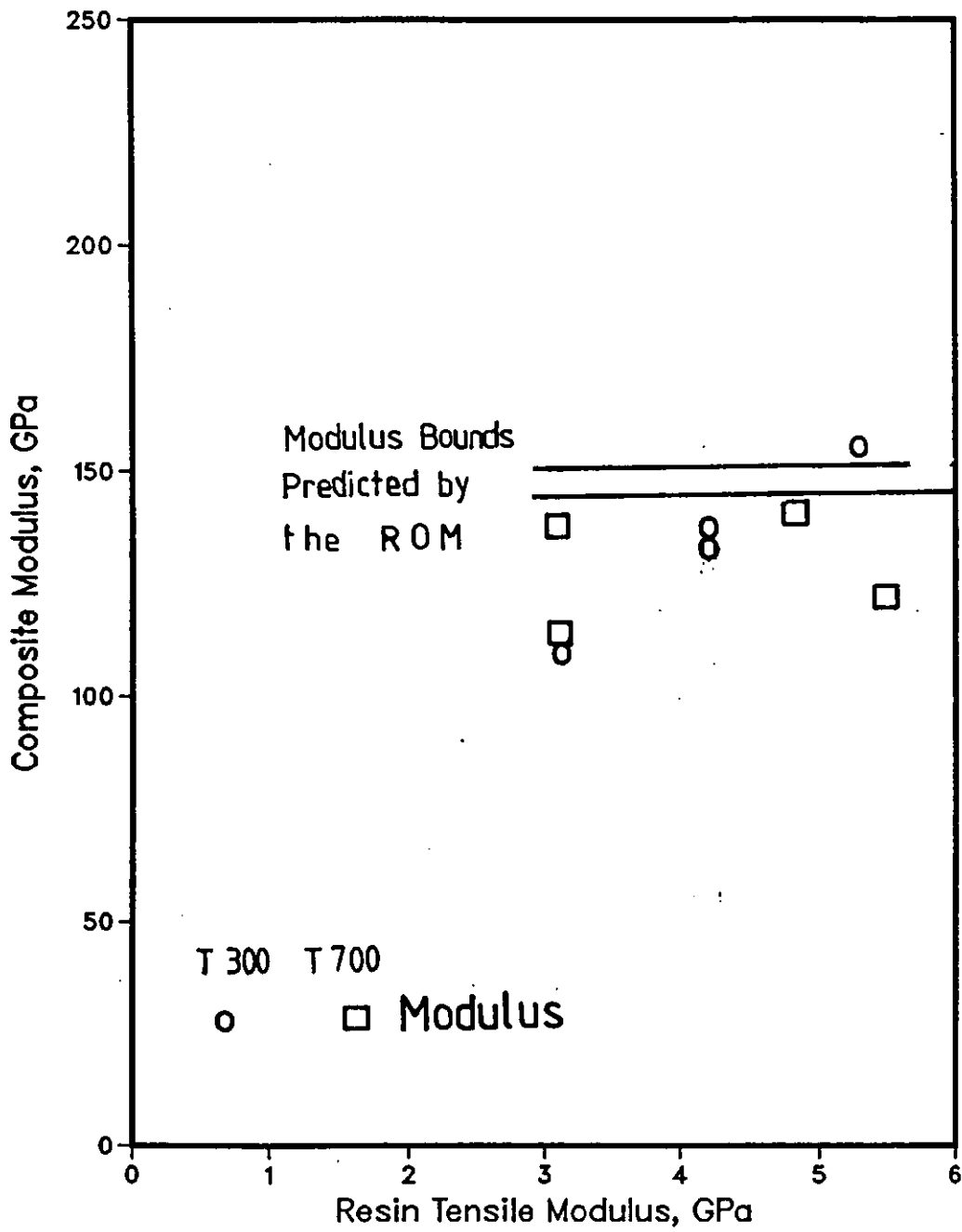
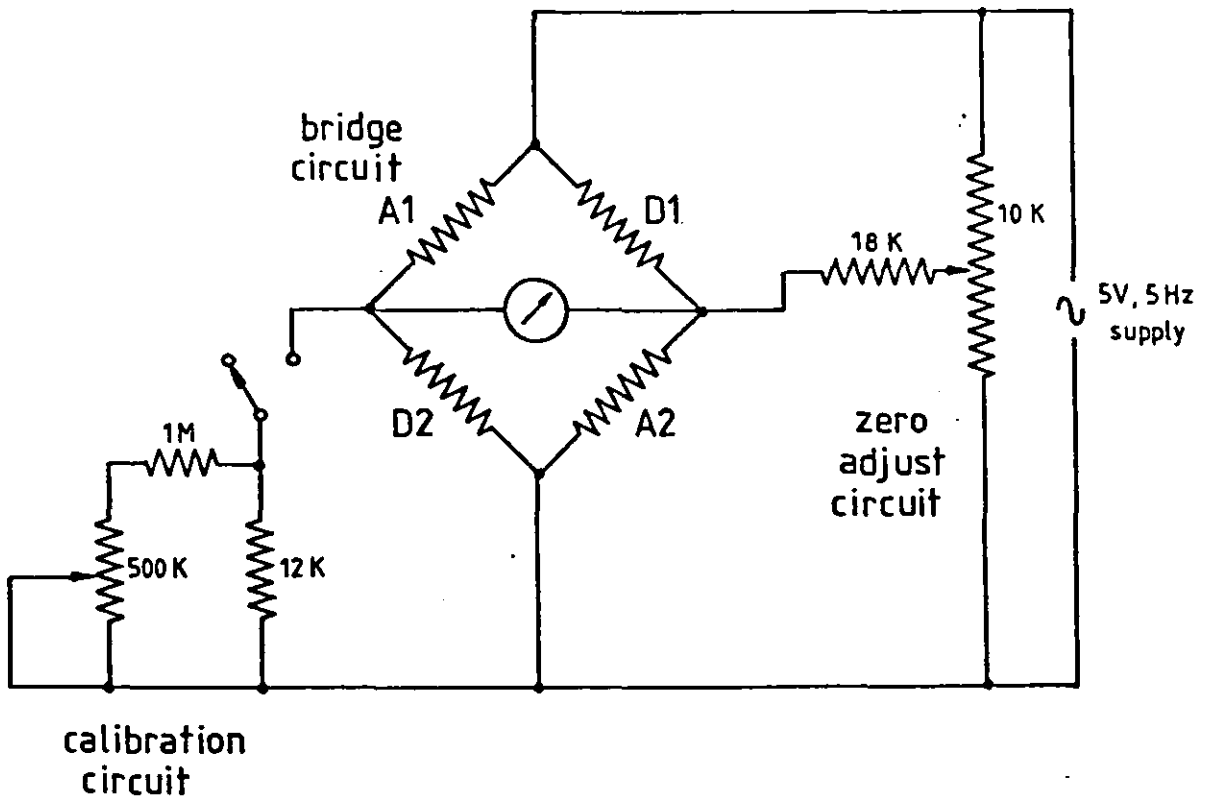


FIGURE 2.12: EFFECT OF RESIN TENSILE MODULUS ON MODULUS OF T300 and T700 COMPOSITES UNDER COMPRESSION OBSERVED BY HAHN AND WILLIAMS (From Ref 24)



- A1 } active 120 $\Omega$  strain gauges  
 A2 }  
 D1 } dummy 120 $\Omega$  strain gauges ( mounted inside SGCB )  
 D2 }

FIGURE 3.13 THE STRAIN GAUGE BRIDGE CIRCUIT

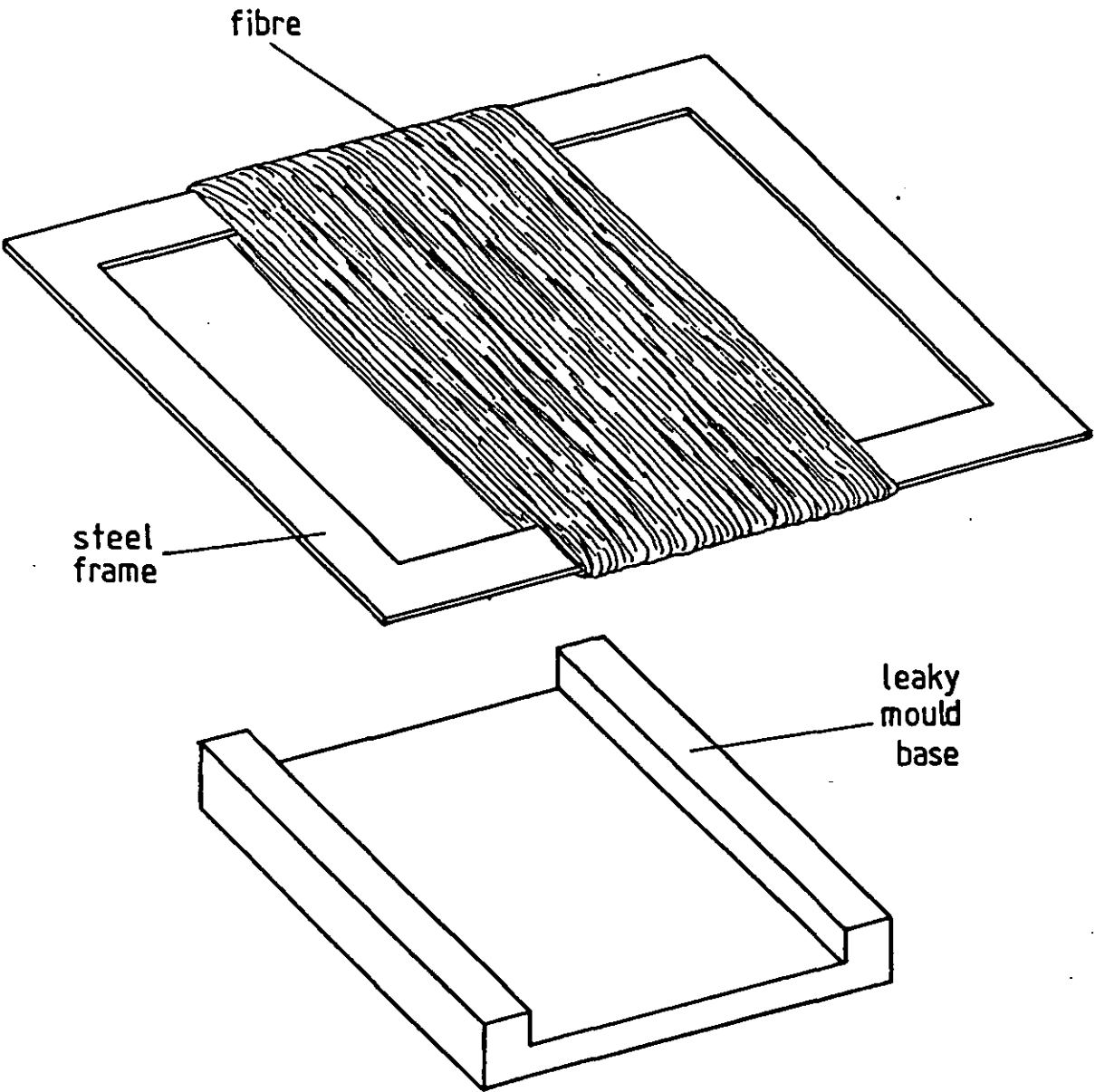


FIGURE 3.14 A FIBRE WOUND STEEL FRAME READY FOR RESIN IMPREG-  
NATION BY THE WET LAY-UP TECHNIQUE

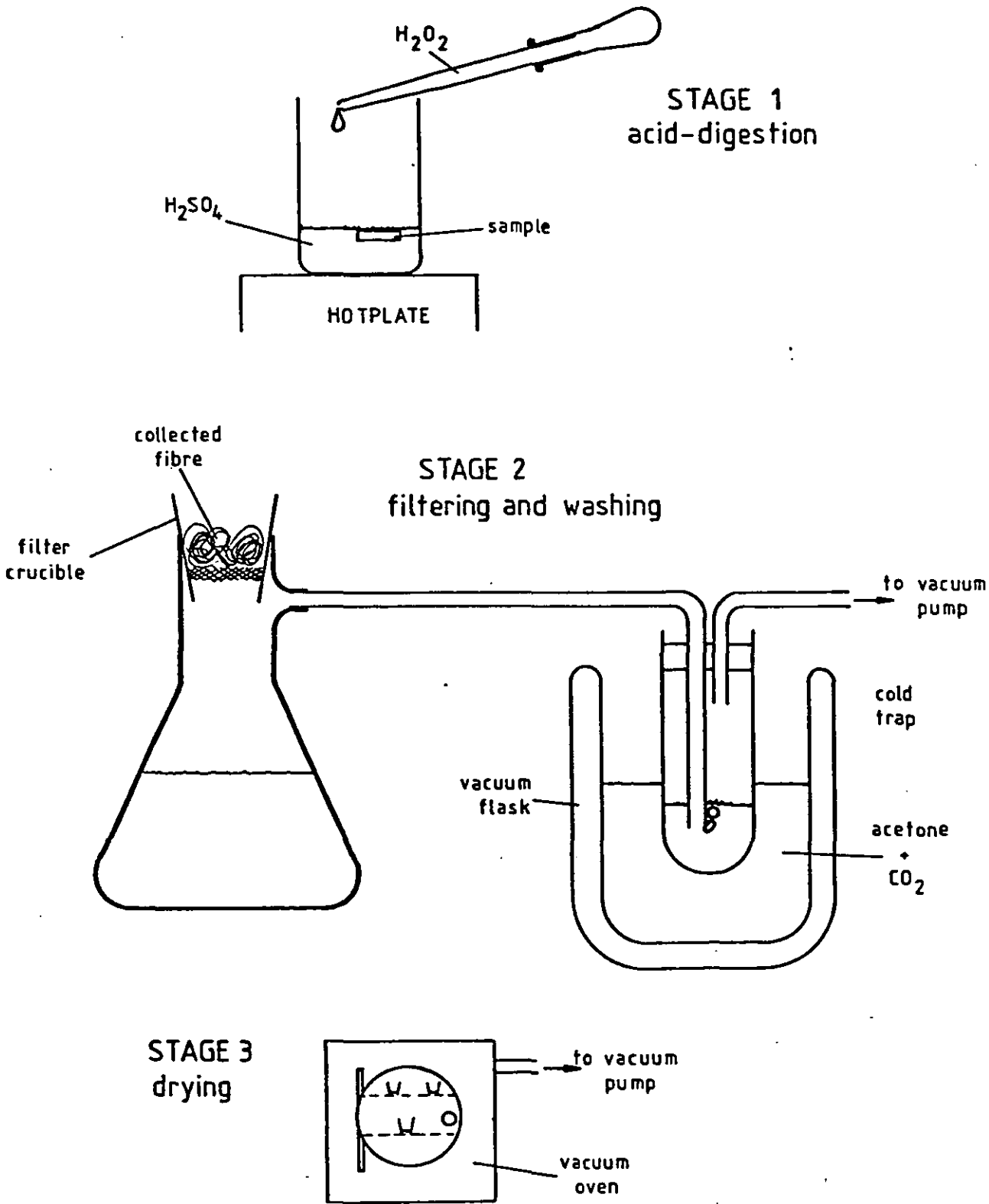


FIGURE 3.15: THE ACID DIGESTION PROCESS OF VOLUME FRACTION MEASUREMENT

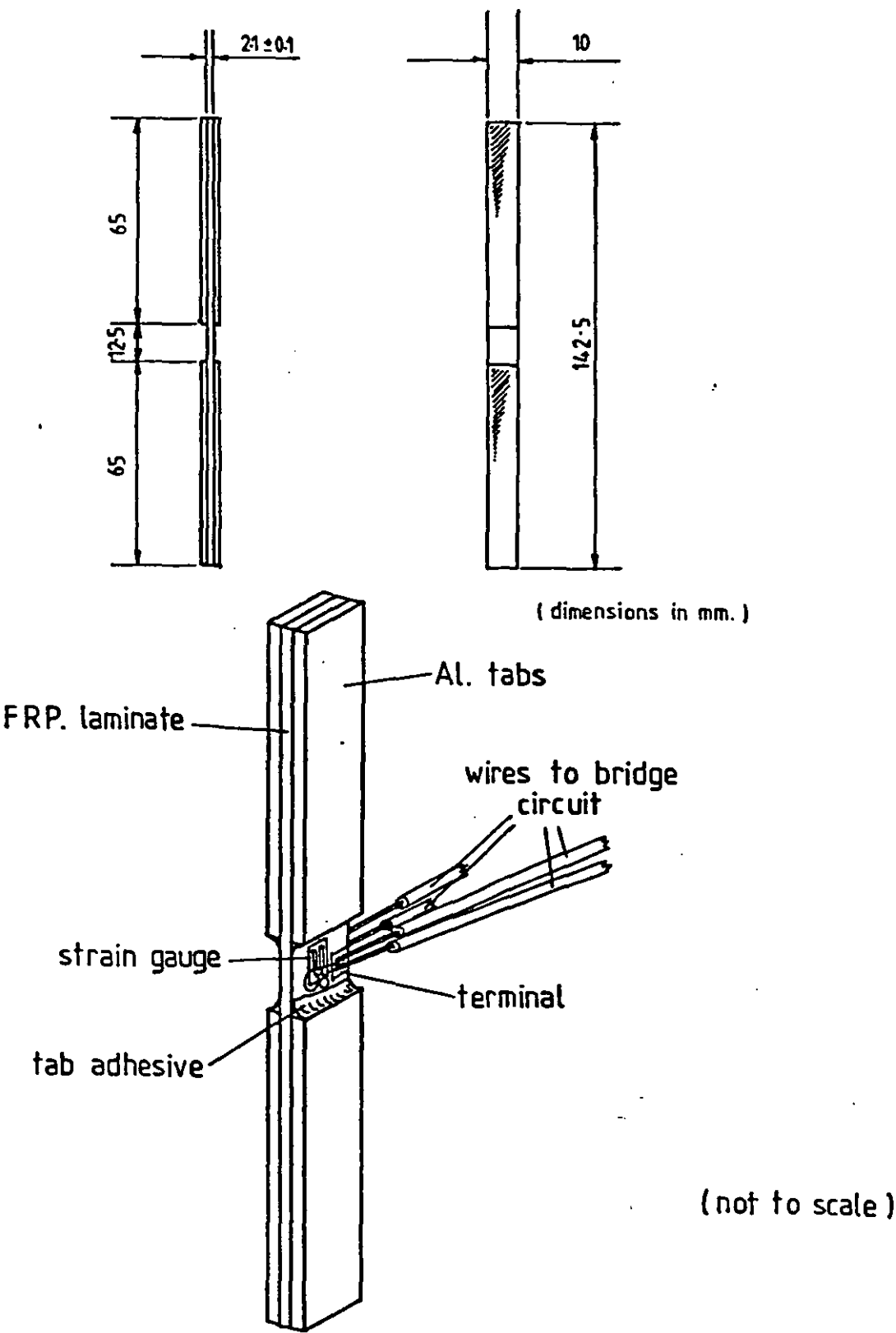
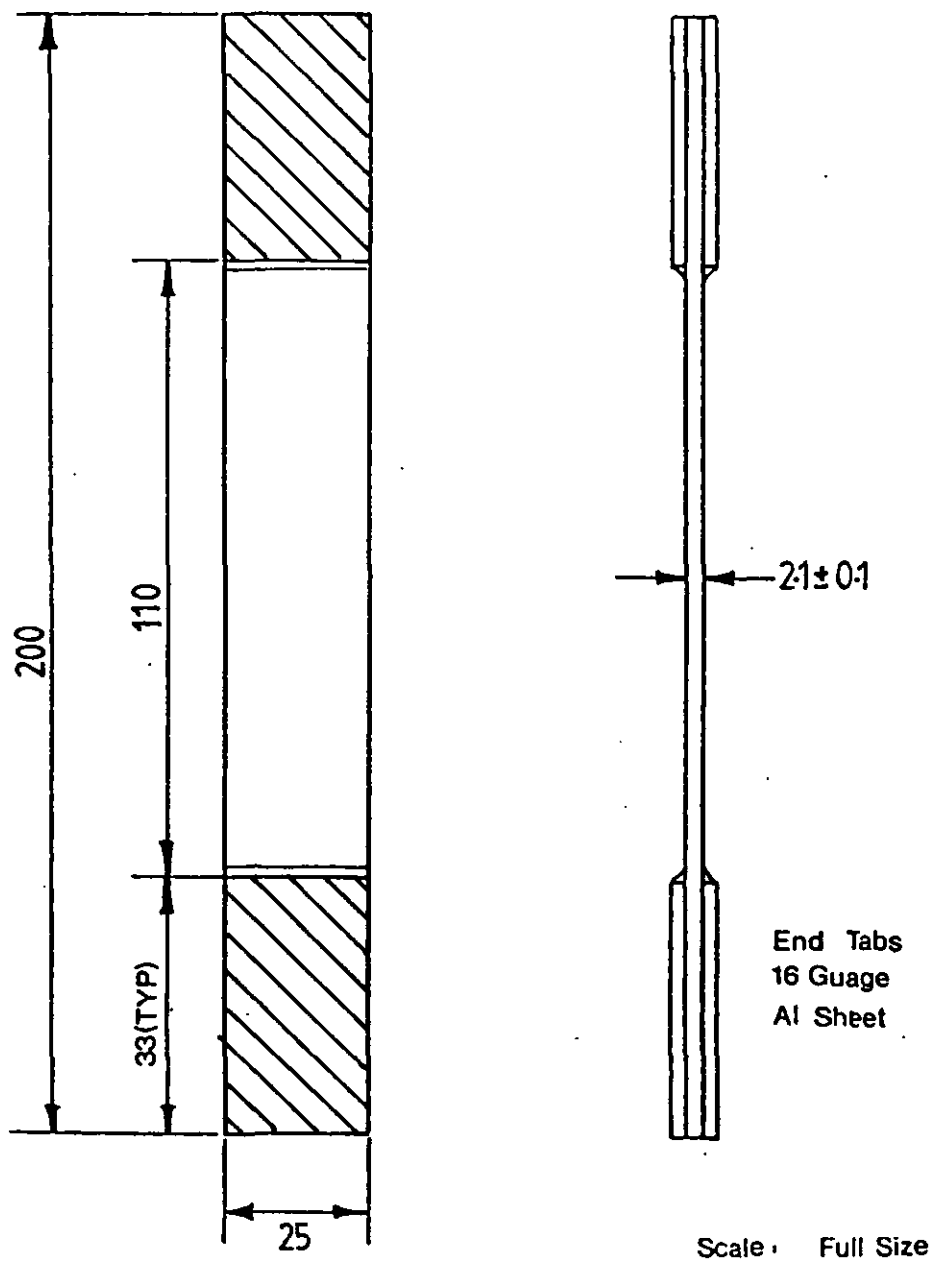
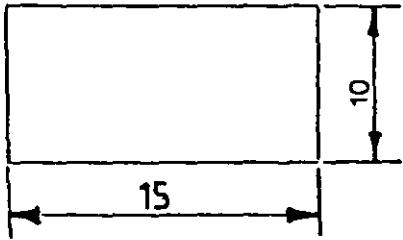
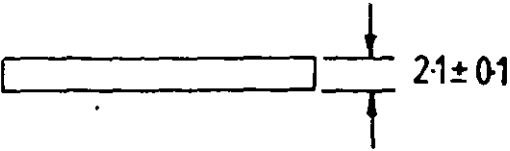


FIGURE 3.16: THE COMPRESSIVE TEST SPECIMEN



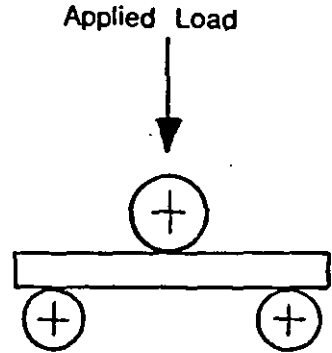
All Dimensions in mm.

FIGURE 3.17: THE TENSILE TEST SPECIMEN



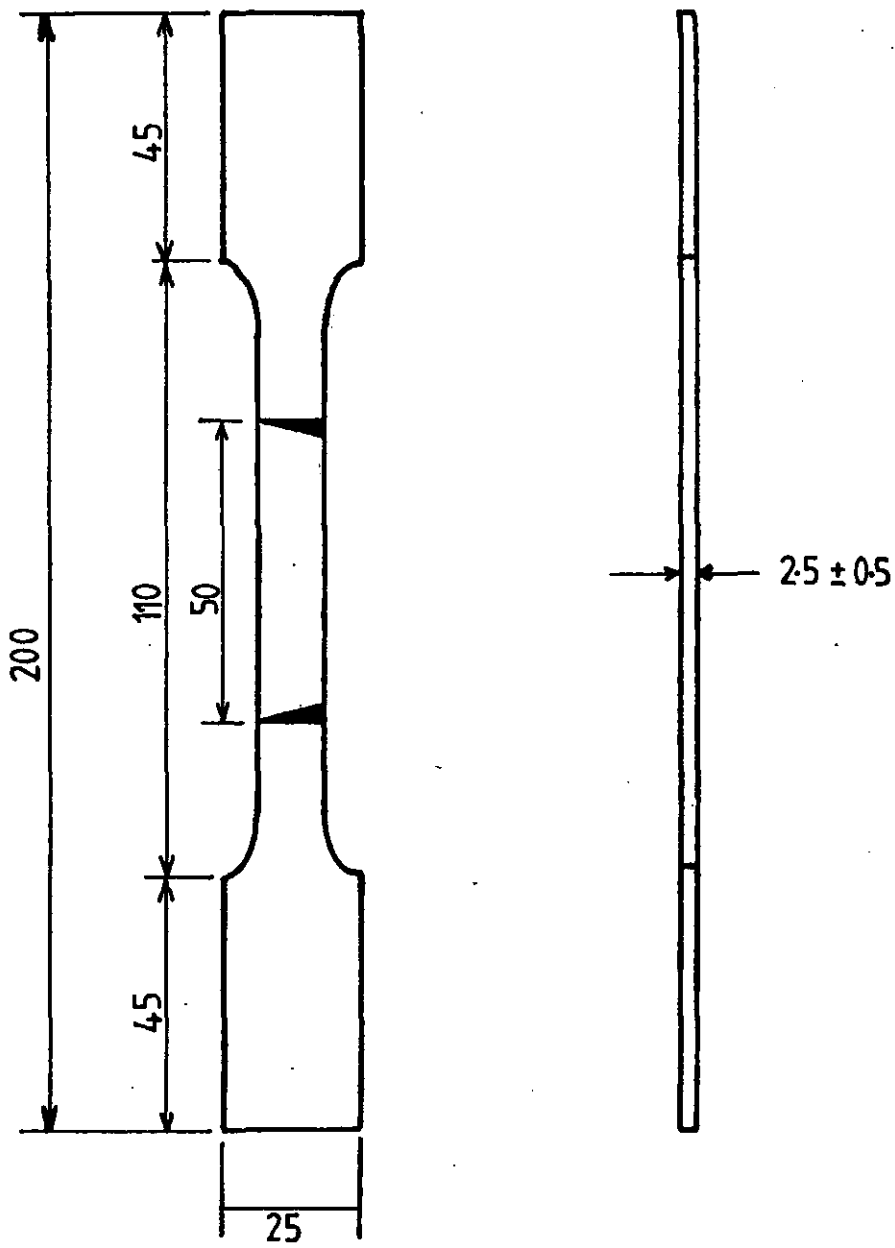
Scale : 2:1

All Dimensions in mm.



Schematic of ILSS Testing

FIGURE 3,18: THE INTER-LAMINAR SHEAR TEST SPECIMEN



All Dimension in mm.

FIGURE 3.19: THE RESIN TENSILE TEST SPECIMEN

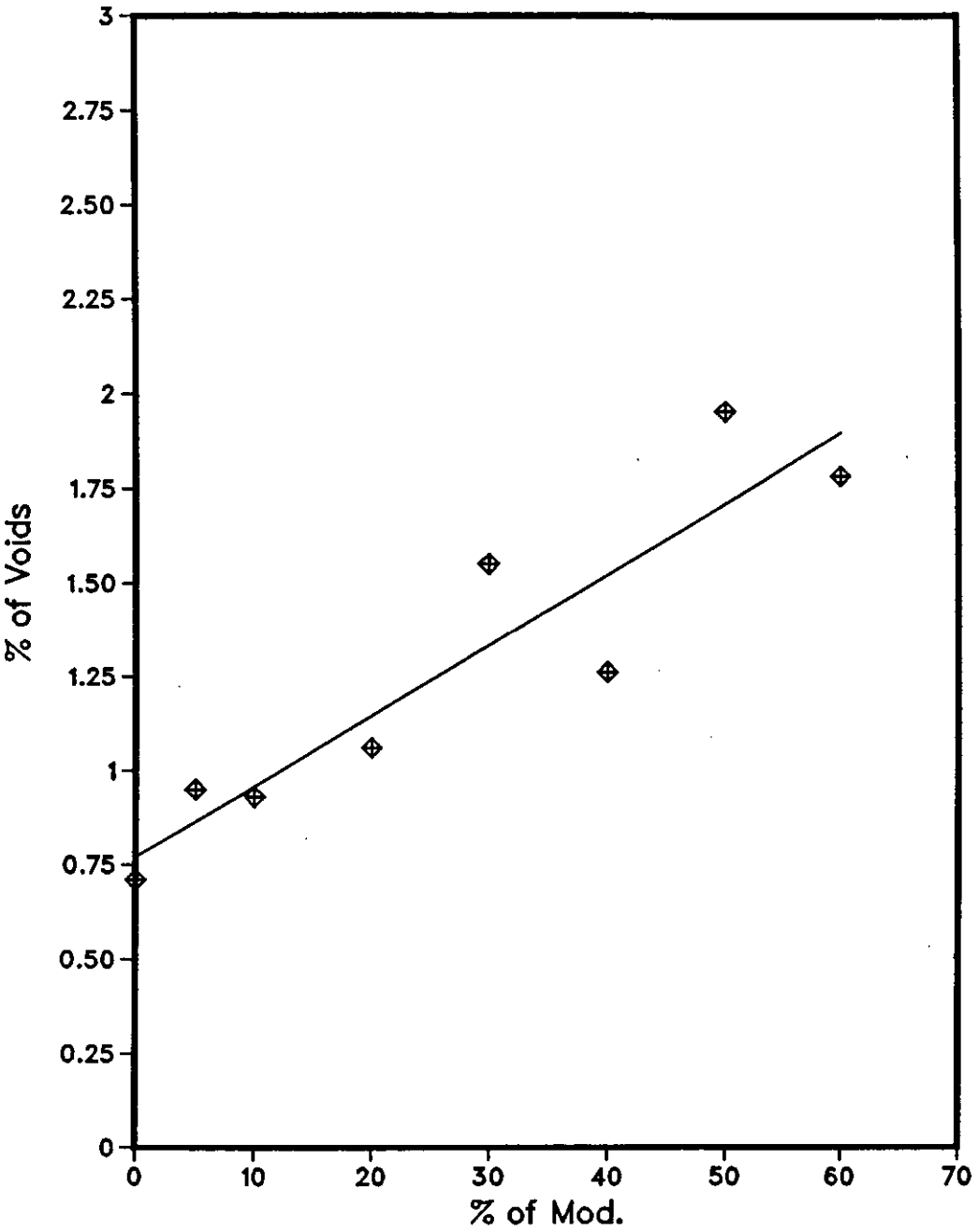


Fig.4-20: Percentage of Voids in Matrix vs.  
% of Modifier

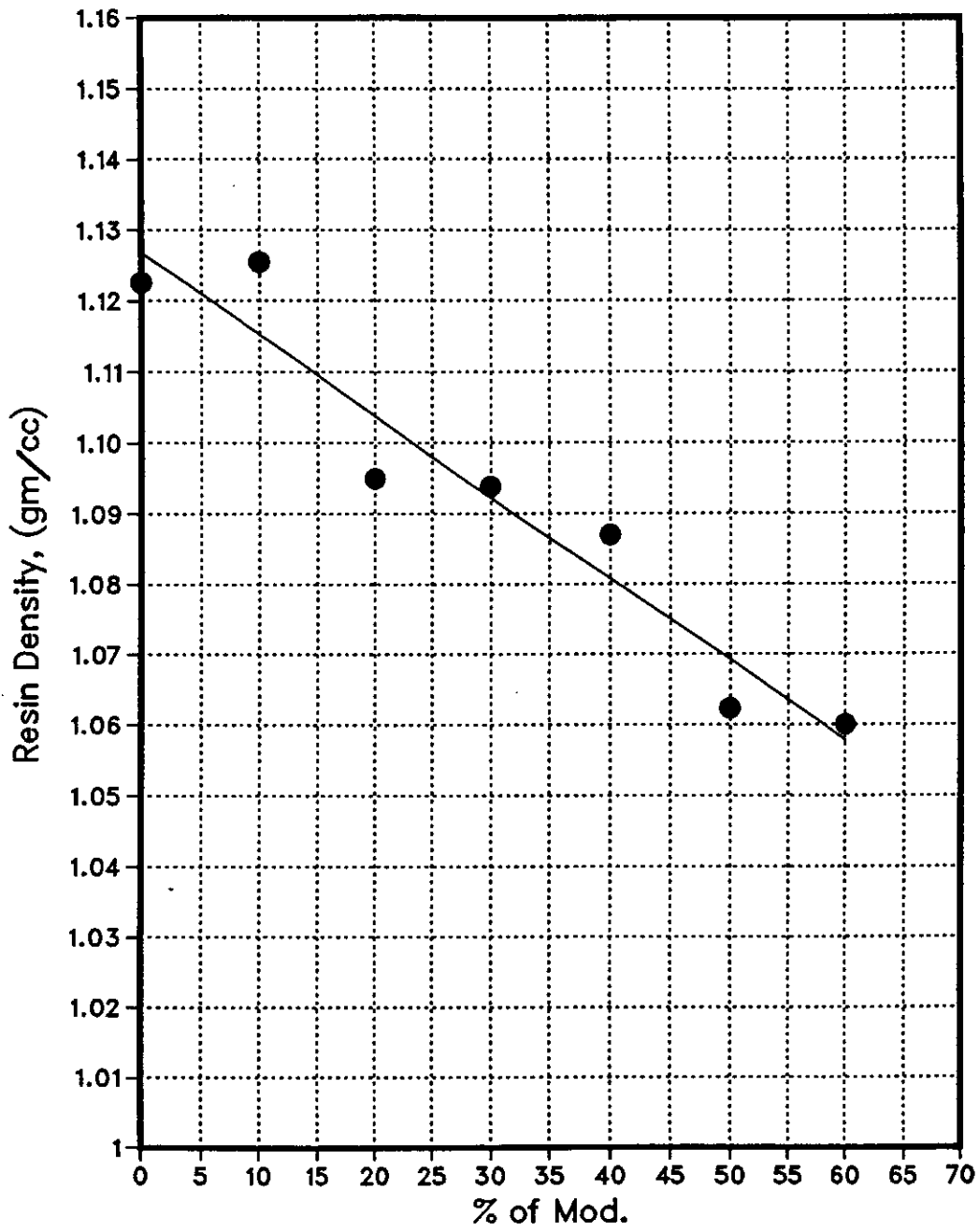


Fig.4-21: Matrix-Resin Density vs.  
% of Modifier

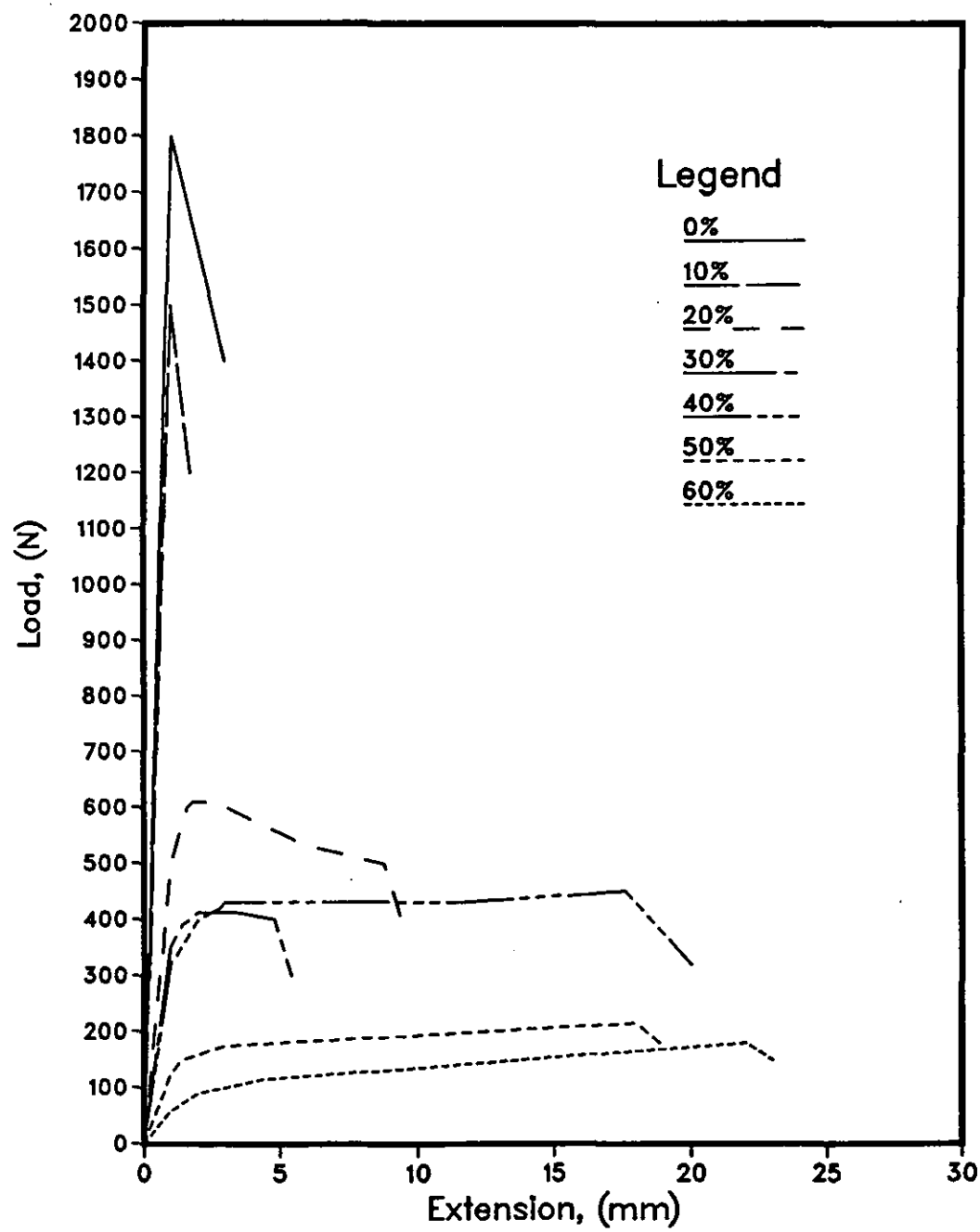


Fig.4-22: Load vs. Extension  
of Resin-Matrix Systems

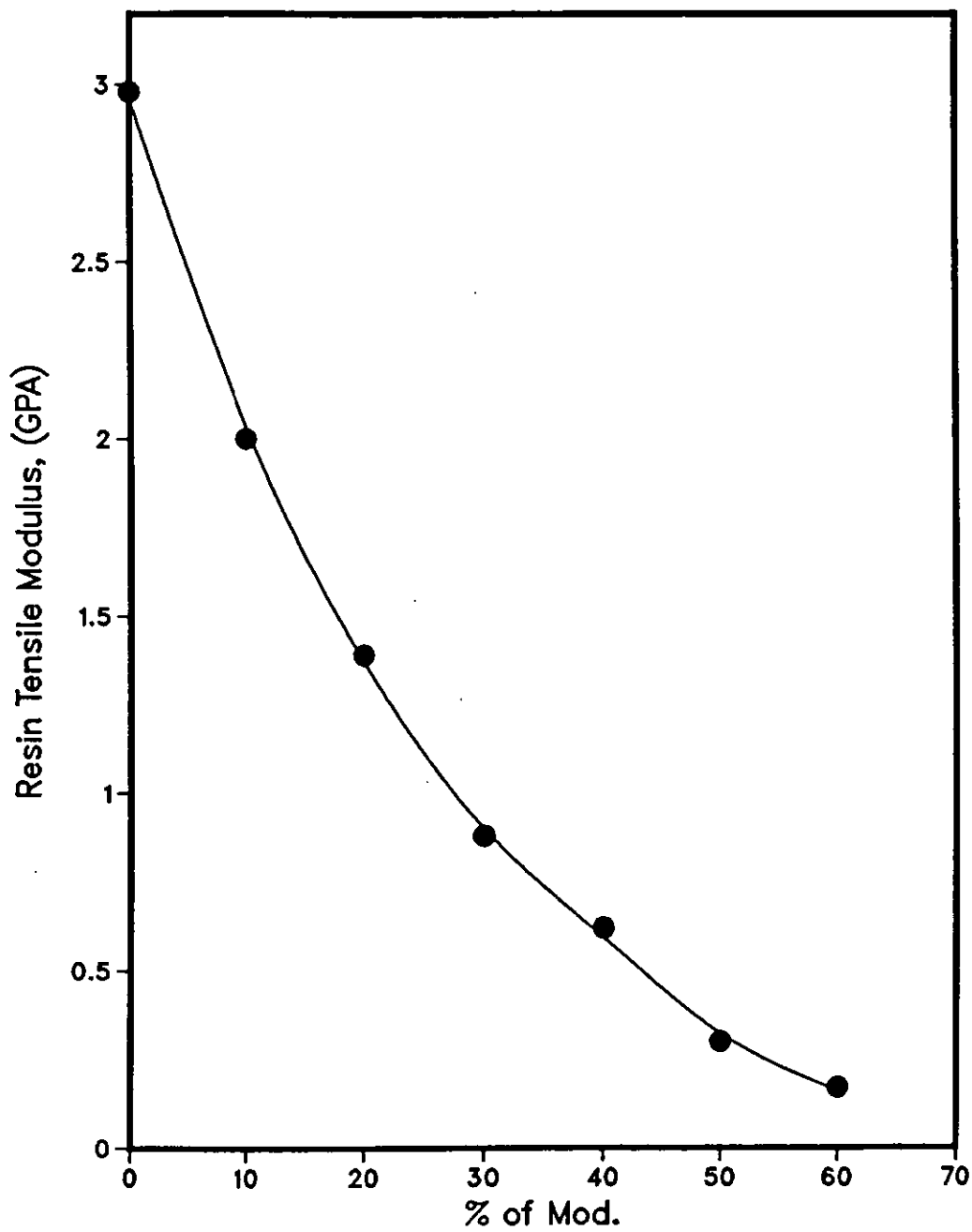


Fig.4-23: Matrix Tensile Modulus vs. % of Modifier

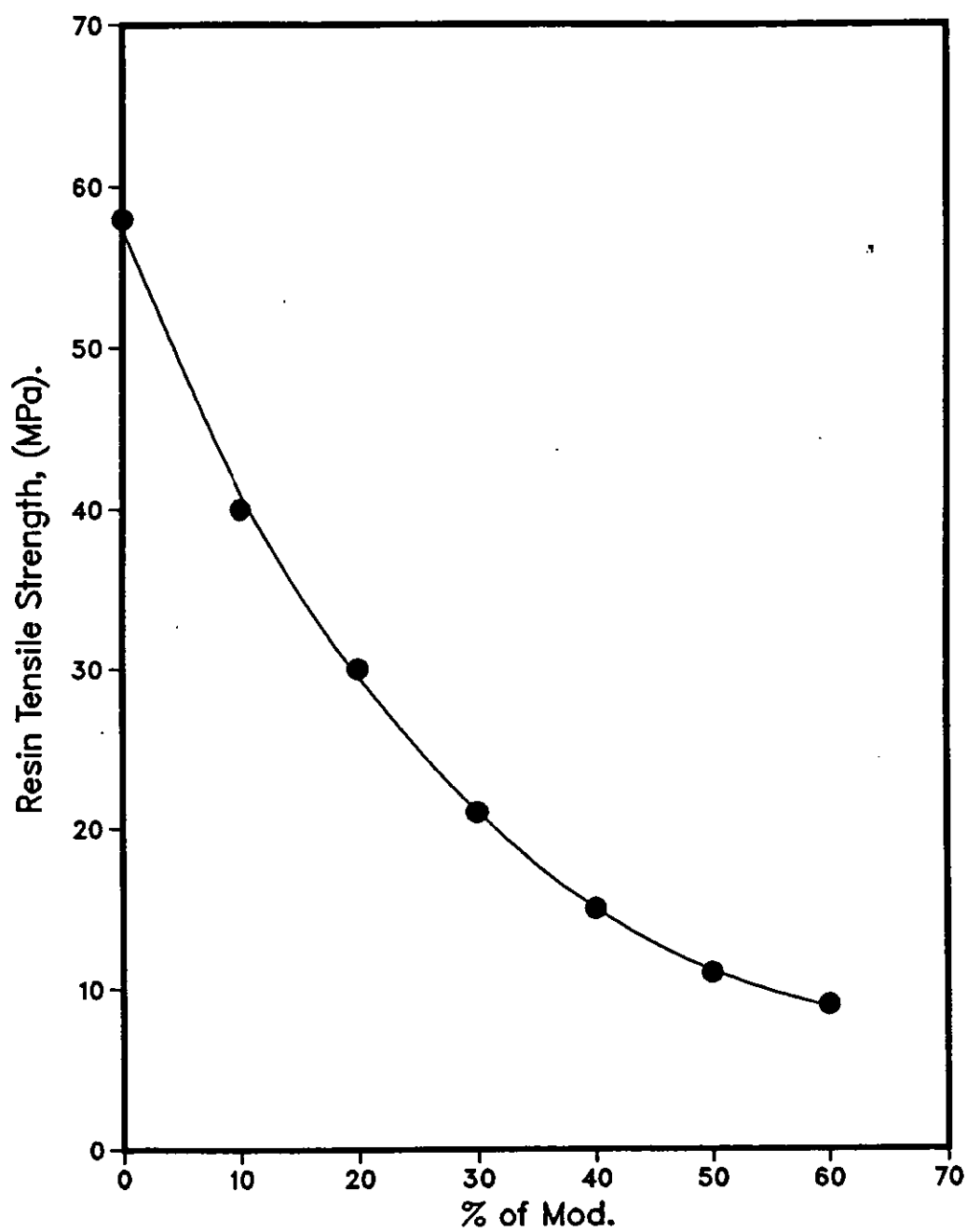


Fig.4-24: Resin Tensile Strength vs.  
% of Modifier

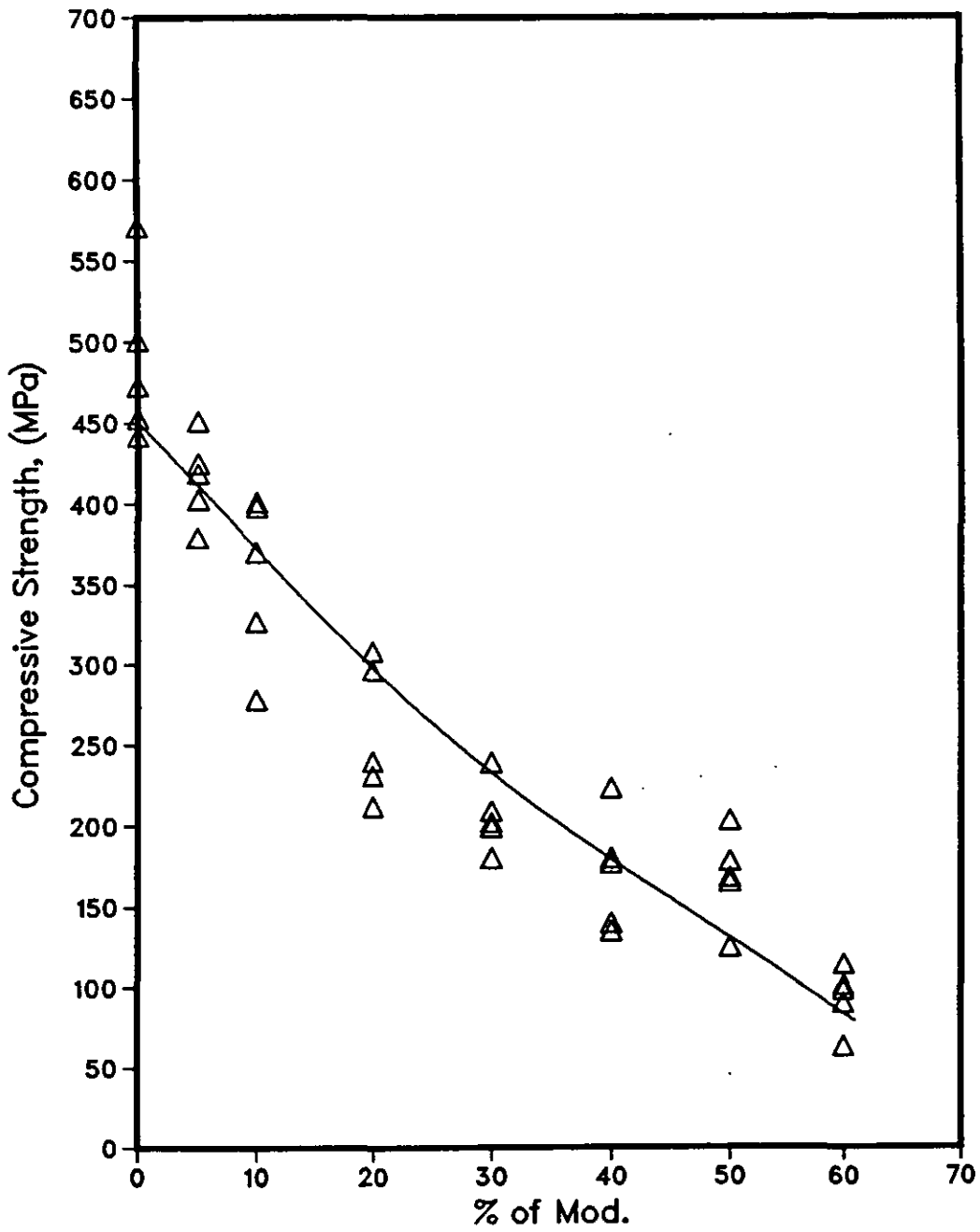


Fig.4-25: Compressive Strength of (GRP) vs. % of Modifier

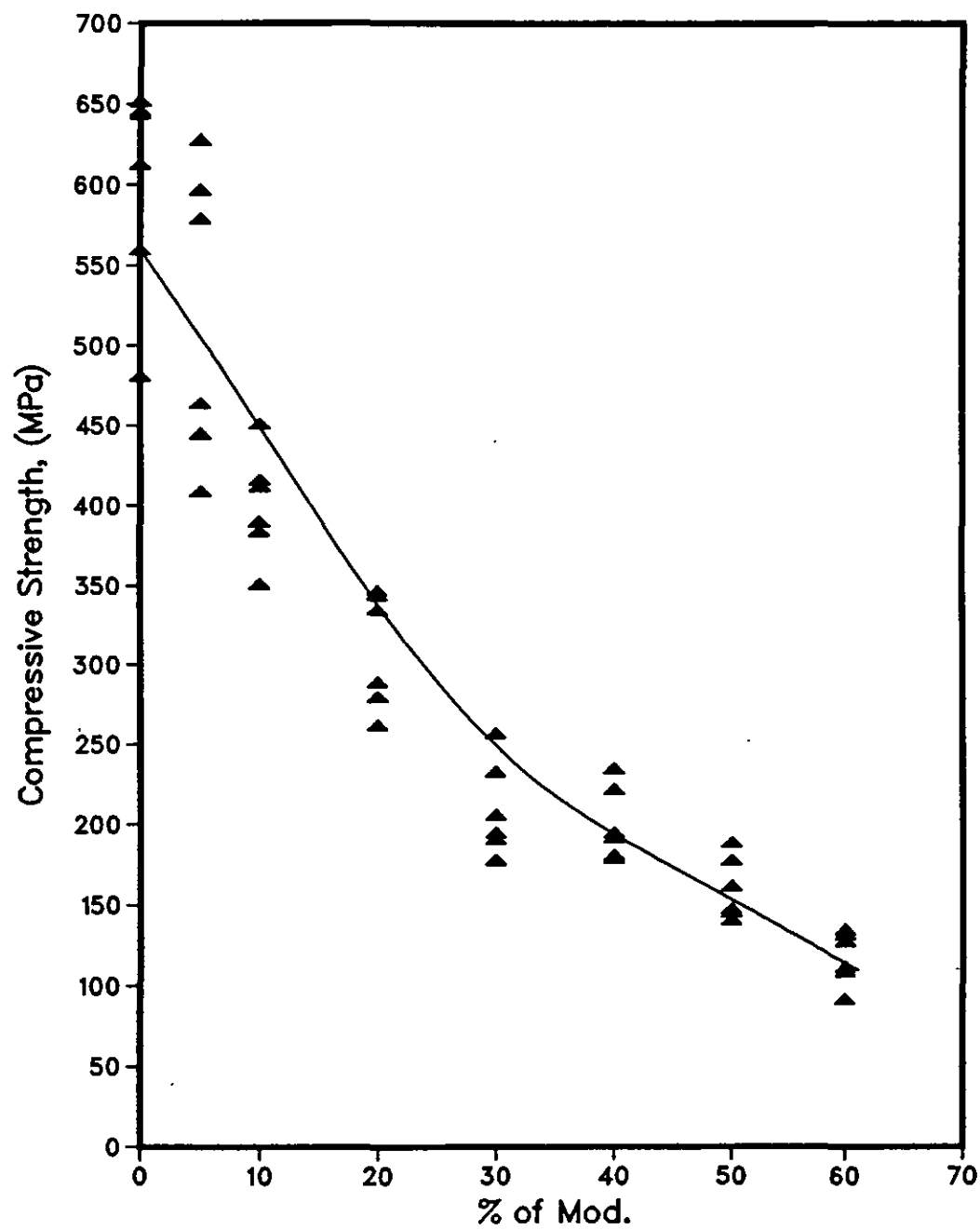


Fig.4-26: Compressive Strength of (CFRP) vs. % of Modifier

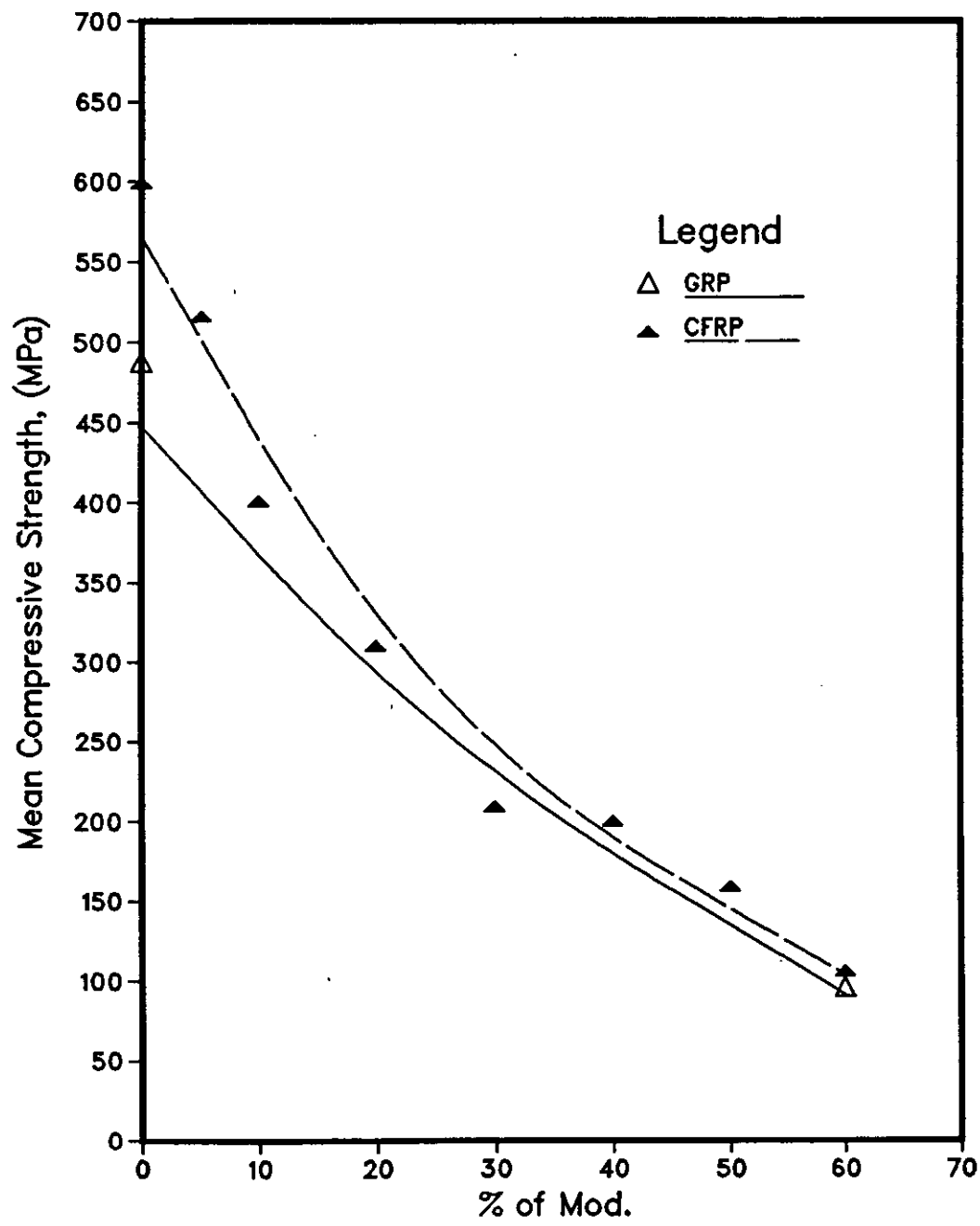


Fig.4-27: Mean Compressive Strength vs. % of Modifier

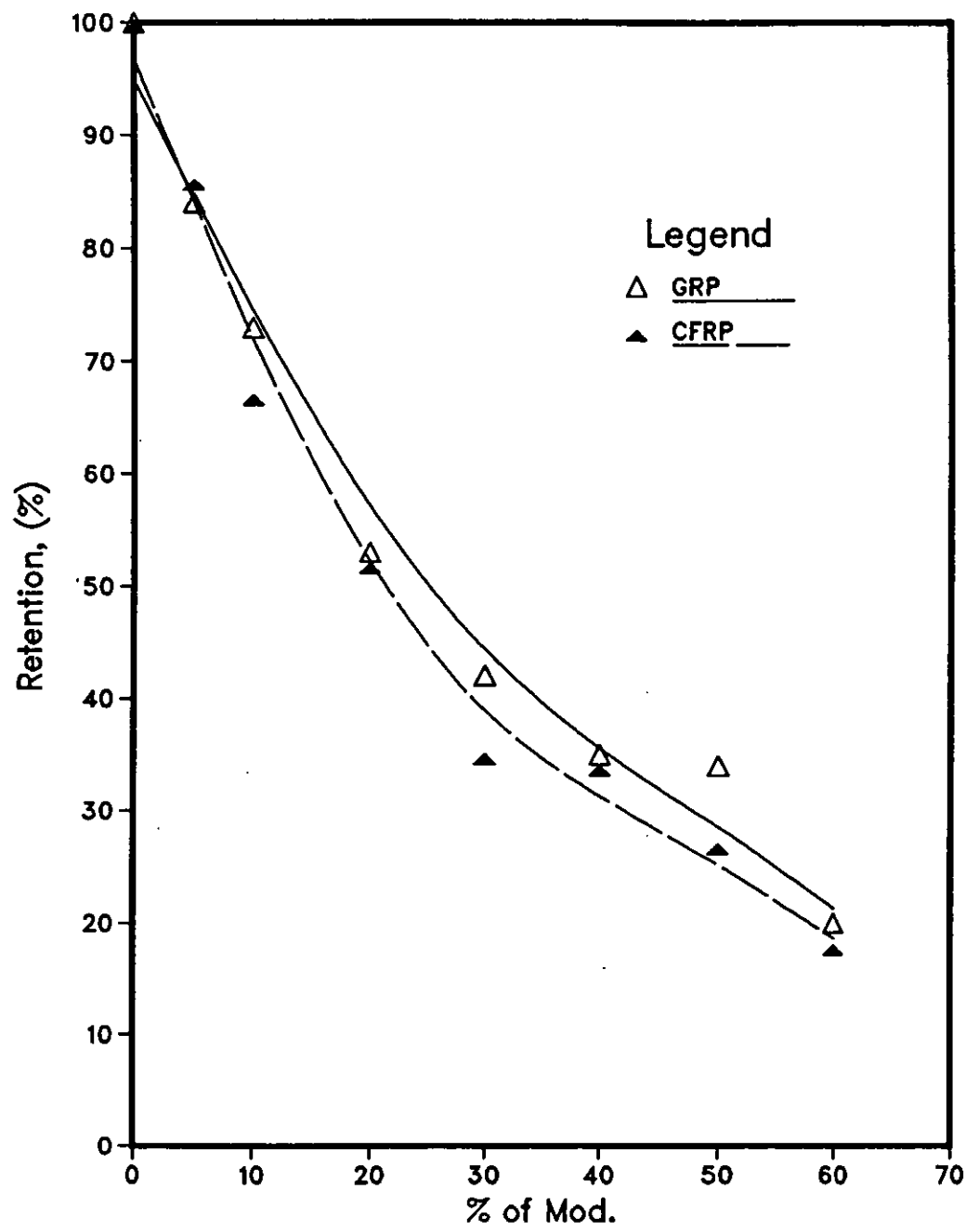


Fig.4-28: Compressive Strength Retention vs. % of Modifier

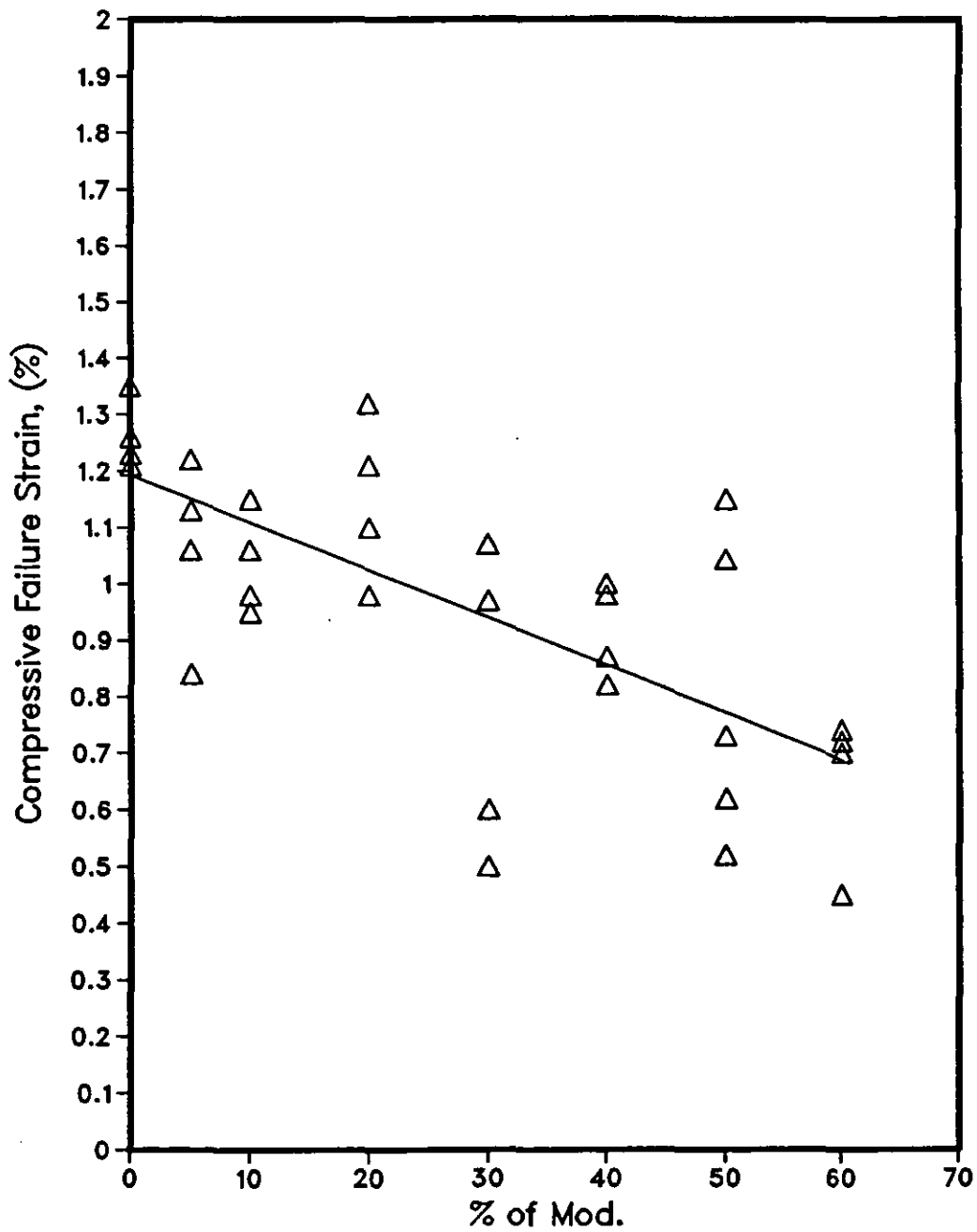


Fig.4-29: Compressive Failure Strain of (GRP) vs. % of Modifier

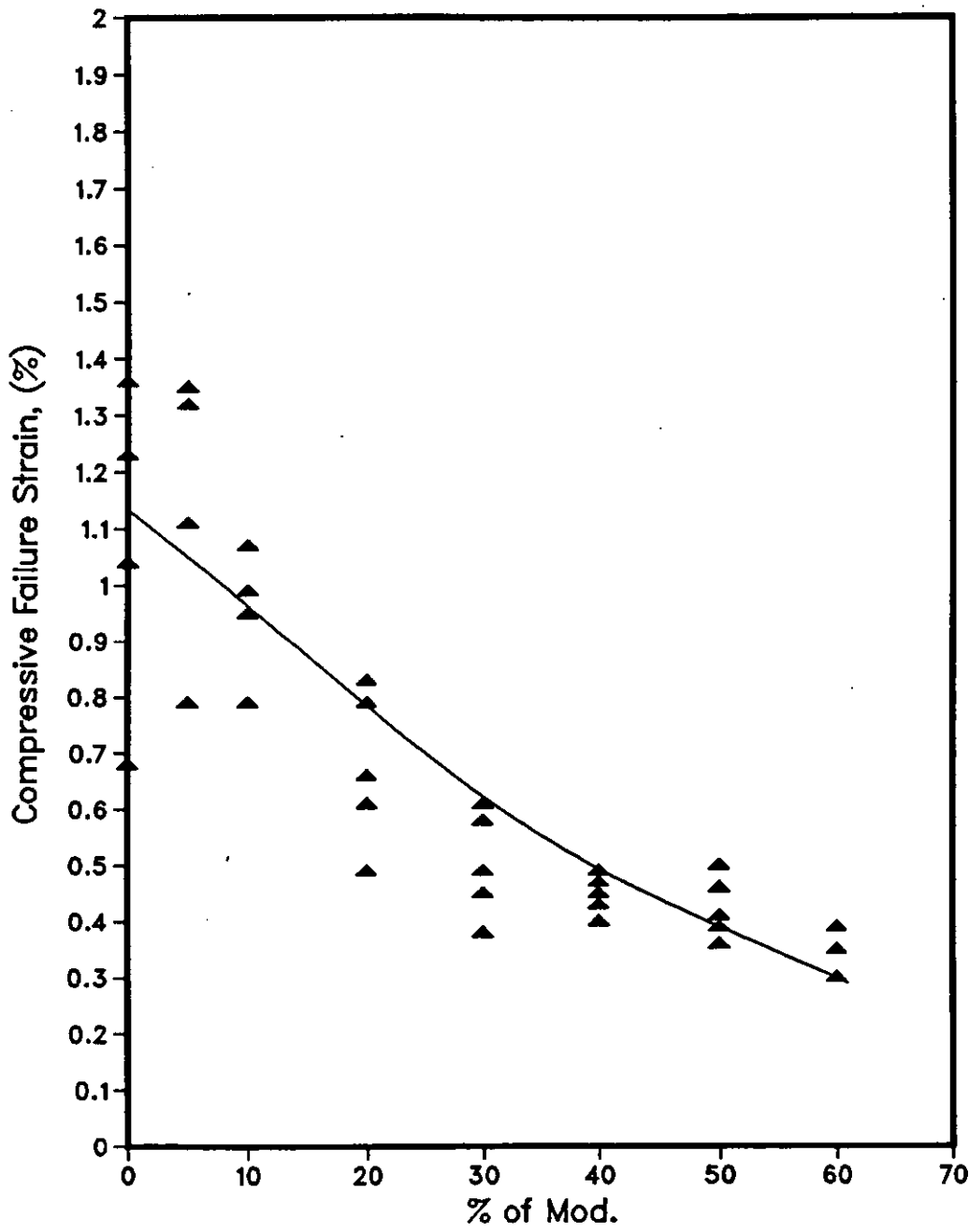


Fig.4-30: Compressive Failure Strain of (CFRP) vs. % of Modifier

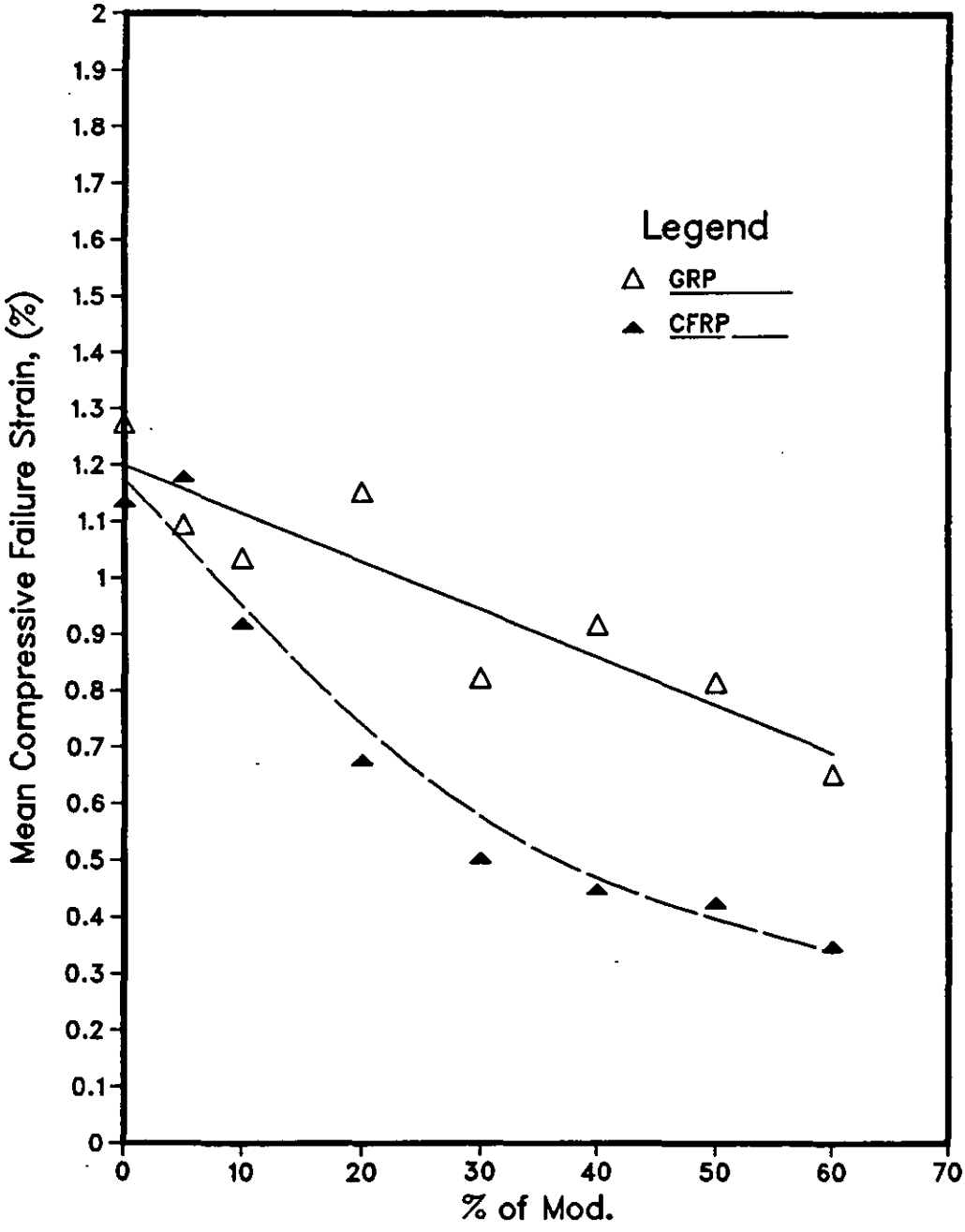


Fig.4-31:Mean Compressive Failure Strain vs. % of Modifier

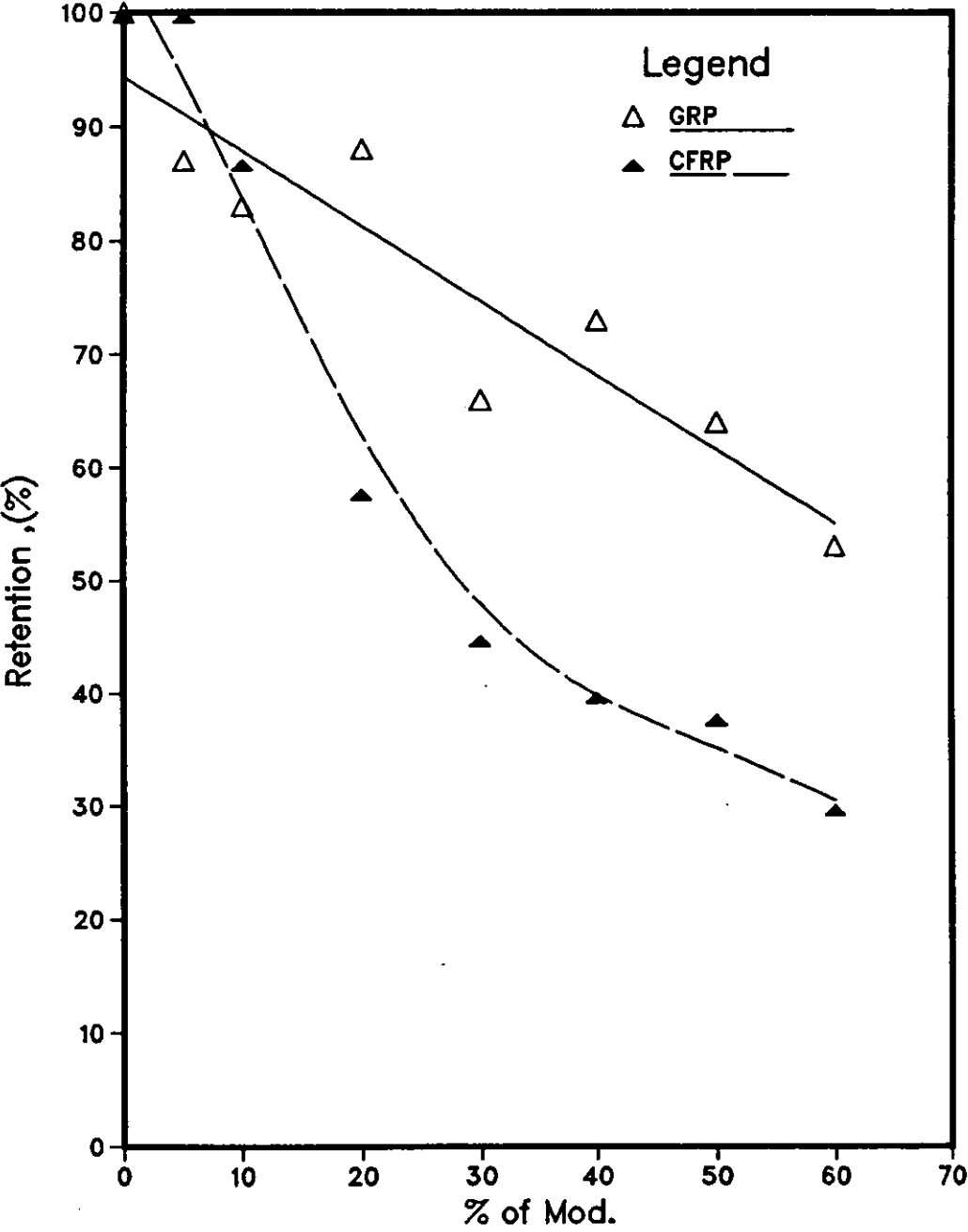


Fig.4-32: Compressive Failure Strain Retention vs. % of Modifier

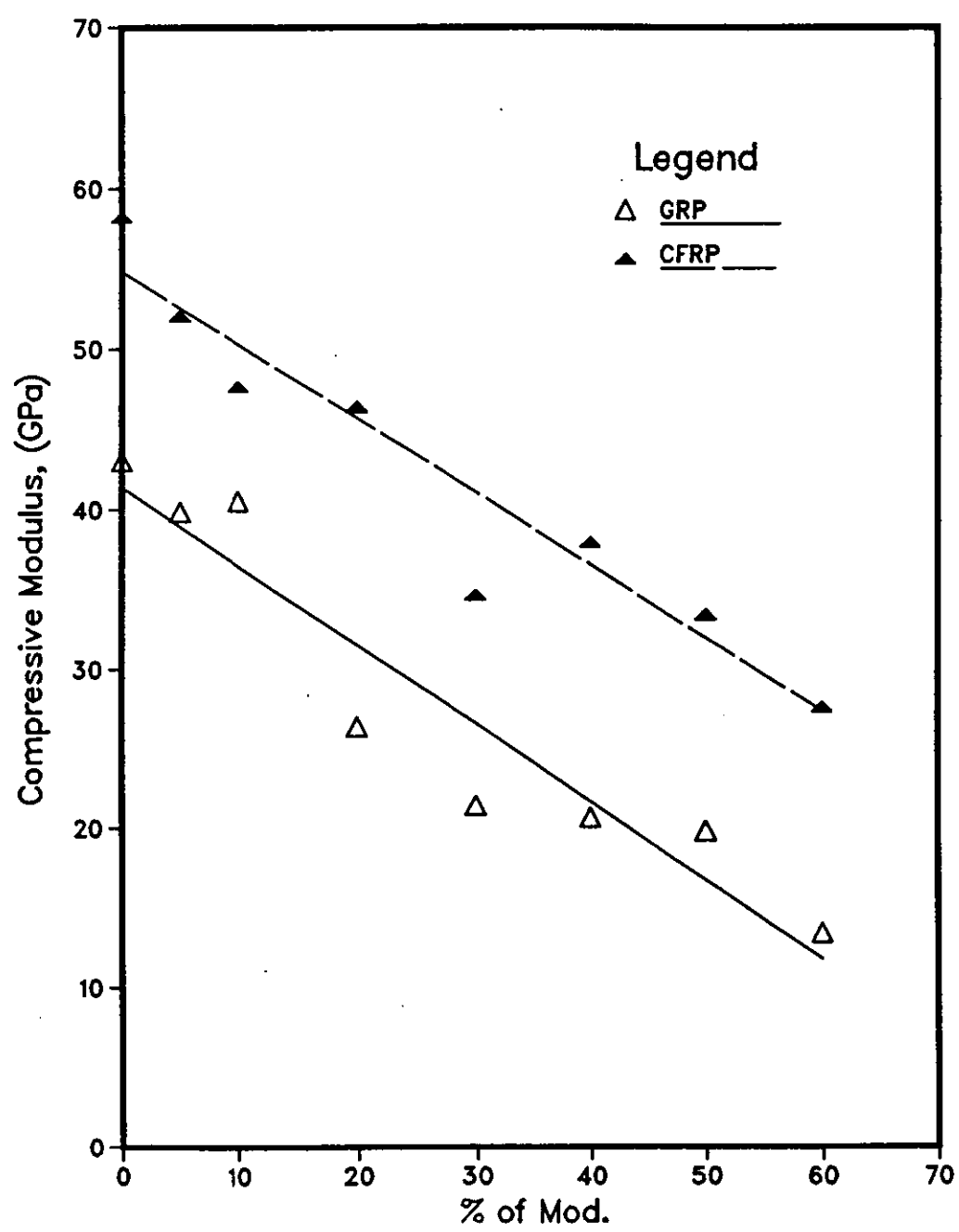


Fig.4-33: Mean Compressive Secant Modulus vs. % of Modifier

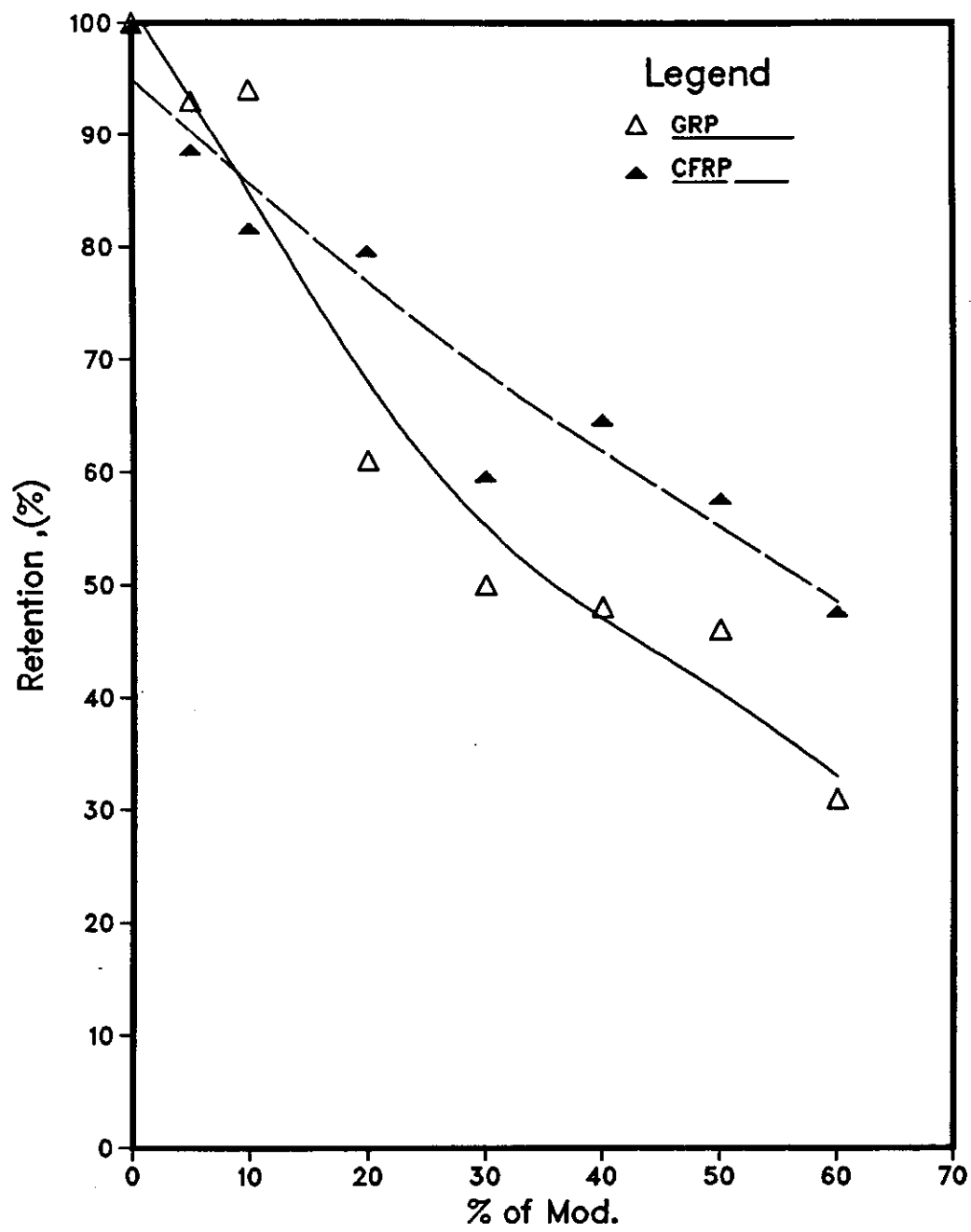


Fig.4-34: Compressive Secant Modulus Retention vs. % of Modifier

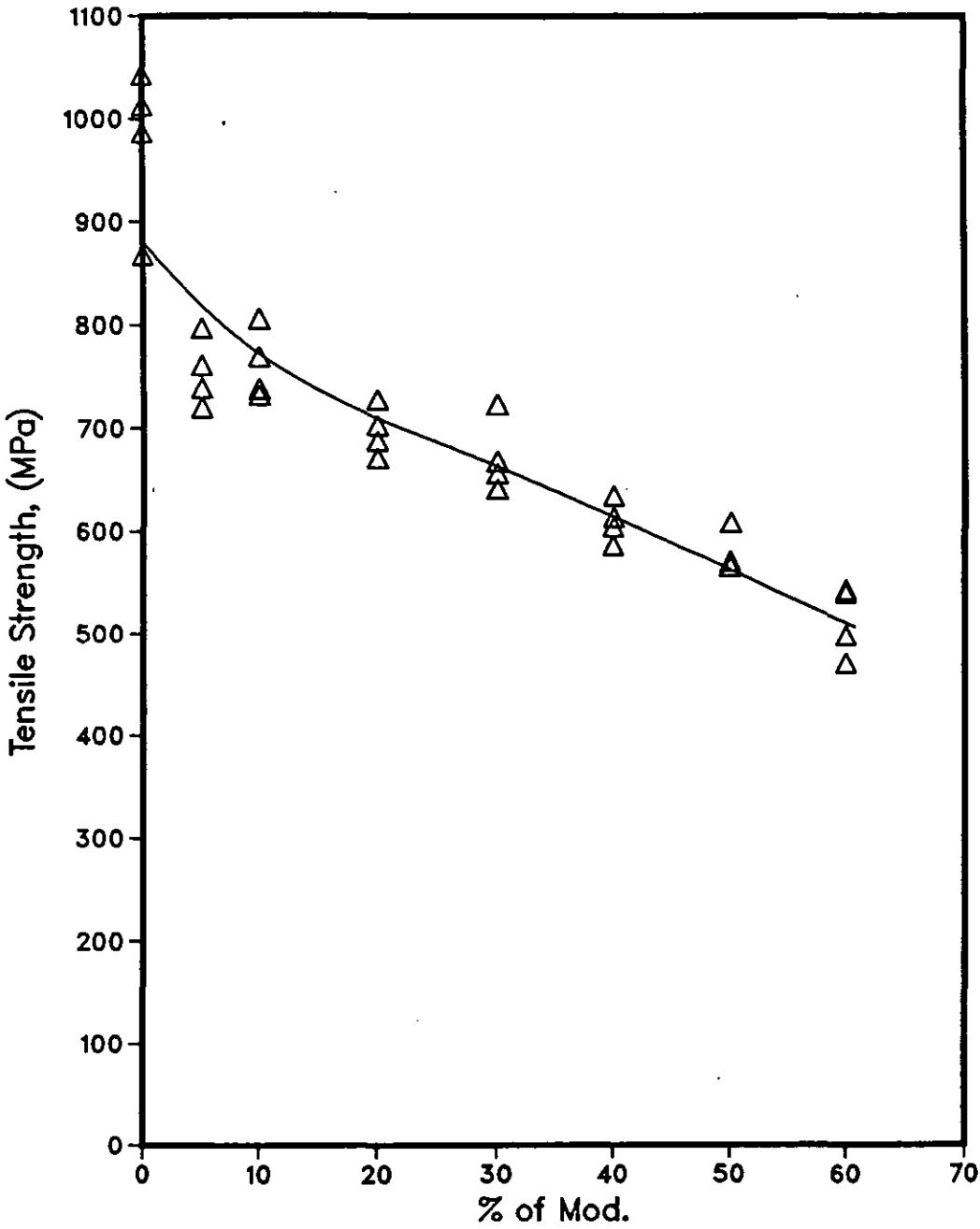


Fig.4-35: Tensile Strength of GRP vs.  
% of Modifier

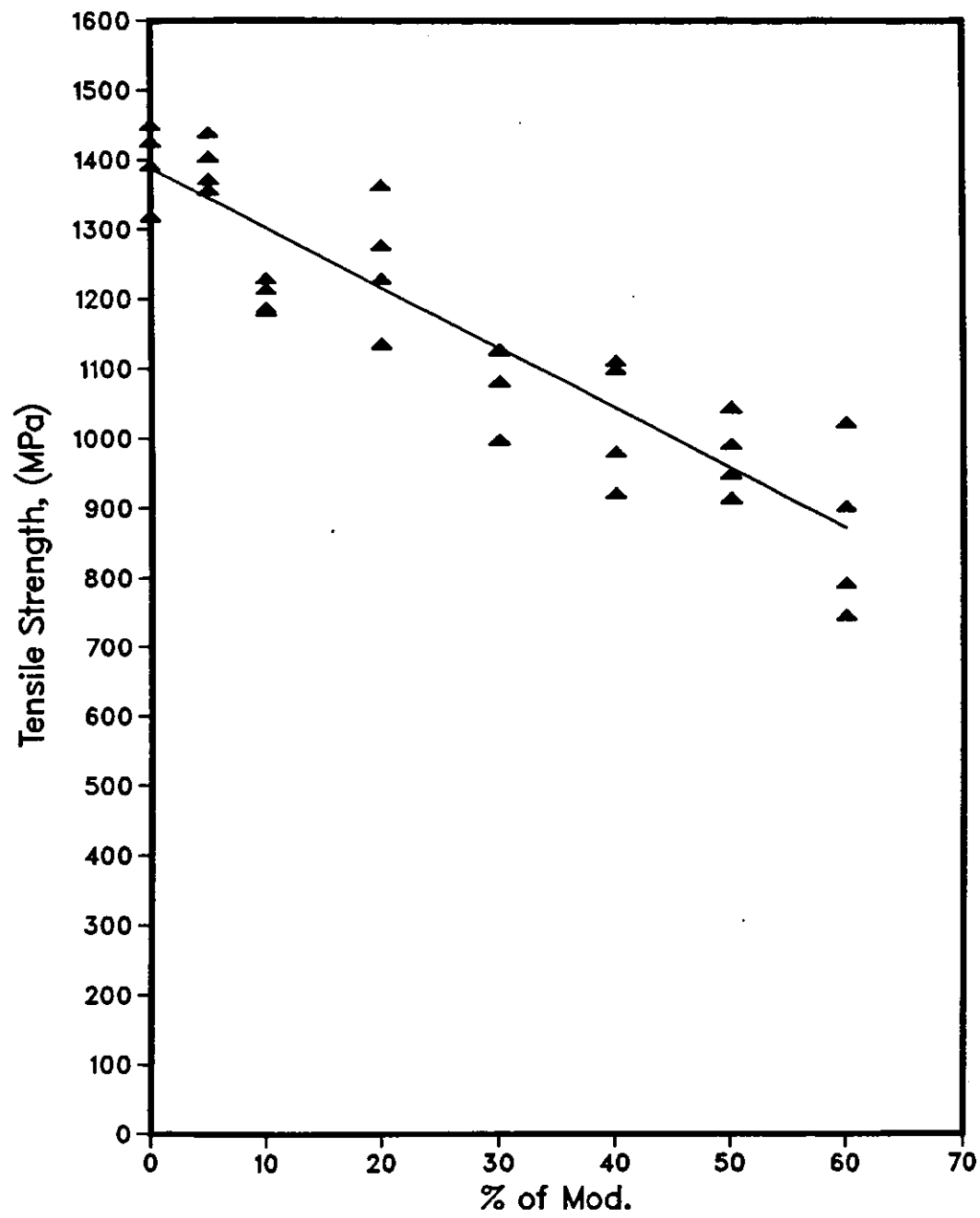


Fig.4-36: Tensile Strength of (CFRP) vs. % of Modifier

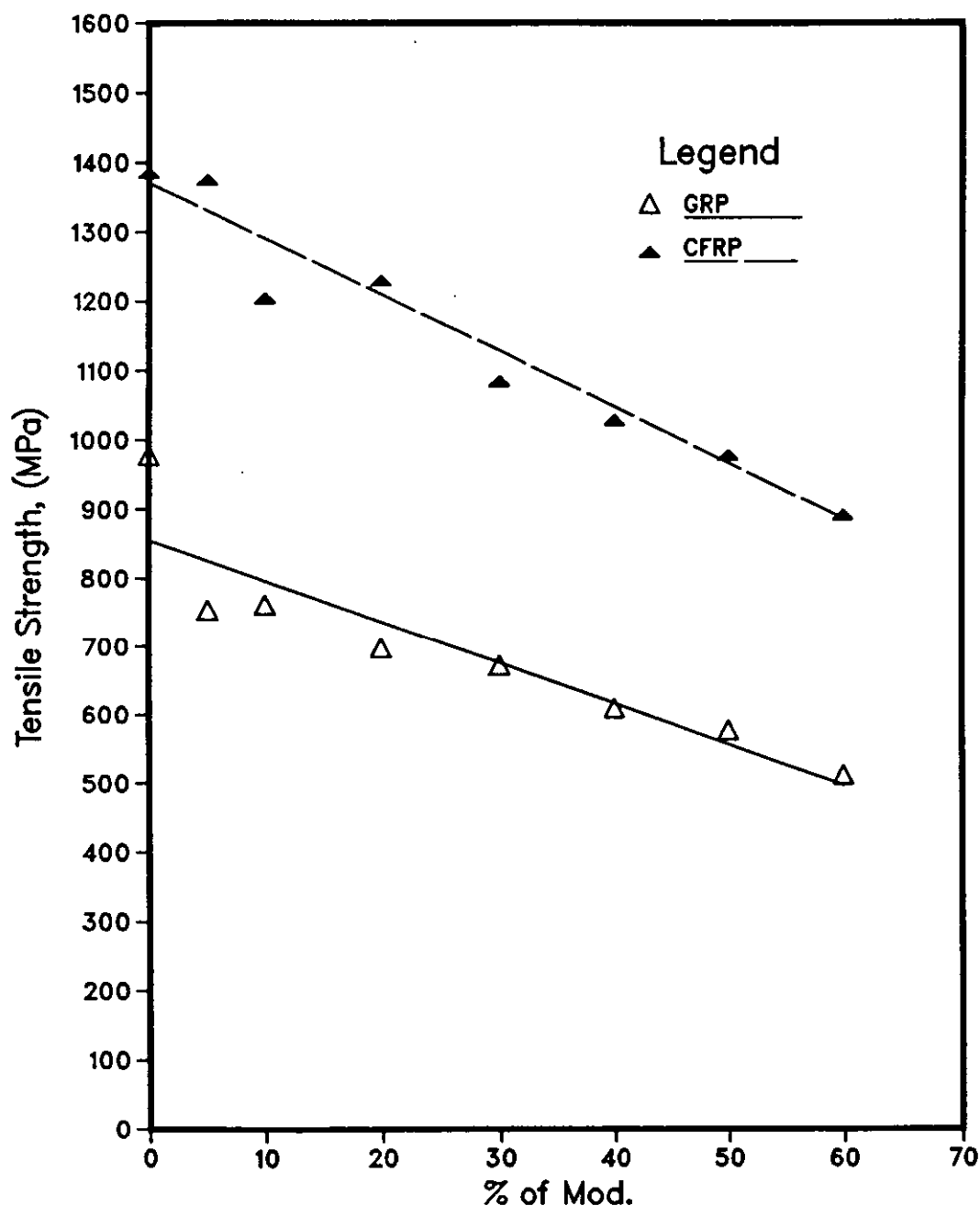


Fig.4-37: Mean Tensile Strength vs. % of Modifier

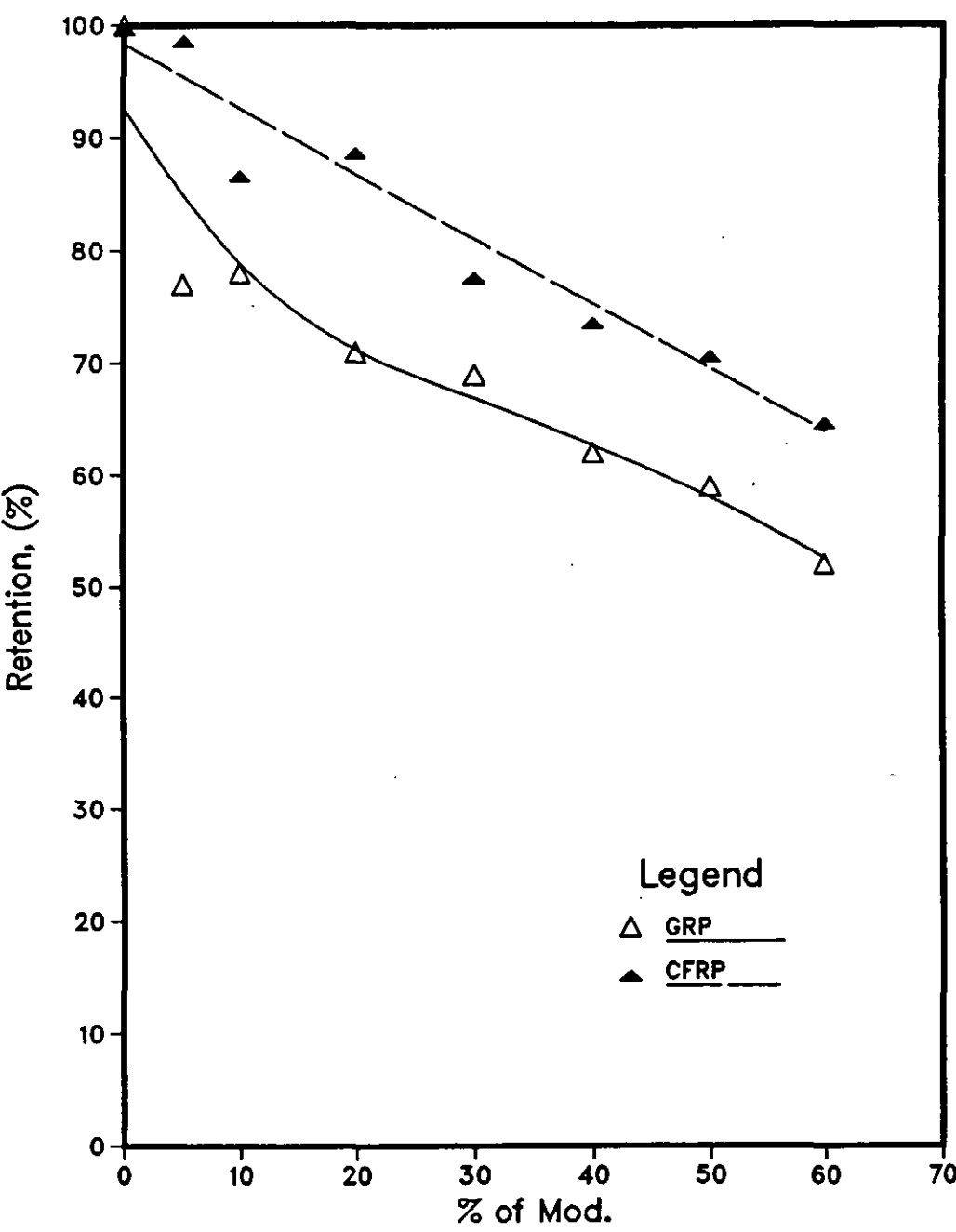


Fig.4-38: Tensile Strength Retention vs. % of Modifier

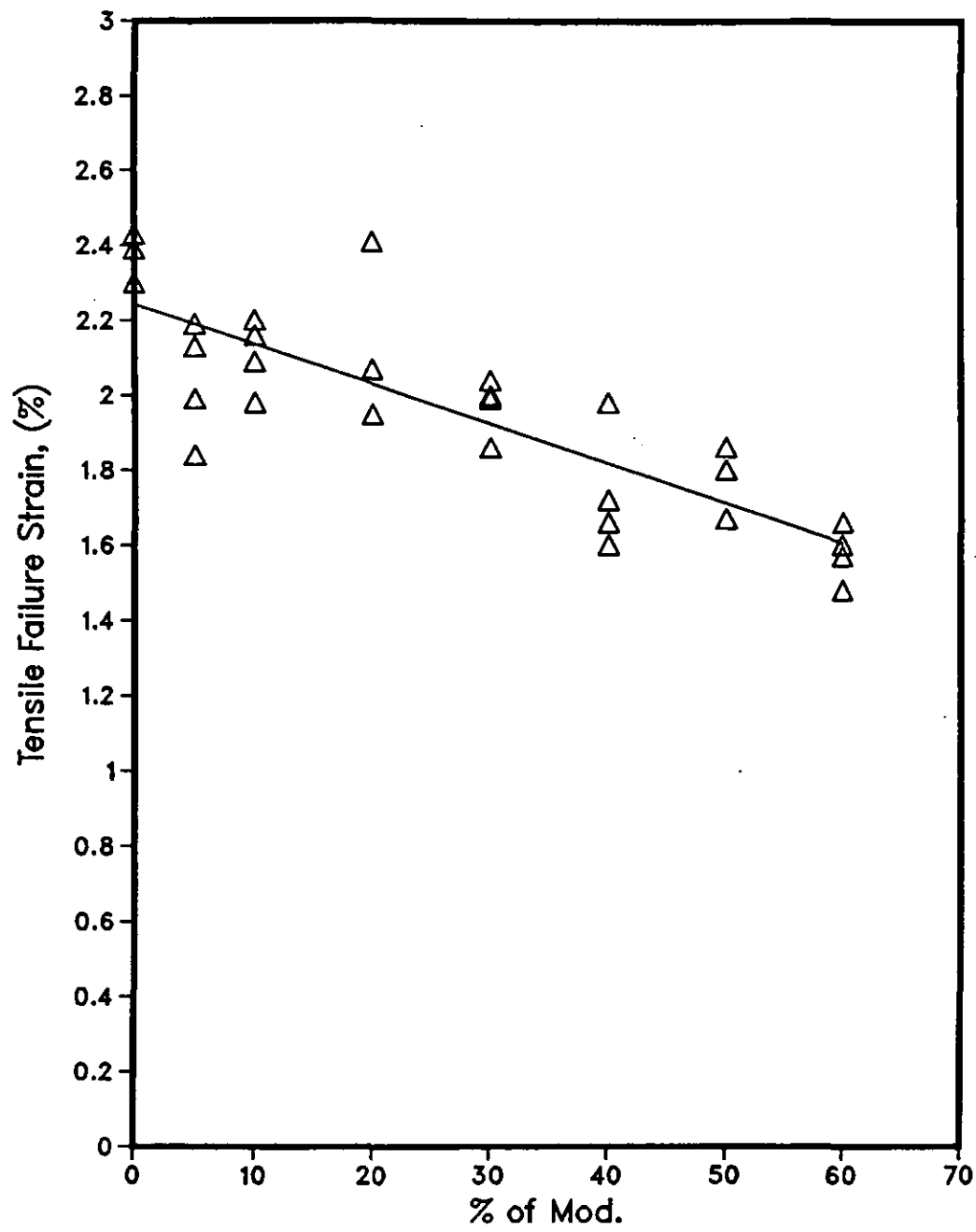


Fig.4-39: Tensile Failure Strain of (GRP) vs. % of Modifier

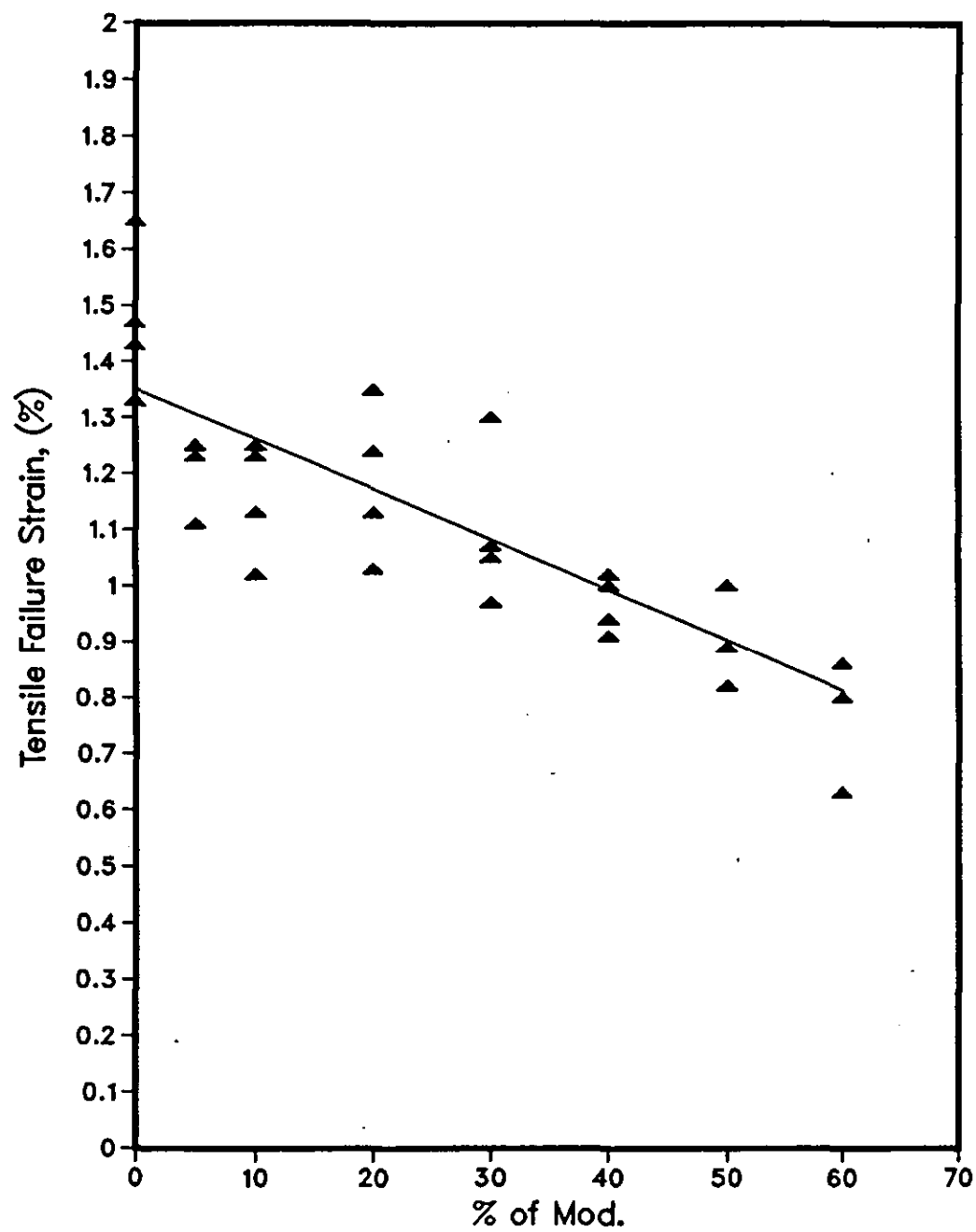


Fig.4-40: Tensile Failure Strain of (CFRP) vs. % of Modifier

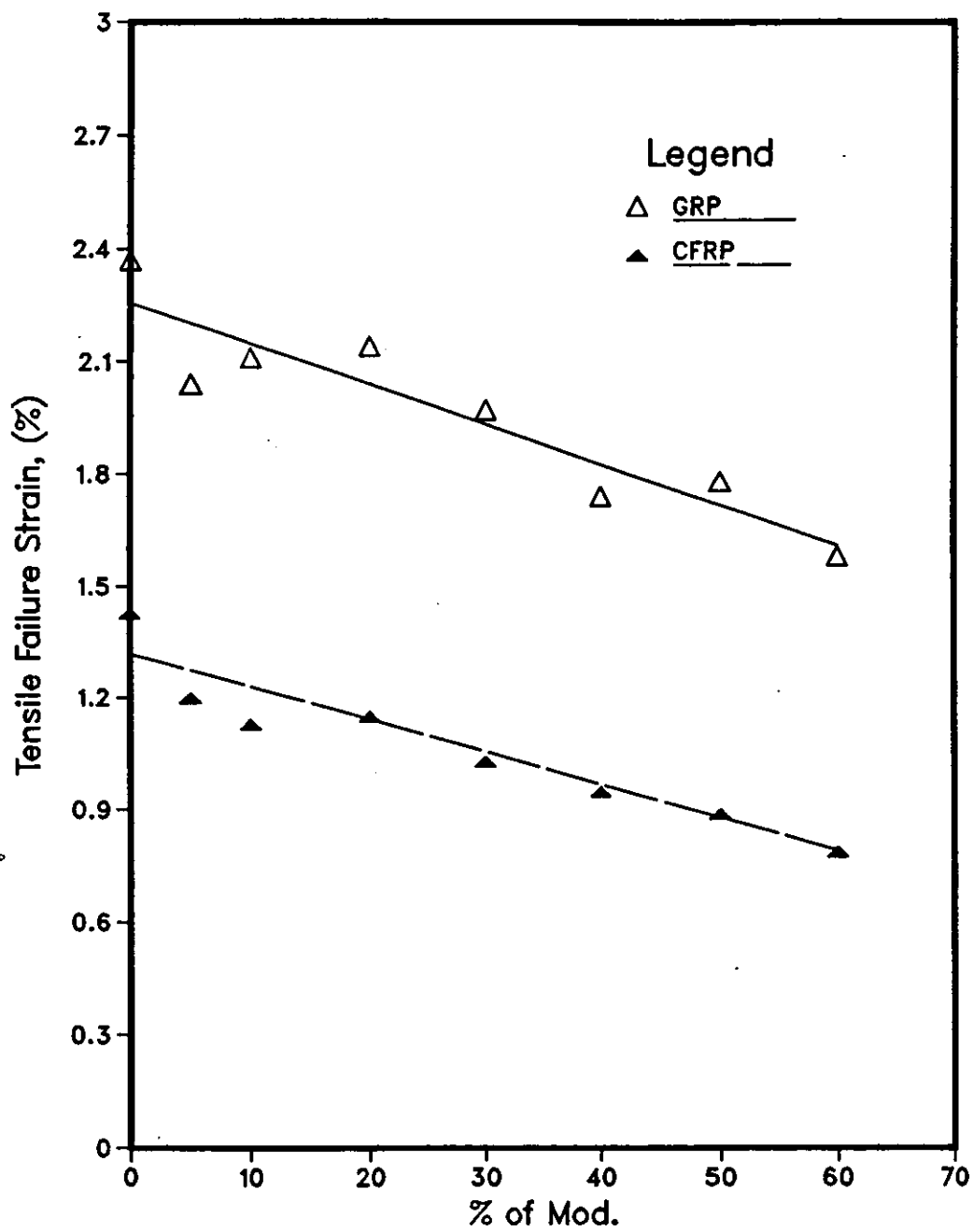


Fig.4-41: Mean Tensile Failure Strain vs. % of Modifier

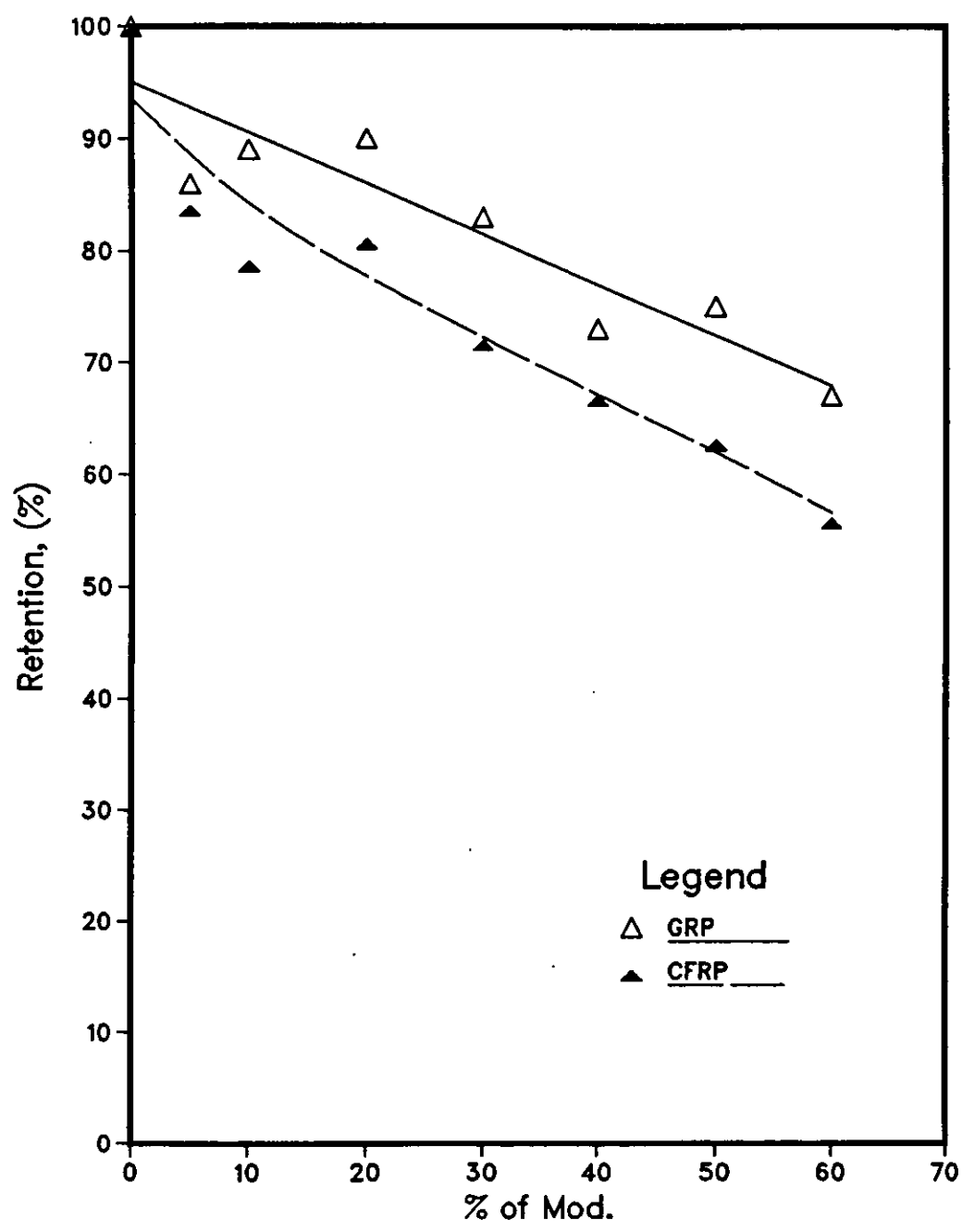


Fig.4-42: Tensile Failure Strain Retention vs. % of Modifier

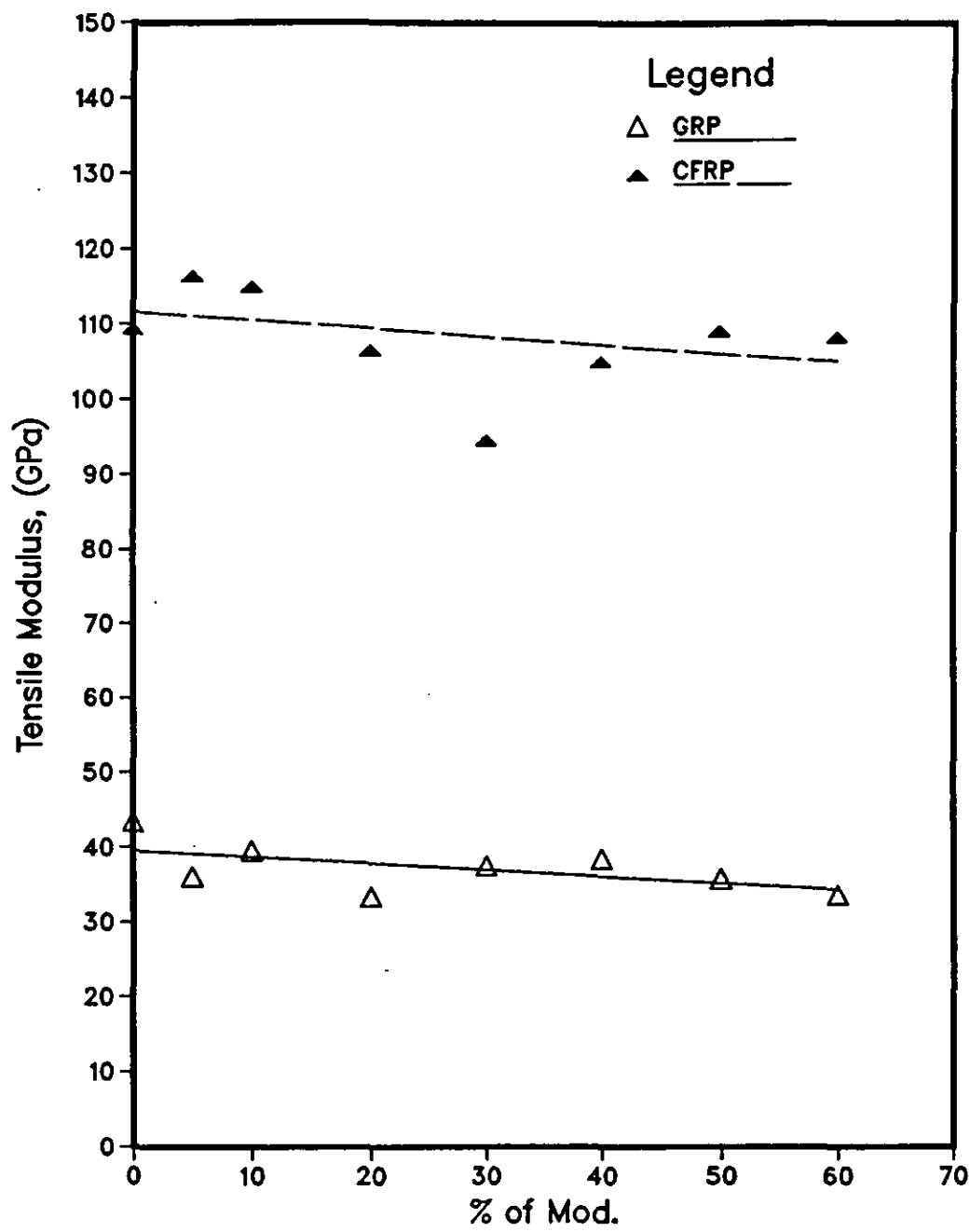


Fig.4-43: Mean Tensile Secant Modulus vs. % of Modifier

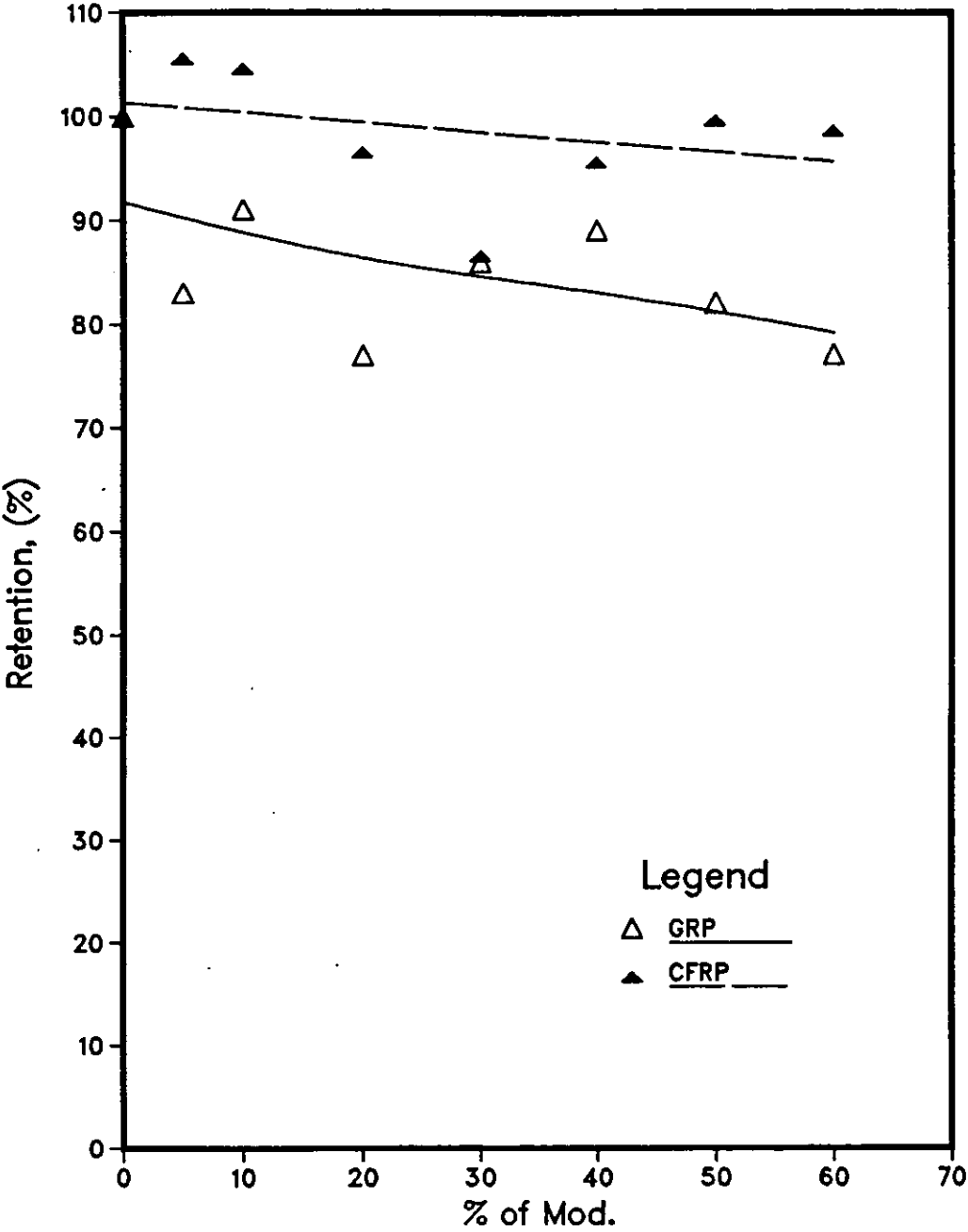


Fig.4-44: Tensile Secant Modulus Retention vs. % of Modifier

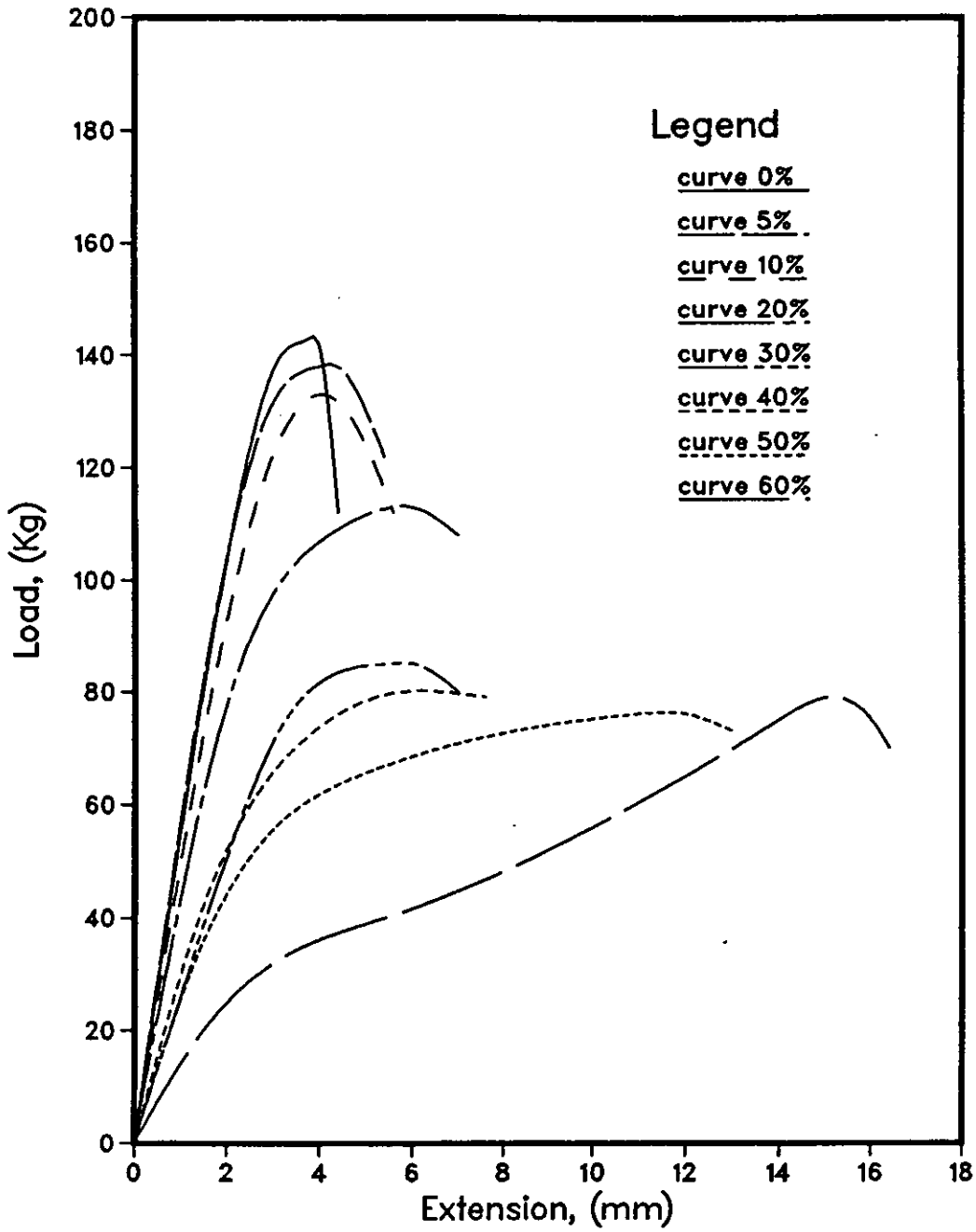


Fig.4-45: General Form of Curves for Inter-Laminar Shear Strength Test (GRP)

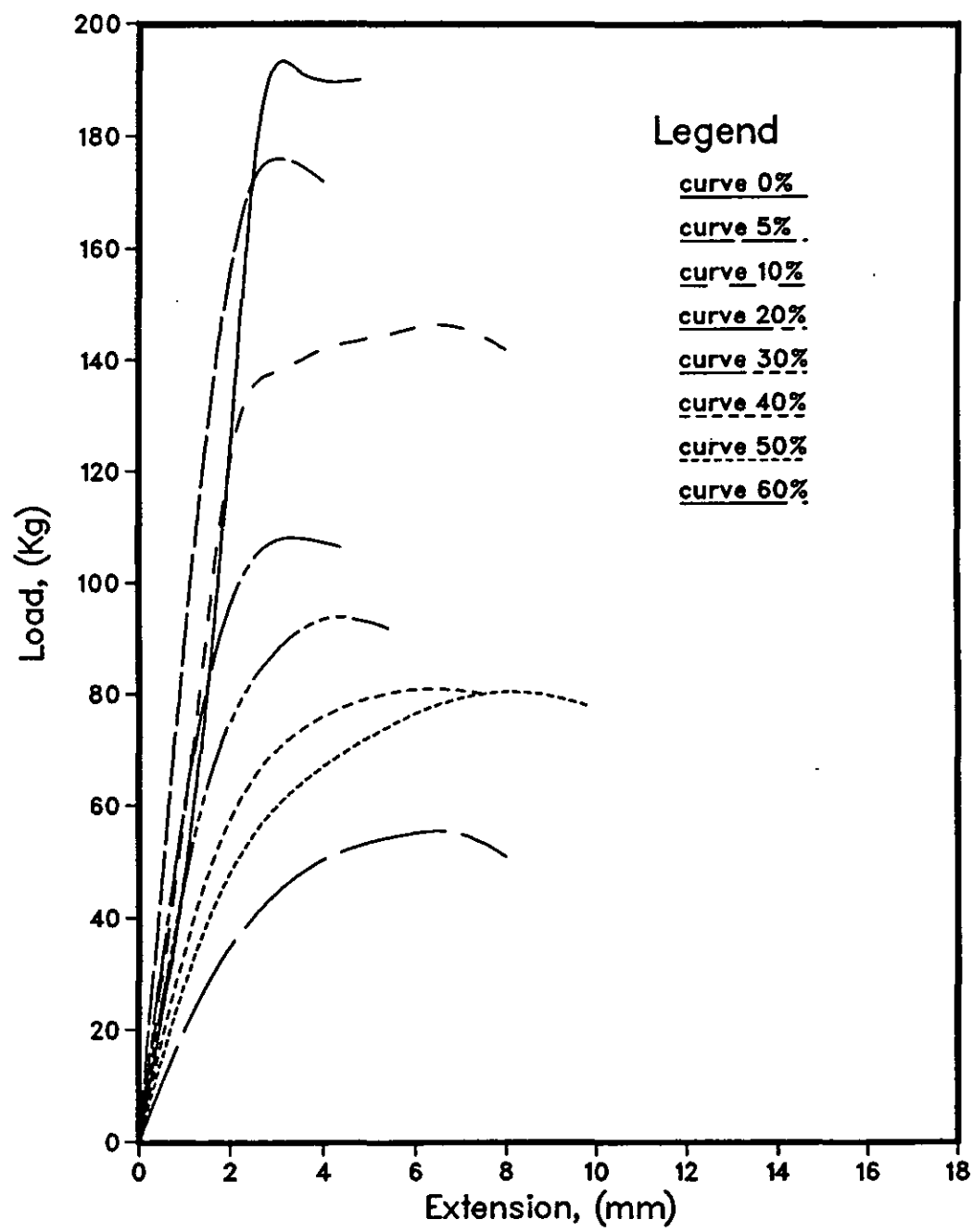


Fig.4-46: General Form of Curves for Inter-Laminar Shear Strength Test (CFRP)

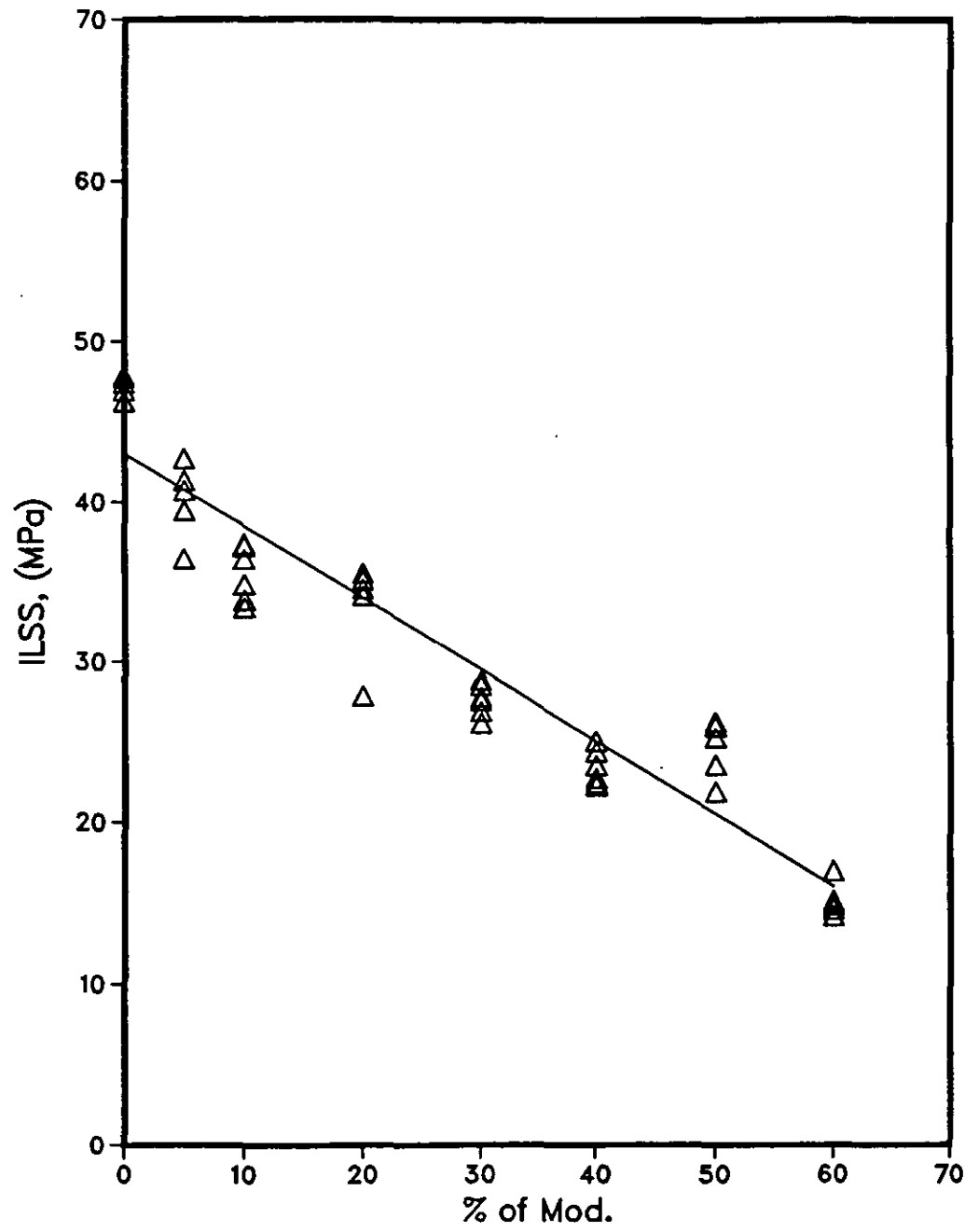


Fig.4-47: Inter-laminar Shear Strength vs. % of Modifier (GRP)

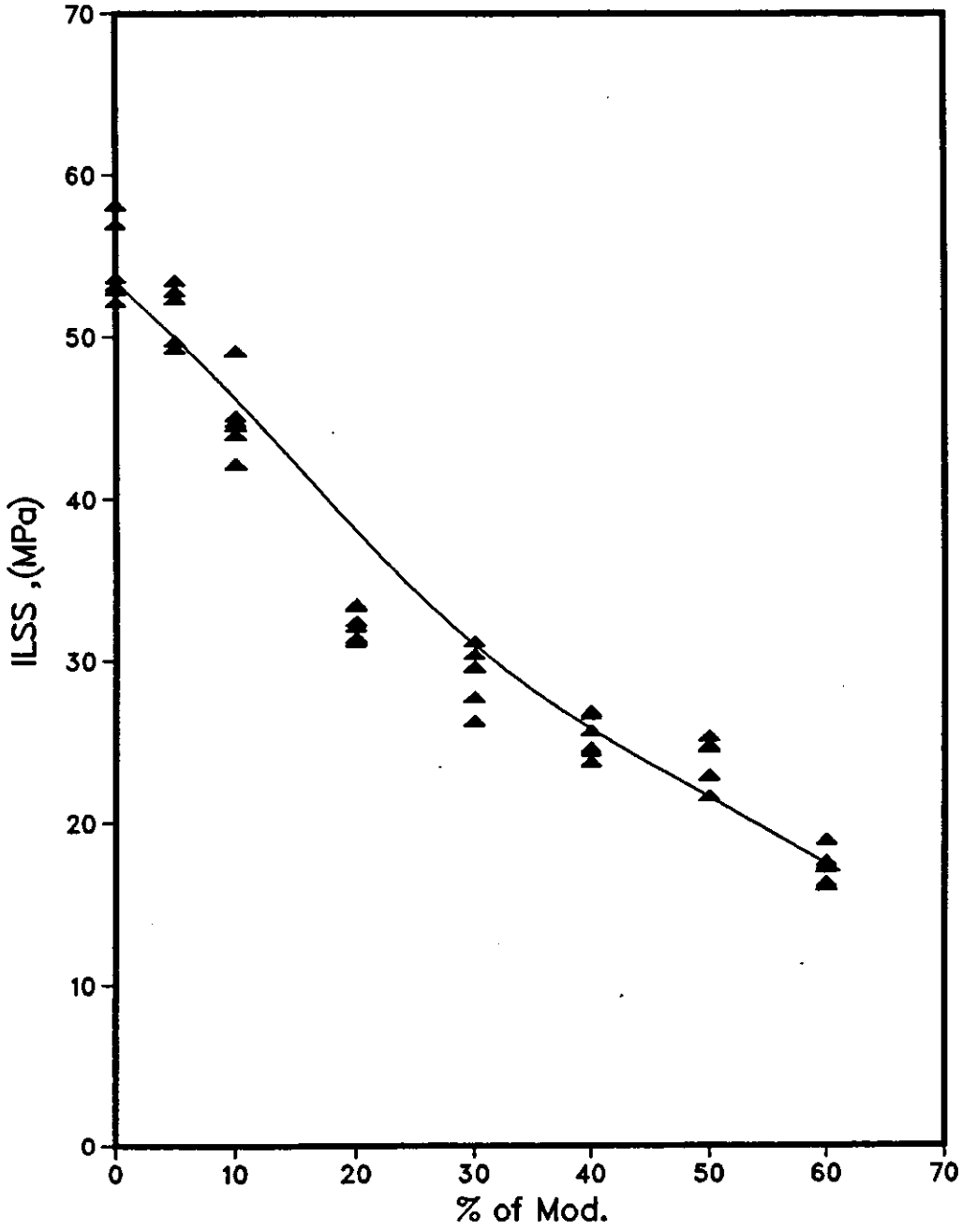


Fig.4-48: Inter-Laminar Shear Strength vs. % of Modifier (CFRP)

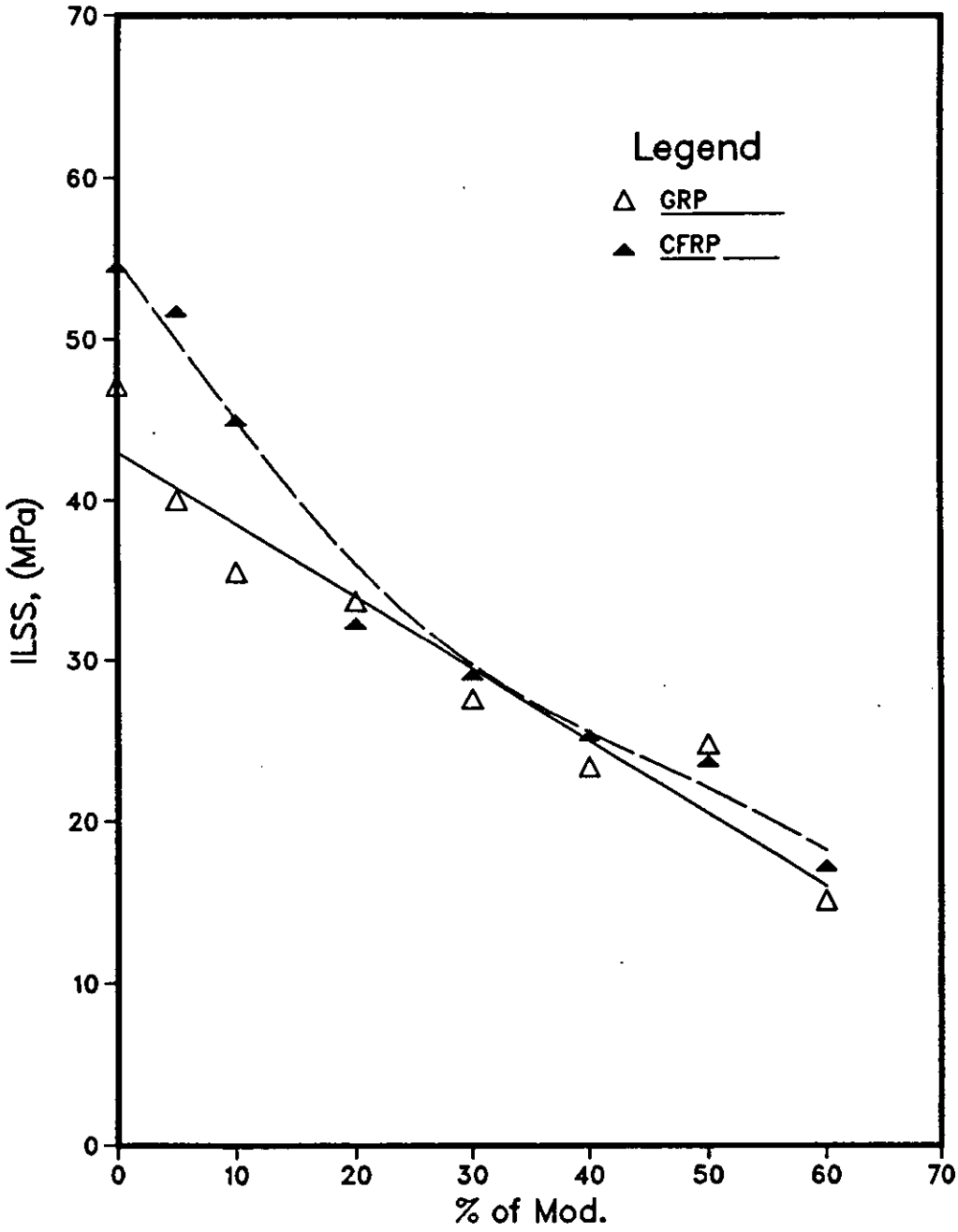


Fig.4-49: Mean Inter-laminar Shear Strength vs. % of Modifier

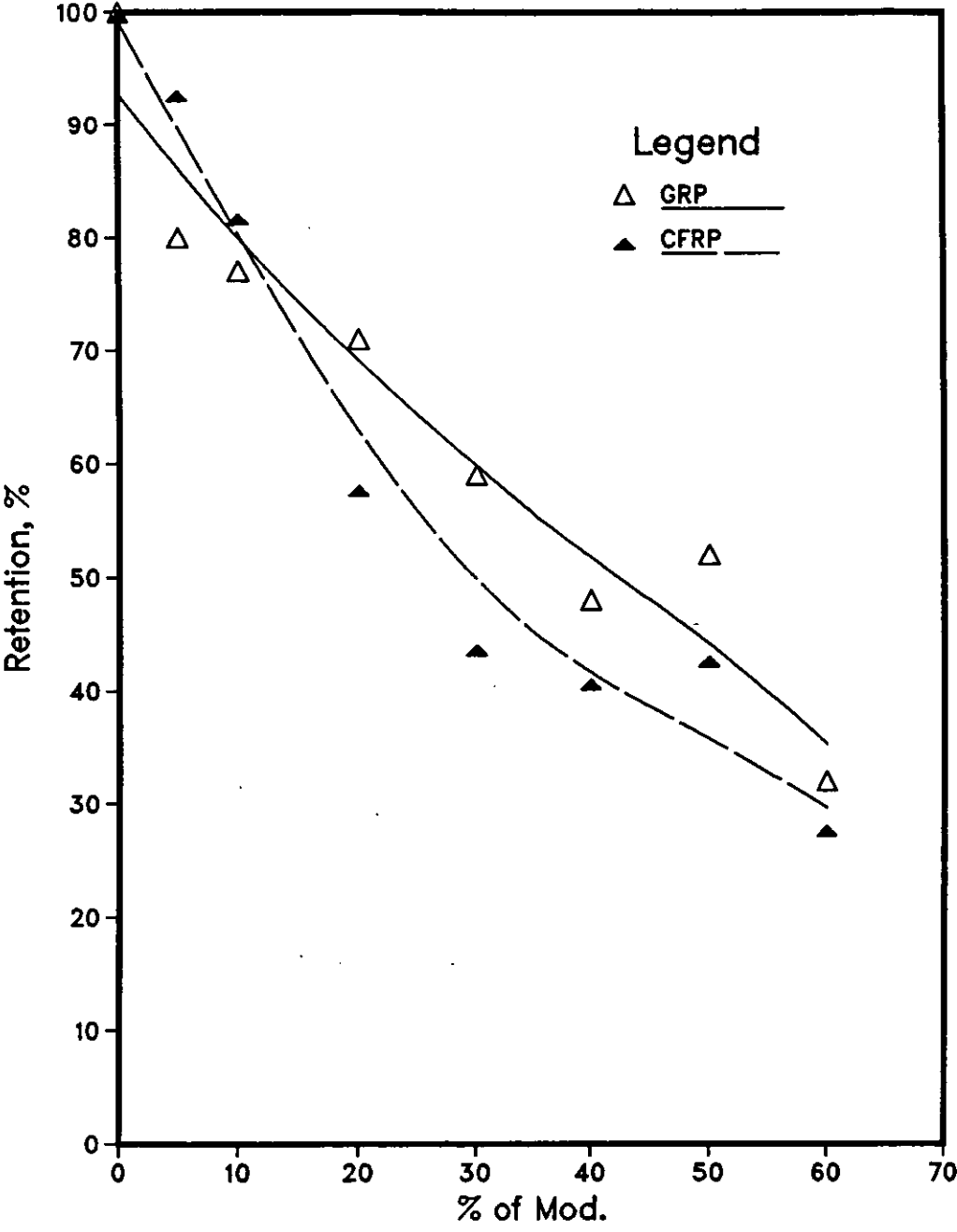


Fig.4-50: ILSS Retention vs.  
% of Modifier

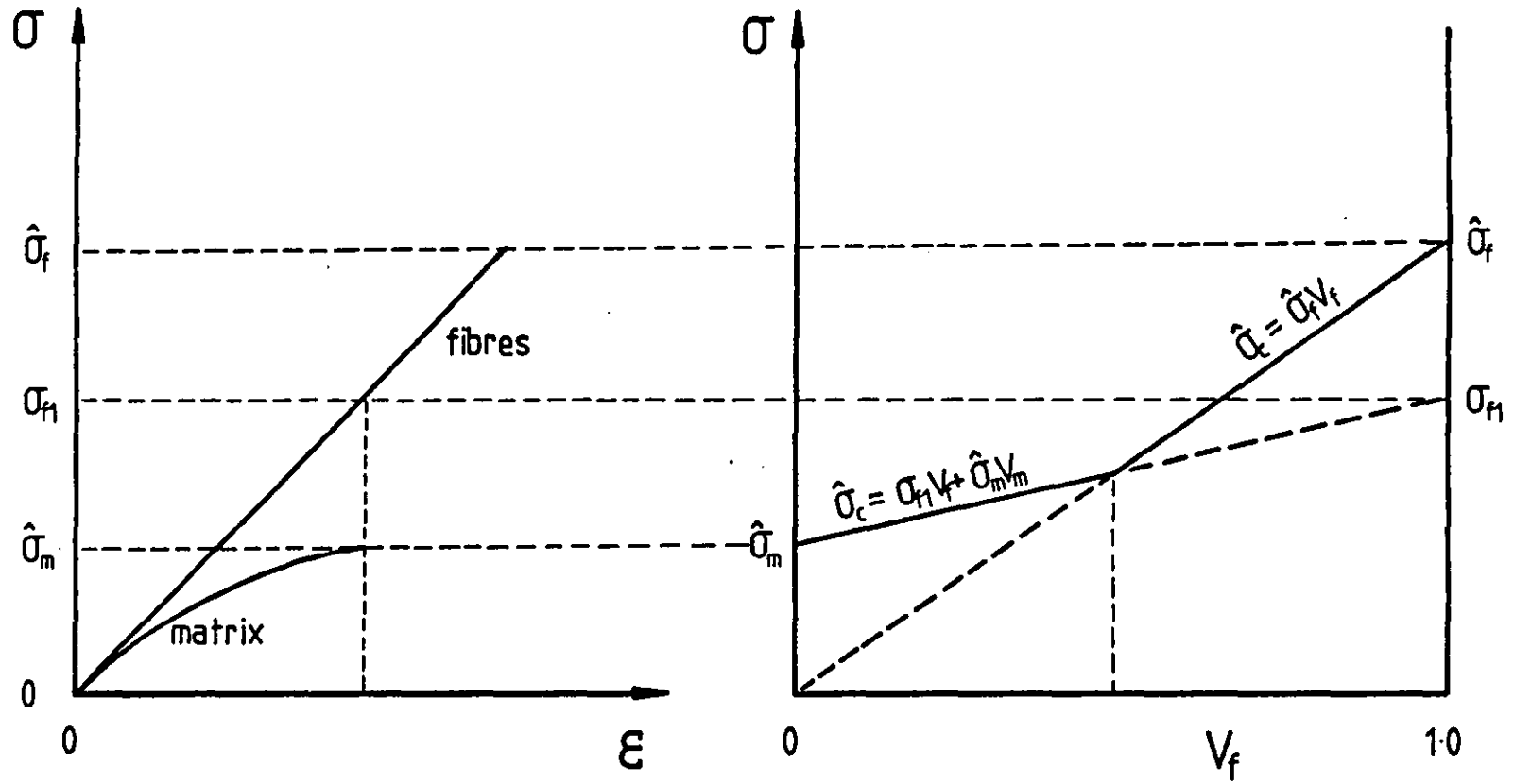


FIGURE 5.51: THE RULE OF MIXTURES RELATIONSHIP FOR THE STRENGTH OF UNIDIRECTIONAL COMPOSITES  
IN WHICH  $\hat{\epsilon}_f > \hat{\epsilon}_m$

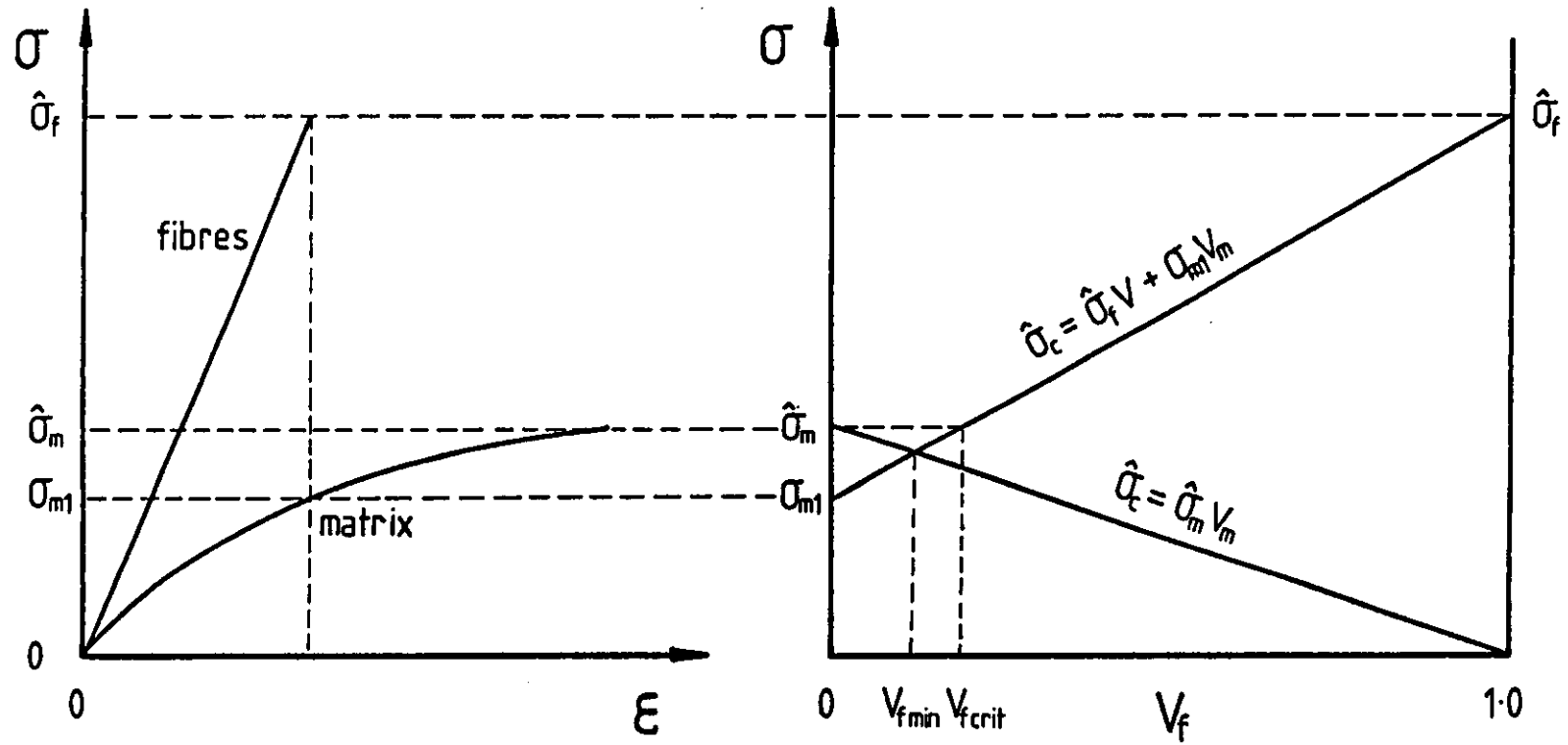


FIGURE 5.52: THE RULE OF MIXTURES RELATIONSHIP FOR THE STRENGTH OF UNIDIRECTIONAL COMPOSITES  
IN WHICH  $\hat{\epsilon}_m > \hat{\epsilon}_f$

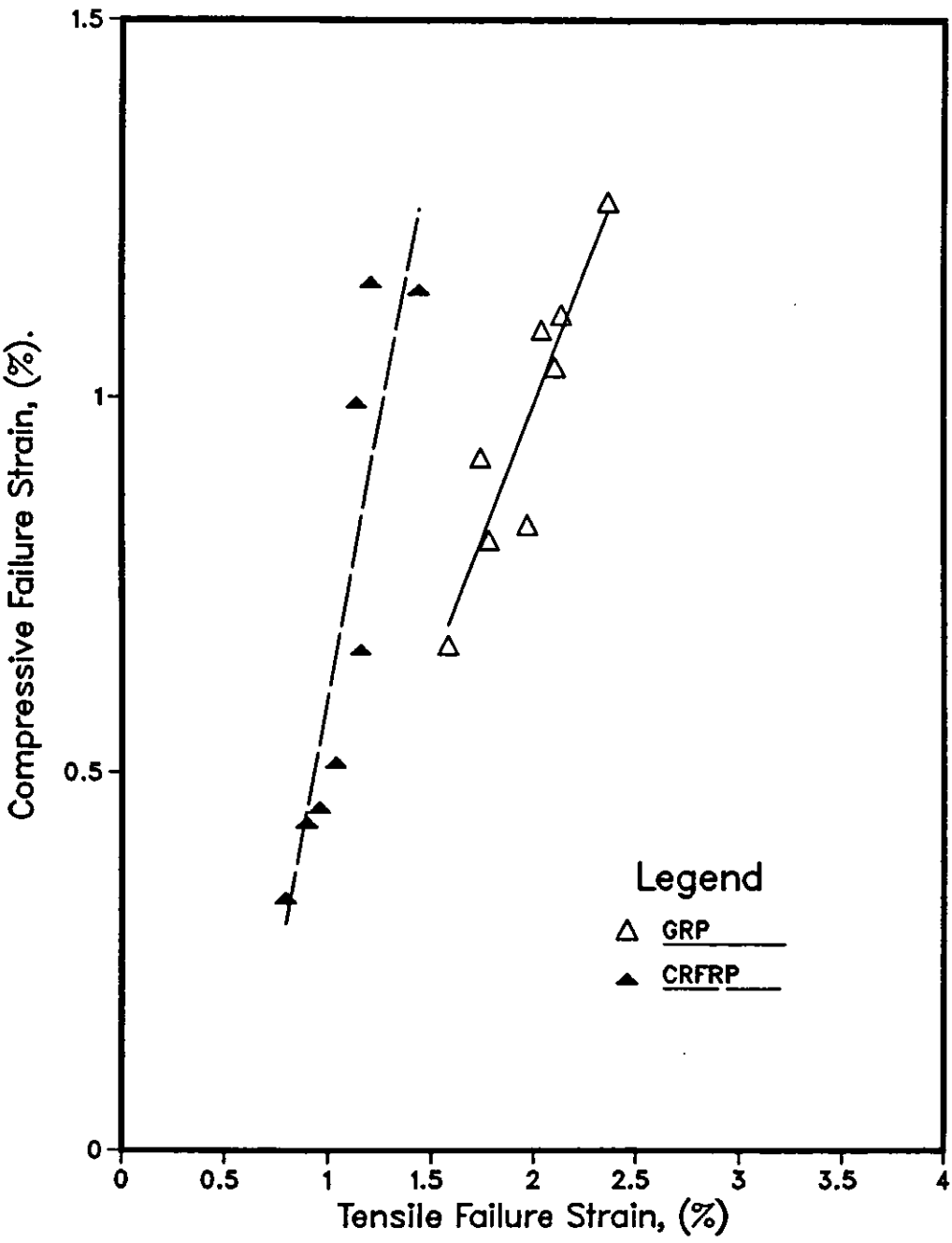


Fig.5-53: A Correlation between Compression and Tensile Failure Strain

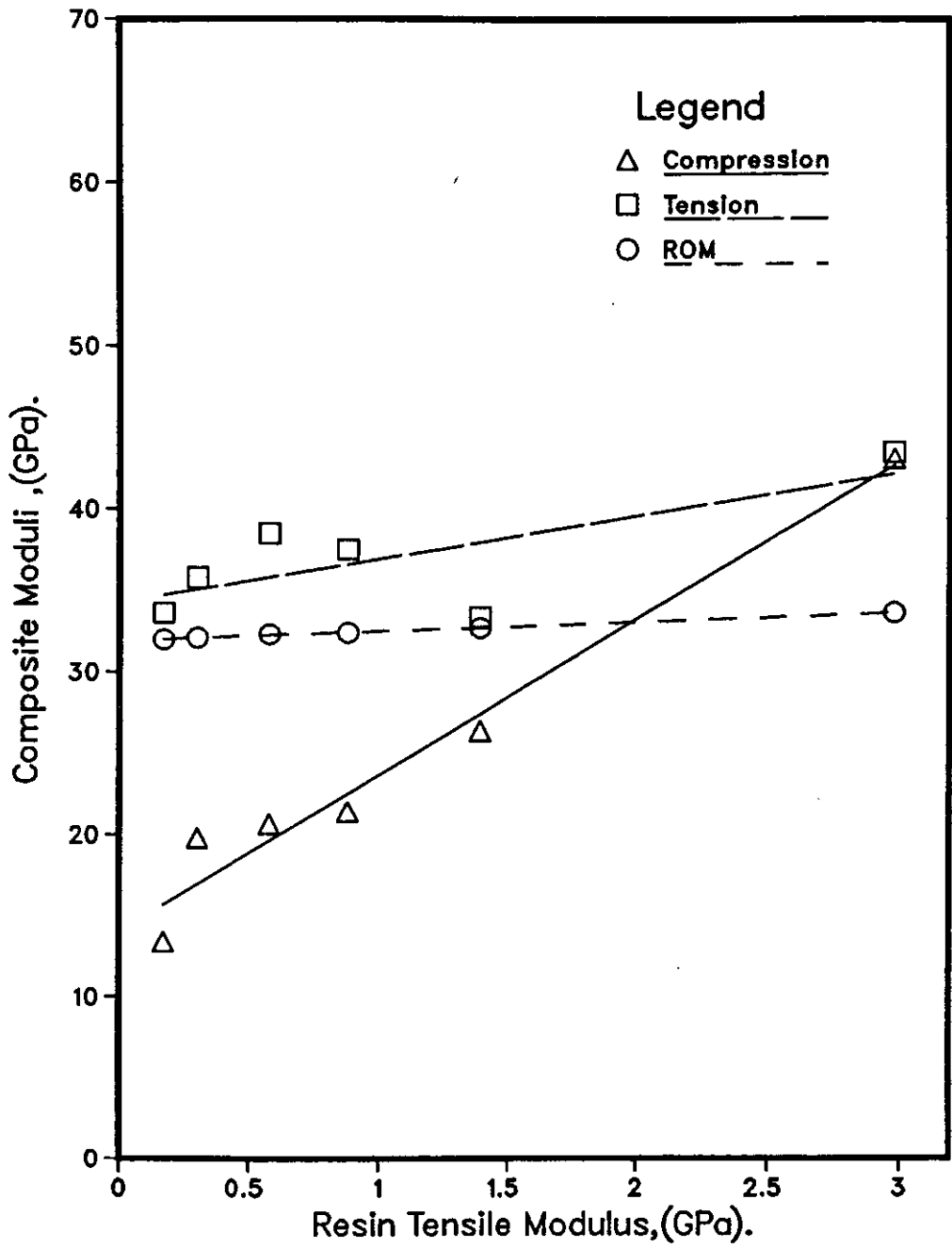


Fig.5-54: Effect of Resin Tensile Moduli on Compressive and Tensile Moduli of GRP

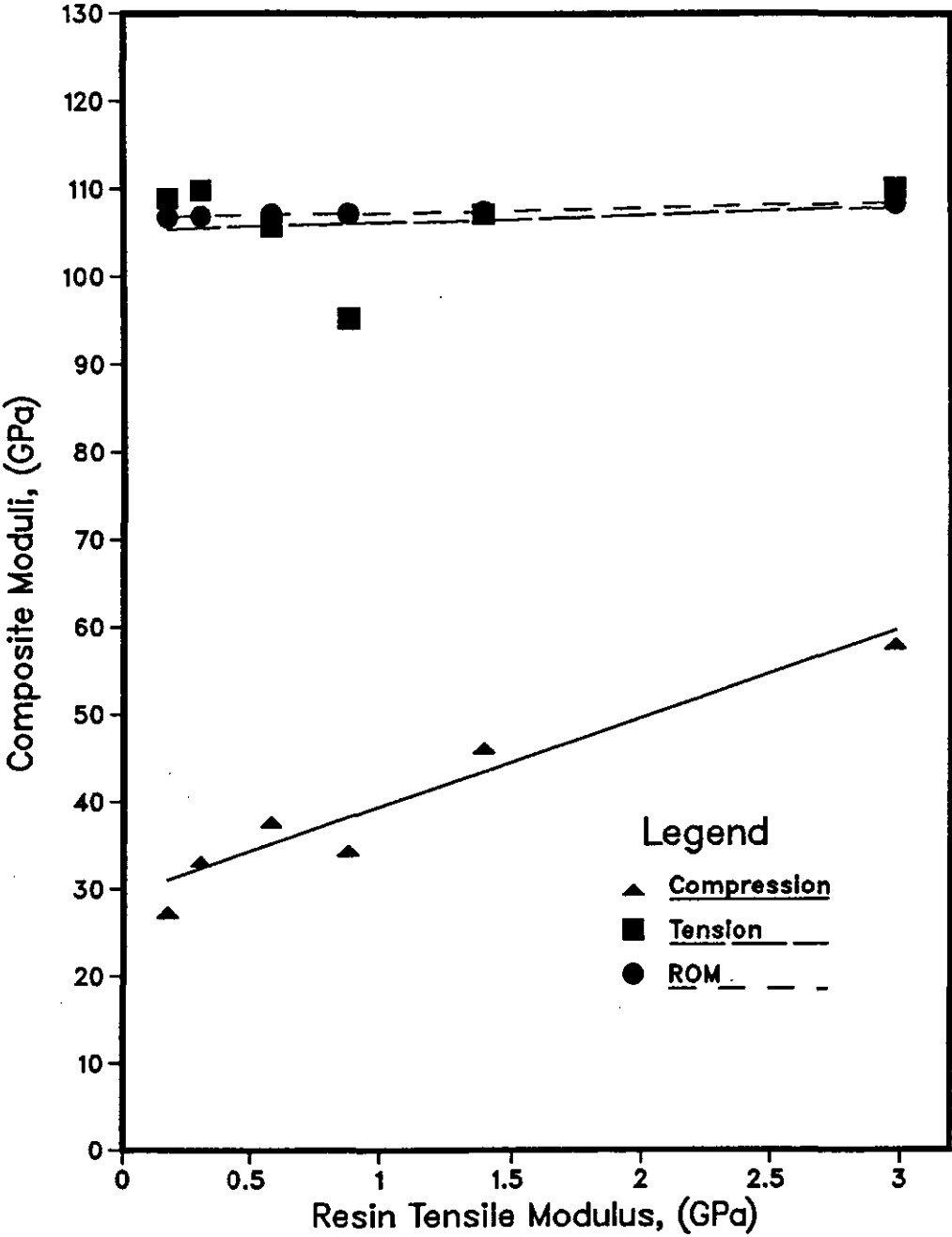


Fig.5-55: Effect of Resin Tensile Moduli on Compressive & Tensile Moduli of CFRP

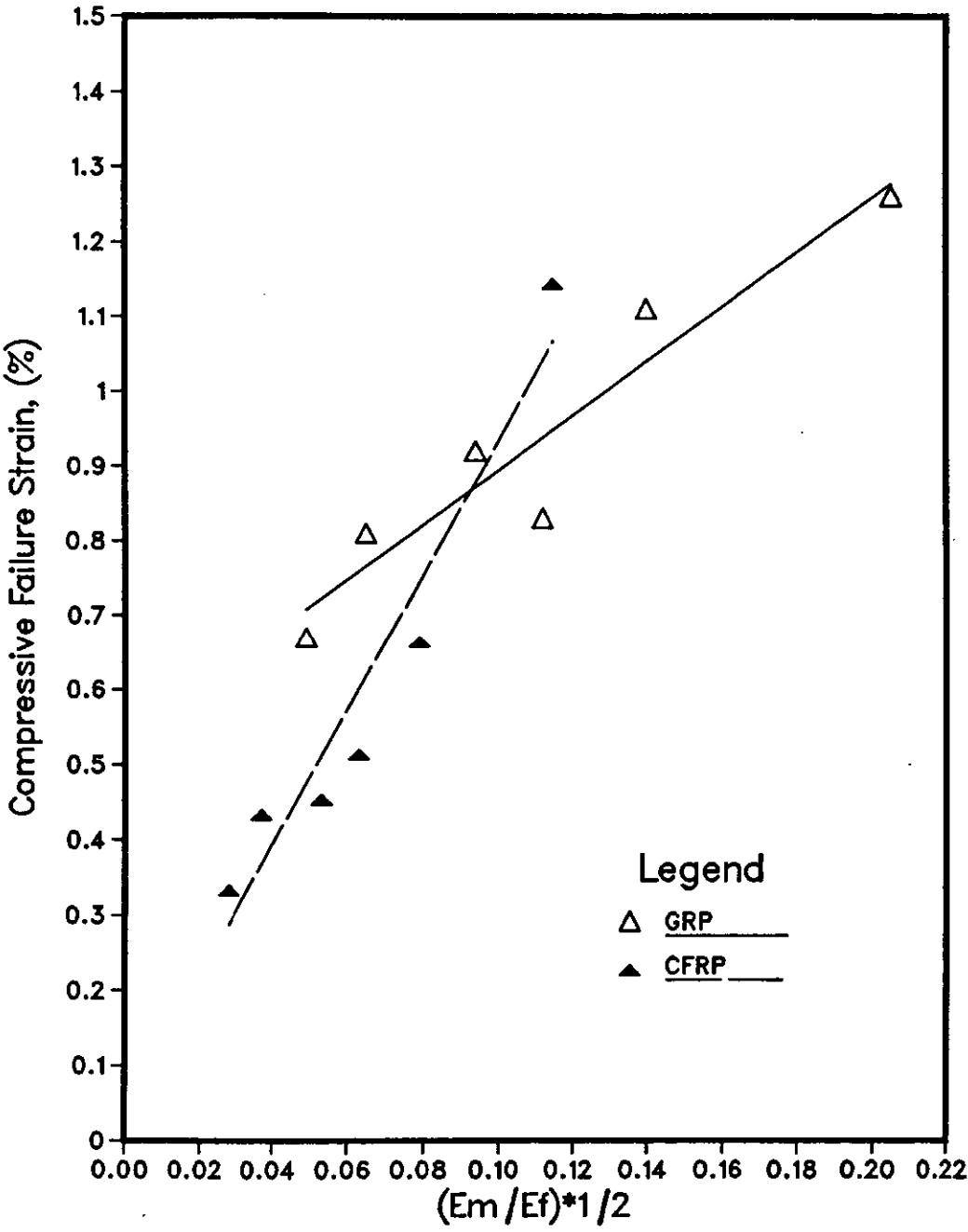


Fig.5-56: Compressive Failure Strain vs. Square Root of the Matrix-to-Fibre Modulus Ratio

# PLATES

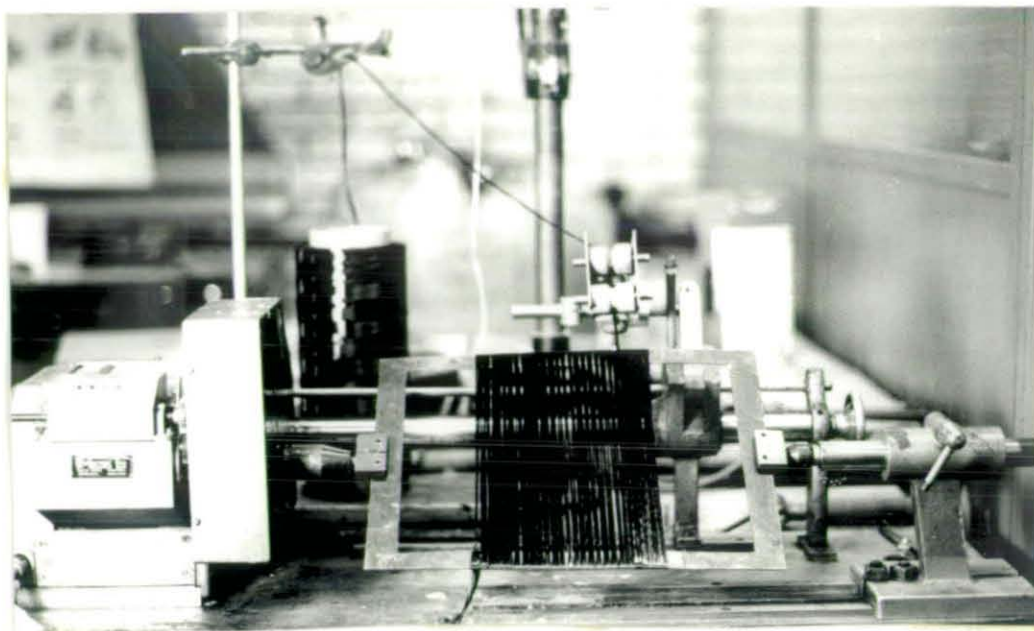


PLATE 1: THE WINDING MACHINE



PLATE 2: THE LEAKY MOULD USED IN THE WET LAY-UP OF EPOXY RESIN COMPOSITES SHOWING FOUR G-CLAMPS



PLATE 3: THE MAND SERVO-SCREW TEST MACHINE WITH WHICH  
COMPRESSIVE TESTS WERE PERFORMED



PLATE 4: THE CELANESE COMPRESSION TEST FIXTURE



PLATE 5: THE DARTEC SERVOHYDRAULIC TEST MACHINE WITH WHICH TENSILE TESTS WERE PERFORMED

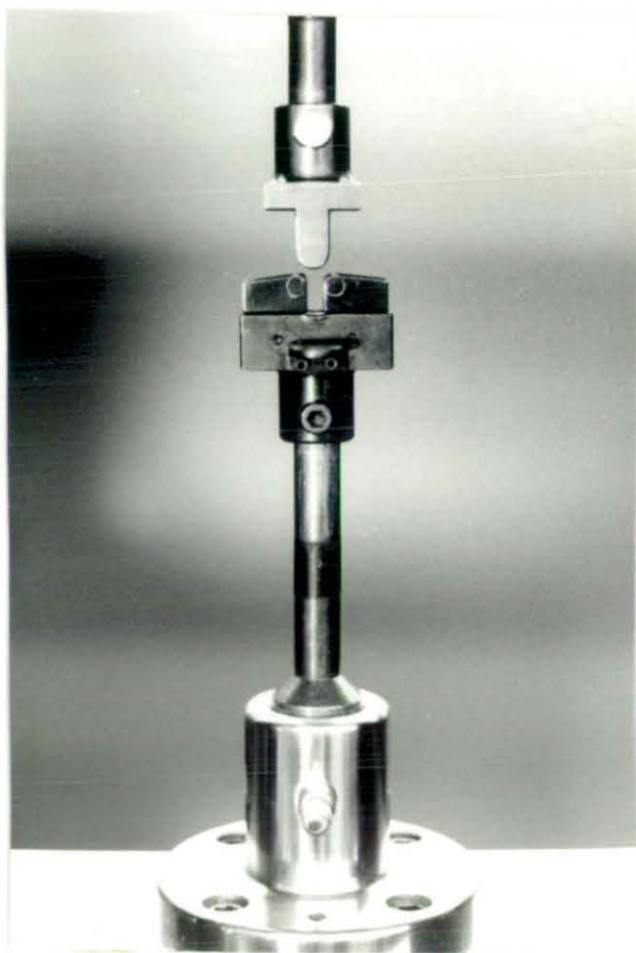
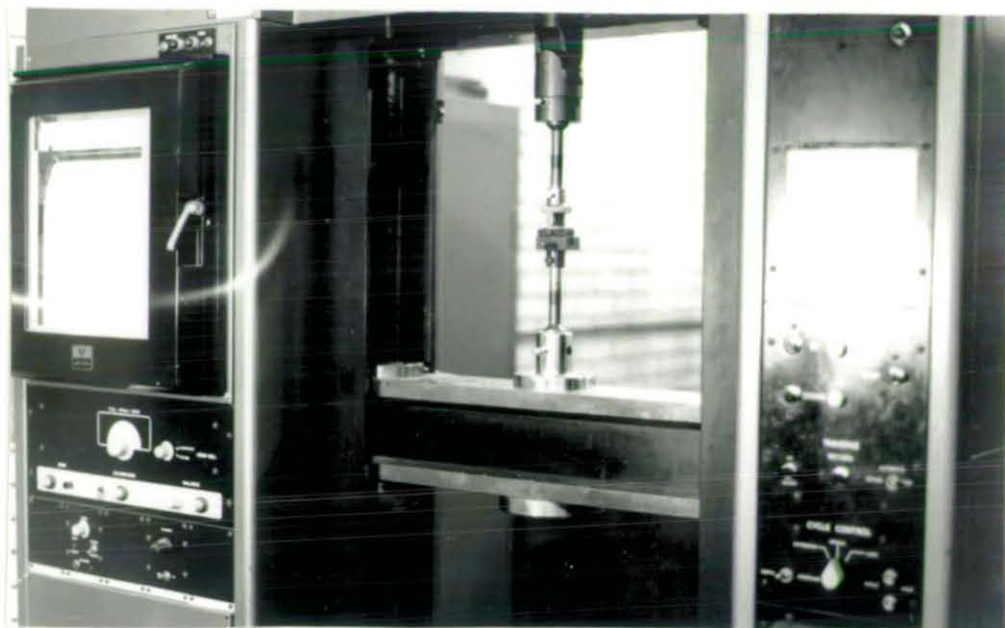


PLATE 6: THE INSTRON TEST MACHINE WITH WHICH INTER-LAMINAR SHEAR TESTS WERE PERFORMED

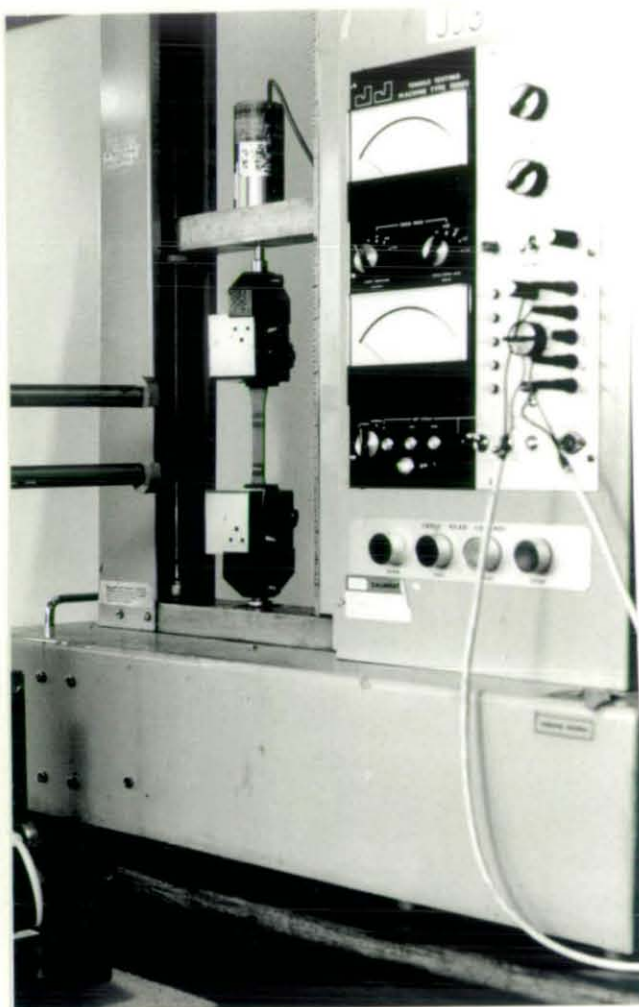
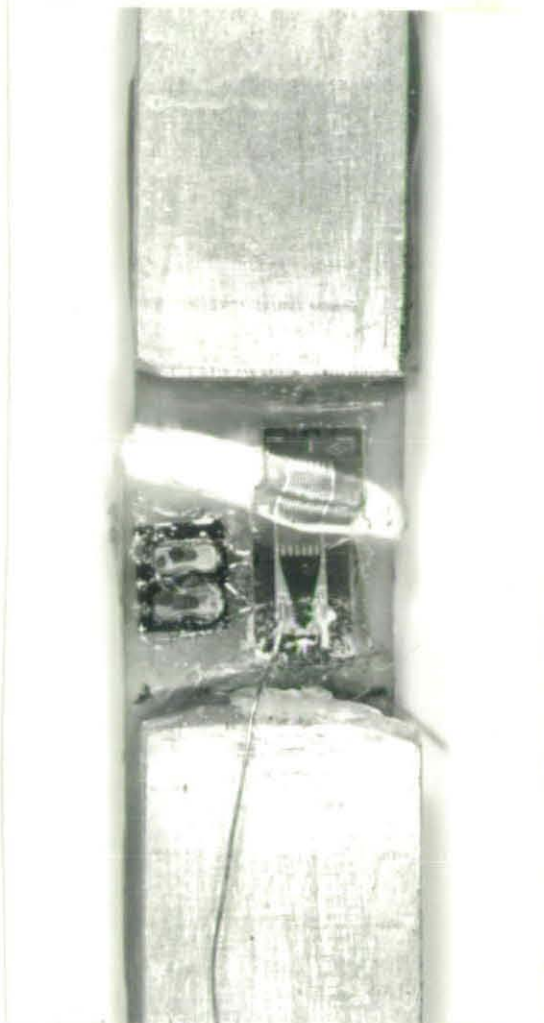


PLATE 7: THE JJ TEST MACHINE WITH WHICH RESIN TENSILE TESTS WERE PERFORMED



(a)



(b)

- PLATE 8: a) MULTIPLE KINK-BANDS IN SOME UNMODIFIED GRP SPECIMENS SHOWING  $70^\circ$  INCLINATION OF THE BANDS TO THE FIBRE AXIS
- b) A SINGLE KINK BAND OBSERVED IN SOME UNMODIFIED GRP SPECIMENS WITH A  $70^\circ$  INCLINATION



PLATE 9: A NARROW SINGLE KINK-BAND IN A 20% MODIFIED  
GRP SPECIMEN SHOWING A  $90^\circ$  INCLINATION TO THE  
FIBRE AXIS

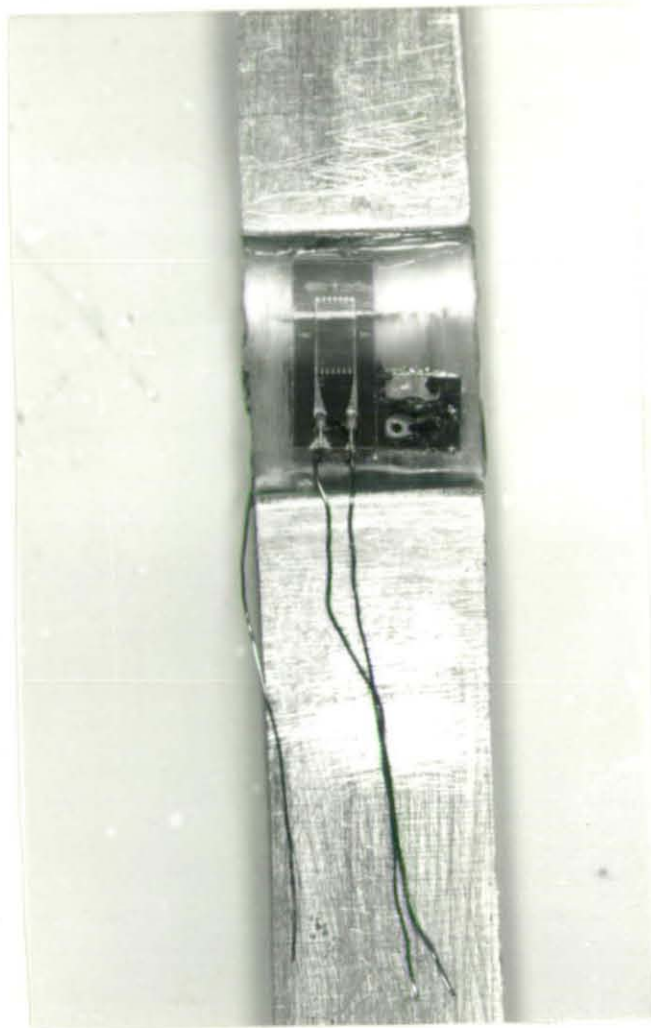


PLATE 10: A WIDER SINGLE KINK-BAND IN A 60% MODIFIED GRP SPECIMEN SHOWING A  $90^\circ$  INCLINATION TO THE FIBRE AXIS

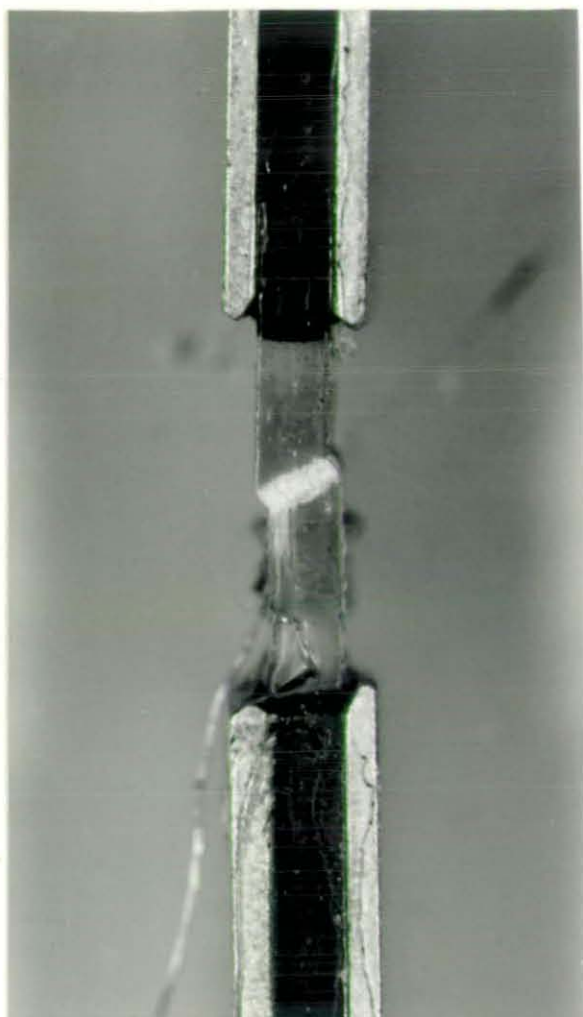


PLATE 11: A THROUGH THICKNESS KINK-BAND IN 5% MODIFIER GRP

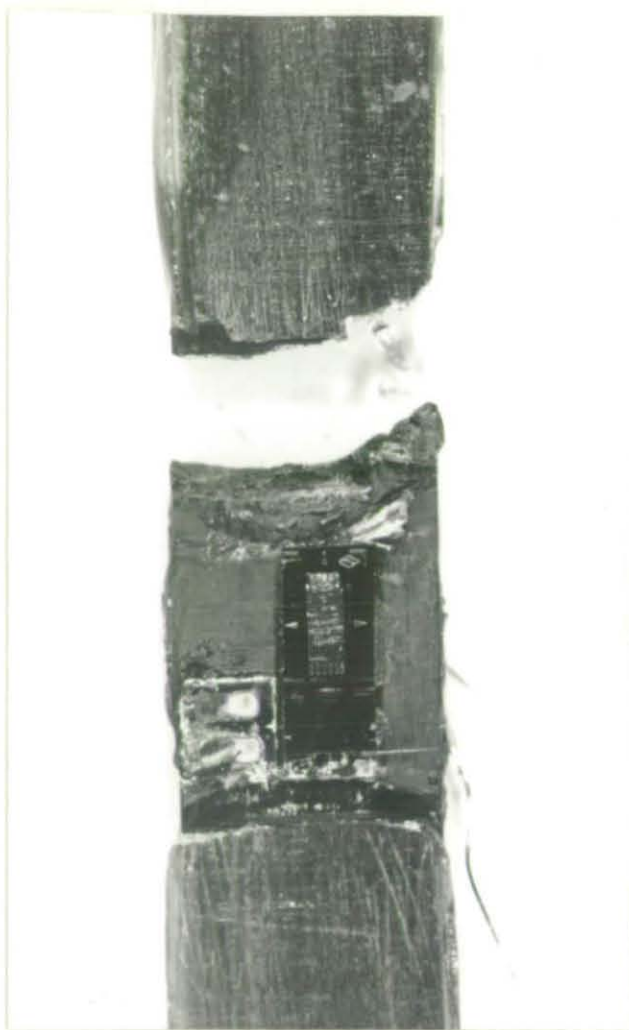


PLATE 12: THE SHEAR FAILURE MODE OBSERVED IN UNMODIFIED  
CFRP SPECIMENS

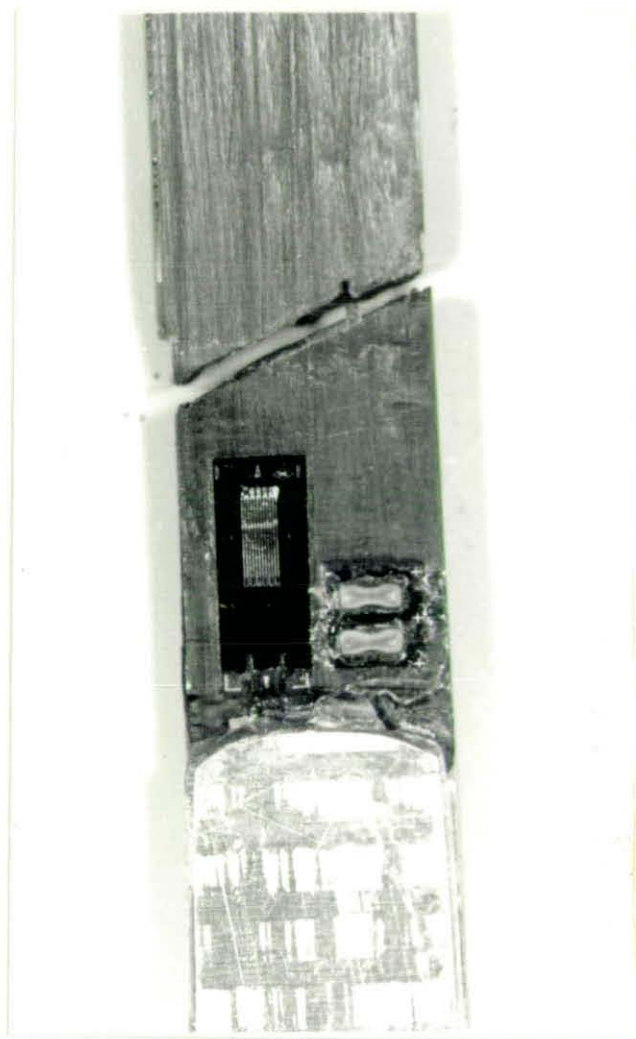


PLATE 13: A MICROBUCKLING MODE AS OBSERVED IN  $\leq 5\%$  MODIFIED CFRP SPECIMENS

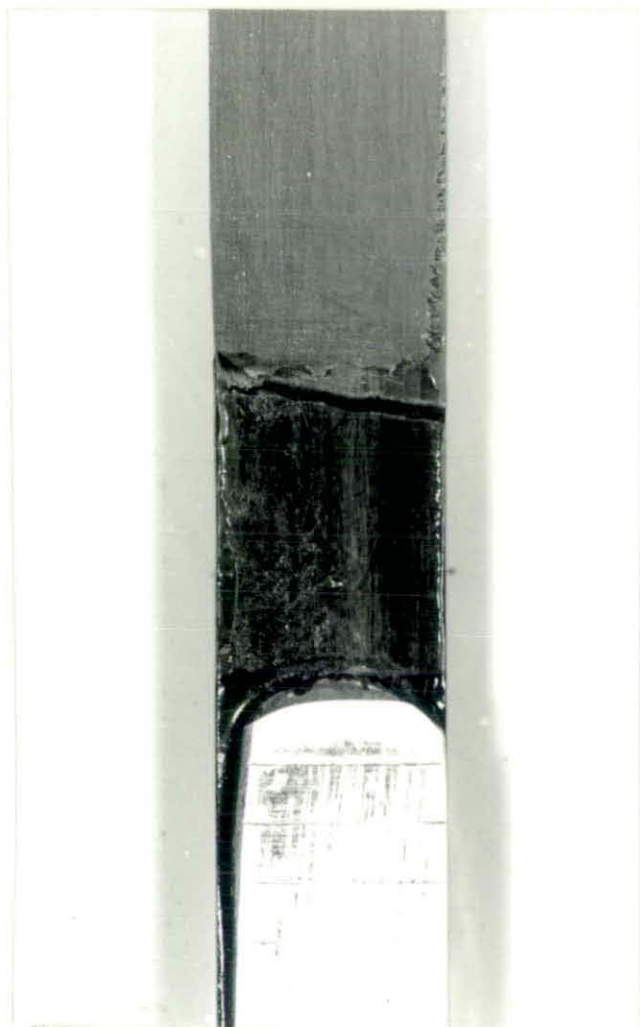


PLATE 14: A KINK BAND OBSERVED IN 30% MODIFIED CFRP SPECIMEN. THE SPECIMEN DID NOT FRACTURE.

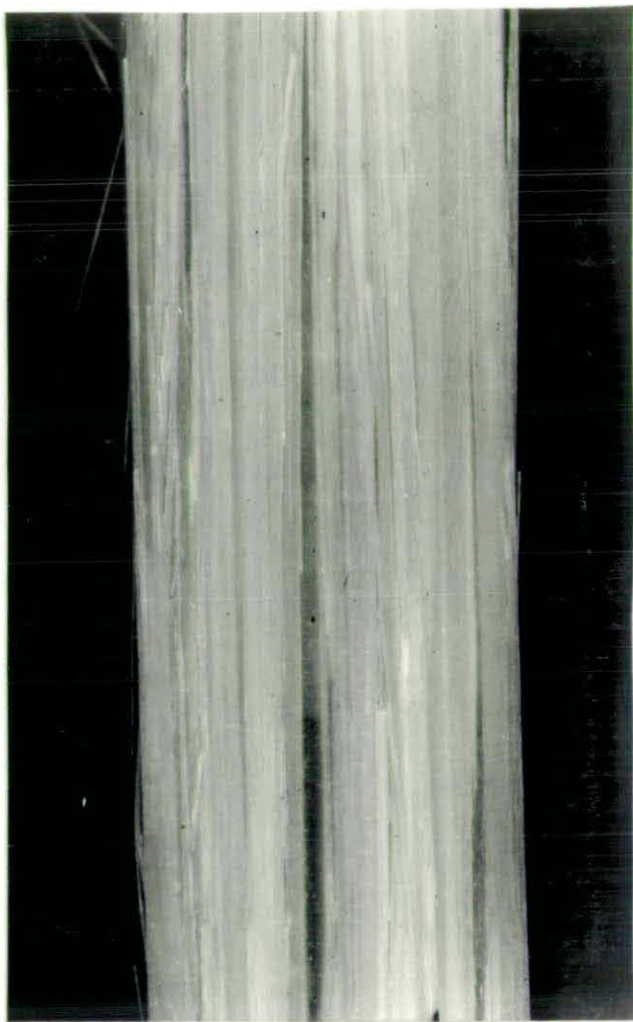


PLATE 15: A TENSILE FAILURE IN AN UNMODIFIED GRP SPECIMEN

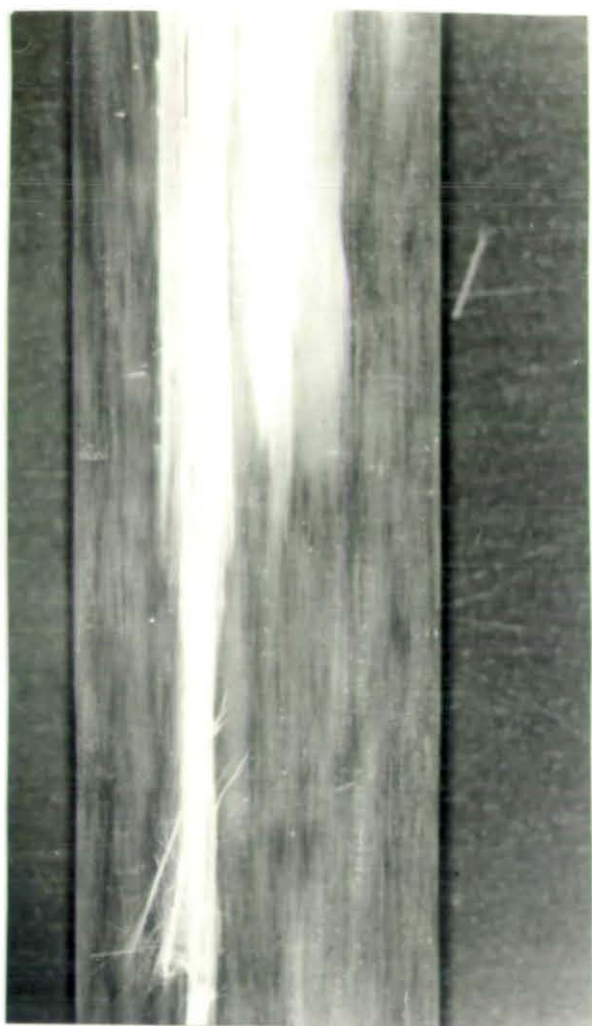


PLATE 16: A TENSILE FAILURE IN 60% MODIFIED GRP SPECIMEN



PLATE 17: A TENSILE FAILURE IN AN UNMODIFIED CFRP SPECIMEN

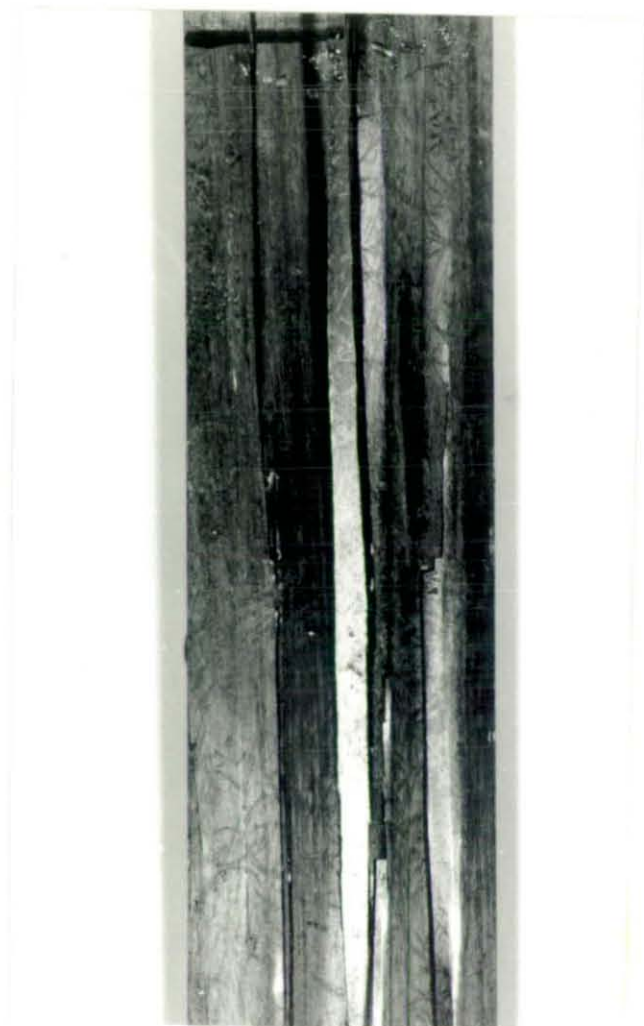


PLATE 18: A TENSILE FAILURE IN A 60% MODIFIED CFRP SPECIMEN

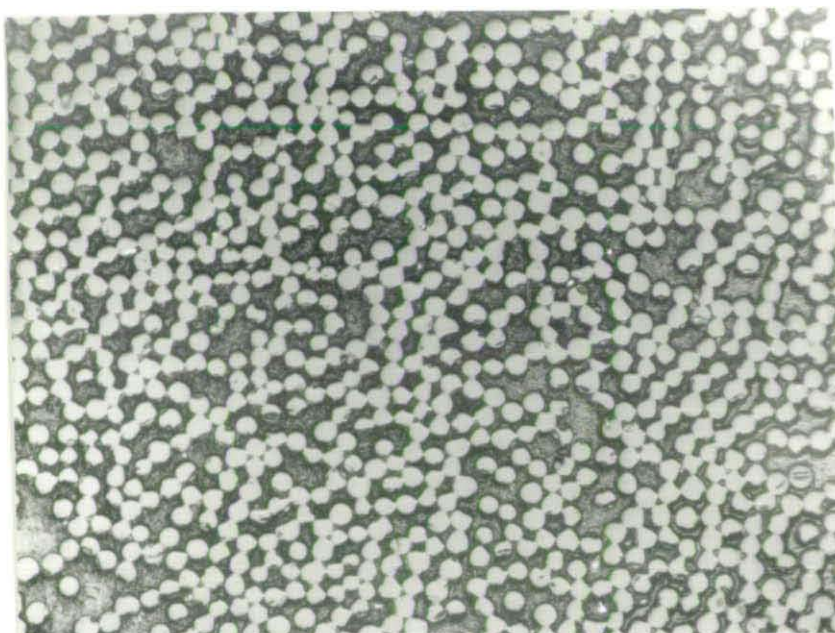


PLATE 19: THE FIBRE DISTRIBUTION IN AN UNMODIFIED GRP SPECIMEN  
(x200)

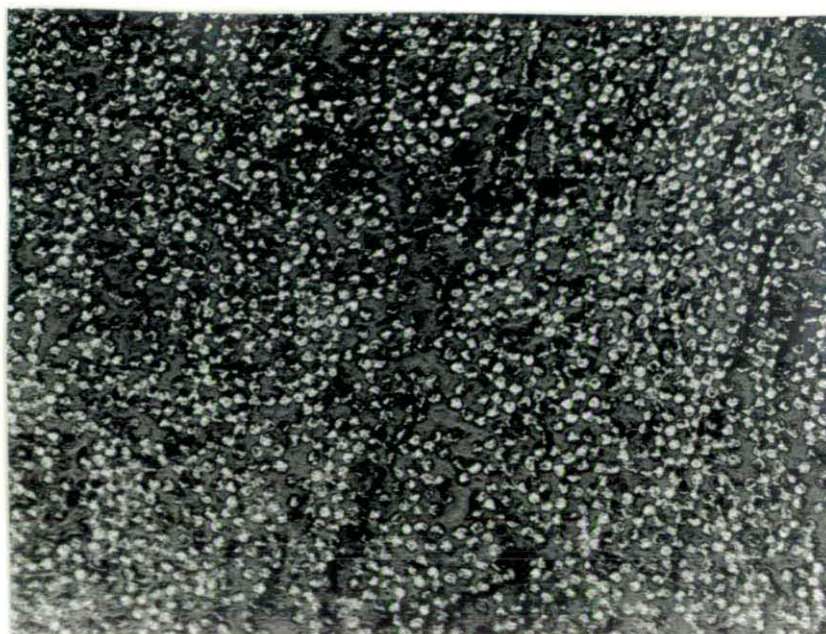


PLATE 20: THE FIBRE DISTRIBUTION IN AN UNMODIFIED CFRP SPECIMEN  
(x200)

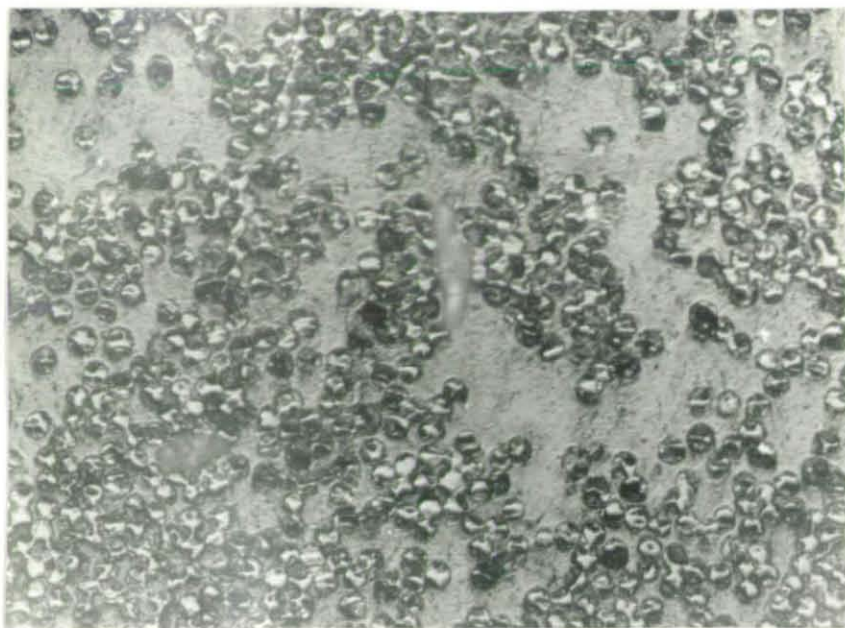


PLATE 21: THE FIBRE DISTRIBUTION IN A 30% MODIFIED GRP SPECIMEN  
(x200)



PLATE 22: THE FIBRE DISTRIBUTION IN A 30% MODIFIED CFRP SPECIMEN  
(x200)

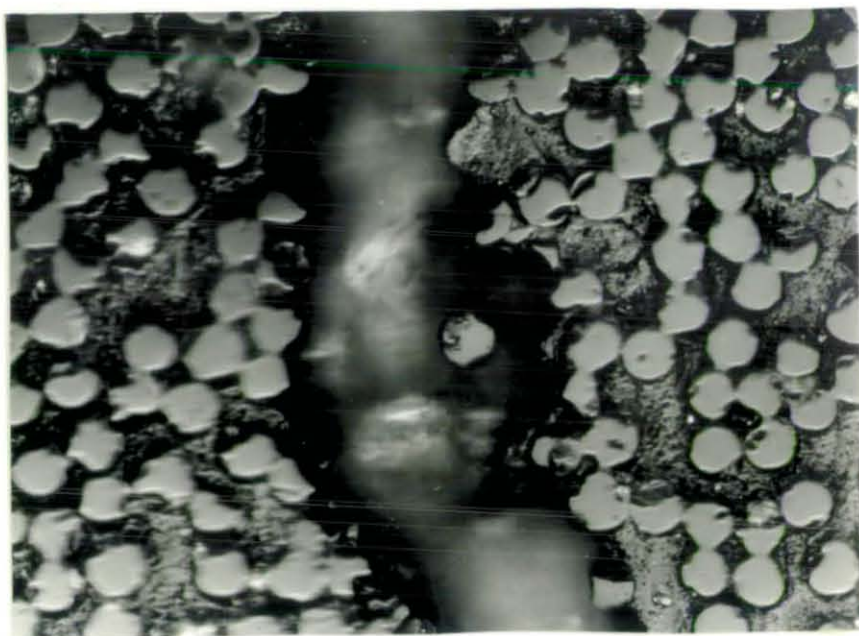


PLATE 23: AN INTERLAMINAR SHEAR CRACK IN AN UNMODIFIED GRP SPECIMEN (x500)

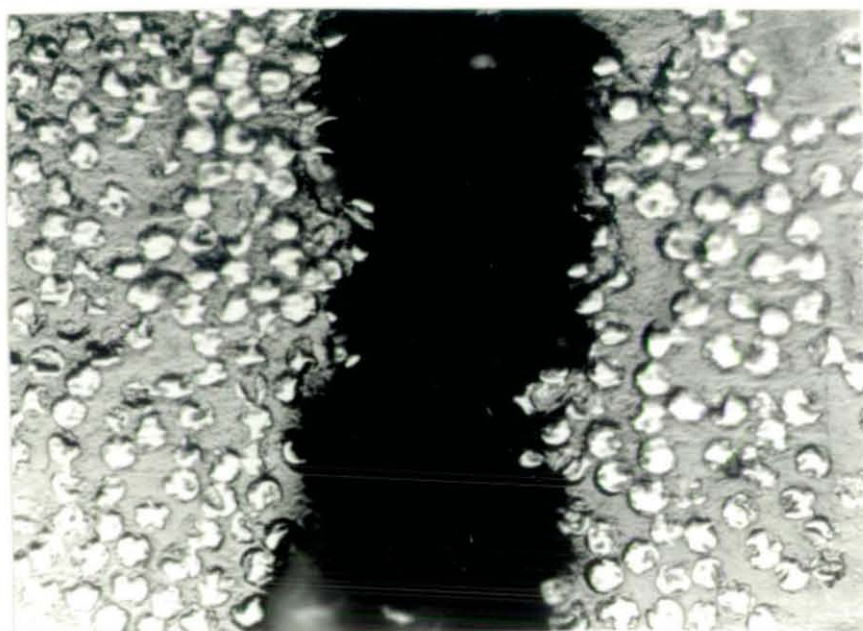


PLATE 24: AN INTERLAMINAR SHEAR CRACK IN AN UNMODIFIED CFRP SPECIMEN (x500)

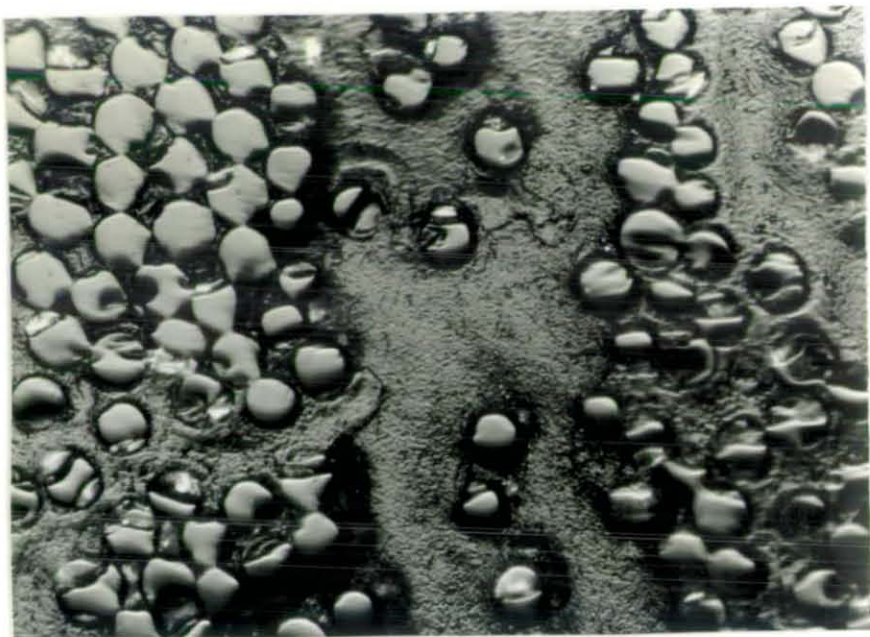


PLATE 25: AN INTERLAMINAR SHEAR CRACK IN A 30% MODIFIED GRP SPECIMEN (x500)

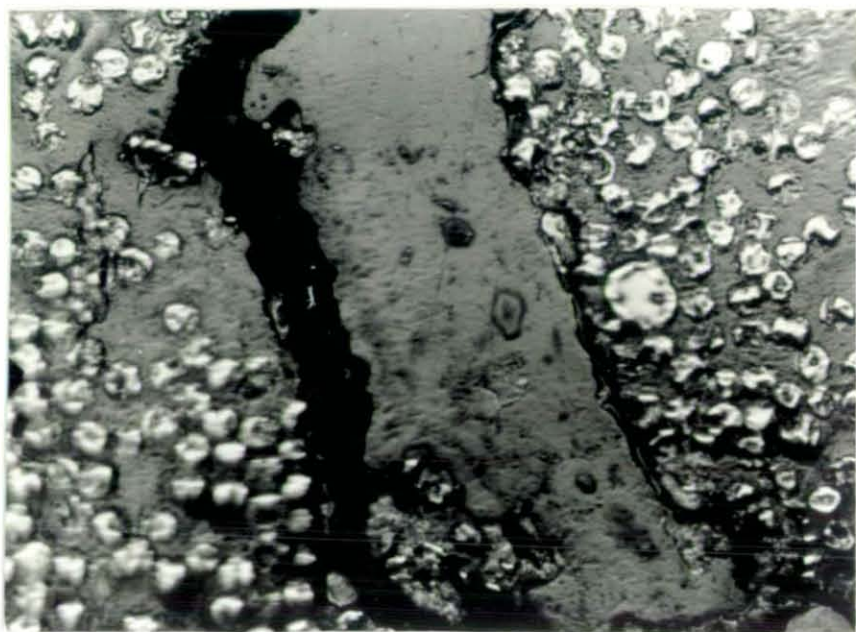


PLATE 26: AN INTERLAMINAR SHEAR CRACK IN A 30% MODIFIED CFRP SPECIMEN (x500)

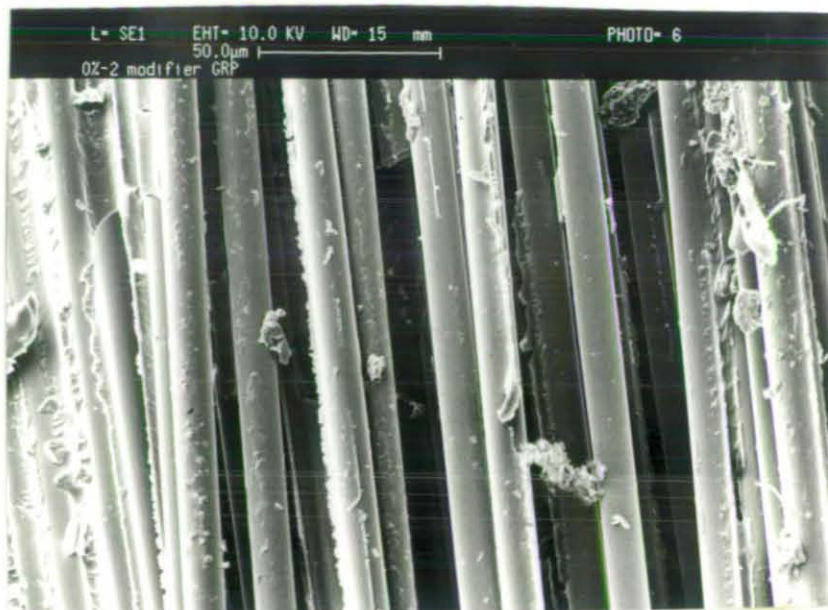


PLATE 27: SEM MICROGRAPH OF THE (ILSS) FAILURE FOR UNMODIFIED GRP (x 660)

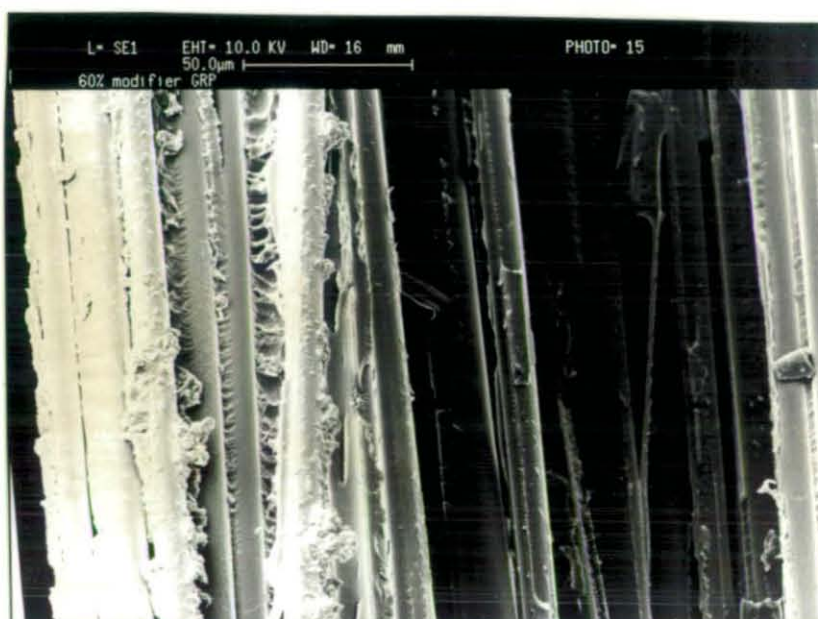


PLATE 28: SEM MICROGRAPH OF THE (ILSS) FAILURE FOR 60% MODIFIED GRP (x 660)



PLATE 29: SEM MICROGRAPH OF THE ILSS FAILURE SURFACE FOR UNMODIFIED CFRP ( $\times 950$ )

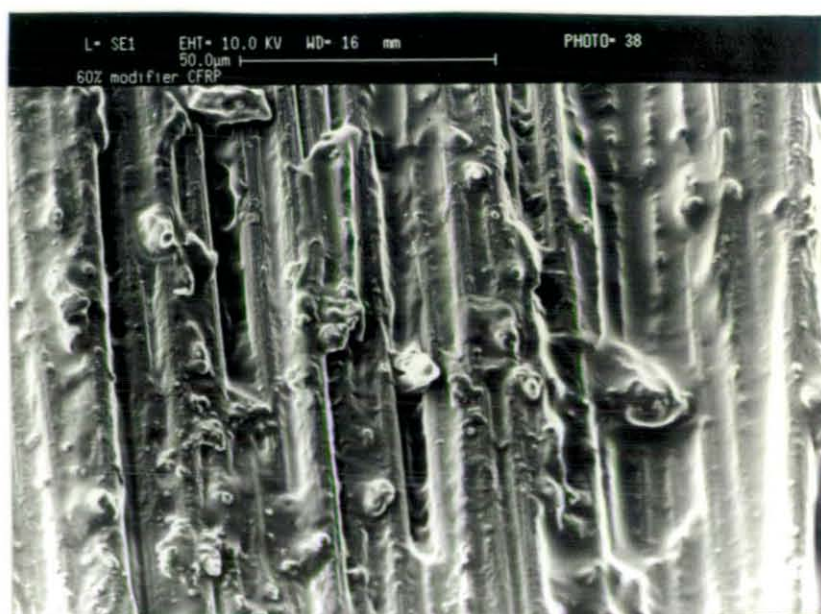


PLATE 30: SEM MICROGRAPH OF THE ILSS FAILURE SURFACE FOR 60% MODIFIED CFRP ( $\times 950$ )



PLATE 31: AN SEM MICROGRAPH OF A PART OF THE TENSILE FAILURE SURFACE OF AN UNMODIFIED GRP SPECIMEN (x450)

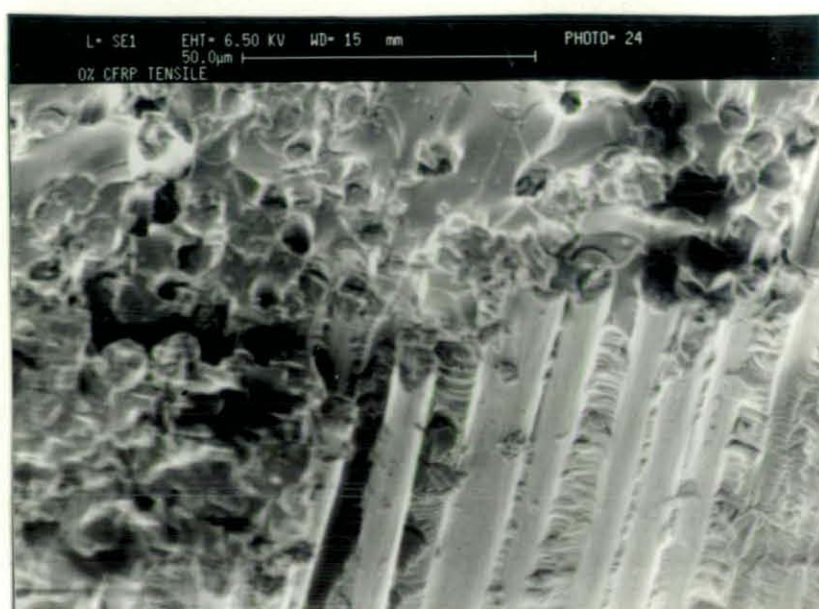


PLATE 32: AN SEM MICROGRAPH OF PART OF THE TENSILE FAILURE SURFACE OF AN UNMODIFIED CFRP SPECIMEN (x450)



PLATE 33: AN SEM MICROGRAPH OF THE SURFACE OF A SHEAR FAILURE AS OBSERVED IN AN UNMODIFIED CFRP COMPRESSIVE FAILURE SPECIMEN (x950)

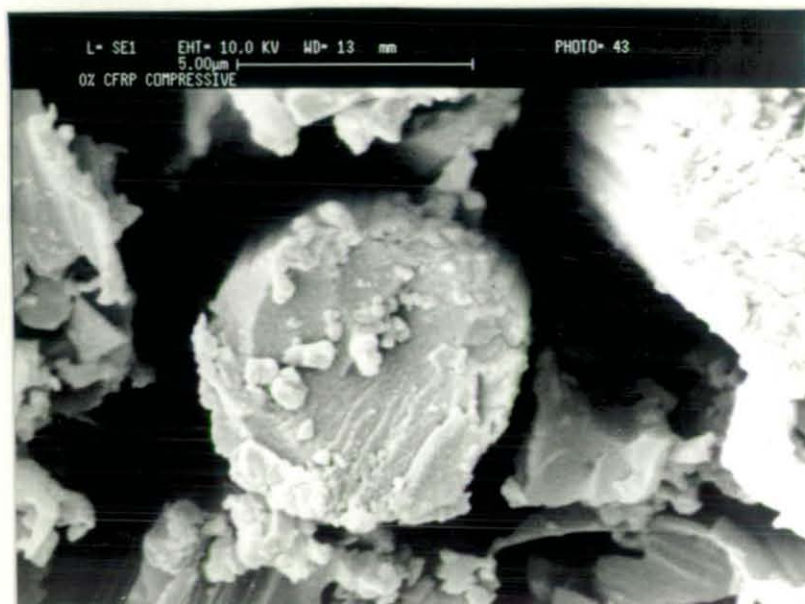


PLATE 34: AN SEM MICROGRAPH OF THE END OF A CARBON FIBRE FROM AN UNMODIFIED CFRP COMPRESSIVE FAILURE. THE FIBRE SHEAR FAILURE MODE IS CLEARLY VISIBLE (x6500)



PLATE 35: AN SEM MICROGRAPH OF THE COMPRESSIVE FAILURE SURFACE OF A 5% MODIFIED CFRP SPECIMEN SHOWING THE CHARACTERISTIC STEPS WHICH ARE THE RESULT OF FIBRE MICROBUCKLING (x250)

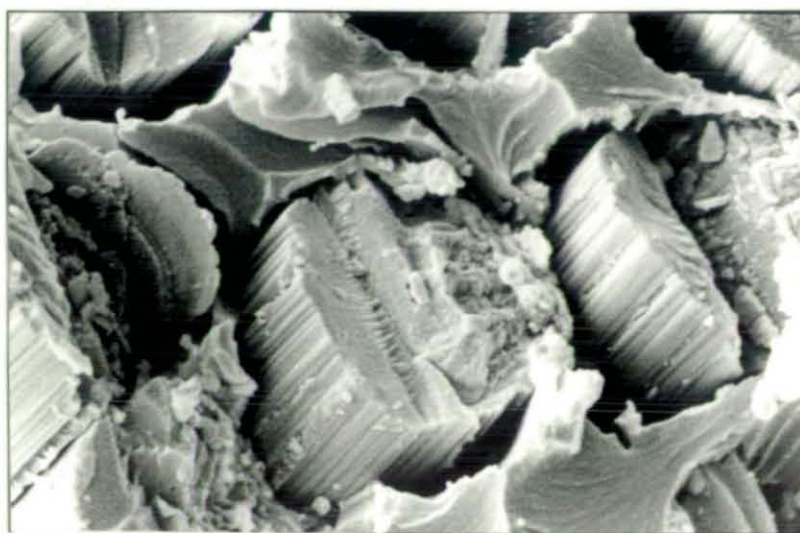


PLATE 36: AN SEM MICROGRAPH OF THE END OF A CARBON FIBRE FROM A 5% MODIFIED CFRP COMPRESSIVE FAILURE. THE FIBRE MICROBUCKLING FAILURE HAS RESULTED IN WELL DEFINED TENSILE AND COMPRESSIVE REGIONS OF FRACTURE BEING VISIBLE (x6500)

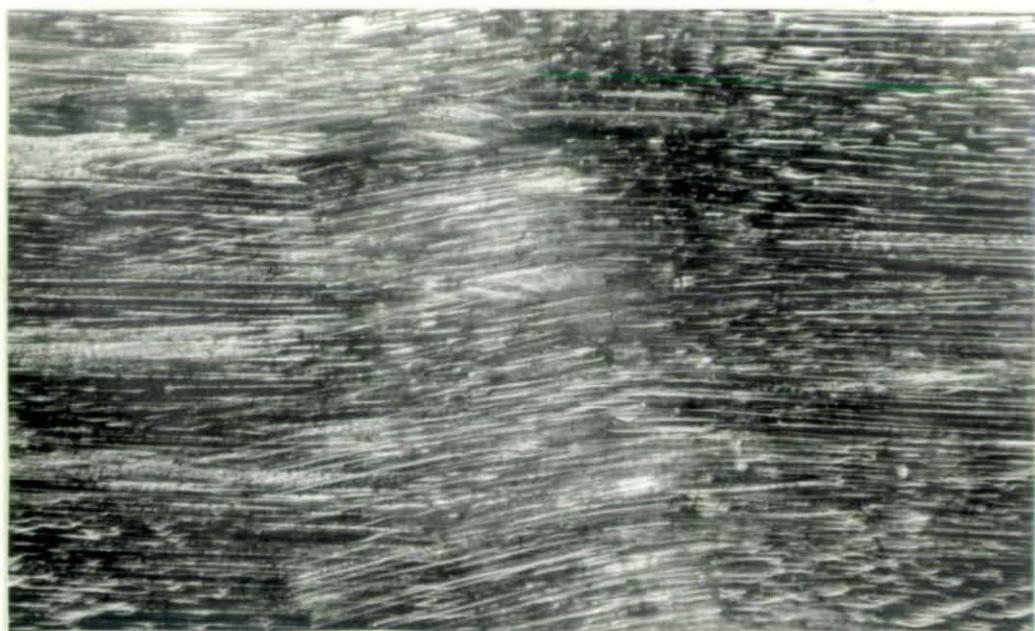


PLATE 37: LOCAL BUCKLING IN THE KINK-BAND OF A 60% MODIFIED GRP COMPRESSIVE FAILURE SPECIMEN (SIDE VIEW) (x50)



PLATE 38: LOCAL BUCKLING IN THE KINK-BAND OF A 60% MODIFIED CFRP COMPRESSIVE FAILURE SPECIMEN (SIDE VIEW) (x50)

# APPENDICES

APPENDICES

APPENDIX A:

Table A-1:	Individual fibre volume fractions, $V_{fg}$ for GRP	.....
Table A-2:	Individual fibre volume fractions, $V_{fc}$ , for CFRP	.....
Table A-3:	Individual voids volume fractions, $V_v$	..

APPENDIX B:

Table B-1:	Individual matrix-resin density	.....
Table B-2:	Individual matrix-resin tensile test results	.....

APPENDIX C:

Table C-1:	Individual compressive test results for GRP	.....
Table C-2:	Individual compressive test results for CFRP	.....

APPENDIX D:

Table D-1:	Individual tensile test results for GRP	
Table D-2:	Individual tensile test results for CFRP	

APPENDIX E:

Table E-1:	Individual interlaminar shear strength results for GRP	.....
Table E-1:	Individual interlaminar shear strength results for CFRP	.....

TABLE A.1: INDIVIDUAL FIBRE VOLUME FRACTION RESULTS FOR GRP

§ Modifier Spec. No	$W_s$ before burn-off (g)	$(W_s+W_{cr})$ after burn-off (g)	$W_{cr}$ after burn-off (g)	$W_{og}$ (g)	$V_{fg}$ (%)
0-1/1	1.3355	61.0120	60.1553	0.8567	44.2
0-2/1	1.2852	62.2430	61.4150	0.8280	44.5
0-1/2	0.9071	60.7461	60.1058	0.5703	42.4
0-2/2	0.7760	15.5848	15.0839	0.5009	44.4
5-1/1	0.8073	14.9835	14.4448	0.5387	46.9
5-2/1	0.9584	15.6981	15.0580	0.6401	46.9
5-1/2	1.2370	64.3770	63.4517	0.8278	47.2
5-2/2	0.7228	16.8448	16.3439	0.5009	44.8
10-1/1	1.1040	61.9895	61.3086	0.6809	41.3
10-2/1	1.1099	61.9719	61.2187	0.6732	40.3
10-1/2	0.8822	14.6522	14.0900	0.5622	41.5
10-2/2	0.7383	61.8000	61.3536	0.4464	39.8
20-1/1	1.2616	14.4717	13.6252	0.8465	46.9
20-2/1	1.0209	63.9017	63.2116	0.6901	47.5
20-1/2	0.6557	62.5449	62.1374	0.4075	41.5
20-2/2	0.6949	15.4487	15.0243	0.4244	40.5
30-1/1	0.6513	19.0520	13.6248	0.4272	44.9
30-2/1	0.9913	14.7764	14.0893	0.6871	45.9
30-1/2	0.7253	62.6228	62.1577	0.4651	43.4
30-2/2	1.1210	62.9270	62.2380	0.6890	40.6
40-1/1	1.3153	64.4257	63.5252	0.9005	47.4
40-2/1	1.3091	62.9905	62.1187	0.8718	45.8
40-1/2	1.5500	64.5975	63.6000	0.9975	43.0
40-2/2	1.0785	64.2821	63.5620	0.7201	46.0
50-1/1	1.4040	62.3513	61.3671	0.9842	49.4
50-2/1	1.4844	61.0975	60.0861	1.0114	47.2

Table A.1 Continued

§ Modifier Spec. No	$W_S$ before burn-off (g)	$(W_S+W_{cr})$ after burn-off (g)	$W_{cr}$ after burn-off (g)	$W_{og}$ (g)	$V_{fg}$ (%)
50-1/2	1.1828	63.9183	63.1720	0.7463	41.3
50-2/2	1.1647	62.8369	62.1086	0.7283	41.2
60-1/1	1.1200	14.8225	14.0898	0.7327	44.2
60-2/1	1.4875	63.2091	62.1959	1.0132	47.0
60-1/2	1.1658	44.3482	43.6074	0.7406	41.9
60-2/2	1.1676	15.8812	15.0990	0.7822	45.7

Note: These results are calculated from equations 4.4 and 4.7.

TABLE A.2: INDIVIDUAL FIBRE VOLUME FRACTION RESULTS FOR CFRP

% Modifier Spec. No	$W_s$ before acid dig. (g)	$(W_s+W_{cr})$ after acid dig. (g)	$W_{cr}$ after acid dig. (g)	$W_{og}$ (g)	$V_{fg}$ (%)
0-1/1	0.8412	37.7290	37.2766	0.4524	42.0
0-2/1	1.0538	37.8496	37.2673	0.5823	43.5
0-1/2	1.1189	37.9517	37.3052	0.6465	46.0
0-2/2	1.0027	37.8813	37.3043	0.5770	45.7
5-1/1	0.8126	35.3757	34.9118	0.4639	45.2
5-2/1	1.0497	35.5145	34.9017	0.6128	46.5
5-1/2	1.2446	35.6105	34.9095	0.7010	44.2
5-2/2	1.1719	35.6272	34.9645	0.6627	44.6
10-1/1	0.8622	37.7400	37.2852	0.4548	40.8
10-2/1	1.0828	36.5470	35.9763	0.5707	40.7
10-1/2	1.2830	40.5158	39.7405	0.7753	48.5
10-2/2	1.1358	36.6961	36.0113	0.6848	48.0
20-1/1	0.8468	35.3827	34.9170	0.4657	42.7
20-2/1	1.1690	37.9609	37.2662	0.6947	47.2
20-1/2	0.9820	37.9205	37.2685	0.6520	54.2
20-2/2	1.1263	38.0120	37.2653	0.7467	54.5
30-1/1	0.8918	37.8490	37.2795	0.5695	51.6
30-2/1	1.1457	36.7077	35.9765	0.7312	51.6
30-1/2	0.9396	35.5337	34.9048	0.6289	55.0
30-2/2	1.2270	35.7599	34.9362	0.8237	55.2
40-1/1	0.7355	35.3691	34.9133	0.4558	49.3
40-2/1	0.7673	35.3882	34.9112	0.4770	49.5
40-1/2	0.8667	37.8535	37.2690	0.5845	55.3
40-2/2	1.2652	36.7424	35.9749	0.7675	47.9

Table A.2 (continued)

% Modifier Spec. No	$W_s$ before acid dig. (g)	$(W_s+W_{cr})$ after acid dig. (g)	$W_{cr}$ after acid dig. (g)	$W_{cg}$ (g)	$V_{fg}$ (%)
50-1/1	0.7857	37.8317	37.3755	0.4562	45.0
50-2/1	1.0345	37.0783	36.3899	0.6884	54.0
50-1/2	0.9324	35.7007	35.1209	0.5798	49.3
50-2/2	1.3351	38.1274	37.2619	0.8655	52.1
60-1/1	0.7759	35.4214	34.9319	0.4895	50.2
60-2/1	1.0471	36.6416	35.9770	0.6646	50.4
60-1/2	0.8461	35.5326	35.005	0.5276	49.4
60-2/2	0.9785	35.5639	34.9335	0.6304	51.4

Note: These results are calculated from equations 4.5 and 4.7.

TABLE A.3: INDIVIDUAL VOIDS VOLUME FRACTION RESULTS

Laminate % Modifier	$W_s$ (gm)	$W_{wo}$ (gm)	$W_{w+s}$ (gm)	$\rho_c$ gm/cm <sup>3</sup>	$W_c$ gm	$W_{cs}$ after burn-off (gm)	$W_{cs}-W_c=W_f$ (gm)	$W_s-W_f=W_R$ (gm)	Voids %
0	1.2938	81.0915	81.6455	1.75	14.4702	15.3068	0.8366	0.4578	0.71
5	0.7776	81.0690	81.4217	1.83	15.8054	16.3511	0.5457	0.2319	0.95
10	1.1729	81.0772	81.5985	1.81	13.7167	14.521	0.8043	0.3683	0.93
20	0.9634	81.0714	81.5026	1.81	14.4213	15.0950	0.6737	0.2897	1.06
30	1.1289	81.0720	81.5810	1.82	14.4439	15.2516	0.8077	0.3212	1.55
40	1.1283	81.0773	81.5753	1.79	16.3440	17.1352	0.7912	0.3371	1.26
50	1.3191	81.0980	81.6402	1.70	14.4176	15.2865	0.8689	0.4495	1.95
60	0.6960	81.0695	81.3745	1.78	20.8745	21.3689	0.4944	0.2016	1.78

Note: These results are calculated from equations 4.6 and 4.7.

TABLE B.1: INDIVIDUAL MATRIX-RESIN DENSITY RESULTS

% Modifier spec. No	$W_S$ (g)	$W_{WO}$ (g)	$W_{WO+S}$ (g)	$\rho_s$ ( $\text{gcm}^{-3}$ )
0-1	1.191	148.259	148.391	1.125
0-2	0.742	148.250	148.330	1.122
0-3	1.191	148.166	148.290	1.116
0-4	0.632	22.402	22.432	1.128
10-1	0.504	148.169	148.218	1.077
10-2	1.113	148.170	148.306	1.139
10-3	1.135	148.184	148.317	1.133
10-4	0.752	148.227	148.309	1.122
20-1	0.888	148.223	148.311	1.110
20-2	0.919	148.208	148.299	1.110
20-3	0.739	148.218	148.273	1.080
20-4	0.705	148.212	148.264	1.080
30-1	0.581	23.064	23.109	1.082
30-2	0.657	148.158	148.221	1.106
30-3	0.558	23.060	23.120	1.121
30-4	1.177	148.198	198.272	1.067
40-1	0.768	148.196	148.250	1.076
40-2	0.769	148.182	148.240	1.082
40-3	1.126	148.170	148.276	1.104
50-1	1.065	148.180	148.260	1.081
50-2	0.653	148.166	148.198	1.052
50-3	1.014	148.191	148.264	1.078
50-4	0.721	148.176	148.203	1.039
60-1	0.941	148.169	148.235	1.075
60-2	1.081	148.162	148.252	1.091
60-3	0.653	148.175	148.184	1.014

Note: These results are calculated from equation 4.7.

TABLE B.2: INDIVIDUAL 'MATRIX-RESIN' TENSILE TEST RESULTS

% Modifier Spec. No	CSA (mm <sup>2</sup> )	Max Load (N)	UTS (MPa)	Failure Strain (%)	Load at 2% Strain (N)	Young's Modulus E (GPa)
0-1	30.17	1950	65	2.00	1950	3.25
0-2	29.76	1650	56	2.00	1650	2.80
0-3	29.36	1700	58	2.00	1700	2.90
0-4	29.94	1580	53	1.80	*	*
20-1	19.42	620	32	17.60	590	1.50
20-1	19.71	590	30	20.60	580	1.47
20-3	20.47	580	28	11.20	540	1.32
20-4	20.38	570	28	8.00	500	1.27
30-1	19.28	420	22	13.60	340	0.88
30-2	20.99	395	19	15.20	345	0.82
30-3	19.29	368	19	13.60	338	0.88
30-4	18.76	412	22	22.80	350	0.93
40-1	28.35	450	16	38.00	350	0.62
40-2	28.40	392	14	30.03	285	0.50
40-3	28.78	425	15	35.20	350	0.61
50-1	18.77	215	12	36.80	125	0.33
50-2	20.39	208	10	39.60	113	0.28
50-3	20.03	192	10	33.20	110	0.28
50-4	17.86	200	11	26.00	115	0.32
60-1	18.30	135	8	26.80	65	0.18
60-2	18.35	180	10	43.20	60	0.16
60-3	18.39	130	7	31.60	60	0.16
60-4	21.20	180	9	44.00	75	0.18

TABLE C.1: INDIVIDUAL COMPRESSIVE TEST RESULTS FOR GRP

% Modifier Spec. No	CSA (mm <sup>2</sup> )	Max.Load P (kN)	UCS (MPa)	Failure Strain (%)	V <sub>fg</sub> (%)	UCS (V <sub>fg</sub> =0.45) (MPa)	Failure Strain (V <sub>fg</sub> =0.45) (%)	Sec. Modulus E (at 0.5% ) (GPa)
0-1/1	22.87	12.76	558	1.20	44.4	571	1.23	35.77
0-2/1	22.73	9.82	432	1.18	44.4	442	1.21	43.19
0-3/2	23.04	10.42	452	1.20	43.4	473	1.25	42.74
0-4/2	22.92	9.96	433	1.29	43.4	452	1.35	47.49
0-5/2	22.74	10.88	478	1.20	43.4	501	1.25	46.02
5-1/1	22.96	9.96	434	1.15	46.9	417	1.13	41.70
5-2/1	22.39	9.58	428	1.25	46.9	411	1.22	35.32
5-3/2	21.79	10.03	460	1.24	46.0	450	1.21	40.41
5-4/2	21.79	8.98	412	1.08	46.0	403	1.06	39.51
5-5/2	21.66	8.39	387	0.85	46.0	378	0.83	43.35
10-1/1	23.08	7.59	329	0.95	40.8	370	1.06	43.27
10-2/1	22.75	8.10	356	0.87	40.8	401	0.98	43.42
10-3/1	23.44	8.29	354	1.02	40.8	398	1.15	37.46
10-4/2	22.98	6.39	278	0.95	45.0	278	0.95	38.00
10-5/2	22.99	7.51	327	*	45.0	327	*	*
20-1/1	22.23	6.42	289	0.87	47.2	295	0.89	33.12
20-2/1	22.10	4.58	207	*	47.2	212	*	*
20-3/2	23.87	5.21	218	1.00	41.0	240	1.01	32.19
20-4/2	23.83	6.68	280	1.20	41.0	308	1.32	19.40
20-5/2	23.90	5.03	210	1.10	41.0	231	1.21	20.80
30-1/1	22.57	5.38	239	0.52	45.4	239	0.52	*
30-2/1	22.24	4.42	199	0.60	45.4	199	0.60	17.99
30-3/2	23.65	4.60	195	1.00	42.0	208	1.07	22.65
30-4/2	24.02	4.02	167	0.90	42.0	170	0.97	22.30
30-5/2	23.60	4.44	188	0.90	42.0	202	0.97	22.70
40-1/1	22.79	5.19	228	1.02	46.3	223	1.00	19.75
40-2/1	22.66	4.09	181	*	46.3	177	*	*
40-3/2	22.49	3.07	137	0.80	44.2	140	0.82	20.92
40-4/2	22.97	4.04	176	0.95	44.2	180	0.97	24.04
40-5/2	22.85	3.01	132	0.85	44.2	135	0.87	17.90

Table C.1 (continued)

§ Modifier Spec. No	CSA (mm <sup>2</sup> )	Max.Load P (kN)	UCS (MPa)	Failure Strain (%)	V <sub>fg</sub> (%)	UCS (V <sub>fg</sub> =0.45) (MPa)	Failure Strain (V <sub>fg</sub> =0.45) (%)	Sec. Modulus E (at 0.5% ) (GPa)
50-1/1	22.37	4.83	216	1.22	48.1	203	1.14	17.60
50-2/1	22.40	4.25	190	1.11	48.1	178	1.04	16.74
50-3/2	23.63	3.62	153	0.66	41.2	168	0.73	23.22
50-4/2	23.15	3.48	150	0.56	41.2	165	0.62	22.76
50-5/2	23.45	2.67	107	0.52	41.2	125	0.52	18.72
60-1/1	22.91	2.62	114	0.70	45.2	114	0.70	17.46
60-2/1	22.53	2.27	101	0.72	45.2	101	0.72	11.54
60-3/2	22.28	2.00	90	0.74	43.0	94	0.77	11.27
60-4/2	22.41	1.40	63	0.45	43.0	66	0.47	*
60-5/2	22.54	2.21	98	*	43.0	103	*	*

Note: These results are calculated from equations 4.1, 4.2, 4.3, 4.9 and 4.10.

TABLE C.2: INDIVIDUAL COMPRESSIVE TEST RESULTS FOR CFRP

§ Modifier Spec. No	CSA (mm <sup>2</sup> )	Max.Load (kN)	UCS (MPa)	Failure Strain (%)	V <sub>fc</sub> (%)	UCS (V <sub>fc</sub> =0.45) (MPa)	Failure Strain (V <sub>fc</sub> =0.45) (%)	Sec. Modulus E (at 0.5% ) (GPa)
0-1/1	23.24	13.36	575	1.30	42.7	616	1.37	62.40
0-2/1	24.09	14.55	604	1.30	42.7	647	1.37	66.15
0-3/1	23.78	14.39	605	0.65	42.7	648	0.69	70.91
0-4/2	23.74	11.49	484	1.05	45.8	483	1.05	49.67
0-5/2	22.56	12.69	563	1.24	45.8	562	1.24	43.55
0-6/2	23.61	15.46	655	*	45.8	654	*	*
5-1/1	23.32	10.88	467	0.96	45.8	459	0.94	46.35
5-2/1	23.99	14.39	600	0.80	45.8	590	0.79	46.12
5-3/1	23.66	9.74	412	1.42	45.8	405	1.39	53.99
5-4/2	23.85	13.56	566	1.30	44.4	582	1.33	60.60
5-5/2	24.06	14.85	617	1.30	44.4	631	1.33	54.76
5-6/2	23.42	10.25	438	*	44.4	448	*	*
10-1/1	23.29	8.01	344	0.87	40.7	387	0.96	47.47
10-2/1	23.39	8.71	373	0.90	40.7	419	1.00	53.23
10-3/1	23.59	8.23	349	1.04	40.7	393	1.15	42.18
10-4/2	24.20	11.73	485	1.14	48.0	454	1.08	56.17
10-5/2	23.96	9.04	377	0.85	48.0	354	0.80	40.69
10-6/2	23.49	10.40	443	*	48.0	415	*	*
20-1/1	23.08	6.57	285	0.62	44.9	291	0.62	49.94
20-2/1	23.25	7.94	342	0.84	44.9	349	0.84	46.38
20-3/1	24.02	7.98	330	0.70	44.9	337	0.70	47.98
20-4/1	23.59	6.51	276	*	44.9	282	*	*
20-5/2	24.02	5.93	247	0.46	44.9	265	0.50	45.09
20-6/2	23.37	9.72	416	0.80	54.3	347	0.67	44.00
30-1/1	23.44	5.25	224	0.52	51.6	198	0.46	35.76
30-2/1	23.46	4.68	198	0.57	51.6	175	0.50	35.01
30-3/1	23.85	5.22	219	0.66	51.6	193	0.58	29.60
30-4/2	23.47	7.44	317	0.75	55.1	259	0.62	34.86
30-5/2	23.12	5.90	255	0.47	55.1	209	0.39	39.65
30-6/2	23.84	6.85	287	*	55.1	235	*	*

Table C.2 (continued)

% Modifier Spec. No	CSA (mm <sup>2</sup> )	Max.Load (kN)	UCS (MPa)	Failure Strain (%)	V <sub>fc</sub> (%)	UCS (V <sub>fc</sub> =0.45) (MPa)	Failure Strain (V <sub>fc</sub> =0.45) (%)	Sec. Modulus E (at 0.5% ) (GPa)
40-1/1	22.94	4.56	199	0.42	49.3	181	0.38	39.24
40-2/1	23.90	4.77	200	0.64	49.3	183	0.59	34.37
40-3/2	22.58	4.99	221	0.46	51.6	195	0.41	41.03
40-4/2	22.87	5.12	224	0.50	51.6	198	0.44	38.58
40-5/2	23.39	5.95	254	*	51.6	224	*	*
40-6/2	23.16	7.11	307	0.62	51.6	238	0.48	38.10
50-1/1	22.12	3.19	144	0.40	49.3	133	0.37	35.08
50-2/1	21.68	3.51	162	0.50	49.3	149	0.46	33.68
50-3/1	22.35	4.49	201	0.46	49.3	181	0.42	34.71
50-4/1	21.68	3.63	168	*	49.3	151	*	*
50-5/2	23.00	4.90	213	0.52	50.7	192	0.46	38.59
50-6/2	23.68	4.33	183	0.56	50.7	166	0.51	26.61
60-1/1	22.46	2.80	125	0.34	50.3	112	0.31	28.05
60-2/1	21.71	2.65	122	0.36	50.3	109	0.33	21.00
60-3/2	23.26	2.95	127	0.40	50.4	114	0.36	34.82
60-4/2	23.40	2.40	103	0.40	50.4	92	0.36	27.69
60-5/2	22.31	2.35	105	*	50.4	95	*	*
60-6/2	22.00	3.20	145	*	50.4	131	*	*

Note: These results are calculated from equations 4.1, 4.2, 4.3, 4.9 and 4.10

TABLE D.1: INDIVIDUAL TENSILE TEST RESULTS FOR GRP

% Modifier Spec. No	CSA (mm <sup>2</sup> )	Max.Load (kN)	UTS (MPa)	Failure Strain (%)	V <sub>fg</sub> (%)	UTS (V <sub>fg</sub> =0.45) (MPa)	Failure Strain (V <sub>fg</sub> =0.45) (%)	Sec. Modulus E (at 0.5% ) (GPa)
0-1/1	54.60	55.70	1020	2.40	44.4	1043	2.43	43.46
0-2/1	55.59	55.04	990	*	44.4	1013	*	*
0-3/2	52.76	43.75	829	2.20	43.4	868	2.30	42.00
0-4/2	53.26	50.20	943	2.28	43.4	987	2.39	44.80
5-1/1	55.18	43.75	793	2.22	46.9	761	2.13	36.09
5-2/1	53.45	40.10	750	2.08	46.9	720	1.99	35.74
5-3/2	55.84	45.48	815	2.24	46.0	797	2.19	35.74
5-1/2	54.44	41.11	755	1.88	46.0	739	1.84	36.66
10-1/1	58.25	42.80	735	2.00	40.8	806	2.20	37.68
10-2/1	58.74	41.20	701	1.80	40.8	769	1.98	41.11
10-3/2	59.50	38.72	651	1.92	40.3	732	2.16	38.60
10-4/2	58.63	38.42	656	1.86	40.3	738	2.09	40.68
20-1/1	56.34	41.38	734	2.16	47.2	703	2.07	35.35
20-2/1	55.25	38.75	701	2.04	47.2	671	1.95	34.66
20-3/2	59.70	39.59	663	*	41.0	728	*	*
20-4/2	58.37	36.60	626	2.20	41.0	688	2.41	30.09
30-1/1	55.91	40.50	724	2.04	45.4	723	2.04	37.20
30-2/1	56.27	37.65	669	2.00	45.4	668	2.00	39.10
30-3/2	58.16	34.77	598	1.74	42.0	641	1.86	36.84
30-4/2	58.65	35.90	612	1.86	42.0	656	1.99	36.84
40-1/1	56.16	36.47	649	2.02	44.6	634	1.98	34.84
40-2/1	56.29	34.80	678	1.70	44.6	604	1.66	41.71
40-3/2	57.17	32.78	573	1.68	44.5	586	1.72	39.36
40-4/2	57.72	34.80	599	1.56	44.5	613	1.60	38.00
50-1/1	55.38	37.27	609	1.92	48.3	566	1.80	35.89
50-2/1	55.22	34.76	608	1.98	48.3	565	1.86	31.92
50-3/2	57.72	32.36	561	1.52	41.2	608	1.67	39.56
50-4/2	59.33	31.19	526	*	41.2	570	*	*
60-1/1	55.23	27.63	500	1.66	45.6	497	1.66	34.76
60-2/1	55.75	30.31	543	1.60	45.6	539	1.60	33.72
60-3/2	54.30	24.36	448	1.41	43.0	470	1.48	32.00
60-4/2	55.95	29.00	518	1.50	43.0	542	1.57	34.00

Note: These results were calculated from equations 4.1, 4.2, 4.3, 4.10 and 4.11

TABLE D.2: INDIVIDUAL TENSILE TEST RESULTS FOR CFRP

§ Modifier Spec. No	CSA mm <sup>2</sup>	Max.Load (kN)	UTS (MPa)	Failure Strain (%)	V <sub>fc</sub> (%)	UTS (V <sub>fc</sub> =0.45) (MPa)	Failure Strain (V <sub>fc</sub> =0.45) (%)	Sec. Modulus E (at 0.5% ) (GPa)
0-1/1	58.74	81.15	1382	1.55	42.7	1457	1.66	107.65
0-2/1	58.34	77.38	1326	1.38	42.7	1399	1.48	108.39
0-3/2	57.88	82.94	1433	1.34	45.8	1408	1.34	115.43
0-4/2	57.98	75.88	1326	1.29	45.8	1303	1.29	108.46
5-1/1	57.85	78.91	1364	1.12	45.8	1340	1.10	118.89
5-2/1	58.91	81.25	1379	1.24	45.8	1355	1.22	116.75
5-3/2	56.68	78.22	1380	1.24	44.4	1399	1.26	110.87
5-4/2	58.32	82.45	1414	1.24	44.4	1433	1.26	121.65
10-1/1	59.12	65.26	1104	1.14	40.7	1221	1.24	119.69
10-2/1	58.13	62.76	1080	1.14	40.7	1194	1.26	114.12
10-3/2	58.66	74.46	1269	1.08	48.0	1190	1.02	107.08
10-4/2	58.71	77.38	1318	1.10	48.0	1236	1.03	121.40
20-1/1	59.34	82.26	1386	1.25	44.9	1370	1.25	118.23
20-2/1	59.72	76.50	1281	1.36	44.9	1284	1.36	110.80
20-2/2	55.63	76.30	1371	1.24	54.3	1143	1.03	92.88
20-4/2	57.83	79.45	1374	1.08	54.3	1145	0.90	106.64
30-1/1	55.83	72.50	1299	1.20	51.6	1133	1.05	93.72
30-2/1	56.89	71.02	1248	1.32	51.6	1089	1.15	61.32
30-3/2	56.42	69.26	1228	1.20	55.1	1005	0.98	92.64
30-4/2	57.63	79.92	1387	1.20	55.1	1135	0.98	99.20
40-1/1	58.71	59.63	1000	0.92	49.3	928	0.85	108.83
40-2/1	57.59	62.27	1081	1.12	49.3	987	1.03	95.10
40-3/2	55.65	70.51	1267	1.14	51.0	1118	1.05	107.82
40-4/2	55.68	69.76	1253	1.04	51.0	1106	0.92	110.93
50-1/1	54.46	62.32	1144	0.90	49.3	1051	0.83	124.03
50-2/1	54.93	57.18	1041	1.10	49.3	956	1.01	99.70
50-3/2	57.57	58.89	1023	1.12	50.7	921	1.01	101.76
50-4/2	57.91	65.10	1124	0.82	50.7	1012	0.74	113.42
60-1/1	52.11	59.55	1143	0.96	50.3	1021	0.87	113.09
60-2/1	52.95	47.03	1018	0.90	50.3	909	0.81	101.18
60-3/2	56.13	57.14	1018	0.96	50.4	909	0.87	95.44
60-4/2	56.84	47.53	836	0.71	50.4	753	0.64	125.67

Note: These results were calculated from equations 4.1, 4.2, 4.3, 4.10 and 4.11

TABLE E.1: INDIVIDUAL ILSS TEST RESULTS FOR GRP

% Modified Spec. No	CSA (mm <sup>2</sup> )	Max Load (kg)	ILSS (MPa)	V <sub>fg</sub> (%)	ILSS (V <sub>fg</sub> =0.45) (MPa)
0-1/1	22.09	144	47.91	44.4	48.56
0-2/1	20.62	134	47.78	44.4	48.43
0-3/1	20.52	132	47.43	44.4	48.07
0-4/2	22.69	143	46.32	43.4	48.03
0-5/2	21.75	139	46.97	43.4	48.70
0-6/2	20.97	132	46.26	43.4	47.97
5-1/1	24.72	139	41.34	46.9	39.67
5-2/1	24.44	142	42.70	46.9	40.97
5-3/1	24.21	130	39.46	46.9	37.86
5-4/2	25.08	139	40.73	46.0	39.84
5-5/2	24.19	130	39.49	46.0	38.63
5-6/2	25.19	125	36.47	46.0	35.68
10-1/1	23.18	110	34.88	40.8	38.47
10-2/1	23.26	107	33.91	40.8	37.40
10-3/1	22.19	101	33.44	40.8	36.88
10-4/2	22.40	114	37.41	45.0	37.41
10-5/2	22.43	116	37.27	45.0	37.27
10-6/2	22.20	108	36.46	45.0	36.46
20-1/1	23.76	119	35.20	47.2	33.56
20-2/1	23.57	114	35.54	47.2	33.88
20-3/1	24.92	119	35.10	47.2	33.46
20-4/2	22.18	84	27.83	41.0	30.55
20-5/2	22.09	104	34.60	41.0	37.97
20-6/2	21.51	100	34.17	41.0	37.50
30-1/1	21.67	84	28.49	45.4	28.49
30-2/1	22.43	88	28.83	45.4	28.83
30-3/1	21.69	82	27.79	45.4	27.79
30-4/2	21.87	80	26.88	42.0	28.80
30-5/2	20.81	78	27.55	42.0	29.52
30-6/2	22.47	80	26.16	42.0	28.03

Table E.1 (continued)

% Modified Spec. No	CSA (mm <sup>2</sup> )	Max Load (kg)	ILSS (MPa)	$V_{fg}$ (%)	ILSS ( $V_{fg}=0.45$ ) (MPa)
40-1/1	22.16	71	23.54	46.3	22.88
40-2/1	23.78	81	25.03	46.3	24.33
40-3/1	22.90	76	24.38	46.3	23.70
40-4/2	22.62	70	22.74	44.2	23.15
40-5/2	22.92	70	22.44	44.2	22.85
40-6/2	22.76	69	22.28	44.2	22.68
50-1/1	22.83	68	21.89	48.1	20.48
50-2/1	24.11	86	26.21	48.1	24.53
50-3/1	23.57	81	25.25	48.1	23.62
50-4/2	24.94	88	25.93	41.2	28.32
50-5/2	23.71	76	23.56	41.2	25.73
50-6/2	24.04	85	25.98	41.2	28.37
60-1/1	22.48	52	17.00	45.2	17.00
60-2/1	22.60	45	14.63	45.2	14.63
60-3/1	22.64	46	14.97	45.2	14.97
60-4/2	22.21	45	14.89	43.0	15.58
60-5/2	22.30	46	15.16	43.0	15.86
60-6/2	22.70	44	14.24	43.0	14.90

Note: These results were calculated from equation 4.12.

TABLE E.2: INDIVIDUAL ILSS TEST RESULTS FOR CFRP

§ Modified Spec. No	CSA (mm <sup>2</sup> )	Max Load (kg)	ILSS (MPa)	V <sub>fc</sub> (%)	ILSS (V <sub>fc</sub> =0.45) (MPa)
0-1/1	22.08	160	53.24	42.7	56.11
0-2/1	24.78	182	53.96	42.7	56.87
0-3/1	24.32	177	53.49	42.7	56.37
0-4/2	22.88	182	58.45	45.8	58.45
0-5/2	24.63	192	57.28	45.8	57.28
0-6/2	23.10	165	52.50	45.8	52.50
5-1/1	25.54	174	50.06	45.8	50.06
5-2/1	24.35	176	53.12	45.8	53.12
5-3/1	23.51	172	53.77	45.8	53.77
5-4/2	22.90	164	52.63	44.4	53.34
5-5/2	24.62	178	53.13	44.4	53.85
5-6/2	24.88	168	49.61	44.4	50.28
10-1/1	24.55	142	42.51	40.7	47.00
10-2/1	24.58	152	45.94	40.7	50.24
10-3/1	24.24	148	44.87	40.7	49.61
10-4/2	23.13	142	45.11	48.0	42.29
10-5/2	23.22	140	44.31	48.0	41.54
10-6/2	21.70	146	49.44	48.0	46.35
20-1/1	22.70	98	31.73	44.9	31.80
20-2/1	22.90	101	32.42	44.9	32.49
20-3/1	23.57	108	33.67	44.9	33.74
20-4/2	23.50	108	33.78	44.9	33.86
20-5/2	22.90	102	32.74	44.9	32.81
20-6/2	23.81	102	31.48	44.9	31.55
30-1/1	22.83	93	29.94	51.6	26.11
30-2/1	22.39	81	26.58	51.6	23.45
30-3/1	22.53	86	28.05	51.6	24.75
30-4/2	22.49	94	30.71	55.1	25.13
30-5/2	22.87	98	31.48	55.1	25.76
30-6/1	23.09	99	29.92	55.1	24.48

Table E.2 (continued)

§ Modified Spec. No	CSA (mm <sup>2</sup> )	Max Load (kg)	ILSS (MPa)	V <sub>fc</sub> (%)	ILSS (V <sub>fc</sub> =0.45) (MPa)
40-1/1	21.50	73	24.95	49.3	22.77
40-2/1	21.47	76	26.01	49.3	23.74
40-3/1	21.89	81	27.19	49.3	24.82
40-4/2	21.97	72	24.09	51.6	21.26
40-5/2	20.95	77	27.02	51.6	23.84
40-6/2	21.99	74	24.73	51.6	21.82
50-1/1	23.07	69	21.98	49.3	20.06
50-2/1	23.39	74	23.25	49.3	21.22
50-3/1	23.78	83	25.65	49.3	23.41
50-4/2	23.55	80	24.96	50.7	22.46
50-5/2	23.42	74	23.22	50.7	20.90
50-6/2	23.41	80	25.11	50.7	22.60
60-1/1	21.45	48	16.45	50.3	14.81
60-2/1	21.99	53	17.71	50.3	15.94
60-3/1	23.04	55	17.54	50.3	15.79
60-4/2	23.39	53	16.65	50.4	14.99
60-5/2	22.51	59	19.26	50.4	17.20
60-6/2	22.94	56	17.94	50.4	16.15

Note: These results were calculated from equation 4.12.

